

University of Alberta

Library Release Form

Name of Author: *Renata Kay Wood*

Title of Thesis: *Response of Dense Beach Above Water Tailings To Cyclic Equipment Loading at Syncrude's Southwest Sand Storage Facility*

Degree: *Master of Science*

Year this Degree Granted: *2003*

Permission is hereby granted to the University of Alberta Library to reproduce single copies of this thesis and to lend or sell such copies for private, scholarly or scientific research purposes only.

The author reserves all other publication and other rights in association with the copyright in the thesis, and except as herein before provided, neither the thesis nor any substantial portion thereof may be printed or otherwise reproduced in any material form whatever without the author's prior written permission.



Signature

1970 Tomlinson Green, NW
Edmonton Alberta
T6R 2R6

September 2, 2003

University of Alberta

*Response of Dense Beach Above Water Tailings to Cyclic Equipment Loading
at Syncrude's Southwest Sand Storage Facility*

by

Renata Wood

A thesis submitted to the Faculty of Graduate Studies and Research in partial fulfillment of the
requirements for the degree of *Master of Science*

in

Geotechnical Engineering

Department of *Civil and Environmental Engineering*

Edmonton, Alberta

Fall 2003

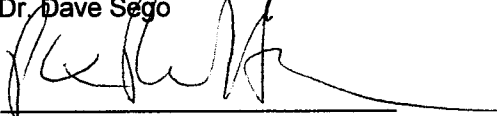
University of Alberta

Faculty of Graduate Studies and Research

The undersigned certify that they have read, and recommend to the Faculty of Graduate Studies and Research for acceptance, a thesis entitled **Response of Dense Beach Above Water Tailings to Cyclic Equipment Loading at Syncrude's Southwest Sand Storage Facility** submitted by **Renata K. Wood** in partial fulfillment of the requirements for the degree of **Masters of Science**.



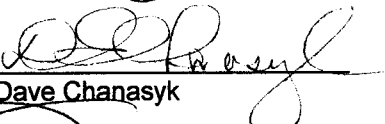
Dr. Dave Segó



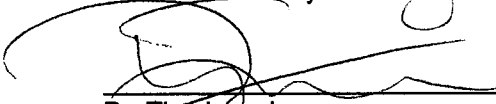
Dr. Peter Robertson



Dr. Kevin Biggar



Dr. Dave Chanasyk



Dr. Tim Joseph

Date: Sept 4, 2003

ABSTRACT

Increased pore pressures and softening of dense beach above water tailings were observed at Syncrude when cyclic equipment loading was applied, resulting in stoppage of several reclamation projects and presenting challenges for future reclamation activities. The softening was accompanied by the formation of sand boils and appeared to be a liquefaction type behaviour, although swelling and retention of static strength were also observed.

To study whether it was liquefaction that caused softening, instrumented test areas were softened by equipment and human activities that imparted cyclic loading on a Syncrude site. Analyses of in-situ test data and subsequent laboratory test results showed that the tailings were initially dense of their critical state. This and the stress paths observed during cyclic loading are consistent with cyclic liquefaction. Several controlling factors and potential mechanisms for the observed softening were identified, and the field data was used to develop correlations for other sites and loading conditions.

ACKNOWLEDGEMENT

I would like to thank my husband Brad for his support and helpful criticisms. I would also like to gratefully acknowledge the funding from NSERC and Syncrude, for without their generous contributions this research would not have been possible. I would like to thank all the people who helped me with the research and field program including: my supervisors Dr. Peter Robertson and Dr. Dave Segoy; Ted Lord, Gord McKenna, Beat List, Jose Ferrara and Gurpreet Purhar of Syncrude; and Gerry Cyer, Christine Hereygers, Steve Gamble, Sally Petaske, and Dr. Derek Martin of the University of Alberta. Lastly, but not least, I would like to thank my parents for their unwavering support and faith in me.

TABLE OF CONTENTS

	Page
1.0 INTRODUCTION	1
1.1 BACKGROUND	1
1.2 PREVIOUS WORK	2
1.3 OBJECTIVES	3
2.0 REVIEW OF LIQUEFACTION LITERATURE	7
2.1 GENERAL	7
2.2 DEFINITIONS	7
2.3 MECHANISMS	11
2.3.1 General	11
2.3.2 The State of Sands	11
2.3.3 Response to Undrained Monotonic Loading	13
2.3.4 Response to Undrained Cyclic Loading	15
2.3.5 Factors Controlling Cyclic Liquefaction Behaviour	16
2.3.5.1 General	16
2.3.5.2 Density and Void Ratio	17
2.3.5.3 Confining Pressure	17
2.3.5.4 Initial Static Shear Stress	18
2.3.5.5 Fines Content	19
2.3.5.6 Loading Direction	19
2.3.5.7 Location of the Phreatic Surface	20
2.3.5.8 Other Factors	21
2.4 EVALUATION OF CYCLIC LIQUEFACTION SUSCEPTIBILITY	22
2.4.1 General	22
2.4.2 Evaluation of the Applied Cyclic Stress	22
2.4.3 Determining the Cyclic Resistance Ratio	23
2.4.3.1 General	23
2.4.3.2 Standard Penetration Testing	24
2.4.3.3 Cone Penetration Testing	27
2.4.3.4 Becker Penetration Testing	30
2.4.3.5 Shear Wave Velocity Measurements	30
2.4.3.6 Laboratory Testing	32
2.4.3.7 Estimation of the Residual or Liquefied Strength	33
3.0 FIELD PROGRAM DESCRIPTION	43
3.1 GENERAL	43
3.2 SITE SELECTION	43
3.3 PARAMETERS MEASURED	45
3.3.1 General	45
3.3.2 Material Type and Variability	46

TABLE OF CONTENTS

	Page
3.3.3	Density and Void Ratio..... 46
3.3.4	Pore Pressure 48
3.3.5	Stress..... 48
3.3.6	Stiffness 49
3.4	EQUIPMENT AND PROCEDURES USED 49
3.4.1	General 49
3.4.2	Cone Penetration Testing..... 49
3.4.3	Pore Pressure Transducers..... 50
3.4.4	Data Acquisition 50
3.4.5	Particle Velocity Monitoring 51
3.4.6	Nuclear Moisture and Density Gauge..... 51
3.4.7	Vibrating Wire Earth Pressure Cell and Piezometer 52
3.4.8	Loading Equipment 52
3.5	DESCRIPTION OF SITE ACTIVITIES 52
3.5.1	General 52
3.5.2	Site Reconnaissance and Characterization 53
3.5.2.1	General..... 53
3.5.2.2	Topography and Ground Water 53
3.5.2.3	Nuclear Density and Moisture Content Readings..... 54
3.5.3	Characterization of Main Test Site..... 54
3.5.3.1	General..... 54
3.5.3.2	Cone Penetration Testing 55
3.5.3.3	Test Pits..... 56
3.5.3.4	In-Situ Density Measurements 56
3.5.3.5	Frozen Sampling..... 57
3.5.4	Instrument Installation 58
3.5.4.1	General..... 58
3.5.4.2	Piezometers..... 59
3.5.4.3	Vibrating Wire Instruments..... 60
3.5.4.4	Seismograph..... 61
3.5.5	Light Equipment Loading..... 61
3.5.6	Heavy Equipment Loading 64
3.5.7	Post Loading Testing..... 65
3.5.7.1	General..... 65
3.5.7.2	Cone Penetration Testing 65
3.5.7.3	Frozen Sampling..... 66
3.5.7.4	Nuclear Gauge Testing 66
3.5.8	Quick Tests 66
3.5.8.1	General..... 66
3.5.8.2	Quick Tests 1 2 and 3 67
3.5.8.3	Quick Test 4 68
3.5.9	Trafficability Study..... 69

TABLE OF CONTENTS

	Page
4.0 LABORATORY PROGRAM.....	88
4.1 GENERAL.....	88
4.2 LABORATORY PROCEDURES	88
4.2.1 General.....	88
4.2.2 Moisture Content Determinations	88
4.2.3 Grain Size Analyses	89
4.2.4 Density and Void Ratio Measurements.....	89
4.3 LABORATORY TEST RESULTS	91
4.3.1 General.....	91
4.3.2 Moisture Contents	91
4.3.2.1 Disturbed Bulk Samples.....	91
4.3.2.2 Frozen Samples.....	92
4.3.3 Void Ratio and Density.....	93
4.3.4 Grain Size Distributions.....	94
5.0 DISCUSSION	99
5.1 GENERAL.....	99
5.2 INITIAL CONDITIONS OF DEPOSIT	99
5.2.1 General	99
5.2.2 Comparison of the Tailings at the Main Test Site with Other Syncrude Sites	100
5.2.3 In-situ State and Expected Behaviour.....	101
5.2.4 Penetration Resistance	103
5.3 RESPONSE OF DEPOSIT TO CYCLIC EQUIPMENT LOADING	105
5.3.1 General	105
5.3.2 Pore Pressure Response	106
5.3.3 Imposed Stresses.....	109
5.3.4 Causes of Softening	112
5.3.4.1 General.....	112
5.3.4.2 Pore Pressure Generation Mechanisms.....	113
5.3.4.3 Evaluation of the Softening Mechanisms	114
5.3.5 Factors Affecting Behaviour	115
5.3.5.1 General.....	115
5.3.5.2 Cyclic Load	115
5.3.5.3 Phreatic Surface Location and Moisture Content	115
5.3.5.4 Fines Content	117
5.3.5.5 Ageing	117
5.3.5.6 Density.....	118
5.4 COMPARISON OF FIELD OBSERVATIONS WITH LIQUEFACTION SUSCEPTIBILITY ANALYSES	118
5.4.1 General	118
5.4.2 Calculation of the Cyclic Stress Ratio and Penetration Resistance	119

TABLE OF CONTENTS

	Page
5.4.3 Comparison of Predicted Behaviour With Observations	121
5.4.4 Factors Influencing Predicted Behaviour	121
5.4.4.1 General.....	121
5.4.4.2 Attenuation Relationship	121
5.4.4.3 Effective Overburden Pressure	122
5.4.4.4 Shear Stiffness	122
5.4.4.5 Penetration Resistance.....	123
5.5 EXTRAPOLATION OF LIQUEFACTION PREDICTION TO OTHER SITES	123
6.0 CONCLUSIONS	140
7.0 REFERENCES	143

LIST OF FIGURES

Figure 1.1 Syncrude Location.....	5
Figure 1.2 Sand Boils Induced by Reclamation Activities	5
Figure 1.3 Results of Small Scale Cyclic Loading Tests, After McKenna, 2002	6
Figure 2.1 Steady State Line and Definition of Soil State Parameter	36
Figure 2.2 Typical Sand Responses to Undrained Monotonic Loading.....	36
Figure 2.3 Monotonic Undrained Stress Paths for Sands and Proposed Interpretation Lines	37
Figure 2.4 Variation in Sand Response to Monotonic Load with Changes in Stress and Void Ratio	37
Figure 2.5 Range of Responses for Sand Subjected to Cyclic Loading	38
Figure 2.6 SPT Blow Count Cyclic Resistance Ratio Relationship.....	39
Figure 2.7 SPT Vs. Cyclic Resistance Ratio with Limiting Strains.....	39
Figure 2.8 SPT Vs. Cyclic Resistance Ratio as Re-evaluated by Fear and McRoberts (1994).....	40
Figure 2.9 CPT Data Evaluation for Evaluation of Cyclic Resistance.....	41
Figure 2.10 CPT Cyclic Resistance Ratio Charts.....	42
Figure 2.11 Shear Wave Velocity – Cyclic Resistance Ratio Relationships	42
Figure 3.1 Location of Southwest Sand Storage Facility.....	70
Figure 3.2 2002 Plan of the Southwest Sand Storage Facility	71
Figure 3.3 Test Site Location.....	72
Figure 3.4 CPT set-up at Main Test Site.....	73
Figure 3.5 Push in Piezometers Used in Field Program.....	73
Figure 3.6 Vibrating Wire Load Cell and Piezometer	74
Figure 3.7 Cross Section of Tailings Beach Near Main Test Site.....	74
Figure 3.8 Southwest Sand Storage Area Near Main Test Site Prior to Testing	75
Figure 3.9 Density, Moisture Content and Saturation Variation Along Beach.....	75
Figure 3.10 Schematic of Sample and Testing Locations at the Main Test Site.....	76
Figure 3.11 CPT Results from the Edge of the Main Test Site.....	77
Figure 3.12 CPT Results from Middle of Main Site	78
Figure 3.13 Shear Window Adapted from Woods (1968) and Target Piezometer Locations.....	79
Figure 3.14 Instrument Locations	79
Figure 3.15 Density and Moisture Content Measurements During Predator Loading... 79	79
Figure 3.16 Pore Pressures and Particle Velocities Measured During Predator Loading80	80
Figure 3.17 Main Test Site After Predator Loading.....	81
Figure 3.18 Main Test Site After Dozer Loading	81
Figure 3.19 Pore Pressure and Particle Velocities Measured During Dozer Loading... 82	82
Figure 3.20 Pore Pressure and Load Cell Reading Between Tracks During Dozer Loading	83
Figure 3.21 Pore Pressure Dissipation at the Main Test Site After Dozer Loading.....	83
Figure 3.22 Location of Quick Test Sites	84
Figure 3.23 Pore Pressure and Particle Velocity to Light Loading at QT1.....	85
Figure 3.24 Pore Pressure and Particle Velocity to Light Loading at QT2.....	86
Figure 3.25 Trafficability Results	87
Figure 4.1 Typical Wax Coated Frozen Sample Prior to Submergence	95
Figure 4.2 Setup for Measurement of Submerged Weight of Wax Coated Sample.....	95

Figure 4.3 Frozen Samples Prior to Trimming	96
Figure 4.4 Grain Size Distribution of BAW Tailings Sand at Main Test Site	97
Figure 4.5 Grain Size Distributions Before and After Softening.....	98
Figure 5.1 Comparison of Grain Size Distribution at Test Sites With Results from CANLEX.....	127
Figure 5.2 Initial State Conditions at the Main Test Site.....	127
Figure 5.3 State Parameter Estimate from CPT Data at Main Test Site.....	128
Figure 5.4 Excess Pore Pressures Measured During Predator Loading	129
Figure 5.5 Excess Pore Pressures Measured During Dozer Loading	129
Figure 5.6 Variation in Maximum Excess Pore Pressure Within Tailings Deposit During Dozer Loading.....	130
Figure 5.7 Variation in Maximum Excess Pore Pressure Within Tailings Deposit During Predator Loading.....	130
Figure 5.8 Contours of Maximum Excess Pore Pressure Generated by Dozer Loading	131
Figure 5.9 Contours of Maximum Excess Pore Pressure Generated by Predator Loading	131
Figure 5.10 Typical Elastic Distribution of Load	132
Figure 5.11 Particle Motions Recorded During Dozer Loading	132
Figure 5.12 Schematic of Assumed Wave Propagation.....	133
Figure 5.13 Stress Path at PN 33 (Depth of 0.5m) During Predator Loading	133
Figure 5.14 Stress Path at PN 33, 32 and 31 (depths of 0.5, 0.9 and 1.8m) During Dozer Loading	134
Figure 5.15 Approximate Stress Path at PN32 During Dozer Loading with a Varying K_0	135
Figure 5.16 Stress Rotation During Dozer Loading.....	135
Figure 5.17 Cyclic Strain - Pore Pressure Generation Relationship Compared to Strains Measured During Field Test	136
Figure 5.18 Resultant Vector Particle Velocities Used in Calculation of Cyclic Stress Induced During Dozer Loading.....	136
Figure 5.19 Predicted Liquefaction Response of the BAW Tailings at the Main Test Site	137
Figure 5.20 Cyclic Stress Ratio Vs Depth for Dozer Loading.....	138
Figure 5.21 Maximum Peak Particle Velocity vs. Depth to Phreatic Surface to Minimize Softening.....	138
Figure 5.22 Tentative Particle Velocity, Equipment Mass and Energy Relationships.	139
Figure 5.23 Tentative Relationship Between Equipment Mass and Required Depth to Phreatic Surface.....	139

LIST OF TABLES

Table 3.1 Instrument Locations	59
Table 3.2 Trafficability Study Results.....	69
Table 4.1 Moisture Content Comparison Between Laboratory and Field Measurements Taken at the Same Location.....	91
Table 5.1 Variation in Phreatic Surface and Water Content at Trafficability Locations	116

LIST OF APPENDICES

APPENDIX A Summary of Field Program Data – Nuclear Gauge Measurements, Piezometer Readings and Calibration	155
APPENDIX B Laboratory Samples, Calculations and Results	166
APPENDIX C CPT Data Analyses, Estimation of State Parameter and Liquefaction Susceptibility	174
APPENDIX D Liquefaction Susceptibility Analyses and Extrapolation of Field Data	202

1.0 INTRODUCTION

1.1 Background

During reclamation activities at Syncrude Canada Limited, unexpected softening was observed when beach below and beach above water tailings were subjected to reclamation equipment traffic. In several instances work was halted as a result of this softening response and in at least one event, equipment sank several meters resulting in significant damage to the equipment. Furthermore, the movement of water to the surface associated with the softening can be detrimental to reclamation processes as it salinizes the area. The phenomenon therefore makes reclamation of beach below water (BBW) and beach above water (BAW) tailings difficult using conventional techniques and thus the following research was initiated to better understand the phenomenon. It should be noted however, that this softening phenomenon appeared to be an operational problem not a stability issue since it is a very local response.

Syncrude was the second company to carry out surface mining of the Athabasca Oil Sand Deposit near Fort McMurray, Alberta. It has been producing oil since 1978 and is currently one of the main oil producers in the region with an average daily production of 250,000 barrels of oil. The Athabasca Oil Sands Deposit contains an estimated total of 1.6 trillions barrels of oil and will likely be exploited by many companies for decades to come. Syncrude's lease covers approximately 100 km², located 50 km north of Fort McMurray as shown in Figure 1.1. Currently there are two main mining locations within the Syncrude lease areas, the original site and Aurora, located further to the northeast with mining activities on-going at each.

The oil sands are mined by truck and shovel or by dragline operations and then processed to extract the bitumen. The bitumen is upgraded and piped to refineries for further processing. The main by-products that remain once the oil is extracted are coke, sulphur, and tailings sand. The sulphur is formed into large blocks and stored on site for future use, sale or disposal. The coke is stored in various containment areas for future utilization. Approximately 1 m³ of coarse tailings and 0.25 m³ of mature fine tailings are produced per barrel of oil, corresponding to 114,062,500 m³ of tailings generated annually at Syncrude. Tailings are generally stored in surface structures, which have become some of the largest man-made structures on earth. In general, there are two components to the tailings: coarse tailings, which are used to construct the tailings embankments, and a finer fraction, which is deposited with process water behind the tailings embankments where it is left to consolidate, although research is ongoing to develop more efficient methods of storing fine tailings. These tailings storage facilities must be reclaimed either during or following mining operations to produce structures that are stable over very long time periods and appear somewhat natural to allow closure of the facilities. It is this latter component of the process that has prompted the following project.

At the main Syncrude site, there are two major tailings storage structures: Mildred Lake and the Southwest Sand Storage Facility. Mildred Lake covers a total area of approximately 49.4km² with a perimeter of approximately 27 km, and the Southwest Sand Storage Facility covers an area of approximately 34.5 km² with a perimeter of roughly 22.4 km. Tailings are piped from the processing plant to the tailings facilities and deposited. In general, tailings can be hydraulically deposited in one of two ways:

above or below water. Beach below water (BBW) tailings are deposited by overboarding of the tailings slurry into a pool. The particles then settle out under gravity generally forming a fairly loose deposit. Beach above water (BAW) tailings are deposited by spigoting of the tailings slurry onto existing tailings. As the slurry runs down the existing tailings beach, the coarse tailings and some trapped finer particles settle out, building up and extending the beach while the finer particles are carried with the water into the pond where they settle out more slowly. Tailings beaches developed in this way typically have slopes of 1 to 2 degrees and are typically relatively dense.

At Syncrude, reclamation activities have been carried out concurrently with mining activities. During these activities, it was observed that equipment traffic caused the tailings to soften significantly and large quantities of water were pumped to surface. In many events, as shown in Figure 1.2, sand boils were observed.

Sand boils are generally considered to be indicative of liquefaction type behaviour, a result of sand particles being carried to surface with the upward migration of water due to the excess pore pressures generated during liquefaction. Liquefaction is an expected response of loose BBW tailings subjected to cyclic loading, however liquefaction was not expected in the denser (typically 95% of the maximum Standard Proctor density) BAW deposits, which lead to subsequent testing and to the research described herein. In general, the affected areas appeared to be approximately five times the area of the equipment causing the softening. This response was observed only in BAW and BBW tailings where the phreatic surface was near the ground surface, not in any tailings compacted in cell construction (McKenna, personal communication, 2002). The softening phenomenon could also be induced in BAW tailings with a shallow phreatic surface by a person's self weight when stepping in place. When this was carried out, it was observed that the BAW tailings appeared to swell, suck in water and soften suggesting that the tailings may have been dilating as they softened, which is typically not associated with liquefaction.

1.2 Previous Work

In response to the observed behaviour of BAW tailings to cyclic loading, several tests have been carried out by Syncrude. A small-scale cyclic loading test was carried out as well as a large-scale trafficability study. During the former tests, a person stepped in place cyclically loading BAW tailings and the density and moisture content of the deposit were measured using a Troxler nuclear gauge at intervals throughout the test. Pore pressures were also monitored during and following the test. A significant decrease in dry density and increase in moisture content was noted throughout the test although the wet bulk density remained fairly constant as shown in Figure 1.3. Measured pore pressures indicated that excess pressure equivalent to the overburden pressure were generated and that pore pressures remained elevated for several hours following loading (McKenna, personal communication, 2002).

A trafficability study was also carried out by Syncrude in 2001 at the Southwest Sand Storage Facility (Syncrude, 2002). The tests were carried out in November when there was ice cover on the tailings. During the study, two types of equipment, a light all terrain vehicle, and a larger backhoe were driven down the tailings beach and locations of "good" and "poor" trafficability were noted. In-situ density and moisture contents were measured using a Troxler nuclear gauge and test pits were dug at intervals along the path. The study indicated that a significant portion of the Southwest Sand Storage

Facility, approximately 21 percent of the total area and 55 percent of the area to be reclaimed, was susceptible to the softening phenomenon when loaded by existing light reclamation equipment. Furthermore, it appeared that only 1.4 percent of the total area and 3.7 percent of total area to be reclaimed was accessible to large equipment because of the softening response of the BAW tailings.

Similar observations of softening behaviour were also made during the Canadian Liquefaction Experiment (CANLEX). It was observed that as drilling or other in-situ testing progressed, the tailings began to soften such that people walking on the surface of the deposit could cause large undulations of the ground surface and water was observed on surface. Plate load testing determined that the tailings retained significant static strength even in their softened state (Robertson, personal communication, 2001).

The observed softening phenomenon of BAW tailings could therefore represent a significant problem to reclamation activities at Syncrude if reclamation is to be carried out using conventional methods. Furthermore, as the BAW tailings at Syncrude are similar to BAW tailings at other oil sands developments, it is likely that all oil sand tailings could exhibit the observed behaviour.

1.3 Objectives

The general observations of increased pore pressure, softening and sand boils tended to indicate that liquefaction was occurring in BAW tailings subjected to equipment loading, however, the observed swelling appeared to indicate a more dilative response than is typically associated with liquefaction behaviour. The apparent retention of static strength was also somewhat unexpected for liquefaction type behaviour. The proposed hypothesis was therefore that cyclic liquefaction or cyclic mobility was responsible for the softening of dense BAW deposits when subjected to cyclic loading, rather than flow liquefaction. It was proposed that because of the low confining pressures in the upper portions of the deposit, the cyclic stresses applied by the equipment, due primarily to the tracks and motor vibrations, were sufficient to cause increases in pore pressure equal to the overburden pressure resulting in essentially zero effective stress and significant softening.

The objective of the research was to carry out representative field tests and sufficient laboratory testing to confirm the proposed hypothesis or to identify an alternate explanation for the observed behaviour. An understanding of the mechanisms occurring to cause the softening and some the factors that affected the behaviour was to be developed. Once explained, it was hoped that some type of guidance with respect to softening as a function of in-situ conditions and equipment type could be developed to aid in site activities.

In order to carry out the objectives outlined, a field program was developed to allow monitoring of the softening behaviour under realistic loading conditions. Prior to any loading, the test site was to be characterized sufficiently to identify its initial state and representative samples of the initial conditions were to be gathered for subsequent laboratory testing. It was also intended to incorporate the extensive amount of published data available regarding Syncrude tailings into the study. Field tests recreating the softening of dense, BAW tailings deposits using equipment generally used in daily operations were to be carried out with sufficient instrumentation and monitoring to identify and explain the observed behaviour. Following softening, the site was to be

characterized again and more samples gathered to enable comparison of the conditions before and after softening. Several test sites were to be created to study the effects of different equipment, and different tailings properties such as density and fines content. It was also proposed to carry out a small trafficability study similar to that previously carried out by Syncrude and described previously to allow comparison between the two studies.

The data gathered during the field tests, laboratory testing and from a review of published data was analyzed to provide an understanding of the mechanisms occurring. Conventional methods of liquefaction analyses were applied to the gathered data to examine their applicability to the problem under consideration and possibly allow extrapolation of the test data to other sites and conditions.

This report begins with a review of the literature regarding the liquefaction phenomenon in general. The literature review was carried out to provide an understanding of the mechanisms expected to control the behaviour and to aid in planning the field test. The field program is then described in detail and the results of the field tests are presented. The laboratory testing carried out is then presented. A discussion of the field and laboratory data follows focusing on the state of the deposit prior to loading and the observed stress response followed by an explanation for the observed behaviour. The field data is then analyzed using conventional liquefaction analyses methods and the results are tentatively extrapolated to other conditions.

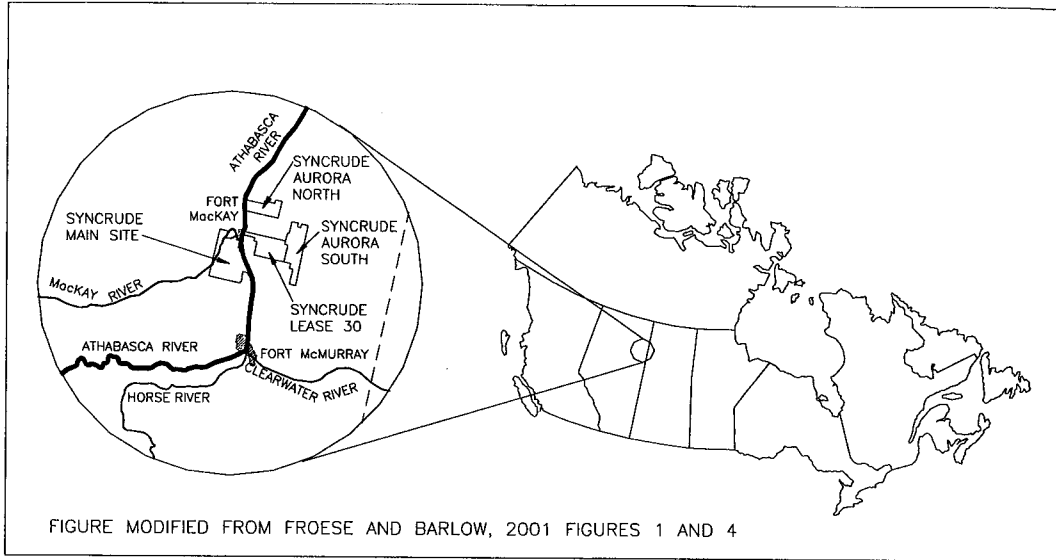


Figure 1.1 Syncrude Location

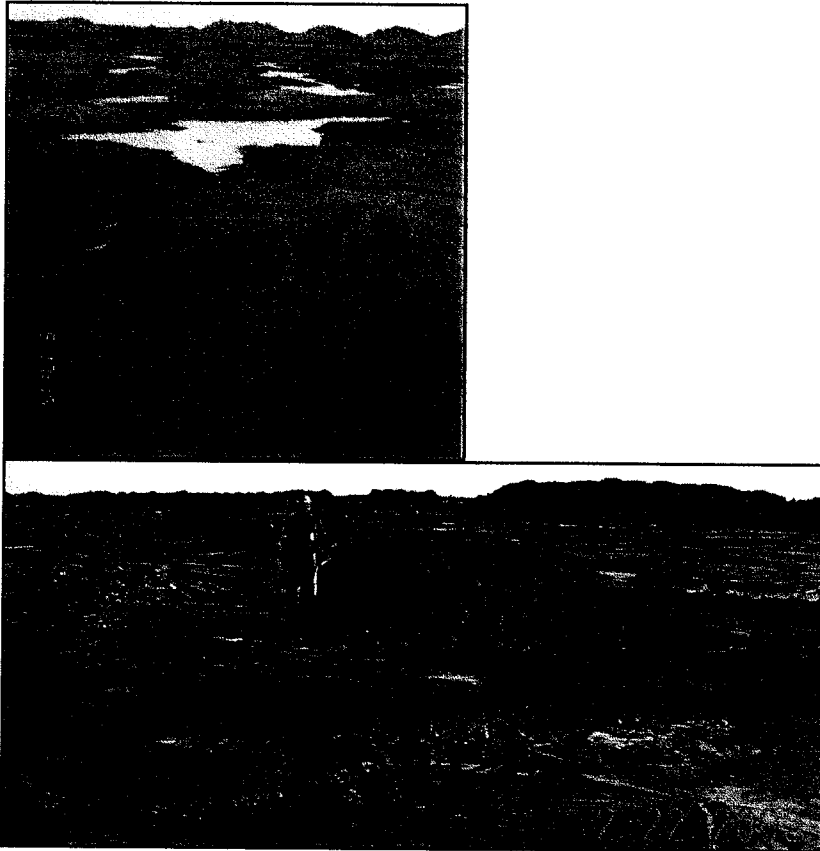


Figure 1.2 Sand Boils Induced By Reclamation Activities

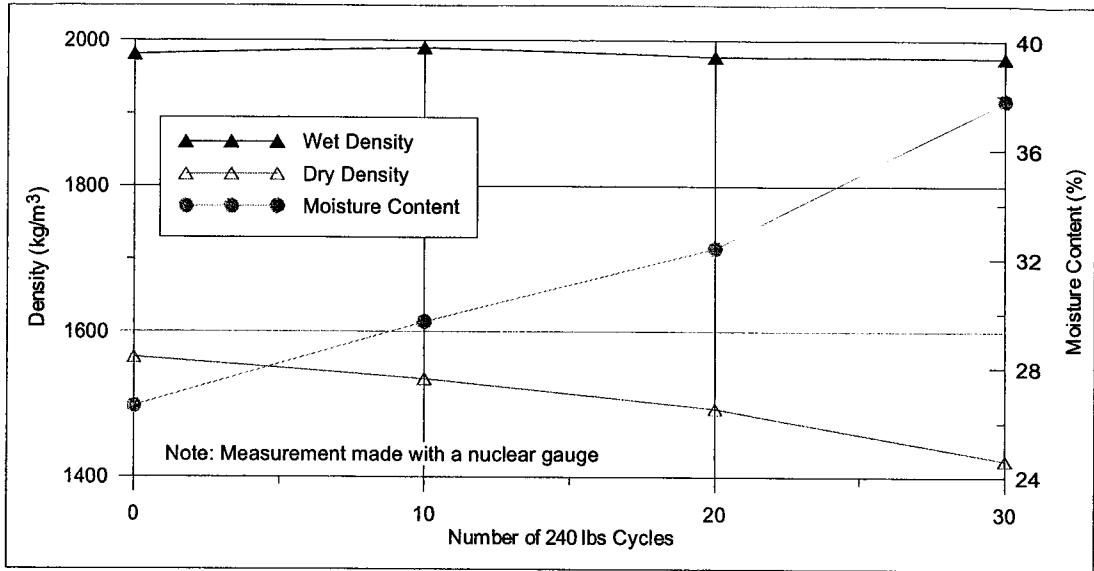


Figure 1.3 Results of Small Scale Cyclic Loading Tests, after McKenna, 2002

2.0 REVIEW OF LIQUEFACTION LITERATURE

2.1 General

This section presents a summary and discussion of the current literature regarding liquefaction. It was found that there is a large volume of work published regarding liquefaction related issues and there appears to be some debate in the literature regarding issues ranging from the appropriate definition of liquefaction to the applicability of steady state soil mechanics. The information contained in the following discussion is by no means exhaustive but an attempt has been made to include a wide cross section of available knowledge. In general however, the topic of static liquefaction was not included in the literature review presented, as the phenomenon under investigation is clearly a result of cyclic loading.

The following review begins by summarizing some of the different definitions of liquefaction. The response of sands to monotonic loading is then presented and linked to the various liquefaction definitions. A brief review of steady state soil mechanics as it pertains to soil liquefaction is then presented. The factors controlling the liquefaction response of sands to cyclic loading are reviewed and discussed followed by a review of the many methods for evaluating the susceptibility of deposits to liquefaction under cyclic loading. Finally a brief summary regarding the determination of the strength of soils during liquefaction is presented.

2.2 Definitions

Throughout the geotechnical literature the term liquefaction has been used to describe a variety of soil behaviour. Not all of the definitions will be presented here but some of the more commonly encountered definitions will be summarized.

One of the first uses of the term liquefaction was found in Hazen's 1920 paper regarding hydraulic fill (Hazen, 1920). He used the term "liquefied" to express a soil condition "practically equivalent to quicksand". He suggested that this condition was caused when the pore pressure rises to the point where it carries the entire load at which point the soil "is almost a liquid, and is capable of moving or flowing or of transmitting pressure in the same measure as a liquid". Following this use, the term liquefaction was used until 1966 only to describe the response of saturated loose sand to strains or shocks resulting in substantial loss of strength with the potential for flow slides (Casagrande, 1979). For example, Terzaghi and Peck (1996) used the term "spontaneous liquefaction" to describe the sudden change of loose sand deposits into a viscous fluid-like flow following a small disturbance.

In 1966 however, Seed and Lee (1966) presented a series of results from cyclic triaxial tests in which a medium dense sand was cyclically loaded through a state of hydrostatic stress generating excess pore pressures equivalent to the confining stress and significant straining. It appeared that they considered the conditions of zero effective stress as liquefaction. At that time, Casagrande had argued that the behaviour observed by Seed and Lee was not true liquefaction and was caused mainly by the redistribution of water content. He further argued that dilative sands, such as the medium dense sands tested by Seed and Lee, subjected to cyclic loading from a cyclic triaxial test were subjected to conditions where peak pressure becomes equal to the confining pressure only momentarily during each cycle and was not associated with any significant loss in

strength and should not be termed liquefaction (Casagrande, 1979). In 1969, Casagrande and several other colleagues had attempted to find another term for the laboratory response and agreed on the term "cyclic mobility". There was not widespread acceptance of their term however so in 1976, Casagrande "reluctantly" used the term "cyclic liquefaction" for the response of a dilative sand to cyclic loading in a triaxial test. He reserved the term "actual liquefaction" for the response of loose saturated sands that experienced strain softening.

Many researchers appear to have followed Casagrande (1979) in their definition of liquefaction and argue that the collapse of loose saturated sands is in fact the only true form of liquefaction (e.g. Castro and Poulos, 1977; Fear and McRoberts, 1995; Sladen et al., 1985; McRoberts and Sladen, 1992; Japanese Geotechnical Society, 1998). This philosophy is embraced in the following definition of liquefaction proposed by Castro et al. (1982): "Liquefaction is a phenomenon wherein a mass of soil loses a large percentage of its shear resistance, when subjected to undrained monotonic, cyclic or shock loading, and flows in a manner resembling a liquid until the shear stresses acting on the mass are as low as the reduced shear stresses."

Sladen et al. (1985) modified this definition slightly by omitting the qualifier "undrained" with respect to the term loading, as they argued that it is possible for the response to be drained right up until the moment of failure.

With researchers who follow this type of definition, the term cyclic mobility has remained in the literature to describe both field and laboratory responses of a dilative materials. Castro and Poulos (1977) define cyclic mobility as the "progressive softening of a saturated sand when subjected to cyclic loading at constant void ratio". They note that softening is accompanied by high pore pressures, increasing cyclic deformation and in some cases by permanent deformation, but, contrary to liquefaction, does not lead to a significant loss in strength or to continuous deformation.

Seed in his state of the art paper regarding cyclic liquefaction in 1979 in fact used definitions of liquefaction and cyclic mobility very similar to those just presented. It does not appear however, that these definitions were subsequently adopted in future work by Seed and his co-workers (e.g. Martin et al., 1975; Seed et al., 1985; Seed 1987.).

Kramer (1996) also differentiates between flow liquefaction and cyclic mobility. He defines flow liquefaction as the phenomenon in which the static equilibrium is destroyed by static or dynamic loads in a soil deposit with a low residual strength. He emphasizes that while the cyclic stresses may bring the soil into an unstable state triggering flow, it is the static shear stress that causes deformation. Cyclic mobility is defined by Kramer as lateral spreading, which can result in very large permanent displacements, driven by both static and cyclic stresses. In these cases the static stresses are less than the liquefied strength of the soil. Kramer (1996) defines level-ground liquefaction as a particular type of cyclic mobility in which significant settlement, flooding and sand boils can occur due to the upward flow of water due to the dissipation of seismically induced pore pressures from below.

Many other researchers use the term liquefaction in a manner similar to that of Seed and Lee (1966) related mainly to the development of excess pore pressures. The National Research Council (1985) presented a summary of the state of the art with respect to designing against earthquake induced liquefaction and defined liquefaction as

encompassing all phenomena involving excessive deformation of saturated cohesionless soils. More recently, the National Center for Earthquake Engineering Research held a workshop concerning the evaluation of liquefaction resistance and liquefaction was defined as “the transformation of a granular material from a solid to a liquefied state as a consequence of increased pore pressure and reduced effective stress” after Marcuson (1978) (Youd and Idriss, 2001). They state that as liquefaction occurs the soil softens and in loose deposits, a loss in strength occurs concurrently with softening and can lead to large shear deformations and flow failure.

Laboratory testing has also lead to another definition of liquefaction. Typically liquefaction is considered to have occurred in a cyclic laboratory tests at specified levels of strain. For a triaxial test this limit is typically set at a strain level of five percent double axial strain while for a simple shear test the limit is often set at three to four percent double amplitude strain (Ishihara, 1993). Double amplitude stain is the total amount of strain experienced by a soil subjected to half a cycle of loading. It is worth noting that for loose samples, these strains are often roughly coincident with the occurrence of zero effective stress. In dense samples however, this is rarely the case (Robertson and Wride, 1995).

Other definitions of liquefaction have arisen from the back analyses of case histories. In these cases, liquefaction has been defined based on ground response and the appearance of surface phenomenon (e.g. Seed and Idriss, 1971; Seed et al., 1985; Andrus and Stokoe, 2000; Stark and Olson 2002). Liquefaction in this sense tends to encompass a wide range of behaviours. For example, Seed and Idriss (1971) state that “liquefaction as used herein describes a phenomenon in which cohesionless soil loses strength during an earthquake and acquires a degree of mobility sufficient to permit movements ranging from several feet to several thousand feet”. Seed et al. (1985) provide further details regarding field phenomena that indicate liquefaction. They consider that “evidence of ‘liquefaction’ in the field is provided by such phenomena as sand boils at the ground surface, ground cracking with some sand boiling, small lateral movements in the ground etc., as well as, in some cases, by major settlements of buildings, bearing capacity failures, major translation of foundation or uplifting of buried pipelines and tanks.” There are several authors (e.g. Fear and McRoberts, 1995) who have questioned whether all of these observations are truly indicative of liquefaction, and it would appear that several of the identifiers listed fall into Kramer’s definition of cyclic mobility rather than flow liquefaction. Seed et al. (1985) do qualify their definition of liquefaction somewhat by stating that the condition of liquefaction involves different behaviours in soils of different penetration resistances.

More recently, liquefaction type responses were divided into three main categories for use in the Canadian Liquefaction Experiment (CANLEX). These three categories were defined in Robertson (1994) and are as follows:

➤ Flow Liquefaction:

- Requires a strain softening response in undrained loading resulting in constant shear stress and effective stress (i.e. ultimate steady state or critical state).
- Requires that in-situ shear stress is greater than undrained residual or steady state shear strength.
- Can be triggered by either monotonic or cyclic loading.

- For failure of a soil structure to occur such as a dam or a slope, a sufficient volume of material must show strain softening response. The resulting failure can be a slide or a flow depending on the material characteristics and slope geometry. The resulting movements are due to internal causes and can occur after the trigger mechanism.
- Can occur in saturated, very loose granular deposits, very sensitive clays and loose loess deposits.
- Cyclic Liquefaction:
 - Requires undrained cyclic loading where shear stress reversal or zero shear stress can develop (i.e. where in-situ gravitational shear stress is low compared to cyclic shear stress).
 - Requires sufficient undrained cyclic loading to allow effective confining stress to essentially reach zero.
 - At point of zero effective confining stress no shear stress can exist. When shear stress is applied pore pressure drops and a very soft initial stress strain response can develop resulting in large deformations. Soil will strain harden with increasing shear strain.
 - Deformations during cyclic loading when effective stress is approximately zero can be large, but deformations generally stabilize when cyclic loading stops. The resulting movements are due to external causes and only occur during the cyclic loading. Subsequent movements can occur due to pore pressure redistribution. However, this will depend on ground conditions and soil stratigraphy.
 - Can occur in almost all sands provided size and duration of cyclic loading is sufficiently large. For dense sands the size and duration of cyclic loading will be large and hence, the condition of zero effective confining stress may not always be reached.
 - Clays can experience cyclic liquefaction but deformations at zero effective stress are generally small due to the possible cohesive strength at zero effective stress and deformations are often controlled by rate effects (creep).
- Cyclic Mobility:
 - Requires undrained cyclic loading where shear stress is always greater than zero, i.e. no shear stress reversal develops.
 - Zero effective stress does not develop.
 - Deformations during cyclic loading will essentially stabilize. The resulting movements are due to external causes and only occur during cyclic loading.
 - Can occur in almost any sand provided size and duration of cyclic loading is sufficiently large and no stress reversal occurs. Can also occur in dense sand with shear stress reversal provided cyclic loading is not sufficient to cause zero effective stress to develop.
 - Clay can experience cyclic mobility but deformations are often controlled by creep effects.

Robertson and Fear (1995) add slightly to the CANLEX definitions presented above by indicating that for design, cyclic liquefaction often implies the point at which the soil experiences large uncontrollable deformations. Based on these definitions, any soil can experience cyclic liquefaction provided the shear stresses applied are sufficiently large to cause a condition of zero effective stress to be achieved. Flow liquefaction appears to correspond to the case of "actual liquefaction" proposed by Casagrande whereas the condition described as liquefaction by Seed and Lee characterized by zero effective

stress appears to be encompassed by flow and cyclic liquefaction in the CANLEX definitions. Cyclic mobility as defined by CANLEX is slightly different than the definitions given by Kramer (1996) and Castro et al. (1982), in that it encompasses a narrower range of soil response.

The preceding discussion presents only a few definitions but clearly illustrates the importance of identifying what is being implied by the term liquefaction when reading the geotechnical literature. For the purpose of this study, the definitions proposed by CANLEX will generally be used.

2.3 Mechanisms

2.3.1 General

Flow liquefaction, cyclic liquefaction and cyclic mobility, as is evident from the definitions presented above, are associated with the generation of excess pore pressures typically caused by rapid changes in loading conditions and an undrained soil response. Therefore, because of their hydraulic conductivities and frictional strengths, sands and silty sands are the materials typically associated with liquefaction. Generally, gravelly soils have a high hydraulic conductivity that limits the build up of excess pore pressures generated during loading and thus gravelly soils typically do not exhibit undrained behaviour. Under certain conditions of impeded drainage or in cases where a fine-grained matrix exists, undrained behaviour can be triggered in gravelly materials and liquefaction of these materials can occur (Andrus et al., 1991; Valera et al., 1994). Clays are generally considered to be non-liquefiable because of their cohesion. Cohesive soils have a different component of shear strength than do cohesionless soils and therefore increased pore pressures do not affect cohesive soils in the same manner as cohesionless soils (Ishihara, 1993). Cohesive soils can exhibit significant losses in strength (e.g. Leda and Norwegian quick clays), however their response in general is controlled by different mechanisms (e.g. salt leaching).

The mechanisms causing liquefaction in cohesionless soils will be discussed in this section. Although there is still debate in the literature regarding the applicability of steady or critical state soil mechanics to liquefaction, the theory is widespread in the literature and a brief summary will follow. The response of soils to monotonic loading has greatly influenced the understanding of the liquefaction behaviour of soils and therefore this will also be briefly discussed. Finally an overview of responses to cyclic loading will be presented.

2.3.2 The State of Sands

Steady or critical state soil mechanics is based on the general premise that a soil will deform under shear until it reaches a critical or steady state that is dependant only on the original void ratio and stress state of the soil. Steady state is defined by Poulos (1981) as the state of a soil that is deforming at constant volume, constant normal effective stress, constant shear stress and constant velocity. It is attained when a flow structure originally proposed by Casagrande (1979) is formed within the soil such that the original structure is completely destroyed and any particle breakage and particle re-orientation has occurred. Critical state is defined slightly differently than steady state as the state of a soil that is deforming at constant volume under constant normal effective stress and constant shear stress (Roscoe et al., 1958). Been et al. (1991) have

suggested that for sands critical and steady state are essentially the same and Sladen et al. (1985) report that it has been shown by Castro et al. (1982) and Lupini et al. (1981) that for sands there is no practical difference between steady and critical states as just defined. As such the terms critical state and steady state can be used interchangeably when dealing with sands.

In void ratio – log effective stress space, the steady state line for sands has been found to be reasonably well represented by a bilinear relationship (Been et al., 1991; Robertson et al., 2000) steepening at high effective mean stresses as shown schematically in Figure 2.1. It has been suggested that the steepening of the curve may be attributed to grain crushing (Been et al. 1991) so that in effect the curve crosses a variety of unique critical state lines for materials of different gradation as the material becomes finer due to grain crushing. The steepening may also be an artifact of the semi-log plot (Been, 1999). There is some debate in the literature with respect to the uniqueness of the steady state line. It has been suggested that the location of the steady state line, particularly in void ratio - mean effective stress space can depend on initial soil fabric, loading path, initial density and strain rate (e.g. Vaid and Chern, 1985; Alarcon-Guzman, 1988; Vaid et al., 1990; Konrad, 1993; Vaid and Sivathayalan, 2000; Sivathayalan and Vaid, 2002). All of these researchers however appear to use the minimum strength to define the steady state line rather than the steady state strength, which is likely the main cause of the debate. Vaid and Sivathayalan (2000) indicate that their reasoning in combining the minimum undrained strength with steady state is that the minimum strength is the strength of practical interest. While this is likely true, it does not indicate that the steady state line is not unique. Further complications arise when assessing steady state conditions from samples that dilate significantly, from very dense samples or from samples tested in extension. In very dense samples or samples that dilate significantly, it has been shown that the final phase of shearing is often localized along bands creating void ratio and water content redistribution within the sample. Therefore, the measured average void ratio of the sample at very large strain would not be representative of the void ratio on the failure plane (McRoberts and Sladen, 1992; Desrue et al., 1996; Ayouban and Robertson, 1998). McRoberts and Sladen (1992) also report work by Thurairajah (1961), which indicates that at strains of greater than 2 to 3 percent very significant non-uniformities develop in extension tests which make average void ratio measurements erroneous. Work carried out by Castro et al. (1977), Castro and Poulos (1982), Sladen et al. (1985), Been et al. (1991), McRoberts and Sladen (1992) and Ishihara (1993) support the suggestion that steady state as defined previously is unique and independent of initial density, strain rate, sample preparation, and stress path.

In deviator - mean effective stress space steady state conditions form a straight line with angle "M" representing a condition of Mohr Coulomb failure (Sladen et al., 1985) as indicated in Figure 2.2. This line is also nearly coincident with the locus of minimum undrained strengths (Vaid and Chern, 1985; Alarcon-Guzman, 1988; Vaid and Sivathayalan, 2000). Typically M is considered to be slightly different in extension than in compression however (e.g. Vaid and Sivathayalan, 2000).

Unlike classical critical state soil mechanics (e.g. Cam Clay Model) in which a soil (generally a clay) is associated with two unique lines, the normal consolidation line and the critical state line, that control or define its behaviour, the critical state framework for sands usually refers only to the critical state line. Sands are typically considered to have an infinite number of normal consolidation lines depending on how they were deposited

(Roscoe et al., 1958; Been et al., 1991; Jefferies, 1999) and thus the normal consolidation line cannot be used as a unique reference point. Some researchers (e.g. Coop and Atkinson, 1993; Ishihara, 1993; Pestana and Whittle 1995) have suggested the use of an intrinsic normal consolidation line as a second reference line for sands equal to the loosest state at which a sample can exist. The concept is similar to the intrinsic consolidation line for clays suggested by Burland (1990) but does not seem to have gained widespread use.

Unless a soil is at critical state, the void ratio and effective stress of a sand is not a unique relationship and unlike clays cannot be determined based on stress history. In order to correctly determine the in-situ state of a sand, both the stress state and the void ratio must therefore be known. The use of a state parameter describing the physical conditions of a deposit to define the in-situ conditions was therefore proposed by Been and Jefferies (1985). The state parameter is the difference between the in-situ void ratio and the void ratio at critical or steady state for constant mean effective stress as shown in Figure 2.1. The state parameter can be estimated from in-situ tests based on empirical correlations. This is not discussed in the current review but is presented briefly in Section 5.2.3.

Criticism in the literature regarding the use of steady state methods for liquefaction assessments appears to be due to questions regarding the uniqueness of the steady state line and the appropriateness of the steady state strength for use in engineering practice (McRoberts and Sladen, 1992). Debate regarding the uniqueness of the steady state line has been discussed above and although it would appear more work needs to be carried out, it seems as if the steady state line is unique. It is true however that the steady state strength is not always appropriate for use in design. An understanding of the complete soil response, and not simply steady state may therefore be required in certain cases. The response of sands to undrained monotonic loading will be discussed in the following section followed by a discussion of the response under steady state loading.

2.3.3 Response to Undrained Monotonic Loading

In general, there are three main categories into which the response of a sand to undrained monotonic loading can be classified. These responses are shown in Figure 2.2 and can be described as strain softening, limited strain softening followed by strain hardening and strain hardening. Associated with each of these responses is a different potential for liquefaction. A strain softening response can result in flow liquefaction, a limited strain softening response can cause limited liquefaction with the severity and type of liquefaction dependant upon the magnitude and duration of strength reduction prior to strain hardening, and finally strain hardening responses would typically be associated with cyclic mobility or cyclic liquefaction (e.g. Vaid and Chern, 1985; Alarcon-Guzman et al., 1988; Ishihara, 1993; Vaid, 1994; Robertson and Fear, 1995).

Various researchers have proposed explanations for the observed responses of sand to undrained loading and the following discussion is based on an integration of a variety of concepts. Examining the stress paths obtained from many laboratory tests on sands several relationships have been proposed to interpret the behaviour of sands. Ishihara et al. (1975) defined a phase transformation line, a constant deviator to mean effective stress ratio (q/p') at which subsequent unloading causes significant pore pressure increase even in dense deposits which would normally continue to dilate to steady state

under continued monotonic loading. The phase transformation line also corresponds to the state of minimum strength or transition from contractive to dilative behaviour during monotonic loading. Vaid and Chern (1985) noted that the initial peak stresses attained by limited strain softening sands also occurred at a constant q/p' ratio and termed that line, extending back to the origin, the critical stress ratio. A third line in q - p space, the collapse surface, was proposed by Sladen et al. (1985). It is defined by the locus of peak strengths attained by very loose, contractive sands and terminates at critical or steady state. Ishihara (1993) also confirmed the existence of a collapse surface. McRoberts and Sladen (1992) have suggested that the collapse surface and critical stress ratio lines may merge but this has not been verified. These lines are shown in Figure 2.3 with a typical steady state line and several typical undrained loading paths. With the exception of the steady state line, the location of these lines are expected to vary with soil fabric, loading direction, etc. particularly in void ratio – effective stress space (Vaid and Chern, 1985; McRoberts and Sladen, 1992; Yoshimine et al., 1999) and may also be non-unique in stress space. Sivathayalan and Vaid (2002) have presented data to indicate that the phase transformation line is unique in stress space with respect to stress path and anisotropy but that the critical stress ratio line is not.

As pointed out by Been and Jefferies (1985) the initial portion of the stress paths are similar regardless of the initial condition of the sand, as can be seen from Figure 2.4. Once one of the lines or surfaces is reached however, the behaviour of the different sands becomes remarkably different. If the collapse surface is reached, the sand is expected to strain soften from that point to steady state. Since Figure 2.3 represents a constant void ratio plane, this condition can be achieved only if the initial confining stresses are larger than those at steady state. If the critical stress ratio is reached during loading, the sand will soften from that point until the stress path crosses the phase transformation line. The phase transformation point corresponds to the minimum undrained strength of the material in these cases and is often referred to as the quasi steady state (e.g. Vaid and Chern, 1985; Robertson and Fear, 1995; Yoshimine et al., 1999; Sivathayalan and Vaid, 2002). From this point, further straining under increasing load should result in strain hardening to steady state conditions. For a constant void ratio this behaviour would be expected to occur for initial states with stresses similar to those at critical state. At lower initial stress levels, located significantly to the left of steady state in Figure 2.3, the phase transformation line and critical stress ratio line are nearly coincident and no significant peak strength is expected, the sand should essentially strain harden to steady state. It should be noted that as void ratio increases, the steady state point in q - p space would move left and the boundaries between the various types of behaviour would likewise increase in stress.

In general, it is considered that very loose soils are associated with strain softening behaviour while very dense sands tend to response in a dilative manner. Sands in between these two states generally exhibit limited strain softening. However, as discussed, changes in confining stress can cause dramatic changes in the response and therefore loose and dense is typically defined in relation to steady state. These variations in behaviour are clearly exhibited in test results reported by Ishihara (1993) and illustrated in Figure 2.4.

It is obvious how these different responses could fundamentally affect the liquefaction behaviour of a sand deposit. Clearly a sand that undergoes substantial loss in strength during undrained shear would have a much more severe liquefaction response than a sand that gains strength during undrained shear. It is noted however that even the

dense strain hardening soils do exhibit initial contractive behaviour which along with other mechanisms discussed in the following section can cause build up of pore pressures when cyclically loaded (McRoberts and Sladen, 1992). An initial dividing line has been proposed by Ishihara (1993), which is a curve drawn in void ratio – mean effective stress space separating sands which exhibit a minimum strength during shear from those that only undergo phase transformation and strain harden completely to steady state. Other researchers have also adopted its use (Yoshimine et al., 1999) and it appears that the initial dividing line lies below the steady state line at low stresses passing above the steady state line as the steady state line steepens at higher stresses. The initial dividing line does appear to be affected by soil fabric, load path and anisotropy (Yoshimine et al., 1999). In addition to the soil response however, the in-situ static shear stresses also affect the possible severity of liquefaction. If the static shear stresses are less than the steady state strength for strain softening sands or less than the minimum strength for limited strain softening sands, then liquefaction can only be driven by imposed cyclic stresses. The effect of in-situ shear stresses will be discussed in greater detail in the following section.

2.3.4 Response to Undrained Cyclic Loading

Several researchers (e.g. Ishihara et al., 1975; Ishihara, 1985; Alarcon-Guzman, 1988; Robertson and Fear, 1995) explain the behaviour of sands under undrained cyclic loading based on the concepts previously discussed for the response of sands to undrained monotonic loading. As noted by Castro (1975) however, steady state concepts are not strictly applicable during cyclic loading as the loading conditions are not constant therefore not steady state (constant deformation at constant volume under constant stresses) is not possible. Nonetheless, the framework as illustrated in Figure 2.3 is useful and the responses can be explained as follows. If a sand is initially loose and is in an in-situ state with static shear stresses greater than those supported at steady state, flow liquefaction is possible under cyclic loading. As cyclic loading commences, pore pressures increase, causing the effective stress path to move to the left as shown in Figure 2.5a. When the cyclic load causes the stress state to reach the collapse surface, pore pressure builds up rapidly and the material fails or flows (e.g. Alarcon-Guzman, 1988; McRoberts and Sladen, 1992; Davies et al., 2001). A similar process would occur if a limited strain softening material with in-situ shear stresses greater than the minimum or quasi steady state strength were subjected to cyclic stresses with the collapse surface replaced by the critical stress ratio line as shown in Figure 2.5c. If the in-situ shear stresses were less than the minimum strength of the material but the applied cyclic stresses were greater than the minimum strength, limited liquefaction or cyclic liquefaction could occur as shown in Figure 2.5 b and d. The process is essentially the same as that just described but the deformations should halt once the driving cyclic stresses are removed.

Sands that exhibit no minimum strength during shear or soils that have in-situ shear stresses lower than their minimum strength behave somewhat differently. As illustrated in Figure 2.5 e and f, the stress path moves left with cyclic loading as pore pressures increase until the phase transformation line is reached at which point there is a drastic change in behaviour. Ishihara et al. (1975) indicate that at this point although under monotonic loading dilation and strain hardening would occur, when unloaded from this point or any stress state at greater stress ratio, significant pore pressure increases occur. Alarcon-Guzman et al. (1988) also indicate a change of mechanism at the location of phase transformation with the onset of dilation causing particle arrangement

possibly including the formation of meta-stable holes. It appears that from the point when the phase transformation line is intersected, the phase transformation line is nearly followed along the loading paths and paralleled on the unloading paths. If conditions of zero effective stress occur, the behaviour is termed cyclic liquefaction (see Figure 2.5f). Cyclic mobility is associated with softening and elevated pore pressures without shear stress reversal or conditions of zero effective stress (see Figure 2.5e). Removal of the load in cases of both cyclic liquefaction and cyclic mobility should cause deformations to halt since the static shear stresses are less than the minimum strength of the material and any further straining would result in dilation.

The descriptions of the responses above do not indicate how the increases in pore pressure are generated, particularly when considering deposits that are initially dense of critical state. The initial pore pressure generation has been attributed to various mechanisms by different researchers. It has been suggested that the initial contractive behaviour of almost all saturated sands when load is applied is responsible for the initial increase in pore pressure (Sladen and McRoberts, 1992; Robertson and Fear, 1995). Nova and Hueckel (1981) suggest that the unloading and reloading of sands at stresses less than those previously attained (i.e. the stress paths followed during the majority of cyclic loading) occurs within a yield locus and is controlled by the phenomena of hysteresis and cyclic compaction. They propose that a piecewise path independent constitutive law that indicates that all volumetric strains along these portions of the stress path are compressive can define the phenomena. Others attribute the increase in pore pressure to the tendency for cohesionless soils to densify under vibratory loading, similar to the cyclic compaction suggested by Nova and Hueckel (1981), which in an undrained condition would cause increased pore pressure (Castro, 1975; Alarcon-Guzman et al., 1988). Martin et al. (1975) proposed a model for the prediction of pore pressure increase due to cyclic loading based on a similar mechanism. They suggested that upon application of a cyclic load, cohesionless soils tend to decrease in volume and in an undrained condition this causes an increase in pore pressure, the magnitude of which is dependant on the rebound characteristics of the sand skeleton. Casagrande (1940) suggested that, in his opinion, vibratory loading could only cause densification if it was applied over a relatively long duration, longer than the duration of earthquakes. Casagrande (1979) suggested that the only mechanism for increased pore pressure of dense deposits in the field was slight rearrangement of the sand grains caused by breakage of the edges and corners of the sand particles. Clearly there is work to be done with regards to this aspect of cyclic mobility but regardless of the cause, it does appear that pore pressures can be generated in essentially any sand deposit subjected to undrained cyclic loading of sufficient magnitude and duration.

2.3.5 Factors Controlling Cyclic Liquefaction Behaviour

2.3.5.1 General

There are a multitude of factors that affect the liquefaction susceptibility of a deposit including properties of the deposit such as void ratio, density, in-situ stresses, grain characteristics, stress history, geologic age, location of the phreatic surface and degree of saturation. When assessing the effect of the various factors on the liquefaction potential of a sand it is important to identify what aspect of the soil response is being used to evaluate the effects. If the onset of flow liquefaction is being used to evaluate the effect of variations in sand properties very different conclusions will be reached with regards to those effects than if the stress needed to cause the generation of excess pore

pressures equal to the overburden or cyclic resistance (the ratio of the cyclic shear stress and the initial effective vertical pressure) is used as a basis for comparison. Factors related to the applied load such as duration and magnitude of cyclic load and the effects of local topography on the attenuation or amplification of earthquake induced stresses also affect the response of a soil deposit, as will be discussed in the following section.

2.3.5.2 Density and Void Ratio

Researchers appear to agree that a major controlling factor in the liquefaction susceptibility of a sand deposit is its initial void ratio or density (e.g. Casagrande, 1940; Seed and Idriss, 1971; Ishihara, 1985; Vaid and Chern, 1985; Finn, 1994; Robertson and Fear, 1995; Vaid et al., 2001). From the point of view of initiation of flow liquefaction, for a given mean effective stress, a decreasing void ratio would tend to move the state of the soil lower in void ratio – effective stress space, suggesting a more dilatant behaviour. In terms of cyclic resistance an increased density, or decreased void ratio, is associated with greater overall strength. It is thus generally accepted that a decrease in void ratio, or an increase in density, results in an increased liquefaction resistance.

2.3.5.3 Confining Pressure

Confining pressure has also been identified as a controlling factor with regards to the liquefaction susceptibility of sands. Its effects however vary with the particular aspect of liquefaction behaviour being considered.

Seed (1987), Seed and Idriss (1971), Seed and Lee (1966), and Vaid and Finn (1979) reported that when subjected to cyclic loading, the shear stress required to generate pore pressures equivalent to the confining stresses increased as confining stress increased. This led Seed and Idriss (1971) to conclude that liquefaction susceptibility decreased with increasing confining stress. Castro and Poulos (1977) also indicate that the cyclic mobility stress, which is equivalent to the shear stress required to produce a certain strain, increases with effective consolidation pressure. These findings appear to be generally consistent with the typical increase in peak strength observed with increasing effective confining pressure. Vaid and Finn (1979) however noted that the cyclic loading resistance required to cause a specific strain increased, decreased or remained constant with confining stress depending on the initial density, the specified strain level of interest and the magnitude of the initial static shear.

Casagrande (1979) indicated that the liquefaction susceptibility decreased with increasing confining pressure, stating that when heavily loaded even a medium dense sand may be susceptible to liquefaction whereas the same soil would not be at lower confining stresses. This latter statement resulted because Casagrande was referring to the effect of confining stress on the triggering of flow liquefaction. As demonstrated by Castro and Poulos (1977) at constant void ratio, an increase in confining stress causes the state of a soil move to the right (i.e. towards and past the steady state line) increasing its susceptibility for flow liquefaction. Similarly they demonstrated that if a sand was allowed to compress with an increase in confining stress, the state would either remain the same or move towards and/or past the steady state line. Vaid et al. (2001) also indicated that increasing the effective confining pressure caused more contractive behaviour.

2.3.5.4 Initial Static Shear Stress

There have been considerable differences of opinion with regards to the effects of initial static shear stress. The differences do not appear to arise solely from the use of different reference behaviours but appear to be mainly due to the complicated effect of initial static shear stress. Casagrande (1979) reported that Lee and Seed (1967) concluded that “the liquefaction potential decreases with increasing initial principal stress ratio” by which they meant that there was an increase in required shear stress or number of stress cycles to cause excess pore pressures equal to the confining pressure. This finding later led to the following, somewhat controversial statement by Seed (1987) in reference to soils with relative densities of at least 45 percent and subjected to shear stress/normal stress ratios generally encountered in practice:

“Since higher and steeper embankments may make it more difficult to build up pore pressure and trigger liquefaction [due to increased confining pressure and static shear stress], it would appear that these embankments can sometimes be constructed on sands with lower N_1 values and still not cause liquefaction to be triggered, than can embankments with lesser heights and flatter slopes.”

Casagrande (1979) however, presented evidence for a substantial increase in liquefaction susceptibility for a loose sand sample loaded with a principle stress ratio of two (i.e. higher horizontal or static shear) compared to isotropically loaded samples. Test results presented in Vaid and Finn (1979) suggested that the effect of initial static shear stress was fairly complicated and apparently dependant on several other factors, so no general conclusions were reached. Castro and Poulos (1977) suggest that for contractive type sands able to exhibit flow liquefaction, higher initial shear stresses results in a decrease in the applied shear stress required to trigger liquefaction and an increase in the magnitude of the movements that will occur, i.e. liquefaction potential and potential deformations will be increased. They further suggest that for sands exhibiting cyclic mobility as per their definition presented previously, initial static shear stress has two opposing effects. Increased initial shear stress tends to move the sand closer to failure, thus decreasing the amount of applied shear stress required to trigger failure. However, they also state that increased initial static shear stress means that shear stress reversal does not occur until cyclic stresses equal to at least $\frac{1}{2}(K_0-1)$ are applied which they indicate is required to cause large strains. Vaid and Chern (1985) similarly indicated that the effect of initial static shear stress on the resistance to cyclic loading depends on the volumetric response of sands to shear. They show that if flow or limited liquefaction occurs, increased static shear stress causes a decrease in the cyclic stress ratio required to trigger softening. Conversely, if cyclic mobility develops they indicate that an increase in the initial static shear stress always causes an increase in the cyclic shear stress required to cause a given axial strain.

In more recent research (e.g. Finn, 1994; Robertson and Fear, 1995; Youd and Idriss, 2001), it now appears to be generally accepted that the effect of initial static shear stresses depend on the initial state of a sand. Contractive sands tend to show an increase in liquefaction potential with increasing initial static shear stress whereas dilative soils tend to show an increase in liquefaction resistance with increasing initial static shear stress.

2.3.5.5 Fines Content

The effect of fines content on the liquefaction susceptibility of sands is also widely discussed in the literature. Seed (1987) indicates that for the case of equal penetration resistance a sand with increased fines content will have a greater liquefaction resistance. Robertson and Wride (1998) also indicated that greater resistance to cyclic liquefaction is generated by sandy soils containing some fines. They found that for the same liquefaction resistance, an increase in the fines content of a sand tended to cause a decrease in the permeability and an increase in the compressibility of a deposit, thus decreasing the penetration resistance. Sladen et al. (1985) however stated that everything else being equal (i.e. confining pressure and void ratio) the liquefaction potential of a dirty sand is greater than that of a clean sand. Vaid (1994) similarly showed that at a given void ratio the cyclic resistance decreases with an increase in silt content. As pointed out by Finn et al. (1994), the effect of fines depends on the comparison being made. For a given penetration resistance, increased fines will actually correspond to an increase in relative density and thus an increase in liquefaction resistance. For constant void ratio however, the presence of fines will tend to decrease the peak undrained strength and thus increase the liquefaction potential. Thus the two statements presented above do not in fact contradict each other.

Ishihara (1993) indicated that the plasticity of the fines has a significant influence on the liquefaction resistance. Citing test results from Ishihara et al. (1978) he showed that the required cyclic stress ratio (the applied shear stress divided by the effective confining pressure) to cause 5 percent double amplitude strain increased significantly with the plasticity of the fines once the Plasticity Index was above 10. Ishihara (1993) suggests that the increased resistance is due to the adhesion developed between the fine particles as their plasticity increases. The effect of plastic or cohesive fines is somewhat captured by the "Chinese Liquefaction Criteria" summarized in Robertson and Wride (1998) which indicates that if a soil has greater than 15 percent fines, a Liquid Limit greater than 35 percent and a natural water content less than 90 percent of the liquid limit, the soil is likely not susceptible to liquefaction.

There is also an indication that fines content may affect the location of the steady state line (Ishihara, 1993) and this could also be expected to affect the liquefaction response of sands. Sladen et al. (1985) and Poulos et al. (1988) indicated that increased fines tend to lower the steady state line in void ratio-effective stress space. Test results reported in Castro and Poulos (1977) tend to indicate that the location of the steady state line may also depend on other soil properties such as gradation and grain compressibility. Analyses of laboratory data by HBT AGRA (1992) did not indicate any significant variation in the location of the steady state line with respect to the fines content of tailings sand. As illustrated in Kupper (1991) however, Sobkowitz and Handford (np) indicated that the steady state line of tailings sand moved upwards when fines content increased from 4 to 11 percent.

2.3.5.6 Loading Direction

The importance of stress paths is discussed by Arthur et al. (1980) in a paper entitled "Principal Stress Rotation: a Missing Parameter". They discuss the differences between stress paths followed in laboratory testing and those followed by a soil element in the field and suggest that rotation of stresses could be the missing parameter that invalidates much current laboratory data. It is therefore not surprising that the direction

of loading or stress path influences the response of sands to cyclic loading. The effects of variation in stress path and loading direction have been reported by Vaid and Chern (1985), Vaid et al. (1990), Yoshimine et al. (1999) Vaid and Sivathayalan (2000) and Sivathayalan and Vaid (2002). In general, it appears that triaxial compression, simple shear and triaxial extension cause increasingly contractive behaviour when carried out on samples initially at the same void ratio and confining stress. Yoshimine et al. (1999) also indicated that a larger intermediate stress (σ'_2) causes more contractive behaviour. It should be noted however that these simple shear and triaxial extension tests may also cause increasing non-uniformities within the samples compared to triaxial compression tests and average void ratio measurements taken for the entire sample may not be reflective of conditions on the failure plane (e.g. Desrue et al., 1996; Ayouban and Robertson, 1998). Roscoe et al. (1963) report that average measurements cause the soil to appear more contractive than the actual behaviour on the shear plane. Results from CANLEX did appear to generally confirm that extension loading particularly causes a more contractive response than triaxial compression. They showed through modeling and a large scale field test that a soil subjected to mainly compression loading was much less susceptible to flow or static liquefaction than a deposit subjected to extension loading (Byrne et al. 2000).

The direction of loading with respect to bedding planes was also shown to affect the response of sands to undrained loading. Sivathayalan and Vaid (2002) showed that as the major principal stress direction moves towards the bedding planes, sands exhibit more contractive behaviour and that the peak strength also decreased as the principal stress direction became more aligned with the bedding planes. The minimum strength also depended on the direction of the principal stress. They further indicated that rotation of the principal stresses alone, with no increase in deviator stress could cause excess pore pressures to develop. The changing volumetric response to shear with rotation of principal stress increases the potential for flow liquefaction (Sivathayalan and Vaid, 2002). Cyclic loading tests were not reported however to examine the effect of principal stress rotation on cyclic mobility type behaviours. Seed (1979) did report laboratory tests carried out in which multi-directional shaking was applied that indicated that stress ratios required to cause pore pressures equal to the confining pressure were approximately 10 percent lower than for the case of unidirectional shaking.

2.3.5.7 Location of the Phreatic Surface

For liquefaction to occur, an incompressible fluid must occupy the voids of the soil. It would therefore seem reasonable to conclude that soils must be located deeper than the phreatic surface to be potentially liquefiable. Location of the phreatic surface is therefore an important parameter and in general, liquefaction potential decreases with an increasing depth of phreatic surface (e.g. Seed and Idriss, 1971; Ishihara, 1985; Fear and McRoberts, 1995; Kramer, 1996). However, as pointed out in Seed (1979) unsaturated surficial soils can be softened and brought into a "quick" condition by the upward dissipation of pore pressures generated in sands below the phreatic surface.

Ishihara (1985) proposed relationships between the thickness of surficial non-liquefiable deposits and the underlying thickness of liquefiable deposit required to avoid surface effects of liquefaction for varying maximum ground accelerations. The relationships indicate that as the thickness of a non-liquefiable surface layer increases, the thickness of an underlying liquefiable layer that can be present without causing surface evidence of liquefaction also increases. In general the relationships suggest that there is a limiting

surficial thickness, increasing with the magnitude of ground acceleration, beyond which there will be no surficial evidence of liquefaction. Since material above the phreatic surface can generally be considered non-liquefiable, it would seem that these relationships could indicate minimum depths of the phreatic surface to prevent surface effects of liquefaction. The relationships were developed by analyzing field data from a Magnitude 7.7 earthquake in Japan and a Magnitude 7.8 earthquake in China based on the criteria in the Japanese Bridge Code and dividing the locations that exhibited surficial sign of liquefaction from those that did not. Youd and Garris (1995) compared the relationships proposed by Ishihara (1985) with a different set of case histories analyzed based on procedures proposed by Seed et al. (1985) and discussed in Section 2.4.3.2. They found that Ishihara's (1985) relationship could predict certain types of surface disruption but that case histories indicating damage due to ground oscillation or lateral spreading often plotted below the proposed boundary, i.e. in the no damage area, and were not properly predicted.

Grozic et al. (2000) report that gassy soils with saturation values as low as 77 percent can be liquefied if sufficiently large cyclic loads are applied. It is therefore possible that soils located somewhat above the phreatic surface in the partly saturated zone could also be susceptible to liquefaction, although their resistance to cyclic loading is greater than that of a similar saturated soil.

2.3.5.8 Other Factors

Other factors affecting liquefaction behaviour can be more difficult to quantify. For example, ageing of deposits has been shown to increase the resistance of a sand deposit to liquefaction (Seed, 1979; Ishihara, 1993; Wride et al., 2000). In general, it is suggested that ageing of a deposit introduces structure or possibly cementation, which increases the strength of the deposit, thereby decreasing its liquefaction susceptibility. However, the increased strength may also be associated with a more brittle failure (Pestana and Whittle, 1995). These effects are not easily quantified since ageing tends to cause an increase in in-situ test results, such as penetration resistance, which would be difficult to differentiate from other influences. Also, sampling procedures tend to destroy the structure or locked-in anisotropic stresses and the long term processes would be very difficult to simulate in a laboratory.

Similarly the effect of soil fabric is difficult to quantify. Even in the laboratory the effect of different preparation methods has been observed to affect the undrained cyclic response of sands (e.g. Seed, 1979; Vaid and Chern, 1985; Kuerbis and Vaid, 1988; Ishihara, 1993; Vaid, 1994). In general it appears that water pluviated samples are more dilative than moist tamped samples. It also appears that the range of densities which can be achieved by moist placement, dry deposition, water pluviation, and slurry deposition become successively smaller limiting the possible ranges of behaviour (Kuerbis and Vaid, 1988; Ishihara 1993). Seed (1987) summarized the cyclic resistance from previous laboratory tests and showed that there is a significant variation in the cyclic resistance of samples at the same density and effective confining stress with different sample preparation method. It would thus be expected that soil fabric developed in the field would also affect the behaviour.

Particle angularity, compressibility and uniformity also appear to affect the liquefaction resistance of sands. It has been suggested that more uniformly graded sands are more susceptible to liquefaction than well-graded soils (Kramer, 1996). Vaid and Chern

(1985) suggested that the angularity of sands causes them to be more compressible than rounded sands, particularly under high stresses, which tends to cause more contractive behaviour and thus increases the potential for flow or limited liquefaction. Castro and Poulos (1977) also suggest that platy shaped grains create more compressible sands, which influences their liquefaction susceptibility.

Drainage conditions also have an obvious implication in the liquefaction of a deposit. It has been shown (Andrus et al., 1991; Valera, 1994) that the presence of thin, low permeability silt or clay layers can cause a gravel deposit to be susceptible to liquefaction if the layers are sufficiently continuous to impede drainage. Fear and McRoberts (1995) also discussed several case histories in which impeded drainage likely influenced liquefaction. They also stressed the difficulty in locating the low permeability layers during a conventional site investigation program.

2.4 Evaluation of Cyclic Liquefaction Susceptibility

2.4.1 General

Seed and Idriss (1971) presented a basic framework for evaluating the earthquake liquefaction susceptibility of a site. Although developed for the specific problem of the evaluation of liquefaction susceptibility, the steps are logical and similar to procedures followed for any stability analysis. The procedure as described by Seed and Idriss (1971) is listed below, with the text in brackets added to provide an analogy to the problem of slope stability.

1. Determine the design earthquake. (Determine the critical failure mode.)
2. Convert the design earthquake into shear stresses induced throughout the soil profile. (Determine the driving forces.)
3. Evaluate the cyclic stress resistance of the soil profile either by laboratory testing or available field data. (Determine the appropriate soil strength that will provide the resisting forces.)
4. Compare the induced stresses with the soil strength and assess the potential for liquefaction. (Calculate the factor of safety against failure as resisting force divided by driving force.)

If the cyclic resistance is less than the induced cyclic stresses then liquefaction could be triggered and the residual or liquefied strength will be required to assess the consequences of liquefaction. Methods for carrying out the steps identified above will be discussed in the following sections.

2.4.2 Evaluation of the Applied Cyclic Stress

The applied cyclic stress greatly affects the liquefaction susceptibility of a deposit in that larger magnitudes obviously increase the potential for liquefaction. The loading duration also has an impact however and it is possible that a smaller magnitude load, acting over a long period could cause liquefaction where a very short duration large magnitude cyclic load may not. The frequency of the applied motion can also significantly affect the soil response (Seed and Idriss, 1982).

Seed and Idriss (1971) suggested a simplified method for determining a value of average cyclic shear stress based on a known maximum ground acceleration value, a_{max} .

Based on studies of various earthquakes and laboratory tests, Seed and Idriss (1971) proposed the following relationship for average cyclic shear stress:

$$\tau_{avg} = 0.65 \left(\frac{\gamma h}{g} a_{max} \right) r_d \quad \text{Equation 2-1}$$

γ = unit weight of soil

h = depth of interest

r_d = stress reduction factor

The term in the parenthesis is the maximum shear stress induced at depth h in the soil. The stress reduction factor, r_d , accounts for the decrease in stress with depth due to deformation of the soil column. Seed and Idriss (1971) presented a range of r_d values based on ground response analyses of a range of earthquake motions and soil conditions with sand in the upper 15m. Mathematical equations have since been proposed to fit the average range proposed by Seed and Idriss (1971) as in Youd and Idriss (2001). Generally the stress reduction factor has been considered independent of earthquake magnitude but recently, an equation for r_d dependant on both depth and earthquake magnitude has been proposed (Idriss, 1998). The average applied cyclic stress is often divided by the effective overburden pressure giving the cyclic stress ratio (CSR), as this is the value typically correlated with in-situ tests (e.g. Robertson and Campanella, 1985; Seed et al., 1985; Stark and Olson, 1995).

Seed and Idriss (1971) also listed representative numbers of cycles applied during earthquakes of various magnitudes. They then updated these values in a later publication (Seed and Idriss, 1982) based on statistical studies carried out. In order to evaluate the effects of a certain magnitude of cyclic stress with in-situ empirical correlations, it is typically necessary to convert the cyclic stress to an equivalent stress for a Magnitude 7.5 earthquake. This is done by dividing the cyclic stress ratio (τ_{avg}/σ'_v) by a magnitude scaling factor, originally proposed by Seed and Idriss (1982). Magnitude scaling factors are calculated as the ratio of the cyclic stress ratio required to induce liquefaction under the representative number of load cycles for the earthquake magnitude of interest to the cyclic stress ratio required to cause liquefaction in the representative number of cycles for a Magnitude 7.5 earthquake (typically taken as 15 cycles). Many researchers (e.g. Ambraseys, 1988; Arango, 1996; Idriss, 1998) have since studied this aspect of magnitude scaling factors as summarized by Youd and Idriss (2001) and various magnitude scaling factors have been proposed.

There are many more elaborate methods of determining induced stresses based on analyses and transmission of actual earthquake acceleration histories. Wave transmission, reflection and refraction, topography, soil type, changing soil properties and many other factors can be incorporated. These will typically require software programs which are beyond the scope of this review.

2.4.3 Determining the Cyclic Resistance Ratio

2.4.3.1 General

As with the evaluation of most soil properties, there are many methods of estimating the cyclic resistance of a soil. In general, there are two main options: empirical correlations established between in-situ tests and the cyclic resistance of the deposit based on case

histories and laboratory experiments or direct measurement in the laboratory. Methods of assessing the in-situ state of a soil based on in-situ testing also exist and can aid in defining the type of liquefaction behaviour that can be expected, but they do not provide a measure of the cyclic resistance and will not be discussed in this review. They are, however, briefly discussed in Section 5.2.3.

Because of the disturbance induced by conventional sampling methods when applied to saturated sand deposits (e.g. Yoshimi et al., 1977; Marcuson and Franklin, 1980; Seed, 1982) and the cost typically associated with gathering frozen samples, the most common method of assessing the cyclic resistance of a soil is through correlations with in-situ tests. These studies, relating behaviour to in-situ testing, are arguably the most appropriate method of interpreting the behaviour of a site because they incorporate factors that are impossible to model in the laboratory or are difficult to quantify individually. However, it is important when applying any such findings to understand how and under what conditions the correlations were developed and whether they are applicable to the site being evaluated. It is also important to understand the tests used to characterize the in-situ conditions of the site and the factors that can influence the results. Because of the general increase in both resistance and in-situ test results (e.g. penetration resistance, shear wave velocity, etc.) with confining pressure, the cyclic resistance is typically normalized through division by the effective overburden pressure and termed the cyclic resistance ratio (CRR). There are many correlations between a wide variety of in-situ tests and cyclic resistance ratio. Not all of the proposed correlations will be presented herein. In general, only the methods most commonly used in North America will be discussed. A brief summary of the laboratory methods of determining cyclic resistance ratio will also be presented.

2.4.3.2 Standard Penetration Testing

The Standard Penetration Test (SPT) is likely the most commonly used in-situ test. As such, there are correlations between SPT blow count (N value) and a multitude of soil properties. Tokimatsu and Yoshimi (1984) indicate that despite its problems, the SPT reflects the effects of stress history, strain history, soil fabric and in-situ stresses which are difficult to capture in the laboratory but do effect the resistance of sands to liquefaction and also is conducted under undrained conditions making it a convenient parameter to relate to the cyclic resistance of a sand. The most common correlations between SPT blow count and CRR in North America appears to be that proposed by Seed et al. (1985). The many revisions of this chart and the many other SPT-cyclic resistance ratio correlations will not be discussed in detail but a brief and by no means exhaustive history of the development of these relationships is presented followed by a detailed discussion of Seed et al.'s (1985) chart.

Correlations between the SPT N-value and the cyclic resistance ratio are reported by Seed and Idriss (1982) to have been initiated in Japan after the Nigata earthquake in 1964. To develop these correlations, SPT data from a number of sites was analyzed and a boundary was drawn between those sites which did and did not show evidence of liquefaction. In 1971, Seed and Peacock (1971) and Whitman (1971) proposed relationships between the cyclic stress ratio and relative density as determined from SPT values based on other empirical relationships. Also in 1971, Seed and Idriss presented several graphs of SPT N versus depth for various values of maximum ground acceleration and phreatic surface level, which indicated three zones; liquefaction very likely, liquefaction potential dependent on particular soil and earthquake conditions, and

liquefaction very unlikely. These charts were based on results from laboratory experiments and 35 case histories. In 1975, Castro amalgamated the data from various sources and produced a plot of corrected SPT blow count versus cyclic resistance ratio defining zones of ground failure, no ground failure, and a middle uncertain area. Tokimatsu and Yoshimi (1984) presented relationships between normalized SPT blow counts and cyclic stress ratio for various fines contents and maximum strain values. Seed and his co-workers published a suite of papers presenting charts of normalized SPT blow count and cyclic resistance ratio similar to its current form apparently beginning in 1975 (e.g. Seed et al., 1975; Seed and Idriss, 1982; Seed et al., 1983; Seed, 1984; Seed et al., 1985). Most recently the NCEER Workshop modified the chart proposed by Seed et al. (1985) at low $(N_1)_{60}$ values so that the clean sand curve does not pass through the origin (Youd and Idriss, 2001). This latest version is shown in Figure 2.6 and is discussed in detail below.

The database presented in Seed et al. (1985) included data from 125 different sites in North and South America, Japan and China. The case histories included mainly sites with level to gently sloping terrain underlain by Holocene alluvial or fluvial sediment at depths less than 15m. For their analyses, Seed et al. (1985) separated the case histories into clean sand sites (less than 5 percent passing number 200 sieve) and silty sand sites. For each case history, they calculated a representative SPT $(N_1)_{60}$ value, in which raw SPT blow count data was corrected for overburden and normalized to an energy transfer ratio of 60 percent. The energy correction appeared to be based on empirical correlations dependant on hammer type presented in Seed et al. (1984) and the overburden correction factor was read from the charts presented in Seed et al. (1983).

The earthquake induced cyclic stress ratio was then calculated for each case history and, where necessary, converted to an equivalent cyclic stress ratio for an earthquake of Magnitude 7.5 as discussed in Section 2.4.2. The conversion to a Magnitude 7.5 earthquake was done using the magnitude scaling factors proposed in Seed and Idriss (1982). For each case history, they then plotted the corrected SPT $(N_1)_{60}$ value against the associated applied cyclic stress ratio. A line was then drawn essentially separating the liquefied sites from non-liquefied sites, representing the cyclic stress resistance ratio for a soil with a given SPT blow count for a magnitude 7.5 earthquake. Signs of liquefaction included phenomena such as sand boils, ground cracking, small lateral movement as well as bearing capacity failures, uplift of buried structures and major translation. By considering case histories for sites with differing fines content, they developed similar curves for sands with 15 and 35 percent fines.

Although not shown in Figure 2.6, Seed et al. (1985) do note that "liquefaction for a sand with an $(N_1)_{60}$ value of 25 to 30 involves a different form of behaviour than that for a sand with an $(N_1)_{60}$ of say 10 to 15. A sand with an $(N_1)_{60}$ value of 25 may show field evidence of liquefaction in the form of sand boils but it is unlikely to undergo more than about 10 percent shear strain under the influence of earthquake shaking...in contrast sands with an $(N_1)_{60}$ value of 15 may...undergo very large shear strain in excess of 25 to 30 percent." To take this into account, Seed et al. (1984) used results presented in Seed (1979) and Tokimatsu and Yoshimi (1984) to associate maximum strain values with liquefaction at higher $(N_1)_{60}$ values as shown in Figure 2.7. From Figure 2.6, limiting values of penetration resistance appear to exist above which liquefaction is unlikely, ranging from roughly an $(N_1)_{60}$ of 30 for clean sands to an $(N_1)_{60}$ of approximately 22 for

sands with 35% fines. It is noted however, that there are not many case history data points in these areas, particularly for silty sands.

To apply the chart in Figure 2.6 in the evaluation of the cyclic resistance ratio of a sand, field SPT data should be corrected for overburden and energy using the same empirical correlations as were used by Seed et al. (1985). It is important when looking at the data to recall that the charts were verified and are only applicable to level to gently sloping terrain underlain by Holocene aged alluvial or fluvial sediments at shallow depths up to 15m (Youd and Idriss, 2001). In order to extrapolate the chart to other conditions such as different magnitude earthquake, deeper sites or sloping ground, various correction factors have been suggested by a variety of researchers.

Significant amounts of research have been carried out with regards to correction factors for the evaluation of the cyclic resistance ratio (e.g. Seed and Idriss, 1982; Seed, 1983; Ambraseys, 1988; Seed and Harder, 1990; Finn, 1994; Arango, 1996; Andrus and Stokoe, 1997; Youd and Noble, 1997; Idriss, 1998; Hynes and Olson, 1999; Vaid et al., 2001) and there are many different suggested values, but they will not be discussed in detail here. Magnitude scaling factors, as discussed in Section 2.4.2, are used to account for the decrease in the cyclic resistance ratio of a deposit from that estimated based on the chart if the earthquake magnitude is greater than 7.5 and vice versa if the magnitude is smaller. For deeper sites, the cyclic resistance ratio is reduced below that read from the charts by a factor K_σ . In cases where initial static shear stress is present, a K_α factor is applied which reduces the cyclic resistance ratio for loose, contractive sands and increases the cyclic resistance ratio for dense dilative sands (Youd and Idriss, 2001). Finn et al. (1994) suggested that both K_σ and K_α vary greatly depending on the specific soil and point out that the database for K_α correction in particular is "too general for effective use in design". They recommend that correction values be determined specifically for the soil being considered. Youd and Idriss (2001) also note that "applications using K_σ and K_α are beyond routine practice and require special expertise."

Recently, Fear and McRoberts (1995) critically reviewed the work by Seed et al. (1985), focusing largely on reconsideration of the selection of $(N_1)_{60}$ for the various case records. The methodology for calculation of the applied cyclic stress ratio adopted by Seed et al. (1985) was maintained in the review study and the case histories were separated into clean and silty sands as in the original study. Cyclic stress ratio and fines content values were reassigned if necessary based on the new selection of representative $(N_1)_{60}$ values. The original definition of liquefaction used by Seed et al. (1985) presented previously was generally adopted in the review but Fear and McRoberts (1995) did add a new category termed "pressure relief" for cases in which sand boils were the only surface expression of liquefaction in order to differentiate between the different types of liquefaction behaviour and to investigate the statements by various researchers (e.g. Castro, 1975; Casagrande, 1979) that dense sands (e.g. high N values) behave differently under cyclic loading than loose sands.

The main objection raised by Fear and McRoberts (1995) regarding the work done by Seed et al. (1985) was that "the methodology used [for selecting N values] in the Berkeley catalogue was not explicitly stated nor consistently followed" indicating that the original work used a minimum $(N_1)_{60}$ value in some cases, an average $(N_1)_{60}$ value in many cases and a high $(N_1)_{60}$ value in a few cases and have thus created an overly

conservative and unduly expensive criteria for the liquefaction potential of sands. Fear and McRoberts argue that "all else being equal, the layer with the lowest $(N_1)_{60}$ value will have the least resistance to liquefaction". The review carried out by Fear and McRoberts (1995) therefore consistently used the "weakest link in the chain" approach and selected the minimum $(N_1)_{60}$ value reported in sand and/or silt layers from below the phreatic surface. They then calculated the associated CSR and noted the appropriate fines content. They discussed the possibility of CSR variation with depth resulting in a more critical combination of $(N_1)_{60}$ and CSR other than that obtained by selecting the minimum value of $(N_1)_{60}$ and corresponding CSR but argued that because of the shallow nature of the case histories the variation in CSR with depth is relatively small compared to the large variation in $(N_1)_{60}$ values with depth making a more critical combination unlikely.

Based on the re-selected SPT values and the additional behaviour category, McRoberts and Fear (1995) produced the chart shown in Figure 2.8 with the boundary proposed by Seed et al. (1985) and modified in Youd and Idriss (2001) superimposed. In general the boundary lines proposed by Fear and McRoberts (1995) are less conservative than those proposed by Seed et al. (1985). Fear and McRoberts report that the main cause of the differences between the two studies was the reclassification of several case histories with $(N_1)_{60}$ values of greater than 15 as pressure relief rather than liquefaction.

The various boundaries shown in Figure 2.8 are interpreted by Fear and McRoberts (1995) as follows. The lower bound lines, which were located such that all the non-liquefaction case histories were located above the line is the boundary above which liquefaction (resulting from contractant behaviour) is very likely. The upper bound lines, drawn beneath all the liquefied case histories but with some pressure relief cases located beneath it, demark a zone of possible liquefaction between the lower and upper bound lines. The zone between the upper bound lines and the conservative upper bound, which encompasses all the liquefied and pressure relief cases, indicates that boils or settlement are the only likely surface indications of liquefaction. Below the conservative upper boundary, some settlement is possible but other forms of earthquake induced phenomenon are unlikely. Fear and McRoberts suggest limiting $(N_1)_{60}$ values for clean sands of roughly 15 for liquefaction with the possible liquefaction zone extending from $(N_1)_{60}$ values of 5 to 13, while the limiting value for the development of sand boils and settlement is approximately 22. They do suggest however that several case histories that define the former boundary liquefied as a result of impeded drainage and that if only free-draining case histories were considered, the limiting $(N_1)_{60}$ value for liquefaction would be reduced further. In comparing Figure 2.6 and Figure 2.8, it can be observed that the limiting $(N_1)_{60}$ values proposed by Fear and McRoberts (1995) are similar to the limiting $(N_1)_{60}$ for 20 and 10 percent strain suggested by Seed et al. (1984).

2.4.3.3 Cone Penetration Testing

The Cone Penetration Test (CPT) is gaining widespread popularity as an in-situ test method largely because of its repeatability and ability to provide a continuous profile of a natural deposit. The CPT is generally not affected by the myriad of operator dependant factors that influence the SPT (e.g. non standard rods, differing hammer and anvil set ups, widely varying energy transfer to the sampler, etc). The CPT is similar to the SPT however in that it responds to many of the same soil properties as the SPT including density, grain characteristics, soil fabric, ageing, anisotropy, in-situ stresses, etc. and should thus be a reasonable indicator of cyclic resistance. It is not surprising therefore

that CPT results are with increasing regularity being used to evaluate the liquefaction susceptibility of soils based on charts developed from case histories in a similar manner to the SPT.

The charts developed for evaluating the cyclic stress ratio from CPT data are generally based on the measured, corrected or normalized cone tip resistance. As with the SPT, for a given CPT penetration resistance, a sand with higher fines content will have a greater cyclic resistance (Robertson and Fear, 1995). Since the CPT does not gather samples, accounting for this effect is not as straightforward as with the SPT where samples are retrieved.

The method of analyzing CPT data for liquefaction analyses recommended by the NCEER (Youd and Idriss, 2001) is based on the following method proposed by Robertson and Wride (1998). The procedure is shown schematically with the equations proposed by Robertson and Wride (1998) in Figure 2.9. It should be noted, however, that equations proposed by various researchers could be substituted into the procedure to incorporate different equations for fines content or behaviour index for example.

In the Robertson and Wride method (1998), the measured sleeve friction and tip resistance are first normalized according to equations proposed by Jefferies and Davies (1991). When normalized in this fashion, Jefferies and Davies (1993) indicated that concentric circles, the radius of which is termed the soil behaviour type index, I_c , can approximate the soil type boundaries. The soil behaviour index is thus calculated based on the normalized cone tip resistance and friction ratio which identifies the soil type (e.g. clean sand, silty sand etc.). This process is iterative as the correct normalization depends on I_c and the normalization and calculation of I_c must therefore be repeated if I_c is calculated outside the range initially assumed. Knowing I_c the fines content can be estimated based on one of many relationships (e.g. Jefferies and Davies, 1993; Lunne et al., 1997). The cyclic resistance ratio can then be estimated at this point based on the tip resistance corrected for overburden from charts developed for silty sands as shown in Figure 2.10b. Alternatively, a clean sand equivalent cone resistance could be calculated. Ishihara (1985) suggested a correction for the CPT tip resistance to account for fines based on that proposed for the SPT. The relationship suggested by Robertson and Wride and included in Figure 2.9 is based directly on I_c which does incorporate the amount of fines. Once the clean sand tip resistance is obtained, the cyclic resistance can be determined from any empirical relationship between cone tip resistance and cyclic resistance ratio developed for clean sands as shown in Figure 2.10a. It is important to note however that the values of q_{c1N} and q_{c1N-CS} proposed by Robertson and Wride (1998) and included in Figure 2.9 are different than q_{c1} or q_{c1-CS} values commonly found in other charts. Conversions can easily be made between the two sets of values however as shown in Equation 2-2.

$$q_{c1N} = \frac{q_{c1}}{P_{a2}} \quad \text{Equation 2-2}$$

where P_{a2} is a reference pressure of 100kPa in the same units as q_{c1}
(e.g. if q_{c1} is in MPa, $P_{a2}=0.1\text{MPa}$)

As noted by Robertson and Wride (1998) the correlations proposed above (soil behaviour index, fines content, correction factors) respond to many factors such as

plasticity, stress history and mineralogy and therefore are approximate and should not be applied blindly. They note that particular care is required for soils that have an I_c between 1.64 and 2.36 and a fines content of less than 5 percent as they can be classified as either a loose clean sand or a sand containing fines each of which have very different cyclic resistances. In these cases, unless further information is available for guidance, they recommend conservatively treating the soil as a clean sand. Furthermore, if the soil is classified as a silty clay or clayey silt, i.e. I_c less than 2.36, it is suggested that a sample be gathered so that other criteria can be applied. A further complication arises when interpreting the cone tip resistance when there are thin sand layers embedded within a softer deposit (Robertson and Wride, 1998). The CPT responds to the properties of the soil within the zone of influence of the cone and therefore the tip resistance measured in layers thinner than the zone of influence may be in error. Robertson and Fear (1998b) suggest a conservative correction for the CPT tip resistance in thin sand layers embedded based on work by Vreugdenhil et al. (1994).

As shown in Figure 2.10 the correlations between corrected tip resistance and cyclic resistance ratio depend on both median grain size and fines content. Different methods were used to develop the various correlations and therefore they are possibly applicable to slightly varying conditions. The relationships proposed by Robertson and Campanella (1985) and Seed and DeAlba (1986) were developed based on their proposed correlations between CPT and SPT data utilizing the chart proposed by Seed et al. (1985) to determine the cyclic resistance ratio associated with various CPT tip resistance values. These relationships are therefore subject to the same constraints as discussed previously for the SPT-cyclic resistance ratio chart (e.g. level ground, young deposits). Ishihara (1985) used laboratory measured cyclic resistance ratios from undisturbed samples gathered near CPT soundings to develop relationships. Shibata and Taparaksa (1988) developed their relationships from CPT case histories mainly located in Asia in a manner similar to that used by Seed et al. (1985). The correlations proposed by Mitchell and Tseng (1990) were based on laboratory measured values of cyclic resistance ratio and theoretical cone tip resistance values calculated based on cavity expansion theory. Stark and Olson (1995) developed their relationship based on a large number of case studies, including those used by Shibata and Taparaksa (1988). Their database included 180 CPT soundings on sites that were subjected to earthquake shaking. Cyclic stress ratios were estimated as suggested by Seed and Idriss (1971). The case histories were separated based on fines content and median grain size and boundaries between occurrence and non-occurrence of liquefaction were drawn to develop the cyclic resistance – q_{c1} relationships. Although not shown in Figure 2.10, the case histories included a group of gravelly soils for which a tentative cyclic resistance correlation was also developed.

Liquefaction in all of the methods discussed, whether they resulted from case histories or laboratory data, was described in a manner similar to that used by Seed et al. (1985) suggesting that at higher penetration resistance the behaviour may be very different than at lower penetration resistances. Robertson and Wride (1998) suggest that for q_{c1N} values greater than approximately 75, soils are dense and deformations may be limited. It also appears that above q_{c1N} of 150 to 180, any type of liquefaction may be unlikely.

Many other correlations and methods have also been proposed for estimating the cyclic resistance of sands from CPT data (e.g. Zhou, 1980; Suzuki et al., 1995,). In general, they are all based on a similar underlying framework (i.e. estimating soil type from the

CPT results and based on case histories or laboratory data developing an empirical correlation for cyclic resistance) and will not be discussed herein.

2.4.3.4 Becker Penetration Testing

The Becker Penetration Test (BPT) is similar to the SPT but on a larger scale. In the BPT, typically a 168mm outer diameter, 140mm inner diameter, double walled closed ended pipe is driven into the ground by a double acting diesel “Becker” hammer. In a similar fashion to the SPT, the number of hammer strikes (blows) required to advance the casing 1 foot (300mm) is recorded. BPTs are generally carried out in gravels or very dense deposits that cannot be properly penetrated by the smaller SPT split spoon sampler. Various correlations between BPT blow counts and SPT results have been suggested (e.g. Harder and Seed, 1986; Sy and Campanella, 1994; Sy, 1997). A detailed description of the interpretation of BPT data is beyond the scope of this review but a brief overview is presented herein. Once a representative $(N)_{60}$ value has been estimated from the BPT data, overburden correction factors can be applied and the chart proposed by Seed et al. (1985) and modified in Youd and Idriss (2001) can be used to assess the cyclic resistance of a soil.

Prior to correlating a BPT blow count to an equivalent SPT N_{60} value, significant corrections are required to account for variations in energy transfer and testing procedures. Similarly to the SPT, BPT results are corrected for energy transfer, and pipe diameter. Corrections have been proposed by Harder and Seed (1986) however, as suggested by Sy and Campanella (1994) and Stewart et al. (1990) these may be somewhat site specific. Harder and Seed (1986) suggested energy corrections based on the measured bounce chamber pressure. An alternative energy correction was proposed by Sy (1997) in which the blow counts would be normalized to an energy transfer rate of 30 percent of the manufacturers rated energy for an ICE 180 hammer. After calculating the “standard” BPT blow count, N_{bc} after Harder and Seed (1986) or N_{b30} after Sy and Campanella (1993), empirical correlations can be used to calculate the SPT N_{60} . Harder and Seed (1986) proposed a correlation that neglected pipe friction as they indicated it had an insignificant effect. Case history data and theoretical calculations presented by Stewart et al. (1990), Sy and Campanella (1994) and Sy (1997) however indicated that friction did have a very significant effect on the measured BPT blow count and that friction increased with depth, density and coarseness of the material being penetrated. Sy and Campanella (1994) therefore suggested a correlation between normalized BPT and SPT blow counts dependant on the amount of casing friction. In order to apply the latter correlation however a measure or estimate of the casing friction is required. Sy and Campanella (1994) suggest carrying out monitoring with a Pile Driving Analyzer (PDA) to evaluate the actual hammer energy and to provide data for pile driving analysis (CAPWAP) to estimate the amount of casing friction at various depths. Sy (1997) also indicated that a newly developed pull-up test may provide an easy method of measuring casing friction.

2.4.3.5 Shear Wave Velocity Measurements

Shear wave velocity (V_s) is a basic mechanical property of soils related directly to a material’s small strain shear stiffness. It is used commonly in seismic surveys to identify subsurface stratigraphy. As with other in-situ tests, the shear wave velocity of a soil is affected by factors similar to those affecting its liquefaction resistance including void

ratio, stress history and geologic age and is therefore generally considered a logical means for evaluating the liquefaction susceptibility of a soil (Andrus and Stokoe, 2000).

Shear wave velocity does not yet appear to be a common method of evaluating the liquefaction resistance but is becoming increasingly so. The main advantage of using shear wave velocity to characterize a deposit is that its measurement can be carried out in any type of deposit, most notably coarse granular soils that are not easily assessed using more conventional SPT and CPT methods. Disadvantages however include the fact that shear wave velocity is associated with small strain stiffness while liquefaction is typically associated with medium to large strain behaviour. Also, it is possible to miss thin, low velocity layers, usually representative of looser material, if the measurement interval is too large. Furthermore, the measured shear wave velocity is fairly sensitive to weak inter-particle bonding and therefore may not correctly detect the liquefaction potential of weakly cemented soils (Andrus and Stokoe, 2000).

In manners analogous to those discussed previously for developing correlations for other in-situ test methods, many researchers (e.g. Kayen et al., 1992; Robertson et al., 1992; Lodge, 1994; Andrus and Stokoe, 2000) have developed correlations between shear wave velocity corrected for overburden stress and the cyclic resistance ratio as shown in Figure 2.11. The relationship proposed by Tokimatsu and Uchida (1990) was based on laboratory derived cyclic stress ratios (Youd and Idriss, 2001). Detailed discussion of shear wave velocity measurement and data interpretation is beyond the scope of this review, however it is noted that assumptions regarding the coefficient of lateral earth pressure and the direction of particle motion relative to the directions of principal stress affect the normalization (Youd and Idriss, 2001).

Of the correlations presented in Figure 2.11, that proposed by Andrus and Stokoe (2000) appears to be based on the largest amount of data. The database included over 70 sites and 26 different earthquakes, resulting in 225 case histories, with the majority located in the United States. The earthquakes ranged in magnitude from 5.3 to 8.3 and the sites included both natural and hydraulically placed deposits ranging from silts to gravels. The cyclic stress ratio for each case history was calculated and converted to an equivalent stress for a Magnitude 7.5 earthquake following the procedures suggested by Seed and Idriss (1971) and using the lower bound magnitude scaling factors recommended by Youd and Idriss (1997). The critical layer was assumed to be where the normalized shear wave velocity was the lowest and the cyclic stress ratio relative to the shear wave velocity was the greatest. The case histories were separated according to fines and gravel content and identified as liquefied or non-liquefied on the same basis as used in Seed et al. (1985); i.e. liquefaction included large movements and failures as well as sand boils and fissures. The sites considered were level, of Holocene age, with relatively shallow deposits and were considered to be normally consolidated with lateral earth coefficients of approximately 0.5. The relationships proposed by Andrus and Stokoe (2000) appear to be less affected by fines content than other in-situ test correlations and the same relationships appear to apply to both gravel and sands. They suggest limiting normalized shear wave velocity to prevent liquefaction and cyclic mobility ranging from 200 m/s for sandy silts to 215 m/s for clean sands and gravels. Andrus and Stokoe (2000) indicate that, based on a shear wave velocity – SPT correlation, their relationship “provides an overall more conservative prediction of liquefaction resistance than does the SPT-based procedure for these sites”.

2.4.3.6 Laboratory Testing

Various laboratory tests have been used to measure the cyclic resistance of soils ranging from gyratory shear tests (Casagrande, 1979) to hollow cylinder tests (Vaid et al., 1990). The cyclic triaxial test is the most common laboratory method for measuring the cyclic resistance of soil (e.g. Seed and Lee, 1966; Ishihara et al., 1975; Vaid and Chern, 1985; Mitchel and Tseng, 1990; Ishihara, 1993; Sivathayalan and Vaid, 2002) and ASTM standard D5311-92(1996) presents the standard procedures for the test. Cyclic simple shear tests, shaking table tests and triaxial torsion shear tests also seem to have been used fairly frequently to determine the cyclic resistance of soils (Seed and Peacock, 1971). Detailed descriptions of the procedures are beyond the scope of this review and can be found elsewhere (e.g. Seed and Lee, 1966; Finn et al., 1971; Seed and Peacock, 1971; Castro et al., 1982; ASTM D5311-92(1996)). Some of the assumptions and limitations of the most common test procedures will be discussed herein.

Since its use by Seed and Lee (1966), the undrained cyclic triaxial test has been regularly used to measure the cyclic resistance of a cohesionless soil. Although the test does not reproduce the exact field conditions, Seed and Lee (1966) argued that when subject to cyclic changes in deviatoric stress of $\pm\sigma_{dc}$ (the deviatoric stress must be less than the confining pressure) from an initially hydrostatic condition, the stresses produced on a 45 degree plane within the specimen approximate the conditions of an in-situ horizontal plane with no initial shear. That is, the normal stress on the plane remains constant and equal to the confining pressure, while the shear stress is symmetrically cycled by $\pm\sigma_{dc}/2$. They also required hydrostatic initial conditions in order to produce symmetric changes in shear stress on the 45 degree plane. Other researchers have used anisotropic initial conditions (e.g. Castro, 1975).

Casagrande (1979) severely criticized the use of cyclic triaxial tests to determine the cyclic resistance, particularly of dense sands. His major objection was the cycling of stress through a hydrostatic stress. He indicated that this condition was almost never encountered in the field and was a major cause of the increase in pore pressures in the sample. He also cited pumping action caused by vertically applied cyclic loading and non-uniform stress distribution on the specimen boundaries as two other mechanisms, unique to the laboratory situation that artificially increase the pore water pressures compared to field conditions. Casagrande (1979) thus concluded that there is no "common denominator between the principal mechanisms that control the cyclic response of laboratory specimens [of dense sands in a conventional cyclic triaxial test] and the response of an element in-situ" and recommended significant correction factors be applied to the results of cyclic triaxial laboratory tests.

Further limitations of the cyclic triaxial test have been identified by Seed and Peacock (1971). These limitations include the fact that the stress conditions at failure are "substantially different from those causing failure in the field", representing the maximum shear stress which is considerably greater than the shear stress determined in the field condition. They also indicate that the amount of stress rotation during the triaxial test is much larger than experienced under field loading conditions and that the intermediate stress varies from the major to the minor stress during the test whereas in idealized field cases it would reflect plane strain conditions. Castro (1975) indicated that necking and non-uniformities significantly affect the results of cyclic triaxial tests on dense specimens and do not reflect field conditions. The test apparatus for the cyclic triaxial test is

however the most widely available and it is the simplest cyclic test to carry out and thus, despite its limitations, is in widespread use (Seed and Peacock, 1971). Correction factors have been suggested relating the triaxial test to the more representative simple shear test and field conditions and will be discussed in greater detail below.

Cyclic simple shear tests are generally considered to replicate field stress conditions during cyclic loading much more accurately than cyclic triaxial tests (Seed and Lee, 1966; Vaid and Finn, 1979). However, simple shear apparatus modified to carry out constant volume tests are not readily available (Seed and Peacock, 1971). It can also be difficult to ensure uniformity of stress and strain throughout the sample. Stress transfer mechanisms between the cap and sample control the application of uniform shear stress across the width of the sample. Shear stresses must also be developed along the vertical faces of a test specimen to prevent non-uniform stresses and strains. Improved testing apparatus and procedures such as the use of roughened end platens and better load transfer systems can limit the development of non-uniformities. However, non-uniformities induced during cyclic simple shear tests still cause a reduction in the measured strength in the order of 20 percent (Seed and Peacock, 1971). In order to limit the stress concentrations such that they do not significantly affect the results, long shallow test samples mounted on shaking tables have been used (Seed and Peacock, 1971).

In spite of its limitations, the results of cyclic simple shear tests are generally thought to be more reliable than those of cyclic triaxial tests. Unlike the triaxial test, which measures the maximum shear stress, the cyclic simple shear test measures the stresses exerted on a horizontal plane. Without considering experimental error (e.g. non uniform stress distribution at sample boundaries etc.) the results of a cyclic triaxial test must thus be reduced to be comparable to cyclic simple shear or field conditions. A range of correction factors for the results of cyclic triaxial tests, based on different failure criteria and depending on the stress ratio, K_0 , have been suggested by different researchers (Finn et al., 1971; Seed and Peacock, 1971; Castro, 1975; Ishihara, 1993). For normally consolidated samples, $K_0=0.4$, the range of the suggested corrections appear to be from 0.55 to 0.72 while for a hydrostatic condition, there is no correction (Seed and Peacock, 1971; Castro, 1975). Seed et al. (1978) also indicated that the multi-directional shaking experienced in the field can decrease the cyclic resistance by 10 percent compared to the uni-directional cyclic loading induced in the laboratory.

Sample preparation also greatly affects the measured cyclic resistance (Seed, 1979; Kuerbis and Vaid, 1988). It is therefore important to test samples with a soil fabric representative of field conditions. This generally necessitates the testing of undisturbed samples. It has been shown however, that even careful piston sampling tends to cause loosening of dense deposits and densification of loose deposits, thereby altering the cyclic resistance significantly (Castro, 1975). Freezing techniques have been shown to preserve the strength characteristics of a soil (e.g. Yoshimi et al., 1994) provided that care is taken during both freezing and thawing.

2.4.3.7 Estimation of the Residual or Liquefied Strength

Many studies regarding the strength of sands during liquefaction have been carried out and it is an important parameter in assessing the consequence of liquefaction. However, the problem currently under consideration is more concerned with the triggering of cyclic liquefaction or cyclic mobility and the residual strength is not a major

concern. A detailed discussion of this topic is therefore outside the scope of this review and only a few salient points will be briefly discussed herein.

The residual or liquefied strength of sands is applicable only to flow or limited liquefaction responses that reach a minimum strength. It is important to note however that a liquefied soil does have a non-zero strength. If the soil is in a very contractant state such that it contracts directly to steady state, then the steady state strength can be used as the residual strength. The steady state strength can readily be determined from laboratory testing. More commonly however sands do exhibit dilation prior to steady state (Vaid and Chern, 1985; Ishihara, 1993) and the residual state is associated with a quasi steady state. Quasi steady state has been shown to be dependent on soil fabric, loading direction and anisotropy (e.g. Vaid and Chern, 1985; Yoshimine et al., 1999; Sivathayalan and Vaid, 2002). These effects can be very difficult to reproduce accurately in the laboratory and therefore, there are many empirical correlations proposed between various in-situ tests and the minimum liquefied strength.

Many researchers have proposed correlations between SPT blow count or CPT tip resistance and the liquefied or residual strength (e.g. Seed, 1987; Seed and Harder, 1990; Stark and Mesri, 1992; Davies and Campanella, 1994; Yoshimine et al., 1999). The relationships vary due to differences in case histories used to develop them, differences in methods for selecting representative values and differences in methods for back calculating the strength. Some researchers appear to have chosen average penetration resistances (e.g. Seed, 1983; Seed and Harder, 1990; Olson and Stark, 2002) and some have suggested that it may be more appropriate to use lower percentile values (Olson and Stark, 2002). Residual strengths have also been back calculated based on the pre-failure geometry or the post failure geometry with or without consideration of the inertial forces occurring during failure. Theoretical relationships between penetration resistance, and the liquefied strength ratio have also been proposed by Jeffries et al. (1990), Stark and Mesri (1992) and Ishihara (1993). However, field data tend to fall below these theoretical lines (Jeffries et al., 1990; Ishihara, 1993).

Yoshimine et al. (1999) indicate that depending on the details of failure, back calculating the strength based on the final geometry could be conservative or unconservative. If the entire slide occurred in an undrained state and in such a manner that when the driving stress equaled the liquefied strength inertia forces were still acting, then the final angle of repose would be shallower than that required to mobilize the liquefied strength and using post failure geometry would be conservative. If however there was some drainage during sliding or if the soil began to harden at high strains, the final slope attained would be controlled by a strength higher than the liquefied strength and the back calculated strength from the post-failure case history would be higher than the minimum strength of the material.

Methods of accounting for inertial effects include Newmark type deformation analyses (e.g. Seed, 1983) and analyses incorporating kinetics (e.g. Olson and Stark, 2002). The latter method is based on Newton's laws of physics, accounting for acceleration and deceleration during failure. The liquefied strength is mobilized during failure when the velocity is at its maximum and not necessarily reflected by the final geometry. To be explicitly exact, such a method should also incorporate the effects of any changes in strength properties with strain and drainage.

The residual strength can also be determined from monotonic undrained laboratory tests. These tests are common and will not be discussed further. It has been suggested however that residual lab testing often yields higher residual strengths than those back calculated from case histories (Japanese Geotechnical Society, 1998). Poulos et al. (1985) suggested a method of determining the steady state strength of purely contractive sands from measurement of the in-situ void ratio and laboratory testing based on tests carried out on both reconstituted samples and undisturbed samples. Triaxial tests on loose, reconstituted samples with representative grain shape are used to determine the steady state line. The undisturbed specimens are then consolidated to stresses greater than those in-situ to increase the contractive behaviour and to likely reduce sampling effects. Triaxial tests are carried out on these samples to determine the steady state strength at the various consolidated void ratios. The steady state strengths may lie above, below or on the previously determined steady state line depending on differences in grain size distribution between samples. The in-situ strength is then corrected for based on the in-situ void ratio and the slope of the steady state line from the reconstituted samples.

The correlations between penetration resistance and residual strength and the laboratory procedures suggested by Poulos et al. (1985) do not indicate what type of disturbance would be required to trigger liquefaction nor how quickly the material would loose strength. Indications of triggering requirements could be obtained from cyclic tests described previously while monotonic testing would tend to indicate the brittleness and change in strength with strain.

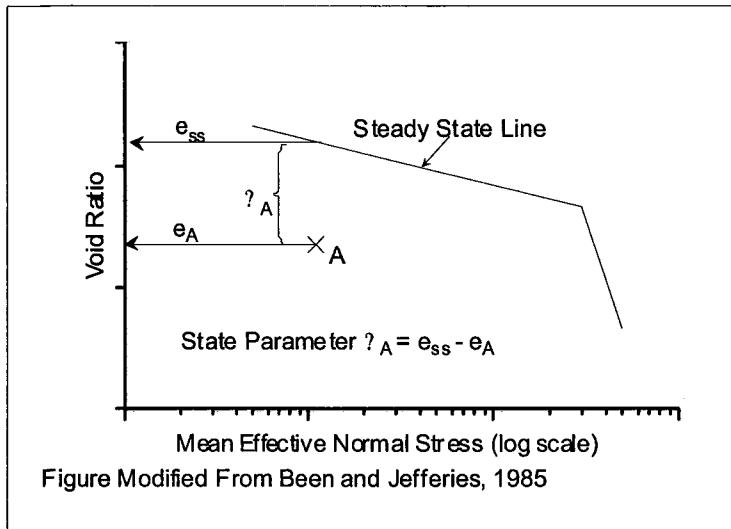


Figure 2.1 Steady State Line and Definition of Soil State Parameter

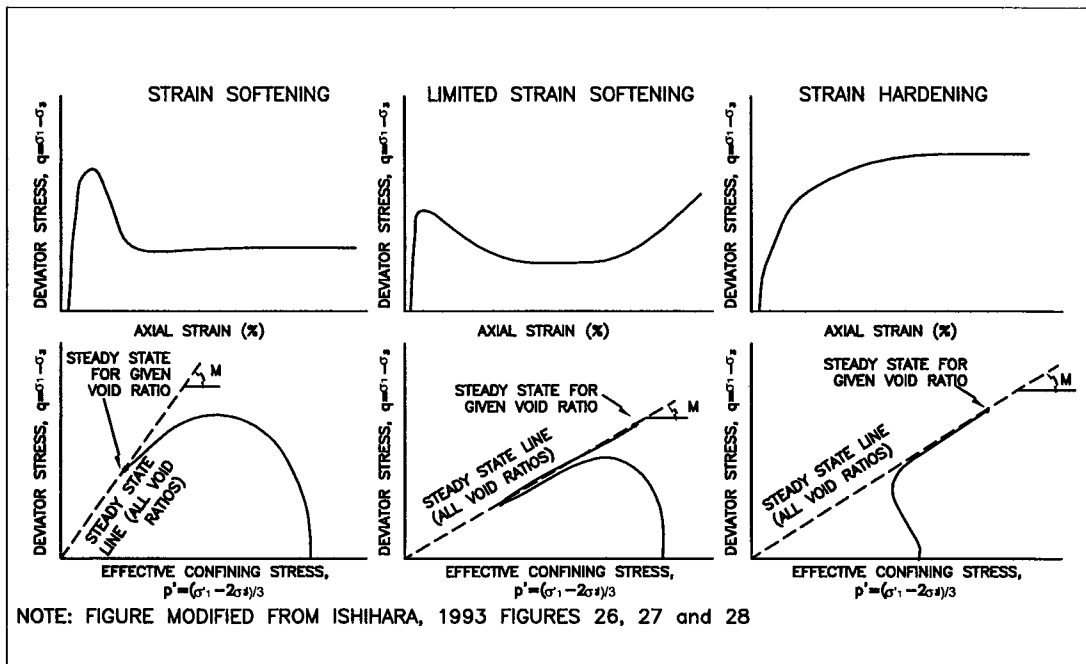


Figure 2.2 Typical Sand Responses to Undrained Monotonic Loading

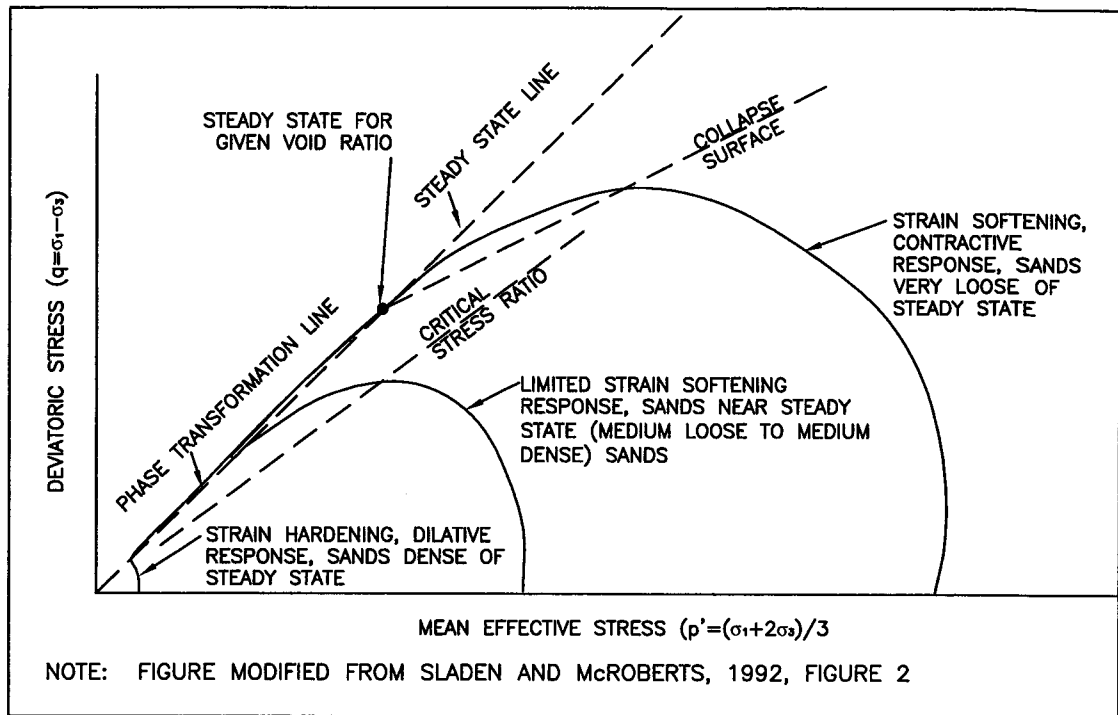


Figure 2.3 Monotonic Undrained Stress Paths for Sands and Proposed Interpretation Lines

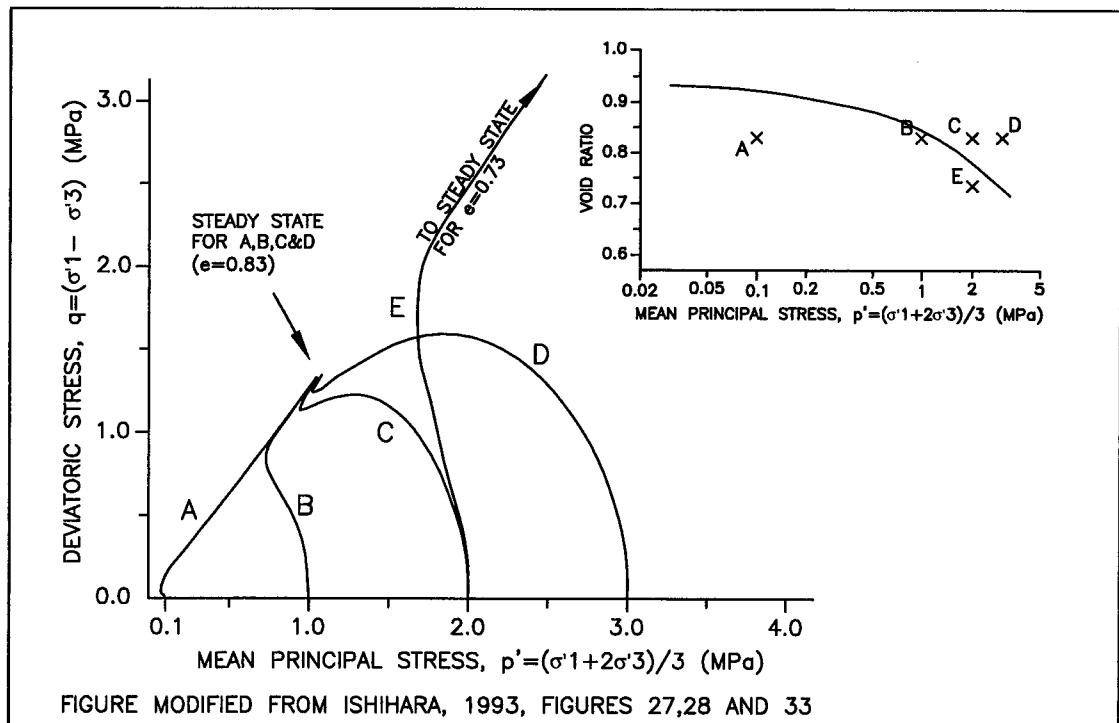


Figure 2.4 Variation in Sand Response to Monotonic Load with Changes in Stress and Void Ratio

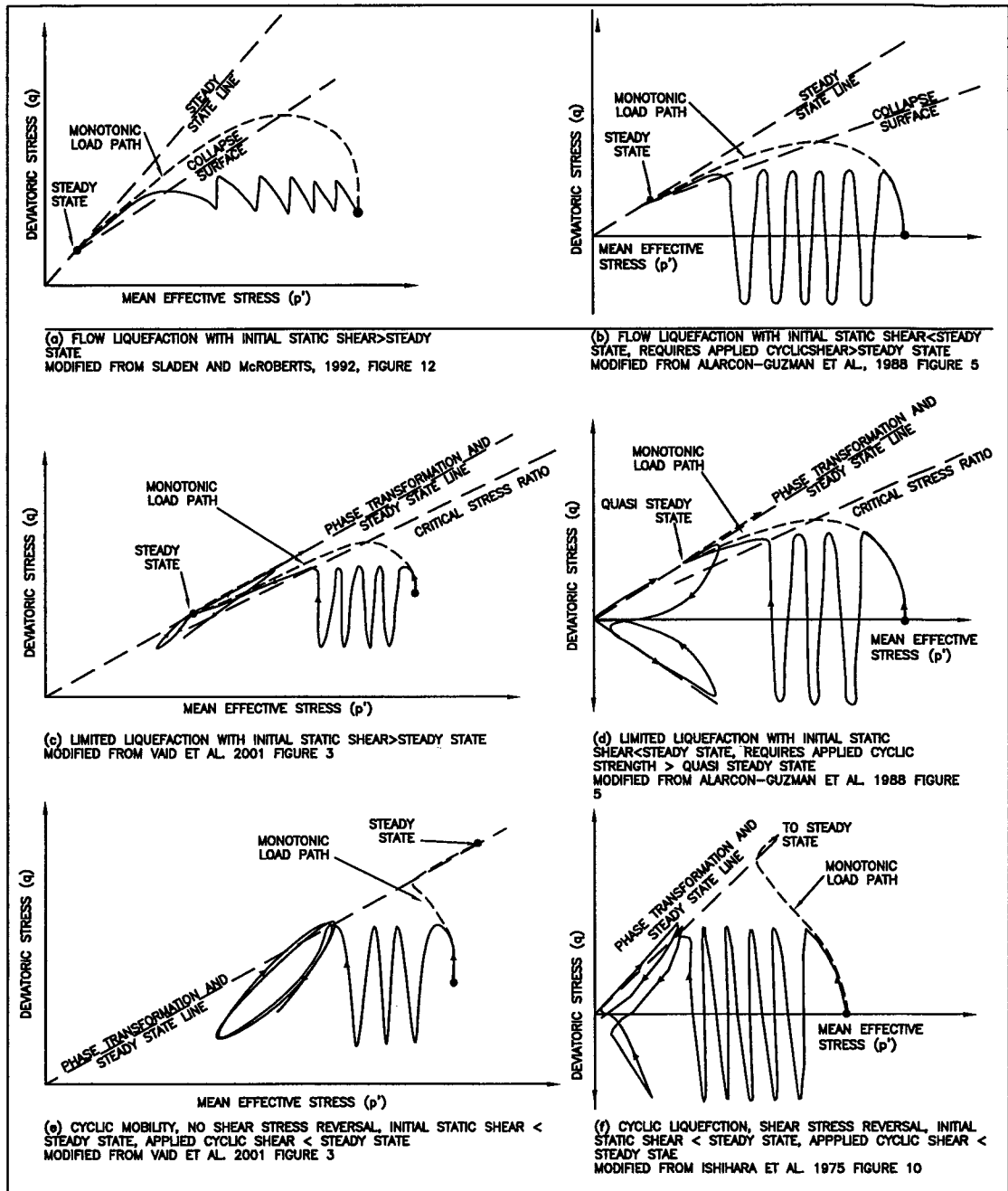


Figure 2.5 Range of Responses for Sand Subjected to Cyclic Loading

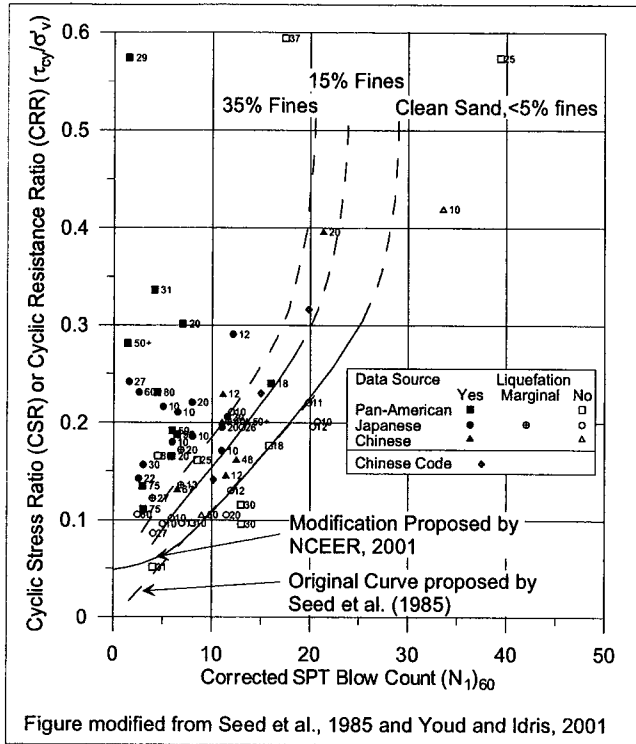


Figure 2.6 SPT Blow Count Cyclic Resistance Ratio Relationship

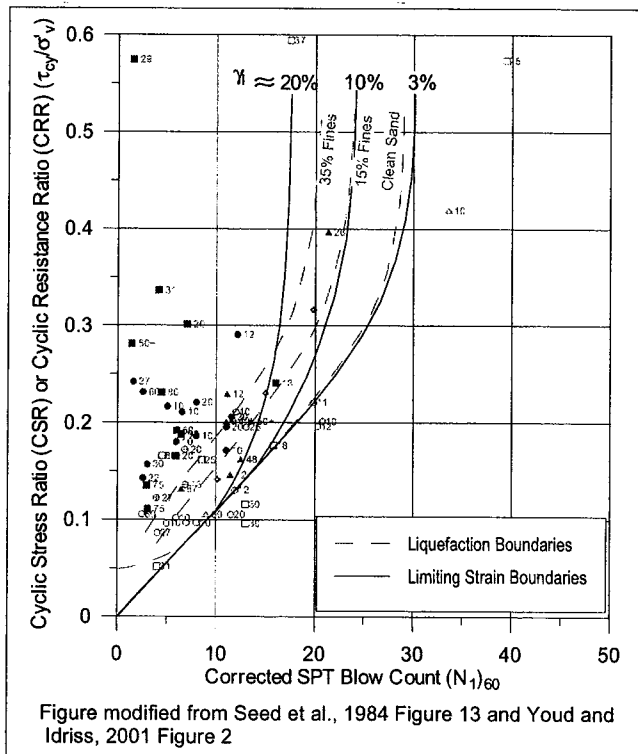


Figure 2.7 Limiting Strains for SPT Cyclic Resistance Ratio Relationship

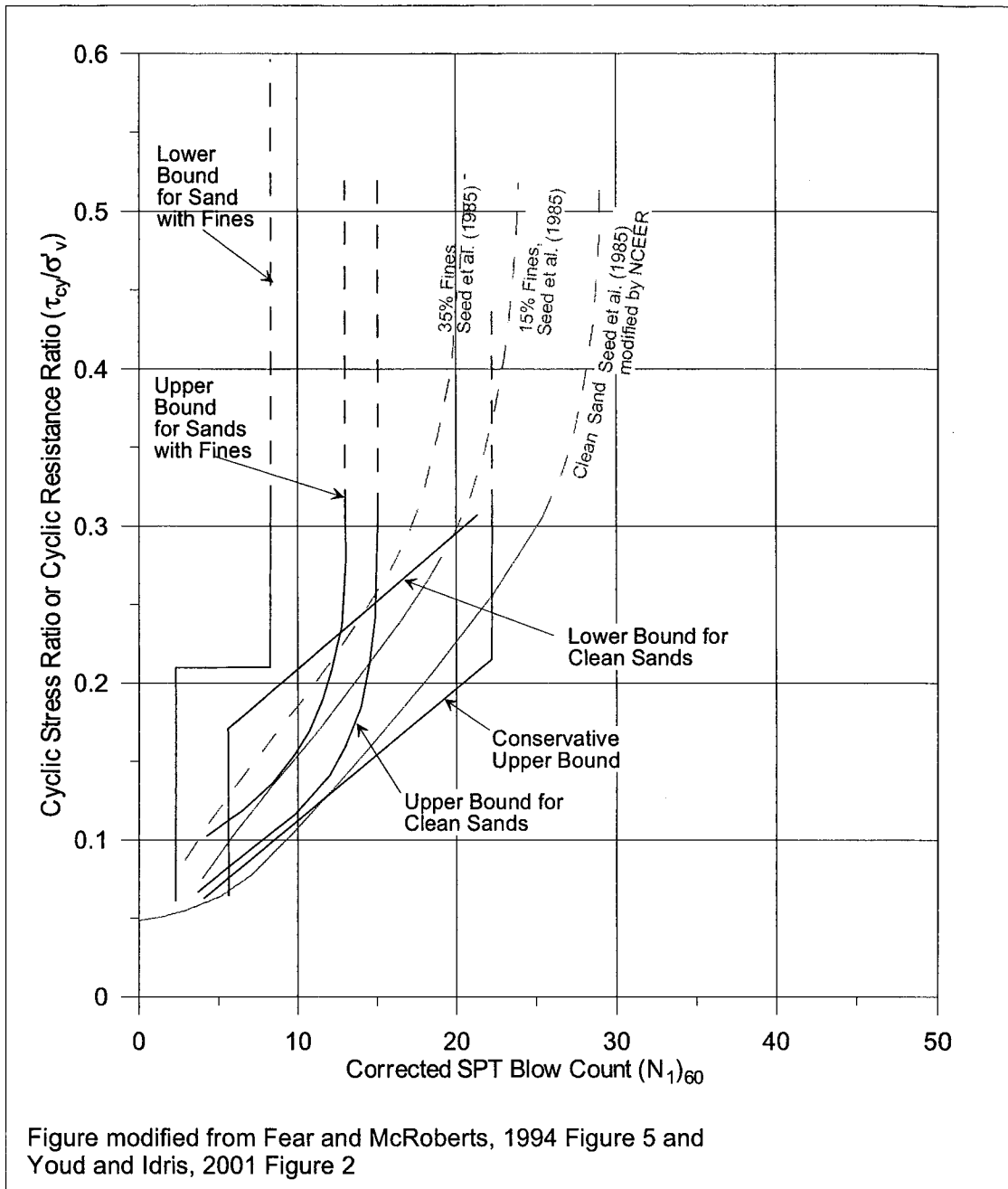


Figure 2.8 SPT-Cyclic Stress Ratio as Re-evaluated by Fear and McRoberts (1994)

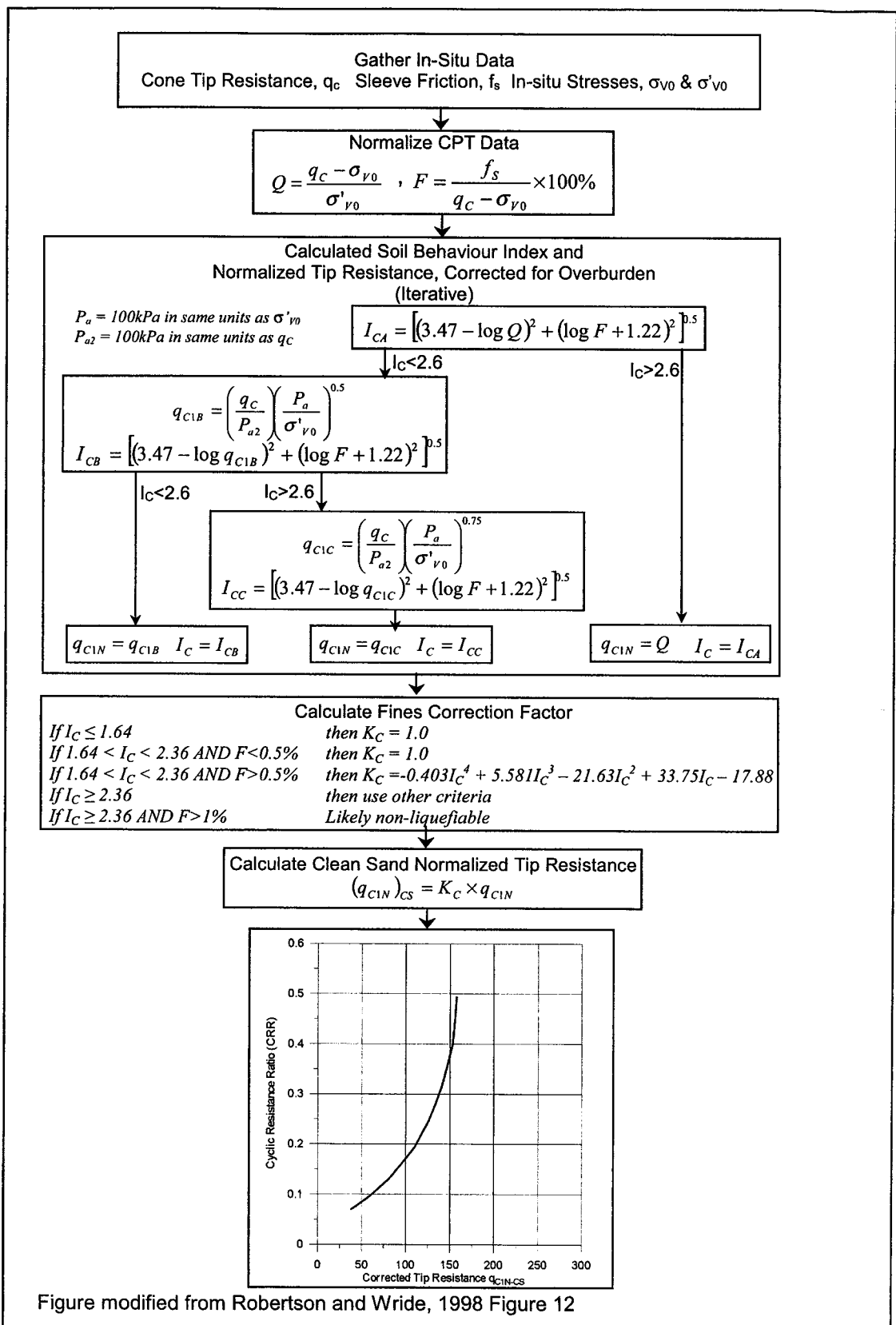


Figure 2.9 CPT Liquefaction Evaluation Procedures

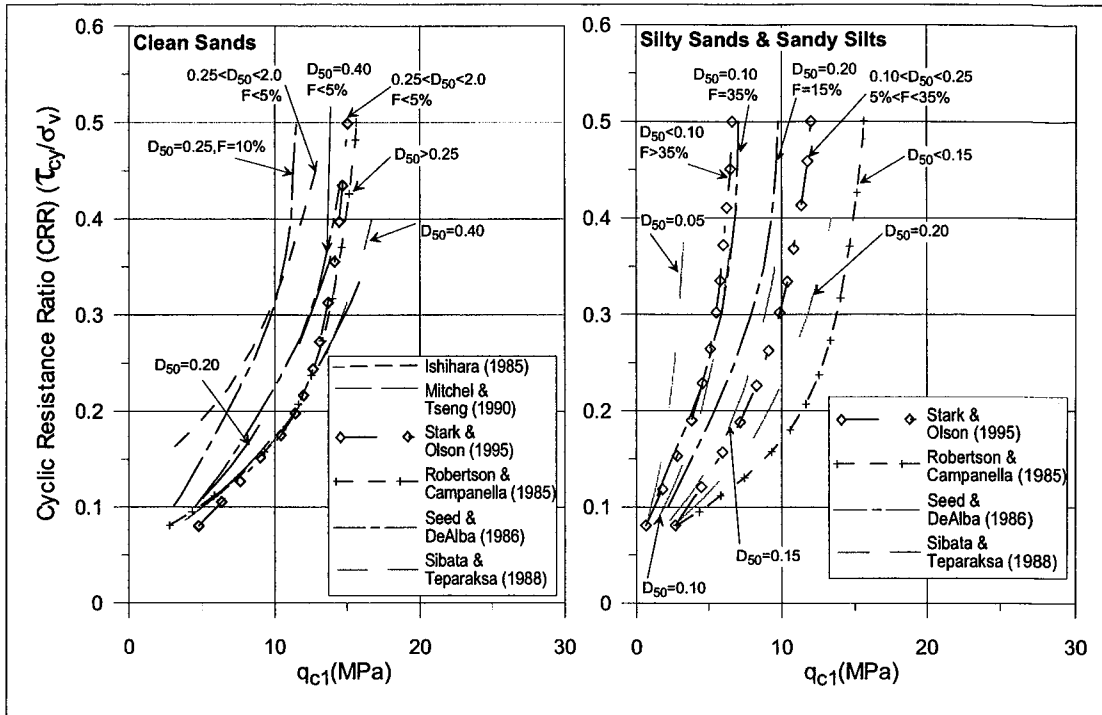


Figure 2.10 CPT Cyclic Resistance Ratio Relationships

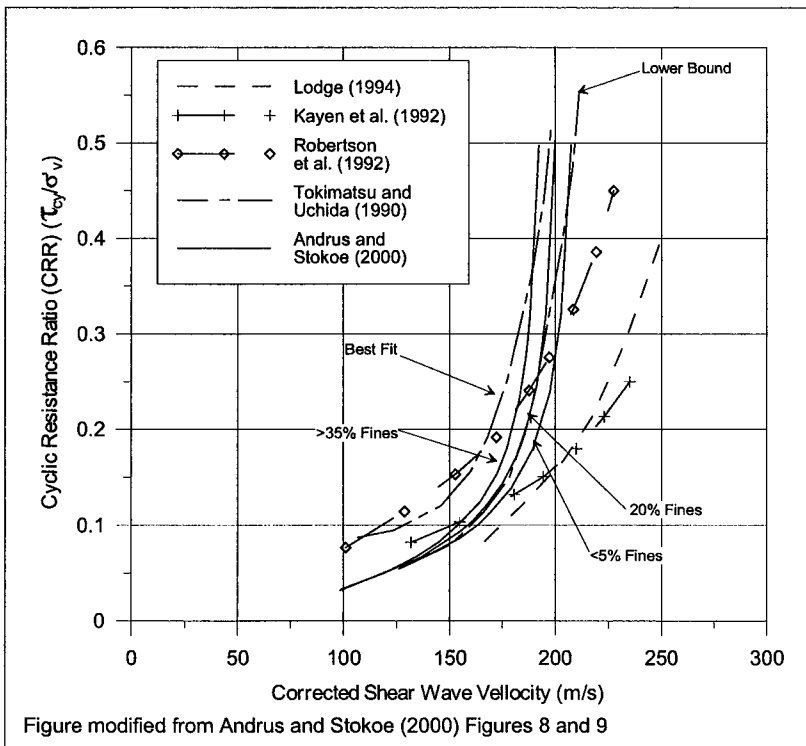


Figure 2.11 Shear Wave Velocity Cyclic Resistance Ratio Relationships

3.0 FIELD PROGRAM DESCRIPTION

3.1 General

The main objective of the field program was to recreate the observed softening of dense beach above water (BAW) tailings deposits under realistic loading conditions and to monitor the soil response in order to explain the behaviour. The proposed hypothesis under investigation was that vibrations from surface equipment triggered cyclic liquefaction of the BAW tailings near the ground surface. The low confining stresses near the ground surface would lead to stress reversal as a result of the vibratory loading imposed by the equipment, thereby allowing pore pressures to increase, causing a state of essentially zero confining stress. A test site was created at Syncrude's facilities in an area identified as problematic because of the softening phenomenon to either confirm the hypothesis or identify an alternative explanation. The area was instrumented and then common construction and reclamation equipment was driven back and forth over the test area while the response of the instruments was monitored. Multiple equipment passes were used rather than stationary equipment because it was thought to be easier to interpret the number of loading cycles under this type of loading and in general seemed to simulate operating conditions more realistically. Analyses and interpretation of the data gathered on site was intended to form the bulk of subsequent research. It was initially intended to carry out several tests at different instrumented sites with different types of equipment to attempt to understand and possibly quantify the effects of variations in initial conditions. Difficulties encountered on site, however, precluded this and only one main test site was instrumented although several different loading conditions were applied.

In order to implement a successful field program, tailings characteristics likely to influence the ground response were identified so that a representative site could be selected and appropriate response parameters could be monitored. The selection of the site and the parameters measured will be discussed in detail in subsequent sections. A detailed description of the field program and procedures used during testing as well as a presentation of the data gathered on site will then follow.

3.2 Site Selection

The Southwest Sand Storage Facility at Syncrude had been identified by Syncrude as a favourable test area for the field program. It was a large area of BAW tailings considered to be typical of the BAW tailings at Syncrude. The facility would not be rendered unsafe by the softening of one small test area and there would be no disruption to tailings placement due to the field program. Also, future reclamation of the Southwest Sand Storage had been identified as potentially difficult because the trafficability of a large portion of the area is expected to be compromised by the softening phenomenon (Syncrude, 2002).

The Southwest Sand Storage Facility is located approximately 10 km southwest of the plant site (see Figure 3.1) and has been receiving tailings since 1991. The facility was developed to store the majority of the coarse tailings produced over 25 to 30 years, with the released fine tailings and process water collected in an internal sump and returned to the Mildred Lake Settling Basin. It has an estimated storage capacity of 750 Mm³ at a height of 40 m and possible expansion to 1000 Mm³ at a height of 60 m (Syncrude, 2003). Until 1993, the structure was constructed using contained beaching techniques

with an external sump used until upstream construction was possible and an internal sump could be developed. The external sump was then used for seepage control. Following 1993, berms were constructed to constant elevations through contained beaching as required, allowing tailings to be deposited by overboarding (List and Lord, 1996). Deposition has been from three tailings lines, each 600 mm in diameter with tailings being deposited on an existing beach as BAW deposits. No filters were installed during the construction of the Southwest Sand Storage Facility (Syncrude, 2003) but recently a filter drain was installed along the east toe of the structure to control seepage in preparation for the expansion of an overburden dump which will eventually buttress the Southwest Sand Storage Facility in this area (Syncrude, 2002). The current configuration of the Southwest Sand Storage Facility is shown in Figure 3.2.

At year-end 2002, the total volume of sand deposited in the Southwest Sand Storage Facility was approximately 287 Mm³ and the volume of mature fine tailings stored in the internal sump was 39.2 Mm³. Tailings deposition has been largely through Lines 3 and 4, consisting of coarse tailings from the cyclone underflow with some contribution from the cyclone overflow tailings Line 5. The latter contains higher fines content, but does not appear to significantly contribute to the total volume of tailings discharged. The discharge locations appear to have been moved fairly regularly with deposition of coarse tailings in Cells 31, 34, 48, 49 and 51 during 2001 and in Cells 46 to 51 and 34 to 36 during 2002. Cyclone overflow tailings were deposited on the Cell 51 beach. The facility has not been raised since 2000 and currently has a maximum elevation of 393.6 m in Cell 31 in the northeast portion of the facility, which corresponds to a maximum tailings thickness of 42.6 m (Syncrude, 2003).

The Southwest Sand Storage Facility was initially visited in August 2002 by the author with four general areas being traversed on foot. The south edge and southeast portion of the site were discarded as possible test areas due to extremely poor trafficability, recent deposition and apparently high phreatic surface. The northeast portion of the Southwest Sand Storage Facility was identified as a potential test area with reasonably competent BAW deposits. The west crest area was also identified as a possible test area because of uniform conditions and competent BAW tailings, but it had a relatively short beach. A second visit to the Southwest Sand Storage Facility was carried out in mid-September, 2002 and the northeast portion was recommended by Syncrude personnel as a test area due to ease of accessibility, safety, age of deposit, and previously observed softening behaviour.

Cells 31, 32 and 33 appeared to be a promising test area because the tailings beach in this area was relatively long with a uniform slope and the tailings had been deposited some time previously. The tailings possessed some degree of trafficability, enabling work to be carried out in the area without causing significant disturbance of the test area prior to loading. Also, there had been previous tests carried out in the area as part of Syncrude's trafficability study (Syncrude, 2002), allowing information to be incorporated and compared between studies. Accessibility to the site was also a major factor in site location; Cells 31 and 32 were close to the main access road to the Southwest Sand Storage Facility and were easily accessible without having to cross any pipelines or drive for great distances along the crest of the tailings embankment. Cell 31 also had a significant number of standpipe piezometers installed in the tailings, particularly in the downstream toe area but also with several in the upper beach area, which would help in understanding the groundwater conditions.

The exact test location was selected based on local topography. The site was selected so that it was not situated in a local low spot to avoid the complication of upward gradients, in an area with fairly uniform slope (approximately 1 to 3 percent), and free from any obviously significant concentrations of bitumen. The distance from the crest to the test site was selected based on light trial loading in similar, adjacent areas in an effort to locate the test site in an area that could be softened with the use of light equipment. It was intended that this area would be softened with the use of light equipment as a test of the instrumentation and procedures. A second site, closer to the crest was then to be used for heavier equipment loading. Complications arose on site however, and only one test site could be used. The main test site, shown on Figure 3.3 was located at N47899, E42815 on the Syncrude Mine Grid (N6317253, E0454583 in UTM coordinates), approximately 230 m from the crest, and 700 m from the pond in Cell 31 of the Southwest Sand Storage Facility.

At the time the site was selected on Friday, September 20, 2002 no tailings were being actively deposited near the site. However, on Monday September 23, 2002, tailings were being deposited from a pipeline in Cell 51 to the north of the test area and a fresh stream of tailings was running towards the pond, in a roughly south to southwesterly direction, approximately 30 m upstream (towards the pond) of the test area. During the field program, tailings deposition occurred only on Monday, September 23.

3.3 Parameters Measured

3.3.1 General

Based on the review of liquefaction literature presented in Section 2.3.5, there were a multitude of factors that could influence the liquefaction or cyclic mobility behaviour of the granular deposit at the Southwest Sand Storage Facility. The ease with which these factors could be measured in the field varied greatly and therefore only certain parameters that were deemed critical to identifying the behaviour were selected for measurement.

To be classified as cyclic liquefaction or cyclic mobility, a deposit has to be dense or dilative, exhibiting strain hardening behaviour at large strains. The difference between the two behaviours according to the CANLEX definitions (see Section 2.2) is whether or not shear stress reversal and zero effective stress occur. The density, void ratio or initial state of the deposit, the change in pore pressure during and after loading and the cyclic stresses or vibrations applied during loading were therefore identified as parameters that should be measured during the trials. Also the large extent of the affected zone was thought to possibly be the result of decreasing stiffness and load shedding during vibration loading and therefore stiffness was identified as a potential parameter to be monitored. As with any geotechnical field investigation, classifying and characterizing the deposit was particularly important. However, unlike typical geotechnical field investigations, the properties of the BAW tailings near surface, in the upper several meters were the main focus in this study as the softening phenomenon was reported to occur at a fairly shallow depth. Deposition history in the test area was also studied to estimate the age of the deposit. Potential methods for measuring these parameters and the selected methods are discussed in the following sections.

3.3.2 Material Type and Variability

Material type can be assessed directly based on visual classification of a soil sample, laboratory testing, or indirectly from empirical correlations applied to in-situ test data. Common methods of retrieving samples are digging test pits and drilling boreholes. Drilling typically requires fairly heavy equipment and is in general not economical for shallow investigations. Cone Penetration Tests (CPTs) are a common method of indirectly assessing soil type. Cone tip and friction resistance are measured and are correlated to material type through empirical relationships. A light-weight, manually operated CPT system was available for use in the field program. This system was not expected to penetrate the deposit to great depths (i.e. greater than 5 m) but it was expected that it could penetrate the upper 2 to 4 m of the deposit. Two methods were thus identified for general classification of material type and variability: test pits and CPTs.

Test pits provided samples with which to confirm the CPT results and also permitted measurement of the phreatic surface. The use of the CPT also had the advantage that a significant amount of past testing on BAW tailings deposits at Syncrude has allowed development of correlations between CPT measurements and a variety of parameters. For example, relationships between CPT and relative density and state parameter also exist and could be used to determine the in-situ state conditions at the test site. These relationships, however, have often been found to have a fairly large scatter and are not always accurate (e.g. Wride et al., 2000).

3.3.3 Density and Void Ratio

There are essentially two main approaches to measuring the density or void ratio of a deposit: retrieval of an undisturbed sample with subsequent measurement of density and void ratio in the laboratory or in-situ measurement. It is well known that it is difficult to obtain an undisturbed sand sample (e.g. Marcusson III and Franklin, 1980; Seed et al., 1982; Tokimatsu and Hosaka, 1986). Common methods of undisturbed sand sampling involve thin walled tube sampling or some type of piston sampler. Konrad et al. (1995) also reported success using a Laval sampler to retrieve a high quality sand sample. In general, these methods of sampling are carried out using drill rigs, which was not practical for this field program.

Ground freezing is generally considered to be the best way of obtaining undisturbed sand samples. The main concern with retrieving frozen samples is that water expands by nine percent of its original volume during freezing. Thus it is important that water be able to escape freely ahead of the freezing front to prevent changes to the soil structure during freezing. Care is also required if the samples are to be thawed without disturbance. Typically ground freezing is expensive and requires extensive support equipment, however, several relatively simple and inexpensive methods of obtaining shallow depth frozen samples were identified. Two methods of retrieving frozen samples from surficial deposits have been used at Syncrude with reasonable success (HBT AGRA, 1992). As part of an investigation for the design of an in-pit dyke system, frozen block samples were gathered by placing a slab of dry ice, covered in insulation and wrapped in plastic, on the ground surface and allowing freezing to occur for 24 hours producing blocks of frozen soil several cubic feet in size. Frozen tube samples were also gathered by inserting a greased, thin walled tube into the ground, excavating around the tube and placing dry ice in the hole around the tube to freeze the sample

(HBT AGRA, 1992). Yoshimi et al. (1977) developed a similar method of obtaining a frozen sample. They inserted a thin walled tube in the ground, excavated the material from inside the tube, sealed the bottom, and then circulated liquid nitrogen in the tube, freezing the surrounding soil radially outward from the cylinder allowing a frozen sample to develop around the tube. They then carried out laboratory tests to validate their method and found that there was significantly less straining due to freezing during radial freezing than during vertical freezing. They found that adjacent to the tube the sand was affected by the insertion of the tube but that it was possible to obtain an undisturbed sample in the outer portions of the sample provided the sample was large enough (they retrieved samples that were 15.5 cm radially thick). They also noted that the size of the affected zone adjacent to the tube decreased with increasing density of the deposit. Based on this, it was decided to collect frozen block samples and frozen cylindrical tube samples using the Yoshimi et al. (1977) method both before and after softening to measure any changes in density as a result of softening.

Sand cone or water replacement methods are more conventional methods used to measure in-situ density of surface deposits. Essentially these methods involve gathering a sample of a known volume and measuring its mass and water content, allowing calculation of the in-situ density. These methods are of limited use in saturated granular deposits however, because saturated granular deposits tend to slough when excavated and therefore it is difficult to accurately determine the volume of the material gathered. It can also be difficult to collect representative moisture content samples if there is a significant amount of free water. A similar method, using a cylinder instead of a cone to gather a sample of known volume, was selected for determining the density at the test site if conditions allowed but it was not planned to be used extensively as collecting the samples caused significant disturbance of the test area, and was cumbersome and time consuming.

For rapid measurements of in-situ density of surface deposits, nuclear gauges are commonly used. These gauges emit a known amount of radiation from a probe that is inserted into the soil and measure how many of the radioactive particles reach the receptor on the ground surface. The measurement at the receptor is then correlated to bulk density and moisture content. Generally, as the amount of radiation that reaches the receptor decreases, the bulk density and moisture content increase. The measurements are limited in depth by the maximum extent of the probe and tend to sample a smaller volume of material with depth so that the results are somewhat biased towards the conditions in the top portion of the deposit. These gauges measure hydrogen content in order to determine moisture content and therefore the measurements can be affected by the presence of organics. Significant bitumen concentrations in tailings deposits can also affect nuclear readings. Generally however, provided that the bitumen is included in the fluid phase, the readings from nuclear gauges agree with other measurement methods (Lord and Cameron, 1985). Nuclear moisture-density gauges are commonly used at Syncrude and in other construction operations as a measure of in-situ density to monitor compaction performance and since the behaviour was expected to be shallow, it was considered a reasonable method with which to measure density. The speed of testing with this method also allowed for density measurement at frequent intervals during loading.

3.3.4 Pore Pressure

The initial pore pressures at the test site were expected to be fairly low because of the relatively shallow depths and, similarly, at shallow depths the increments of pore pressure change due to loading could potentially be quite small. Also, if there were any type of cyclic pore pressure response to loading then the measurements would have to be made continuously in small time intervals in order to capture the response. Accurate, rapid, and continuous measurement of small pore pressures was therefore required in order to detect any cyclic response. These requirements negated the use of standpipe piezometers due to their long response (lag) time and requirement of manual measurement. Vibrating wire and pneumatic piezometers are often used when more rapid responses are required, but in general rapid monitoring of these types of piezometers is expensive. It was therefore decided that electrical pore pressure transducers would be the best way of monitoring the pore pressures as they also required little fluid movement, and thus had a short response time, and could be monitored by a readily available data acquisition system.

3.3.5 Stress

Another parameter identified as important to measure was the stresses induced in the ground due to loading since applied stresses lead to the generation of any excess pore pressure. Furthermore, any modelling of the behaviour would require some type of input stresses to trigger a response. Estimating the stresses due to vehicle loading is very complex and was therefore deemed impractical for the problem under investigation. The total cyclic stresses applied to the soil from vehicle loading are a combination of the dead weight of the vehicle, the cyclic loading of the vehicle passing by, vibrations from the various components of the vehicle, stress concentrations from local protrusions on the tracks of the equipment, and a host of other variables. A brief review of literature related to compaction and to ground vehicle theory was carried out with little relevant data identified. Apart from simple elastic theory based on the spreading of dead weight the more elaborate models required extensive and largely unknown input data (e.g. Raoer and Erbach, 1990, Seed and Duncan, 1986, Schmid, 1995). In-situ measurement of stresses, although somewhat difficult, was thus identified as the best method for determining the applied stresses.

It is in general quite difficult to measure the in-situ stress state directly. There are issues regarding the relative stiffness of the load or pressure cell and the soil deposit and also there is significant disturbance of the soil mass during installation. Blunden et al. (1992) developed a recording system for measuring in-situ soil stresses due to traffic using earth pressure cells; however, the system was very expensive and required a great deal of electronic equipment. A single earth pressure cell was readily available during the field test, however with only one load cell it is not possible to completely define the in-situ state of stress, so it was decided to use the earth pressure cell as a secondary stress measurement device. The main stress measurements were instead made indirectly using a seismograph. From the theory of elasticity, dynamic stresses, both shear and normal, can be related to particle velocities. Hryciw et al. (1990) also used a relationship between peak particle velocity and shear stress to determine the cyclic shear stress induced in a soil and evaluate its liquefaction susceptibility. Furthermore, it is standard practice in earthquake engineering to measure soil or rock acceleration (which is just the derivative of velocity) to determine induced stresses. It was therefore

decided to measure particle velocities by using a seismograph and calculate the induced stresses.

3.3.6 Stiffness

A common method of measuring the in-situ stiffness modulus of the soil is the use of a pressuremeter. This was not an option due to equipment requirements and also pressuremeters are not often used at shallow depths and would likely not be sensitive enough to accurately measure properties at say 1m below ground surface. The shear wave velocity of a deposit is related directly to the small strain shear modulus, which in turn is related to the elastic modulus of the deposit. A common method of measuring the shear wave velocity is to use a seismic cone or to insert a receiver down a borehole, however the required equipment was not available. From previous extensive testing carried out as part of the CANLEX project, relationships between CPT tip resistance and the shear wave velocity for Syncrude tailings have been developed (Wride et al., 2000) and this was determined to be the most feasible method of estimating the in-situ stiffness modulus.

3.4 Equipment and Procedures Used

3.4.1 General

Specific equipment and instrumentation used during the field test and site characterization are discussed in the following section.

3.4.2 Cone Penetration Testing

The CPT equipment was provided by GeoForte Ltd. The cone was very similar to reference CPT equipment that has a 60° angle, a 10 cm² base area and a 150 cm² friction sleeve (Lunne et al., 1997) and was able to measure pore pressure. The cone and sleeve had a diameter of 35.66 mm and their lengths were 35.60 mm and 131.15mm, respectively. These dimensions correspond to a cross-sectional cone area of 9.99 cm² a sleeve surface area of 146.93 cm², slightly less than the international standard of 10 cm² and 150 cm² respectively. The pressure transducers were all electrical strain gauge load cells. The friction and tip resistance load cells were arranged as a subtraction type cone such that the tip resistance is measured by a load cell in compression while the sleeve friction load cell, also in compression, located farther up the instrument measures both cone resistance and sleeve friction. The sleeve friction is thus calculated by subtracting the second reading from the first. The filter for pore pressure measurement was located behind the cone tip in the "u₂" (Lunne et al., 1997) location in the gap between the sleeve and cone.

The various pressure cells in the cone were connected to a Data Dolphin data logger, in turn connected to a battery for constant voltage supply, which was programmed to take readings every three seconds. The data acquisition equipment is discussed in Section 3.4.4.

The CPT pushing frame consisted of a rectangular metal frame, approximately 2m tall, 1m long and 0.15 m wide, with a head plate fitted with a pipe vise that guided and pushed the rods into the ground as shown in Figure 3.4. The head plate was connected to a chain on each side and the chains were connected to gears, driven by a manually

operated pulley type system located on the outside of the frame. The frame was connected at its base to a beam running perpendicular to the frame. Weight placed on the beam provided the reaction force during pushing.

3.4.3 Pore Pressure Transducers

A typical push in electric piezometer used during the field program is shown in Figure 3.5. The piezometers were selected based on appropriate range, sensitivity and ability to be installed by a hand-operated system. They were manufactured by ConeTec and contained standard electrical resistance strain gauge pressure transducers which essentially monitored the deflection of a thin membrane due to changes in pore pressure. The pressure transducers had a range of 172 kPa (25 psi or roughly 17.5 m of water) with a sensitivity of ± 0.15 kPa (0.05 feet or 1.5 cm of water) and measured absolute pressure (i.e. they are sensitive to changes in atmospheric pressure and can measure small negative pore water pressures). The disc shaped metal transducer was approximately 20 mm in diameter and was located inside a plastic cylinder with an outer diameter of 27 mm. Four holes spaced equally around the circumference of the plastic cylinder were located just below the transducer to allow direct interaction between the transducer and the pore water. A porous plastic cylinder, 100 mm in length with an outer diameter of 33.7 mm fitted over the plastic cylinder extending approximately 5 to 10 mm below the transducer, covering the holes in the plastic cylinder, seated against a lip in the plastic cylinder at its upper end. Three meters of cable extended from the transducer passing through the plastic cylinder. Just below the porous plastic, the plastic cylinder was threaded to allow a metal conical tip to be added for installation. The metal pushing cone was approximately 50.8 mm in diameter and 44.5 mm in length (49° tip angle, relative to a vertical axis). A metal cable was secured in a groove around the pushing tip to aid in retrieval of the instruments upon completion of the field test.

3.4.4 Data Acquisition

Data gathered by the CPT and piezometers were monitored using Data Dolphin data acquisition units. These units have 4 standard inputs channels, 8 precision inputs channels and 3 frequency based inputs. The standard inputs record voltage, counts or a simple on-off status with 10 bits of precision. The 8 precision inputs each have an extra 16 bits of precision for a total of 24, which allow voltage measurements down to 90 nanovolts (Optimum Instruments, 2002). During the field test, only precision input channels were used. The data recorded by the Data Dolphin units was stored on an erasable memory chip. Each record was time-stamped and stored in the card in a normalized database fashion that allowed different inputs to be turned on and off without restarting the Data Dolphin.

The Data Dolphin units were designed to operate in the field. The operating temperature ranges is from below -40°C to over 75°C and all of the inputs have static protection. Power can be supplied internally from three "C" sized batteries, or externally from a 12 V battery or a 120 V AC power source (Optimum Instruments, 2002). During the field tests, all units were connected to external batteries and the input power voltage was monitored throughout testing. The minimum recording interval (i.e. highest recording rate) of the Data Dolphin was found to vary somewhat during the field program ranging from 3 to 5 seconds.

3.4.5 Particle Velocity Monitoring

A seismograph was used to measure particle velocities during testing. A Blast Mate Series III unit was selected for its ability to monitor particle motion in three directions, thus defining completely the particle motion, and for its ability to carry out relatively long term monitoring. The unit had four monitoring channels, three that monitored geophones and one that monitored a microphone. The three geophones were mounted in orthogonal directions to measure transverse, vertical and longitudinal ground vibrations. The geophones were housed inside a short metal cylinder, the upper and lower edges of which were in the plane of the longitudinal and transverse geophones, with an arrow pointing in the direction of the longitudinal geophone and the whole assembly was referred to as a transducer. On the base of the transducer there were 3 threaded holes used to attach ground spikes for installation on soft ground. The geophones had a 2 to 300 Hz frequency response and two possible ranges with maximum peak particle velocities of 31.7 mm/s or 254 mm/s. The cable between the Blast Mate and geophone transducer was roughly 1 m long and is the main limiting factor in the depth location of the geophones.

The blast mate unit had a 960 kB memory, which allowed 307,200 readings to be stored. There were many options available in terms of how the data was recorded and how monitoring was initiated and terminated which determined the maximum length of data storage. Essentially however there were two main modes of monitoring ground vibrations, complete waveform recording or histogram recording, and three sampling rates: 1024 readings per second, 2048 readings per second and 4096 readings per second. When recording complete waveforms the unit would store all readings at the selected recording rate as well as the peak particle velocity, the frequency, the acceleration and the peak displacement recorded during monitoring. At the lowest recording rate, the unit could store 5 minutes of data in the complete waveform mode. The histogram mode was available for longer term monitoring. In this mode, readings were taken at the sample rate specified and the maximum positive and negative velocities and frequencies recorded by each channel as well as the peak vector sum would be stored at specified, constant intervals. Using this recording mode allows data to be collected over days rather than minutes. A combination of the two recording modes was also available.

3.4.6 Nuclear Moisture and Density Gauge

A nuclear moisture and density gauge that had been used extensively on site in the past was available at Syncrude and was used for testing during the field program. The gauge available was a Troxler, Model 3430, serial number 30512. It had a maximum rod depth of 300 mm. The rod contained a cesium-137 source and an americium-241:beryllium source. Radiation is emitted with the rod extended in the ground and the detector within the unit on surface records the amount of radiation that travelled through the soil. The cesium-137 source is used for density measurements and emits gamma photons that collide with electrons within the soil. The number of gamma photons that reach the detector on the ground surface is therefore related to the number of electrons in the soil. Since the number of electrons is related to the number of protons, which is related to the mass of the particles, the measurement can be related to bulk density. The americium-241:beryllium source emits neutrons that are slowed or thermalized when they collide with hydrogen. The detector on surface is sensitive only to thermalized or slow neutrons and therefore the amount of radiation it detects is a measure of the

amount of hydrogen atoms in the deposit (Troxler, 2002). As hydrogen is most commonly associated with water this allows measurement of the moisture content, however the presence of organic molecules, which are also hydrogen rich, can be misinterpreted as moisture. Nuclear gauges, therefore, interpret bitumen, which is a hydrocarbon, as moisture. It is common practice, however, to include bitumen in the fluid phase and therefore provided this is understood, the nuclear gauge readings agree with laboratory determined moisture plus bitumen contents (Lord and Cameron, 1985). In general however, the tailings at the Southwest Sand Storage were quite clean with little, if any, significant bitumen concentration.

3.4.7 Vibrating Wire Earth Pressure Cell and Piezometer

A vibrating wire earth pressure cell and piezometer shown in Figure 3.6 were also available for the field program. The earth pressure cell had a fluid filled sensing area 212 mm in diameter connected to a fluid filled line, 184 mm in length leading to a transducer. The sensing area and transducer were surrounded by a thin metal plate for protection and ease of installation. The vibrating wire piezometer was attached to the metal plate surrounding the earth pressure cell approximately in line with the transducer, 290 mm away from the centre of the earth pressure cell sensing area. The piezometer was 35 mm in diameter and therefore its centre was located approximately 18 mm above the sensing area of the earth pressure cell. Both instruments had a range of 345 kPa (50 psi). The instruments were connected to a Data Taker data acquisition unit capable of monitoring vibrating wire instruments for monitoring.

3.4.8 Loading Equipment

Three types of equipment were available for the loading stages: a small all terrain vehicle, a dozer and an excavator. The all terrain vehicle, a Triton Predator 4345, was the lightest vehicle available and is commonly used at Syncrude for transporting personnel and light equipment for instrumentation readings in softer areas. The Predator had eight wheels surrounded by rubber tracks approximately 45cm wide with a 165cm length in contact with the ground. The vehicle itself weighed approximately 1600 lbs (725kg) corresponding to a contact pressure of approximately 4.8 kPa. The predator was diesel powered with between 33.5 and 37.5 hp (25 to 28 kW). A John Deere 450G LGP (low ground pressure) dozer and a John Deere 792D LC excavator, with operational weights of 7,924 and 27,328 kg respectively, were available for heavier equipment loading, both of which were also tracked. The dozer tracks had ground contact areas approximately 61cm wide by 216cm long and the excavator tracks were approximately 80cm wide by 440cm long with average ground pressures of 29 and 38 kPa respectively. The dozer had up to 70 hp (52 kW) power and the excavator had up to 165 hp (123 kW) power.

3.5 Description of Site Activities

3.5.1 General

The field program was carried out between September 20, 2002 and September 26, 2002 at the Southwest Sand Storage area, part of Syncrude's facilities in Fort McMurray, Alberta. The weather during the field program was generally clear and cool with temperatures above freezing during the day but occasionally falling below freezing

overnight. Except for a few hours on the morning of September 26, 2002, there was no significant frost during the field program.

Field activities included a brief site reconnaissance to locate the exact test site, instrument calibration and installation, initial site characterization, loading of the test site, and post loading site characterization. Quick, light loading tests were also carried out to gather additional information. Additionally a short trafficability study was carried out for comparison with previous work. These activities are described in greater detail in the following sections.

3.5.2 Site Reconnaissance and Characterization

3.5.2.1 General

The northeastern portion of the Southwest Sand Storage Area, in which the main test site was located (see Figure 3.3), was visited three times, in August, mid September and at the time of the field program in late September. During the visits, general observations were made and during the field program, test pits and nuclear density and moisture content gauge measurements were made as part of site reconnaissance. It should be noted that the depth to the phreatic surface when determined by test pits was measured as the depth to free water in the tailings. After water was intersected in the test pit, conditions were allowed to equalize until there was no evidence of water flowing into the test pit and the depth from the ground surface to the water level in the test pit was measured.

3.5.2.2 Topography and Ground Water

A cross section of the tailings beach and embankment in Cell 31 through the main test site is shown in Figure 3.7 and photographs of the area are shown in Figure 3.8. The total beach length was approximately 1,000 m with an estimated average slope of approximately 1 to 2 degrees (approximately 60H to 30H:1V) towards the pond to the west, flattening further towards the pond. The crest area of the southwest sand storage area was much steeper with slopes up to 3H:1V and appeared to be greatly affected by wind action. Many piezometers were installed by Syncrude at the Southwest Sand Storage Facility for general monitoring of the facility. Sixteen standpipe piezometers were installed in the tailings sand in Cell 31. Although they were mostly located in the crest and downstream slope of Cell 31, they did help to establish a general phreatic surface in the tailings beach. Piezometer data indicated that there was a drainage divide near the crest of the southwest sand storage where the phreatic surface appeared to be at a maximum elevation, located approximately 5 to 6 m below the ground surface. From the crest, although the actual elevation of the phreatic surface dropped, the depth of the phreatic surface appeared to rise towards the pond as the ground surface elevation decreased at a slower rate than the phreatic surface. The depth to the phreatic surface was approximately 1 m at a distance of 100 m from the crest and appeared to be near the surface at approximately 300 m from the crest. The latter location appeared to be mainly controlled by recent tailings deposition and was observed to vary as tailings deposition changed during the field program. On September 20th the location of saturated tailings on surface appeared to be at a greater distance from the crest but active tailings deposition on the 23rd caused saturated tailings near surface to be located at approximately 300m from the crest. It did not appear that this had any

influence on the phreatic surface at the main test site, located approximately 230 m from the crest, which was at a depth of approximately 0.35 m.

3.5.2.3 Nuclear Density and Moisture Content Readings

Nuclear density gauge readings were taken at regular intervals, approximately every 20 m, along the beach from the crest to near the newly deposited tailings to investigate if there was any systematic change in density or moisture content with distance from the crest. Nuclear gauge testing was carried out in accordance with the safety requirements in place at Syncrude. As such, the equipment had to be operated by certified personnel and thus the tests were carried out by Terracon Geotechnique Ltd. This imposed some restrictions as to the timing and number of tests that could be carried out. The nuclear gauge provided was a Troxler, model number 3430 as described in Section 3.4.6 and had a maximum probe depth of 300 mm. The same Troxler unit was used for all tests and was operated by the same technician. The unit was calibrated by Terracon each day prior to arrival on site. The ground was always levelled and, if necessary, loose or frozen material was removed prior to testing. The probe was always extended to its maximum depth for testing. Percent compaction results were based on standard Proctor tests carried out by Terracon and used routinely at Syncrude's site.

Based on readings from the Troxler nuclear gauge, the density of the tailings did not appear to change significantly or with any type of a pattern between the crest of the Southwest Sand Storage Facility and the location of newly deposited tailings, with dry densities varying between 1590 and 1720 kg/m³ corresponding to between 89 and 97 percent of the maximum standard proctor dry density. The moisture content and saturation of the upper 0.3 m of the deposit, above the phreatic surface, did appear to depend on distance from the crest. The general trend appeared to be a slight decrease in moisture content from 10 percent (approximately 30 percent saturation) to approximately 3 percent (approximately 10 percent saturation) for the first 170 m from the crest at which point the phreatic surface was measured at approximately 0.6 m in a test pit. The moisture content and saturation of the tailings near the surface then appeared to increase dramatically to a maximum measured moisture content of 27 percent, (approximately 95-100% saturation) near the location of newly deposited tailings where the phreatic surface was nearly at the surface, approximately 285 m from the crest. These trends are illustrated in Figure 3.9 and are summarized in Appendix A. The residual moisture content shown in Figure 3.9 was based on typical soil water characteristic curves for uniform sand and silt tailings from GeoSlope (2002). It was noted that the moisture content in the upper portion of the tailings beach, within approximately 200m of the crest, was at or below typical residual moisture contents for these types of materials. Note that the saturation values were calculated based on the nuclear gauge measurements of dry density and moisture content using an assumed tailings specific gravity of 2.66; the value suggested for Syncrude tailings by CANLEX (Wride et al., 2000)

3.5.3 Characterization of Main Test Site

3.5.3.1 General

The main test site was characterized in greater detail through CPTs, test pits, frozen samples and more concentrated nuclear gauge measurements. The locations of the various tests and samples are shown in Figure 3.10.

3.5.3.2 Cone Penetration Testing

Cone penetration testing was carried out using equipment supplied by GeoForte Ltd described in Section 3.4.2. The transducers were calibrated by GeoForte Ltd. prior to arrival on site. The CPT was attached to 25.4 mm (1 in) diameter rods and pushed from the manually operated frame described in Section 3.4.2. The Predator all terrain vehicle described in Section 3.4.8 was used to provide the reaction force for the pushing frame. No depth wheel was available to monitor the location of the cone tip and therefore the time at which the cone attained certain depths was recorded to allow calculation of the push rate and thus depth (push rate x time = depth). The procedures used during CPT testing are listed below.

- The Predator was driven onto the beam beneath the frame and parked such that one of the wheels was directly on top of the beam to provide a reaction force
- The porous stone in the pore pressure transducer was saturated with glycerin and the cone assembled
- The cone was pushed manually from the surface, beginning at an even time such as 3:54:00 PM at a constant rate and the time at which 0.5 and 1 m of penetration was attained was recorded. The time of any stops during push were recorded as well as the location of any significant change in push effort. Note that the time on the data acquisition unit recording the CPT measurements was programmed to coincide with the time of the watch used for monitoring the test.
- The rods were 2 m in length but due to the height of the push frame, only 1 m intervals could be pushed continuously. The start and stop times of any push interval were recorded.

Two CPTs were carried out on September 20, 2002 to obtain initial conditions at the site. One CPT was located at the edge of the area to be loaded and one was located in the middle of the area to be loaded. The increasing resistance of the deposit with depth controlled the maximum depth of the CPTs. The maximum push force was equal to the weight provided by the Predator on the reaction beam. The Predator had a total dead weight of approximately 725 kg but it is unlikely that the entire weight was applied to the reaction beam. In general, it became difficult to push the cone at approximately 1.4 to 1.7 m, and the Predator began to lift off the ground. This factor limited the depth to which CPTs were carried out to a maximum of 2.5 m. Softening was expected to be largely a near surface phenomenon, and therefore deeper CPTs were not necessary. The traces recorded during the CPTs are shown in Figure 3.11 and Figure 3.12.

As indicated in the figures, although there appears to be a drop in tip resistance near the bottom of the traces, this is likely not an indication of a loose layer. The Predator began to lift off the ground near the bottom of the tests and not only was the push rate significantly reduced but the cone was likely pulled up as well. This is indicated by the negative friction values, indicating a reversal in the direction of motion of the cone tip. The remainder of the traces indicate a fine or silty sand material with no obvious loose or dense layer. Characteristic of sand deposits, the CPT data indicated a fair amount of variability within the tailings deposit. The tip resistance varied generally from 1 to 2 MPa suggesting representative q_c values of 1.5 ± 0.5 MPa although some more resistant material was encountered near the base of CPT 1e. It also appeared that in general the

sleeve friction measured during CPT 1m was larger than in CPT 1e. The location of the phreatic surface can also be estimated from the pore pressure traces.

3.5.3.3 Test Pits

Test pits were dug by hand adjacent to the test area to measure the depth of the phreatic surface and to collect bulk soil samples for laboratory testing. They were not dug directly in the test area so as to avoid disturbance prior to loading. The tailings were classified, according to the classification system presented in the Canadian Foundation Engineering Manual (1992), as a uniform fine to medium sand with trace fines and some bitumen inclusions. The phreatic surface was measured at approximately 30 cm below ground surface on September 20th and at 37 to 35 cm on September 23, 24 and 25. The difference in depths was likely due to precipitation events. It had rained heavily during the evening and night of September 19, 2002 but did not rain again in any significant amount for the duration of the field program. Evidence of continued drying above the phreatic surface was observed throughout the field program.

Large bulk samples of material were also gathered from two large test pits dug near the test site with the John Deere 792DLC excavator. One test pit was dug approximately 18 m southwest of the test area on September 25, 2002, approximately 30 minutes after loading. A second test pit was dug on September 26, 2002, one day after loading, in the instrumentation area, essentially at the north edge of the loaded area. The test pits were roughly 2 m by 2 m and 2 to 2.5 m deep, limited in depth by sloughing of the test pit walls. It was noted that although the test pits appeared to penetrate below the phreatic surface, there was a remarkable lack of free water in the test pits, likely due to stress relaxation causing negative pore pressures and the relatively low hydraulic conductivity of the tailings, so the test pits were thus able to penetrate much deeper than expected. Although the large test pits were dug after softening, the large samples gathered from the test pits were considered to have particle distributions representative of the initial conditions. Because of the saturated nature of the tailings, the moisture content was not considered reliable as pore water could have been lost or gained during excavation of the test pit. All samples were double bagged on site, except the large bulk samples, which were placed in plastic buckets. Upon return to the University of Alberta, the samples were placed in a moisture room at a relative humidity of at least 75 percent and a temperature of 4 to 6 °C.

3.5.3.4 In-Situ Density Measurements

Density testing was carried out after the site was instrumented, prior to loading on September 24, 2002 using a Troxler nuclear density and moisture content gauge, with samples gathered at the Troxler locations to check the moisture content measurements. The CPTs carried out did not indicate the presence of a densified crust layer and thus the density measurements were made directly from surface. A profile of density with depth was not measured because digging down to place the unit below the original ground surface would disturb the area and likely loosen the deposit. Also because free water was encountered so near the surface in the test pits, it would not have been possible to dig more than approximately 20 to 30 cm. The tests indicated that the initial dry density of the upper 30 cm of the main test site was approximately 1690 to 1710 kg/m³ (16.5 to 16.8 kN/m³), which corresponded to a compaction of 95 percent standard Proctor. The moisture content was measured at 10 to 11 percent corresponding to a

void ratio of approximately 0.57 and a saturation of approximately 50 percent. A summary of the nuclear gauge testing is included in Appendix A.

An in-situ density sample was also gathered just prior to loading of the test area on September 24, 2002 by inserting a thin walled metal cylinder with a tapered, sharp cutting edge into the ground above the phreatic surface, carefully excavating around the cylinder and capping the bottom to allow moisture content measurement in the laboratory and subsequent density calculation. The measured moisture content of the 1490 cm³ sample was 17.6 percent with bulk and dry densities of 1784 and 1517 kg/m³ respectively. This method could not be used below the phreatic surface because there would be no way of ensuring that the moisture content was representative and retrieving the sample would be very difficult.

3.5.3.5 Frozen Sampling

Frozen samples were gathered on September 25, 2002 after softening had occurred. The samples were not gathered at the time of the initial site characterization on the 22nd because they were intended to represent soil conditions just before softening. Because of the continued drying of surficial materials samples gathered several days prior to softening may not have been indicative of conditions at the time of loading. Therefore because of the uncertainty as to which loading condition would actually produce softening, the frozen samples were gathered following softening approximately 7.5 m southwest of the test area where it appeared that the upper portion of the deposit had not been affected by the testing and conditions were thought to be representative of the initial conditions at the test site.

The procedure used for collecting frozen block samples was fairly simple. Dry ice pellets were placed in a pile on the ground surface causing the tailings in the area to freeze with excess water being allowed to migrate down and to the sides. As freezing occurred, soil was excavated around the frozen zone behind the freezing front and dry ice placed in the void in order to speed up the freezing process. Dry ice was not placed ahead of the freezing front to avoid blocking the movement of water during freezing. At the end of the freezing period the block samples were excavated from the ground and placed in coolers surrounded by dry ice for shipment to the laboratory. The block samples were 13cm in depth and approximately 30cm in length and width however the upper several centimeters appeared very disturbed by the dry ice pellets. At the University of Alberta, the samples were double wrapped in plastic, each layer secured with duct tape and placed with ice inside coolers which were placed inside deep freezers which in turn were located inside a large walk-in freezer. The temperature of the large walk in freezer was maintained at approximately -40°C.

Cylindrical frozen samples were collected using the following procedures. A thin walled tube was carefully inserted into the tailings vertically from the ground surface by hand in a continuous push. The soil inside of the tube was carefully excavated to the base of the tube by hand, without prying against the walls of the tube and collected in a sample bag. Dry ice pellets were then placed inside the metal tube causing the surrounding soil to freeze radially outwards, allowing excess water to escape ahead of the freezing front. Following freezing, the samples were excavated with a shovel and placed, surrounded by dry ice, in a cooler for shipment back to the laboratory. The frozen sample reflecting conditions before loading at the main test site was 27cm deep and formed a bulb around the metal tube with a maximum thickness of 10cm. The whole sample was too large to

fit in the cooler and had to be broken on site with the use of a flat-headed screwdriver acting as a chisel. Once in the laboratory, the samples were stored in the manner described previously for the frozen block samples.

Sample freezing time was dictated by the timing of testing during the day, as there were no provisions to allow freezing to continue overnight. Freezing was started immediately following loading at approximately 10:30 am on September 25, 2002 and the samples were removed from the ground at approximately 4:00 pm of the same day.

3.5.4 Instrument Installation

3.5.4.1 General

Instruments were installed over two days, Friday September 20 and Monday September 23, 2002. Prior to arriving on site, simple finite element modelling was carried out in an attempt to identify the best locations to place instrumentation. However, because of the number of unknowns prior to carrying out the testing, the modelling did not produce reliable results. It was thus decided to place the piezometers in the shear window as defined by Woods (1968) since this was the location in which any shearing and thus liquefaction should theoretically occur. There were not many piezometers placed directly under the loaded area because that area should be dominated by compression loading. The shear window shown in Figure 3.13 was calculated for an elastic half space and may not be entirely correct for a material upon softening, however it could be expected that any shearing would initiate in that area and propagate outwards. From Figure 3.13, it can be seen that the shear window is close to surface near the loaded area becoming deeper with distance. The piezometers were therefore placed in a line perpendicular to the direction of equipment travel in groups of three or four becoming deeper with distance from the load. The piezometers within each group were spaced vertically, with the more distant groups placed deeper, to capture the response within the area of the shear window and to possibly capture any propagation of shearing and pore pressure away from the shear window.

The piezometers, load cell and geophones were placed to monitor the repose of the tailings to light loading, since it was intended to instrument a new test site prior to using heavy equipment to load the area. Due to circumstances on site, however, only one test area was used. Since this was not foreseen, the instruments were placed at fairly shallow depths and relatively close to the loaded area as shown in Figure 3.14 whereas some deeper and more distant installations may have been warranted for heavy loading conditions.

The phreatic surface became shallower towards the pond; therefore the piezometers were laid out parallel to the pond, in a north south direction to minimize static water level fluctuations between them. The direction of equipment travel would thus be towards and away from the pond (west – east) and would occur on the south side of the instruments. The tracks of the light equipment were approximately 45cm wide, and thus a maximum distance of 175 cm (greater than 3B) from the loaded area seemed appropriate. The maximum depth to which piezometers could be installed was limited to 215 cm due to the push force available to install the piezometers being exceeded. An extra piezometer was left open to atmosphere on surface to monitor fluctuations in the atmospheric pressure since this affects the piezometer readings.

The load cell and vibrating wire piezometer were placed under the centre of the loaded area to measure total vertical pressure and pore pressure.

The geophone transducer measuring particle velocities was installed essentially at the ground surface rather than at depth for several reasons. By measuring particle velocity at the surface, subsequent modeling could potentially use the data as a source input, similar to an earthquake acceleration history. Measuring the particle velocity as close to the source as possible would produce more useful results since the amount of attenuation would be limited and extrapolation to different positions would be simpler. Measuring the particle velocities at various depths within the tailings deposit would have been beneficial in order capture the attenuation of velocities with distance from the source and to assess whether different waveforms produced significantly different velocities below surface however multiple geophone transducers were not available. The geophones were not installed directly under the trafficked area to prevent damaging the instrument and were placed as close as practicably possible to the source, in line with the closest pore pressure transducers. The depth of the instruments and their distance from the most southerly piezometer are tabulated in Table 3.1 and a detailed description of the calibration and installation procedures follows.

Table 3.1 Instrument Locations

Instrument ID	Depth (m)	Distance from PN 33 (m)	Instrument ID	Depth (m)	Distance from PN 33 (m)
PN 33	0.518	0.00	PN 37	0.430	1.68
PN 32	0.893	0.08	PN 39	1.059	1.70
PN 31	1.802	0.10	PN 34	1.680	1.70
PN 36	0.432	0.81	PN 35	2.142	1.76
PN 38	0.925	0.92	VW LC 74517	0.30	-1.78
PN 29	1.783	0.90	VW PN 74518	0.28	-1.78

* PN = piezometer number, VW=vibrating wire, LC=load cell

3.5.4.2 Piezometers

The electric piezometers were calibrated at Syncrude on September 20, 2002 using a groundwater well installed inside a shop for the purpose of instrument calibration. The piezometers were grouped into bundles of four and connected to a common Data Dolphin data logger, which was plugged into an outlet supplying constant 120V AC power. No porous plastic was attached to the piezometers during calibration. A zero voltage reading was taken with the transducers inside the well casing but above the water. The bundled piezometers were marked at 1m intervals, with the first mark located between 0.2 and 1 m from the pressure transducers. Voltages were read at one meter depth intervals by lowering the piezometers into the well until the marks were at the top of the well casing. At least 4 points, in addition to the zero reading, were taken for each transducer to generate a calibration curve. Linear regression of the data points taken at one meter depth intervals, carried out using the least squares method within the software *Excel*, indicated correlation coefficients of essentially 1 (0.99998), i.e., the measured voltages and pore pressures were linearly correlated. The intercept was assumed to be the zero reading from the calibration, as it was known with greater accuracy than the actual depth of the transducers. The piezometer calibrations are included in Appendix A.

The piezometers were pushed into the ground using the manual push frame used for carrying out the CPTs described in Section 3.4.2. The piezometers closest to the loaded area were installed first and in general the deeper piezometers within a given row of piezometers were installed first to avoid damaging or disturbing installed piezometers during adjacent installations. Installation of these piezometers was carried out as follows:

- Marks were placed on the piezometer cable at 1 m intervals from the location of the pressure transducer to allow measurement of installed depth (assuming that the cable did not become kinked or significantly distorted during installation).
- The CPT cone was pushed to "pre-bore" a hole for the larger diameter piezometer in order to minimize friction during installation of the piezometer and allow deeper installation.
- The electrical cable was threaded through drill rods. The drill rods were attached to 19 mm diameter pipe at the bottom to allow the piezometer, but not the conical tip, to fit up inside the pipe protecting the piezometer and maintaining it in a vertical position during installation.
- A saturated cylindrical porous plastic, which had been soaking in water for at least 24 hours, was installed around the piezometer transducer.
- The void between the pressure transducer and the end of the plastic cylindrical casing was filled with water and the metal pushing cone was threaded onto the bottom of the piezometer.
- The metal pushing tip was seated snugly against the large diameter pipe at the base of the drill rods and whole assembly was pushed into the ground to the desired depth using the hand operated pushing frame described earlier.
- The drill rods and attached pipe were then raised to surface, leaving the piezometer in the ground.
- The actual depth of the installed piezometer was measured based on the depth markers on the cable exposed above surface.
- The piezometers were left in the ground for at least 12 hours to allow pore pressure to equalize prior to testing.

The pore pressure transducers were connected to three Data Dolphin data acquisition units for monitoring. Each Data Dolphin monitored 4 transducers such that each row of transducers (parallel to direction of equipment travel) was connected to the same Data Dolphin. The two rows closest to the loading area had only 3 transducers installed in the ground, so an additional pressure transducer open to atmosphere was connected to each of the two Data Dolphins to monitor any changes in barometric pressure.

3.5.4.3 Vibrating Wire Instruments

The vibrating wire piezometer and load cell used were provided by the University of Alberta and had been calibrated by the manufacturers. The two instruments were installed on September 23, 2002 in the centre of the area to be loaded. A hole was dug by hand to a depth of 30 cm and levelled. The load cell and piezometer were placed in the bottom of the hole with the piezometer placed behind (East) of the load cell. Because of the configuration of the instruments, the centre of the piezometer was approximately 2 cm above the load cell. The cables from the load cell and piezometer were laid in a hand dug trench roughly 15 cm in depth to the edge of the area to be

loaded and connected to a Data Taker data acquisition unit. These instruments were allowed to equalize for at least 12 hours prior to testing.

3.5.4.4 Seismograph

The Blast Mate seismograph used to measure particle velocities was installed just prior to each loading event because it did not require any equalization time. The important aspects of its installation were the orientation of the geophone transducer and obtaining intimate contact between the transducer and the ground. As described in Section 3.4.5, the transducer contained three geophones oriented in orthogonal directions, which should be oriented in line with the major directions of particle motion. The ground was first excavated 5 to 10 cm to provide a level surface so that the vertical geophone was oriented in a vertical direction. The longitudinal geophone was then aligned in the direction perpendicular to the direction of equipment travel (roughly North-South). The transverse geophone was thus in a direction parallel to the direction of equipment and the rows of piezometers (roughly East-West). Three large metal spikes were provided for installation of the transducer on soft ground and were screwed into the base of the transducer. The transducer was installed by pressing the spikes firmly into the ground, with transducer oriented as described. The small hole created to level the ground was then backfilled with tailings and a sand bag was placed on top of the transducer to encourage intimate contact between the transducer and underlying tailings.

To accommodate the relatively long term monitoring required two different recording modes were employed. A continuous waveform was recorded during critical loading periods, such as initial loading and events that lasted less than 5 minutes. In this mode, the unit was set to record particle velocity from each of the three geophones 1024 times per second. This record rate was substantially faster than required but was the minimum rate at which the unit was program to gather continuous data. Loading events that lasted considerably longer than 5 minutes were initially monitored using the continuous mode but after several minutes were monitored using the histogram mode described in Section 3.4.5 to preserve memory space. Summary information (peak particle velocities and frequencies in each direction and peak vector sum) was stored every 2 seconds. It should be noted that in histogram mode, there is no certainty that the individual peak velocities saved occurred at the same time. When small velocities were expected, such as during Predator loading, the unit was set to the sensitive operating range of 34 mm/s. Conversely under larger loads, such as provided by the dozer, the upper range of 200mm/s was selected. In continuous record mode, monitoring was initiated automatically when particle velocities were greater than 0.015 mm/s when the sensitive range had been selected and greater than 0.51 mm/s when operating in the normal range. In histogram mode monitoring was initiated manually prior to equipment loading. Monitoring could always be terminated manually. In the case of continuous monitoring however, it was possible for monitoring to stop automatically. The particle velocities were automatically checked every 104 seconds and if they were below the trigger level monitoring ceased. In both cases, if loading was halted for a time, to measure density or for other reasons, the Blast Mate was turned off to conserve memory and battery supply and was restarted prior to subsequent loading.

3.5.5 Light Equipment Loading

Following instrument installation on September 23, 2002, very light loading was applied on the north side of the instruments (the opposite side as the actual loading site) to

check that the piezometers were functioning. Load was applied simply by jumping or stepping in place. It appeared that the closest, shallowest piezometers did show some response, confirming that they were functioning. The piezometers were then left overnight to allow equalization of any change in pore pressures caused by their installation.

The main test area was initially loaded the morning of September 24, 2002. The weather was sunny, windy and cool, although well above freezing. The phreatic surface was measured at 37 cm in a test pit approximately 2.5 m north of the loaded area and. Load was applied by driving the eight wheeled, tracked Predator all terrain vehicle back and forth in an essentially east-west direction at the southern limit of the piezometer installations. The track locations were varied to minimize rutting resulting in a total loading width of approximately 2.5 m. A pass was defined as a movement through the test area in one direction (either east or west). The Data Dolphins recording the electric piezometers and the Data Taker recording the vibrating wire piezometer and load cell were set to record at 3 second intervals, the fastest recording rate possible, although, as discussed in Section 3.4.4, it appeared later that data was not always gathered at that rate. The Blast Mate seismograph was installed and set up to record as discussed in Section 3.5.4.4.

An initial ten passes were carried out with the Predator and then loading was stopped to allow nuclear gauge density and moisture content readings to be carried out. The measurements appeared to indicate that the dry density of the upper portion of the deposit was decreasing and that the moisture content and wet density was increasing. Thirty-two more passes were applied followed by more nuclear gauge readings. These readings indicated only small additional changes in the density and moisture content of the deposit and there was no further significant surficial evidence of softening. The direction of equipment passes was then changed to north/south to explore whether that would affect the response and a significant number of passes was applied. Further measurements with the Troxler did not indicate any significant change in the density or moisture content of the deposit. Loading was continued with the Predator again travelling in an east/west direction with greater than 100 passes applied. During this period, the seismograph recording mode was changed to the histogram mode to allow monitoring to continue. A final measurement of density and moisture content with the nuclear gauge did not indicate any significant changes. The Predator continued to make passes sporadically but no surficial evidence of softening occurred.

The density and moisture content values recorded by the Troxler nuclear gauge during the initial period of loading are shown in Figure 3.15. The Troxler measurements were separated into two groups, those taken in the southwestern portion of the test site and those taken in the northeastern portion of the site because the two areas appeared to respond slightly differently. The southwestern portion initially showed small signs that softening may be triggered while there was no evidence of this in the northeastern portion of the test site.

The pore pressures and particle velocities monitored during Predator loading on September 24, 2002 are shown in Figure 3.16 and are also summarized in Appendix B. The seismograph data was shifted slightly because the time in the seismograph did not agree exactly with the time stamp in the Data Dolphins monitoring the piezometers. It should also be noted that the atmospheric pressure recorded by the two transducers open to atmosphere did not agree perfectly. This may be due to differences between

the Data Dolphin acquisition units to which the transducers were connected. Therefore when correcting the piezometer zero values for changes in atmospheric pressure, the readings from the transducer measuring atmospheric pressure connected to the same Data Dolphin as the transducers measuring pore pressure were used.

It can be seen in Figure 3.16 that pore pressures rose slightly in response to loading but not nearly enough to cause any significant reduction in effective stresses and therefore softening could not occur. As shown in Figure 3.16 there was some cyclicity in the monitored pore pressures that appeared to match the ground motions monitored by seismograph, although significantly fewer pore pressure cycles were captured than ground motion cycles due to the lower recording rate of the pore pressure transducers. It can also be noted that the pore pressures rose quickly in response to the applied cyclic load with no obvious delay between the onset of ground motion and an increase in the measured pore pressure.

Since the site had been selected in an area where it had appeared that the Predator would be able to induce softening this was unexpected. Passes were therefore made with the Predator in areas closer to the tailings pond and in an area to the south of the test site, to see if these areas could be softened and to try to identify any differences between the areas that may have affected the behaviour. The Predator could cause the visual softening behaviour in these other areas after approximately 10 to 15 passes. In an effort to understand what was causing the difference, the Predator was used to initiate softening in an area and would then move a few meters towards the crest and apply more passes. It appeared that there was a very definite boundary between the area that could be softened with the Predator and the area that could not, located approximately 10 m west of the test area (i.e. closer to the pond). In general the phreatic surface was slightly shallower than at the test site but there was no drastic change in phreatic surface right at the boundary location between tailings that would and would not soften. It appeared that the main difference between the areas that would and would not soften was the saturation of the tailings above the phreatic surface. It appeared that where there was an essentially dry layer of tailings at the surface, softening of the deposit would not occur as a result of Predator loading. Several samples of adjacent areas that would and would not soften under Predator loading were gathered for further testing in the laboratory.

Another attempt was made to soften the test area in the afternoon of the same day by adding six 5 gallon buckets of wet tailings sand to the back of the Predator to increase the load applied. It was estimated that this increased the weight of the Predator by approximately 225 kg for a total weight of approximately 1,000 kg. The seismograph was again set up to monitor particle velocities in continuous monitoring mode as described previously and the data loggers recorded the other instrumentation. Over 200 passes were carried out with no surficial indication of softening. The monitored pore pressure and particle velocity response to the increased Predator load was similar to that recorded previously with no significant increase in the amount of excess pore pressures generated. Softening of the deposit was also attempted by dropping a heavy beam on the ground with no visible effect. Photographs of the test site after Predator loading are shown in Figure 3.17.

3.5.6 Heavy Equipment Loading

On September 25, 2002, larger equipment was brought to the test area in an effort to induce the softening behaviour. Safety protocol at Syncrude required that there be two pieces of equipment so that if the ground softened and a piece of equipment became stuck, the other could pull it out. The two pieces of equipment available were a John Deere 450G LGP dozer and a John Deere 792DLC excavator. Details of these machines were given in Section 3.4.8. For safety reasons, loading was first carried out with the lighter dozer. The record rate for the data loggers monitoring the piezometers and load cell were set at 3 seconds and their clocks synchronized with the watch on site. The Blast Mate was set to record in continuous mode with the range specified as 254 mm/s and the trigger level as 0.51 mm/s. The area had not been loaded for 17 hours and the piezometers appeared to have returned to equilibrium conditions.

Loading was initiated with the dozer travelling towards the pond in a westerly direction. The dozer remained in essentially the same track locations with the edge of the track closest to the electric piezometers at approximately 55 cm from the first row of piezometers. The vibrating wire load cell and piezometer were located between the two dozer tracks. Signs of softening consisting of surface waving and some cracking were observed after three passes. Loading had to be halted after eight passes due to extreme softening of the deposit, which was beginning to jeopardize the safety of the dozer. The ground surrounding the excavator for several meters was undulating and cracking was observed. The track locations were depressed approximately 30 cm when loaded, rebounding when not.

Immediately following the dozer loading, the ground could support the weight of a person but undulated for several meters around the person as they walked across the ground surface. Significant quantities of water began pumping to the surface through cracks in the ground approximately 30 seconds after loading. The surface of the ground within a distance of approximately 1.5 m of the edge of the tracks then began to wet with water boiling to the surface as shown in Figure 3.18. Cracks were observed on the surface of the ground up to 2 m from the edge of the dozer tracks. Within 45 minutes after loading, although the tailings on the surface appeared to be saturated and there were several pools of water, the area appeared to have hardened significantly; a person could walk on the surface with no deflection occurring.

The pore pressures and particle velocities measured when the John Deere 450G LGP dozer was driven back and forth 0.5 m south of the instruments are shown in Figure 3.19 and summary information is included in Appendix B. The seismograph data was shifted slightly because the time in the seismograph did not agree exactly with the time stamp in the Data Dolphins. The shift was made by matching the last significant vibration with the known time at which loading ceased. Also, as occurred during the Predator loading test, the atmospheric pressure recorded by the two transducers open to atmosphere did not agree, differing by more than 7 kPa. Therefore when correcting the zero values for changes in atmospheric pressure, the readings from the transducer measuring atmospheric pressure connected to the same Data Dolphin as the transducers measuring pore pressure were used. The readings from the vibrating wire piezometer and load cell located between the dozer tracks is shown in Figure 3.20.

The pore pressures generated by the dozer were substantially larger than those generated by the Predator. From Figure 3.19 it appears that the pore pressure was

equal to the overburden pressure in a substantial volume of soil creating conditions of essentially zero effective stress and softening. The figure also indicates essentially immediate pore pressure response close to the location of load application. Excess pore pressures were recorded in the nearest row of piezometers at almost the same time as the initial ground motions were recorded, with the piezometers located further away appearing to lag slightly behind. As with the Predator loading, some cycling of the pore pressures in response to the dozer applied cyclic stresses, particularly in the shallower piezometers can be seen in Figure 3.19. The number of pore pressure cycles is clearly much less than the number of loading cycles, possibly due to the relatively low recording rate of the piezometers (3 to 5 second recording intervals compared to 1024 readings per second from the seismograph). However, the pore pressures cycles can be seen to correspond somewhat with the occurrence of the larger and more intense ground motions recorded by the seismograph.

Initially it had been thought possible that the heavier excavator could be used to load the tailings on the north side of the piezometers. It was apparent however that a single pass would cause softening and that it could endanger the equipment and therefore this was not carried out.

3.5.7 Post Loading Testing

3.5.7.1 General

Cone penetration testing, sample collection and nuclear gauge density and moisture content measurements were carried out at the test site following loading to quantify changes that had occurred in the tailings. The three piezometers located closest to the loading area were also used to monitor pore pressure for 24 hours after loading to investigate the dissipation of excess pore pressures and allow an estimate of the hydraulic conductivity of the tailings. The pore pressure dissipations are shown in Figure 3.21. It appears that pore pressures required at least 24 hours to fully dissipate and that dissipation was slower at shallower depths.

3.5.7.2 Cone Penetration Testing

Cone penetration tests were carried out two hours after loading, located close to the sites of the CPTs carried out to initially characterize the site. The procedures used were the same as presented in Sections 3.4.2 and 3.5.3.2. One CPT was carried out near the edge of the loaded area, approximately 50cm north of the edge of the northern-most dozer track, and one was carried out between the two dozer tracks. It would have been desirable to carry out the CPTs closer to the loading time but due to equipment activities this was not possible. The results of the CPTs are shown in Figure 3.12 and do not appear to indicate any significant loss in tip resistance, generally varying between 1 and 2 MPa as in the CPTs carried out prior to loading with slightly higher tip resistances still indicated near the bottom of CPT 2e. The sleeve friction values measured during the CPTs carried out after softening do appear slightly higher than the measured values prior to loading however. The measured pore pressures were slightly higher than measured initially, indicating that even 2 hours after loading, excess pore pressures still existing in the middle of the test area. As indicated in Figure 3.11 and Figure 3.12 the CPT measured pore pressures actually agree quite closely to the pore pressures measured by the piezometers two hours after loading.

3.5.7.3 Frozen Sampling

The frozen samples gathered to characterize the tailings after loading were taken close to the location of the tracks because that was the area where the shear window should be closest to the surface. It was not possible to dig down from surface to obtain a sample from depth because the tailings in the loaded area had become saturated, causing sloughing soil and water flow in any hole dug. A frozen block sample was gathered from between the two dozer tracks, away from the location of the load cell and piezometer, and a cylindrical sample was gathered just north of the northern dozer track location. Both samples were gathered as discussed in Section 3.5.3.5. Freezing began approximately 45 minutes after loading once conditions appeared to have stabilized and was continued for approximately 6 hours. The frozen samples gathered from the loaded area were significantly smaller than those gathered from the undisturbed area, likely because of the increased amount of water in the tailings, which would slow the progress of the freezing front. The block sample that was retrieved was approximately 10cm deep by 30cm wide and the cylindrical sample was approximately 15 cm deep with a bulb of material around the metal tube with a maximum thickness of 6 cm. Large bulk samples from the loaded area were also gathered and placed in five gallon pails.

3.5.7.4 Nuclear Gauge Testing

Nuclear gauge density and moisture content tests were carried out on September 26, 2002, almost 24 hours after loading by the dozer. It had been desired to carry out these tests immediately after loading but due to the uncertainty in triggering softening and personnel requirements it was not possible. Two tests were carried out in the loaded area where no further disturbance had occurred after loading. Both locations were between the dozer tracks and bulk samples were gathered from these locations and double bagged to check the moisture content measurements. Tests could not be made to the north of the test area where the frozen cylindrical sample had been collected because the area had been disturbed and excavated to retrieve the piezometers. The tests were carried out with the probe extended to its maximum 300mm depth from a level surface approximately 5 to 10 cm below the ground surface. The readings indicated that the dry density of the upper 30cm of the tailings deposit had decreased substantially from an initial average value of 1700 kg/m^3 to values ranging from 1548 to 1568 kg/m^3 (15.2 to 15.4 kN/m^3). Consistent with visual observations, the readings indicated that the moisture contents increased, changing from 10 to 12 percent initially to 23.9 to 25.3 percent after softening (equivalent to a saturation of 94 to 97 percent), corresponding to a calculated final void ratio of approximately 0.71 compared with an initial void ratio of approximately 0.57.

3.5.8 Quick Tests

3.5.8.1 General

Four sites shown in Figure 3.22, located closer to the tailings pond than the main test site, were selected for quick, light loading tests. It was decided to carry out the quick tests to gather more data with regards to the changes occurring to the tailings mainly with respect to density and stiffness, before, during, and after softening. To allow flexibility in the timing of the tests to accommodate personnel requirements, load was applied by a person stepping in place. Density and moisture content could then be measured using the Troxler nuclear gauge at various stages throughout the test and

CPTs could be carried out before and immediately after or during loading. By carrying out the CPTs so close to loading, it was hoped that correlations between tip resistance and Young's modulus could be used to investigate the change in stiffness during loading and perhaps explain the large size of the area affected by loading.

3.5.8.2 Quick Tests 1 2 and 3

Two sites, QT1 and QT2, were located near an area of new tailings deposition where the phreatic surface appeared to be within 10cm of the ground surface. One piezometer was installed at each location on September 25, 2002 and left overnight to allow equalization of pore pressures. The piezometers were located at a depth of approximately 50cm and approximately 40 cm from where the person would stand to load the area.

The quick tests were carried out on September 26, 2002. Temperatures overnight had fallen dramatically to a low of -11°C and there was approximately 3 cm of frost upon arrival to the site, although temperatures had risen above freezing. The frost disappeared rapidly as the day warmed but based on the amount of water observed in the tailings at the ground surface, the phreatic surface at both QT1 and QT2 appeared to have risen essentially to the ground surface. An initial CPT was carried out at QT1, approximately 40 cm from the area to be loaded, to characterize the deposit. The Troxler nuclear gauge was used to take initial density and moisture content readings following the initial CPT, also approximately 40 cm from the area to be loaded. During all of these initial measurements, attempts were made to disturb the area as little as possible. The geophone transducer was installed on the surface near the location of the piezometer and the Blast Mate was set to record in continuous mode in the sensitive range. The site was then loaded with approximately 50 stepping cycles, each of which applied roughly 10 to 20 kPa, after which the density and moisture content of the softened tailings were measured with the Troxler and another CPT was carried out. During the test a piezometer measuring atmospheric pressure was also monitored. This procedure was repeated at location QT2.

The increased amount of water from the melting frost made work in the test areas more difficult than expected and thus a third location, QT3 located slightly more towards the crest was selected to allow testing in an area with a slightly deeper phreatic surface. Pore pressures during loading could not be monitored however as there was no time to allow equalization of pore pressures after installation.

Softening was induced at all three locations although at location QT3 fewer cycles were applied and softening was not as severe. Evidence of softening included severe undulations of the ground, the amplitude of which increased with the number of stepping cycles, cracking and, particularly at sites QT1 and QT2 which underwent greater numbers of loading cycles, water flowing to the surface. A slightly raised area also appeared to develop in a ring around the loaded area. The radius of the surficial evidence of softening at each quick test location was at least 1m. At all locations the nuclear gauge readings indicated that the initial dry density of the tailings was significantly lower than at the main test site ranging from 1614 kg/m^3 at QT3 to 1464 kg/m^3 at QT1 with much higher moisture contents, 26 percent at QT1 and QT2 and 21 percent at QT3. The changes in the density readings recorded by the Troxler nuclear gauge during and after these tests were much smaller than those recorded at the main site in the order of $10\text{ to }20\text{ kg/m}^3$, possibly within the margin of error for the instrument.

Site QT1, the site with the lowest initial density, actually showed a slight increase in dry density after approximately 50 stepping cycles while both QT2 and QT3 recorded slight decreases. The Troxler readings also indicated that the moisture content at all sites increased, although only by 1.5 percent.

The particle velocity and pore pressure responses at QT1 and QT2 are shown in Figures 3.23 and 3.24. The particle velocities recorded were somewhat lower than those induced by the Predator however it should be noted that the Blast Mate was closer to the applied load in this case and therefore less attenuation of particle velocities would have occurred. Similar to when softening was induced by the dozer, the pore pressures appeared to rise to essentially the overburden pressure although due to the shallow installation depth the magnitudes of pore pressure change were fairly small. Unfortunately, there appeared to have been a loose wire or a short in the CPT equipment as there was considerable noise in the data and no meaningful data was obtained. Qualitatively however, it was evident from the reduced effort required to push the CPT that the tip resistance had significantly decreased.

3.5.8.3 Quick Test 4

It had been intended to collect frozen samples from at least one of the instrumented quick test locations. However, the amount of water that was brought to surface during loading made any further work at these locations very difficult. Site QT4, at a slightly higher elevation with a slightly deeper phreatic surface, was therefore selected for light loading similar to the previous quick tests and subsequent sampling. The location was selected to give a large area with uniform conditions so that an "undisturbed" sample could be gathered at some distance from the softened area and still hopefully be representative of the initial conditions of the tailings that were softened.

The phreatic surface at QT4 was approximately 15 cm below ground surface prior to loading. Loading was carried out by applying greater than 30 human stepping cycles at which point the ground surface was undulating significantly for a distance of approximately 1m around the person, and water was pumping to the surface. After softening, a cylindrical frozen sample was gathered approximately 40 cm from the foot locations, 10 cm away from the area of most disturbance and large cracks. A cylindrical frozen sample was also gathered 5.3 m south of the loading area to represent conditions initial conditions prior to loading. The samples were gathered by radial freezing around a thin walled metal tube as discussed in Section 3.5.3.5 with one difference. After careful excavation of the tailings sand inside the metal tube, bentonite pellets were placed in the bottom of the tube to seal the bottom. This was done to stop water flowing up into the bottom of the tube as the base of the tube was below the phreatic surface. Once the pellets became hydrated and expanded, the few centimetres of water in the bottom of the tube was removed and dry ice pellets were placed in the centre of the tube. Freezing was halted after 3 hours, as there was no method to maintain dry ice in the tubes overnight. The sample recovered from the softened area was 20.8 cm deep with a maximum thickness of 6 cm while the one recovered from the undisturbed area was 20.5 cm deep with a maximum thickness of 10 cm. Bulk samples excavated from the middle of the metal tube were double bagged for moisture content measurement and comparison with the results of the frozen samples. Unfortunately, a Troxler nuclear gauge was not available to carry out measurements at this site for comparison.

3.5.9 Trafficability Study

A short trafficability study, similar to the one carried out by Syncrude in November 2001, was carried out after loading of the main test site on September 25, 2002. There were two portions to the study. The trafficability limits of the dozer and excavator were established by driving the equipment down the beach until significant softening or cracking occurred. No obvious bow wave or any type of disturbance was visible ahead of the equipment prior to softening during the trafficability study. At the furthest distance reached in a single pass, a small test pit was dug to measure the depth to the phreatic surface and to gather bulk samples. Density and moisture content measurements were also made at the location with a Troxler nuclear gauge, however due to personnel requirements these measurements occurred nearly 24 hours after the equipment had travelled the area.

The John Deere 450G LGP dozer was also used to study how many runs caused softening to occur, compromising trafficability. The dozer was used rather than the heavier excavator for this portion due to safety issues; if the dozer became stuck, it could be rescued by winch of the larger excavator. The dozer travelled down the beach, south of the main test site to the limits of its trafficability where significant softening was induced and water was brought to the surface. The dozer then retreated backwards up the same tracks to the starting point and returned down the same tracks for a second run again to the trafficability limit. A total of three runs up and down the same tracks were carried out just south of the test site. At the limit of each of the three runs, a test pit was dug and the depth to the phreatic surface was measured and a sample gathered. At each location, nuclear gauge readings of moisture content and density were also made 24 hours after the area had been trafficked.

The limits of trafficability established during the trafficability study as well as the locations of the first signs of softening and water being brought to surface are shown in Figure 3.25. The measured depth to the phreatic surface and the Troxler nuclear density and moisture content readings are summarized in Table 3.2. The location of the trafficability limits in Cell 31 at the Southwest Sand Storage appeared to coincide closely with the location of newly deposited tailings, however signs of softening and cracking did occur well before of these limits.

Table 3.2 Trafficability Study Results

Location	Depth to Phreatic Surface (m)	Nuclear Gauge Readings	
		Dry Density (kg/m ³)	Moisture Content (%)
Excavator Furthest Point	0.56	1576	18
Dozer Further Point	0.23	1518	27
Dozer, End of 2 nd Run	0.38	1660	14
Dozer, End of 3 rd Run	0.38	1695	9.5

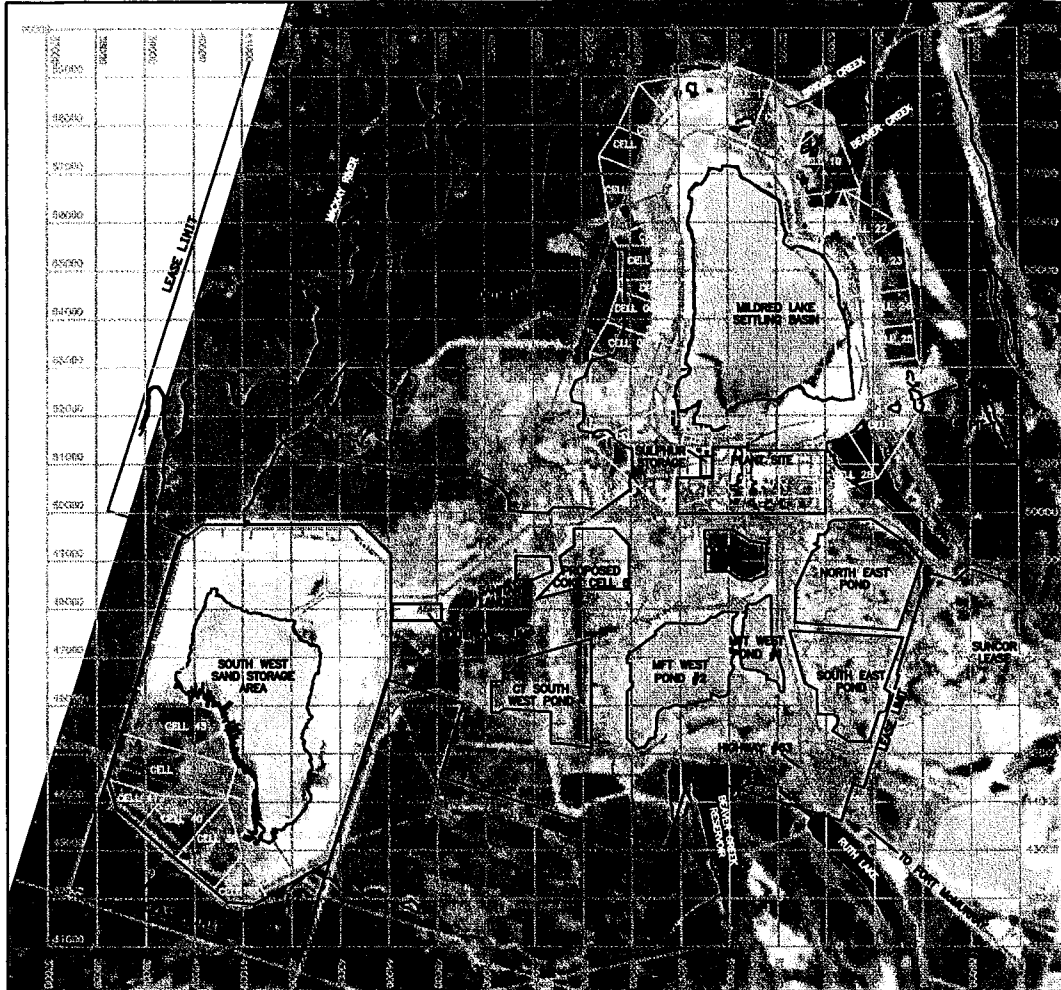


Figure 3.1 Location of Southwest Sand Storage Facility

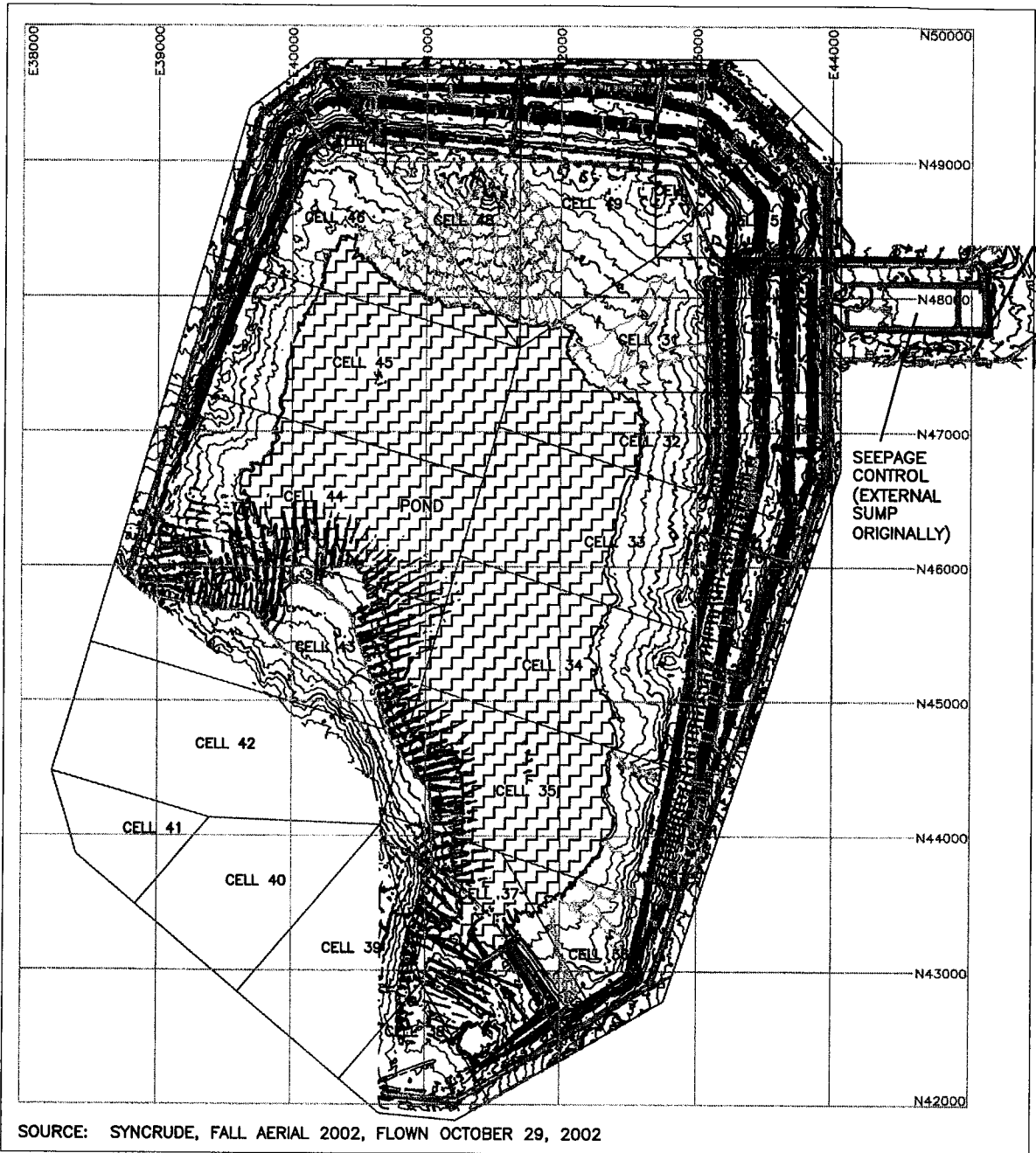
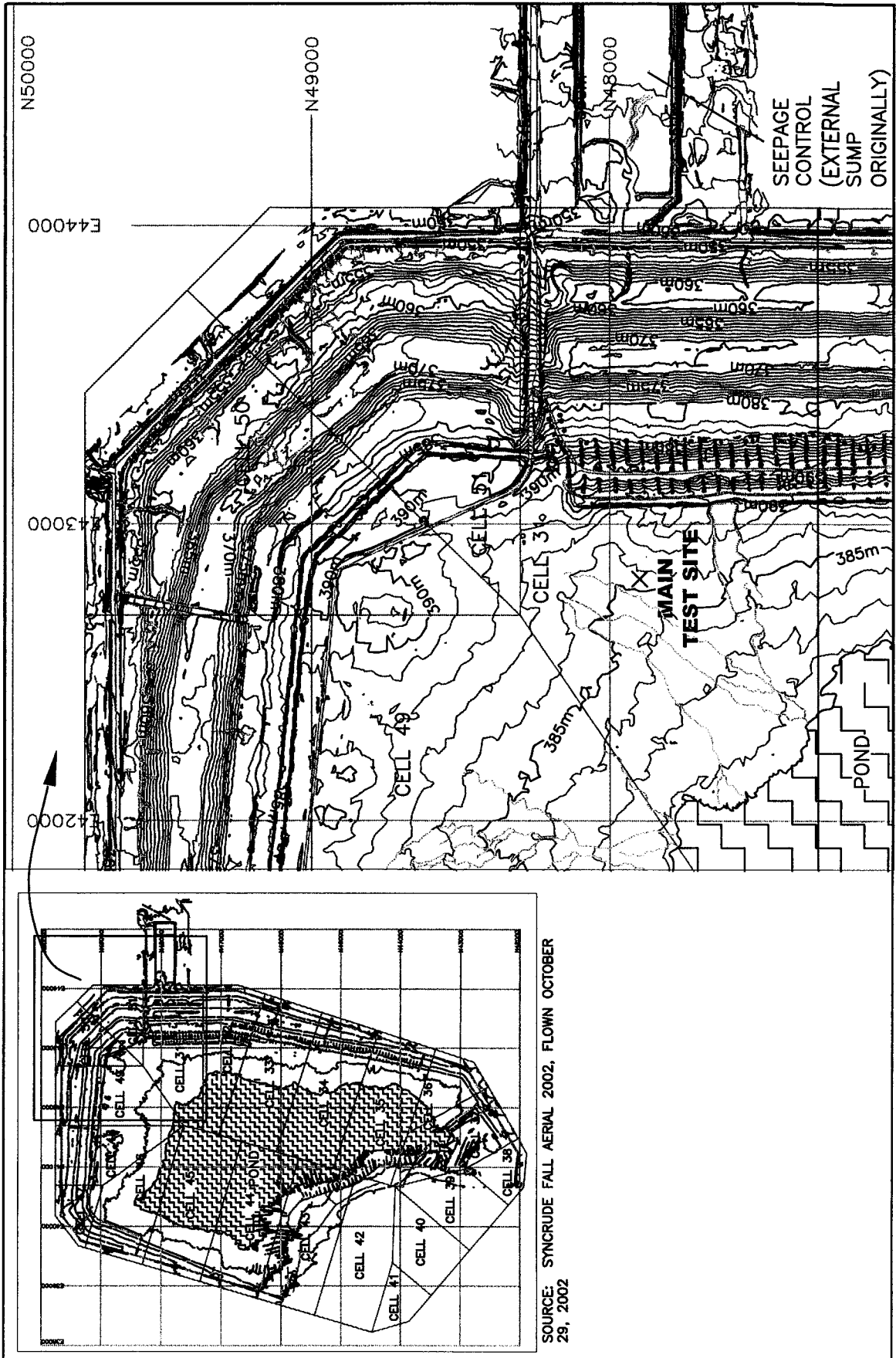


Figure 3.2 2002 Plan of the Southwest Sand Storage Facility



SOURCE: SYNCRUDE FALL AERIAL 2002, FLOWN OCTOBER 28, 2002

Figure 3.3 Test Site Location



Figure 3.4 CPT Setup at Main Test Site

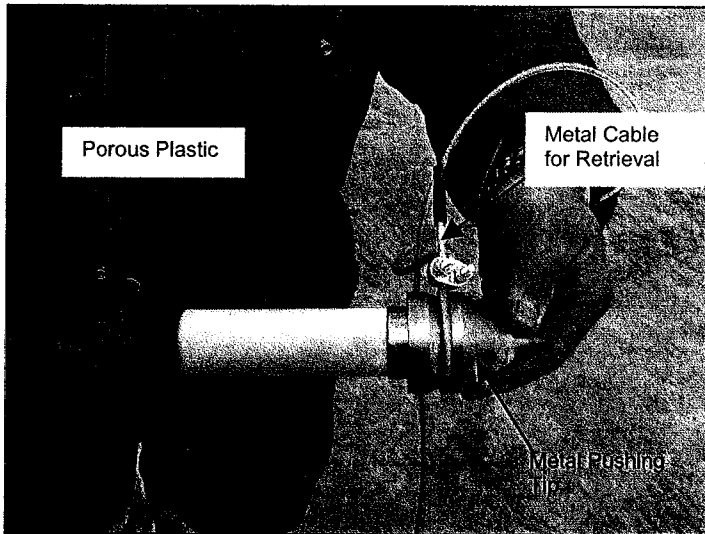


Figure 3.5 Push in Piezometer

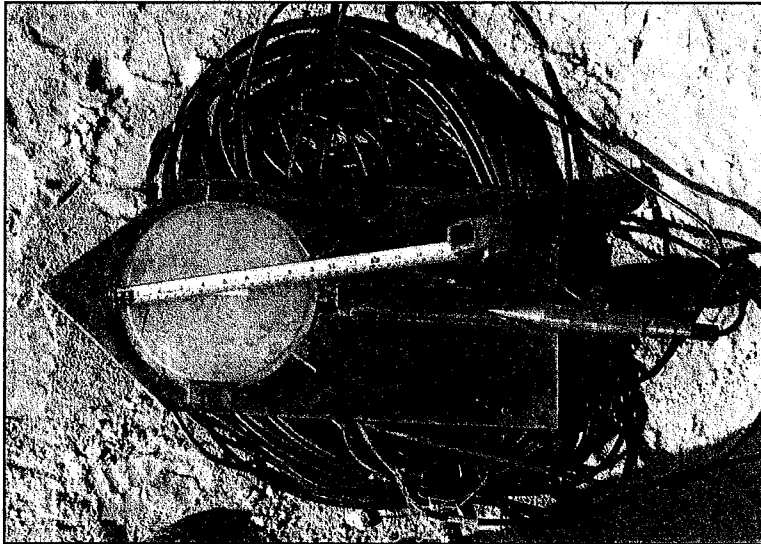


Figure 3.6 Vibrating Wire Load Cell and Piezometer

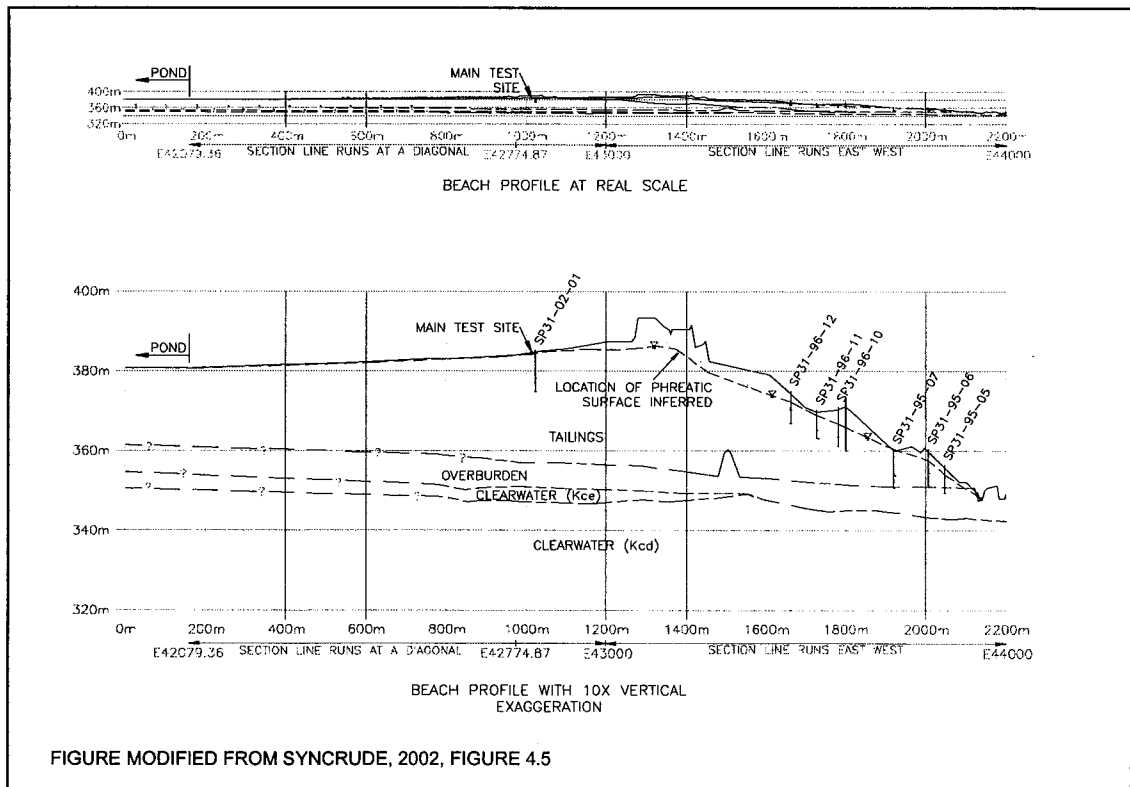


FIGURE MODIFIED FROM SYNCRUDE, 2002, FIGURE 4.5

Figure 3.7 Cross Section of Tailings Beach Near Main Test Site

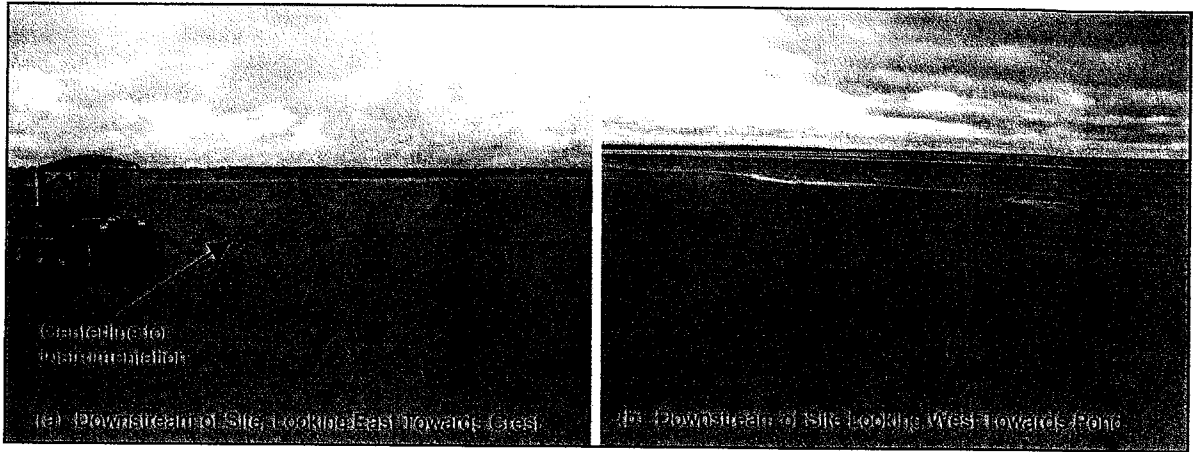


Figure 3.8 Southwest Sand Storage, Main Test Site Prior to Testing

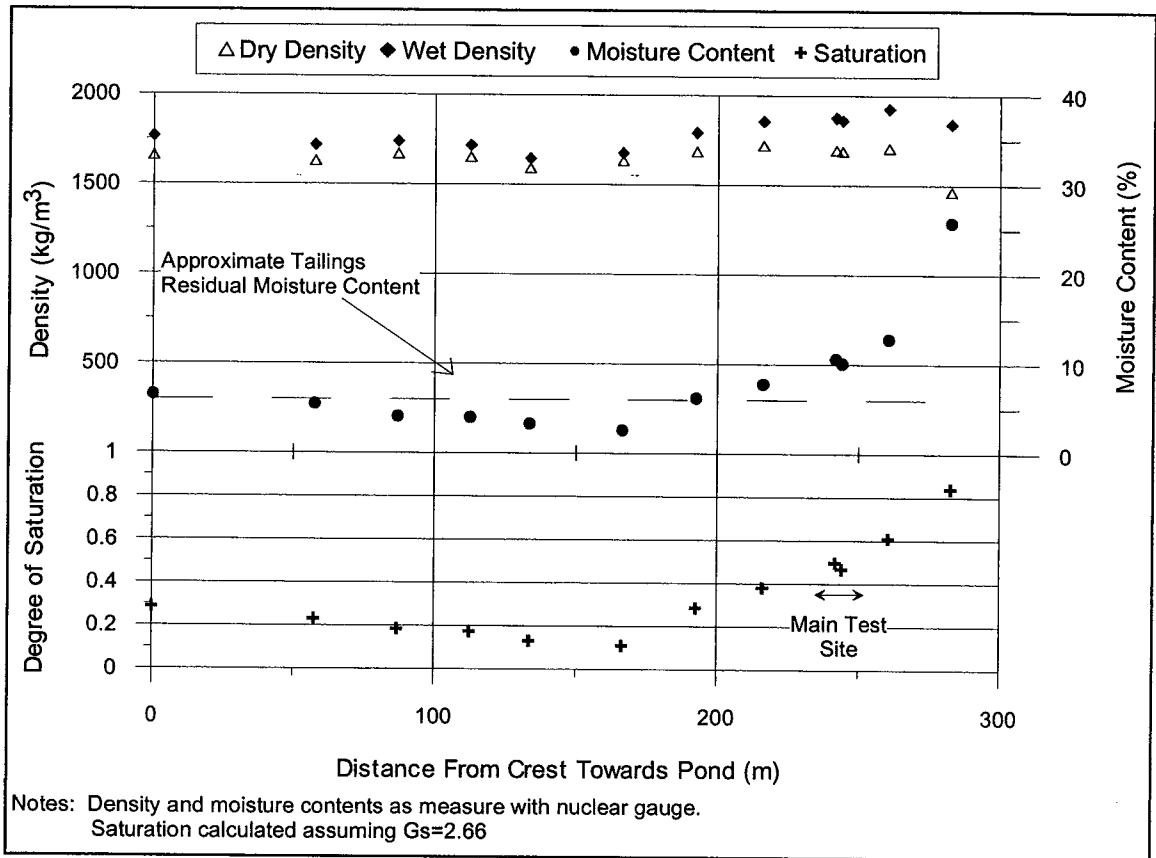


Figure 3.9 Density, Moisture Content and Saturation Variation Along Tailings Beach

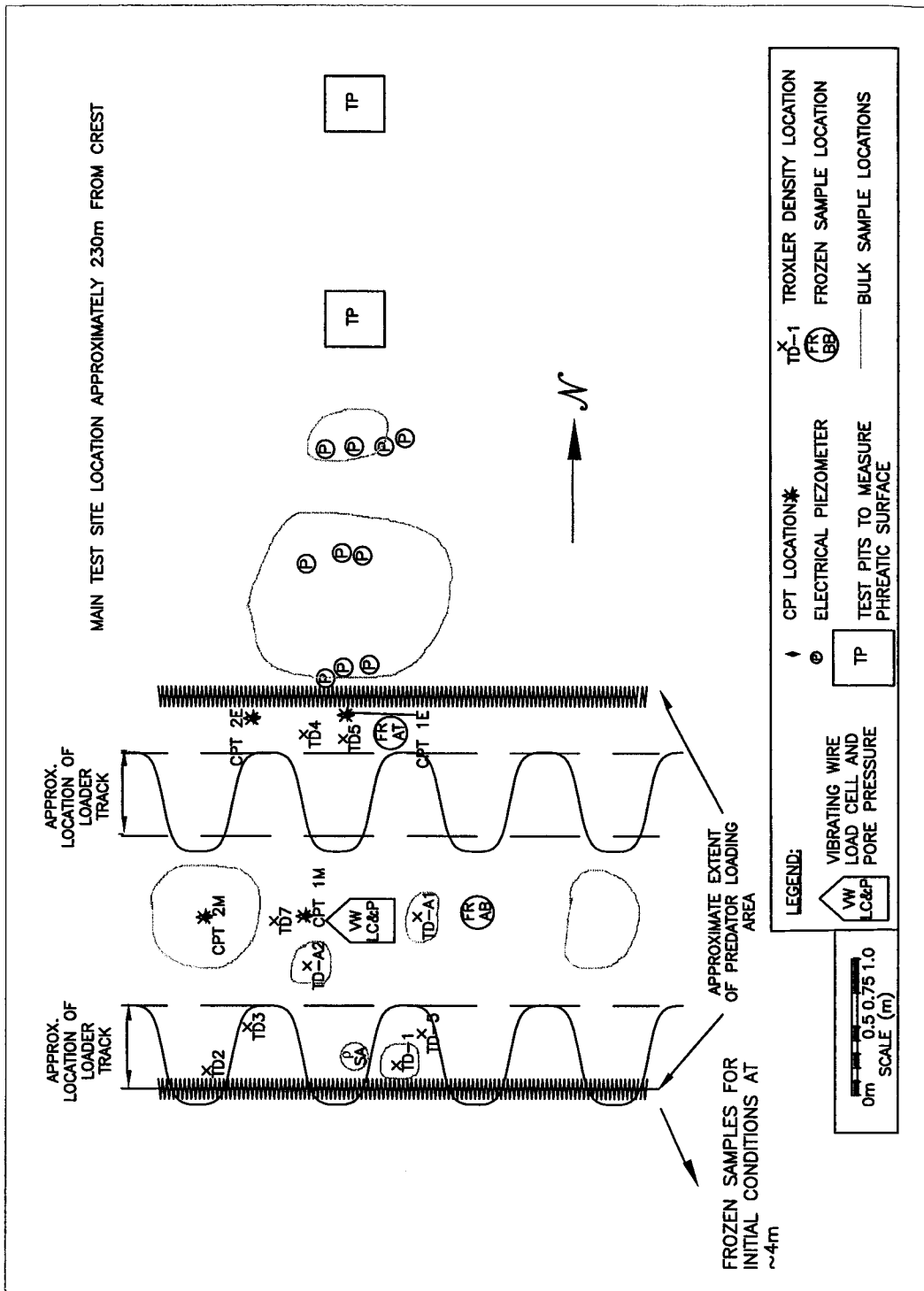


Figure 3.10 Schematic of Sample and Testing Locations at the Main Test Site

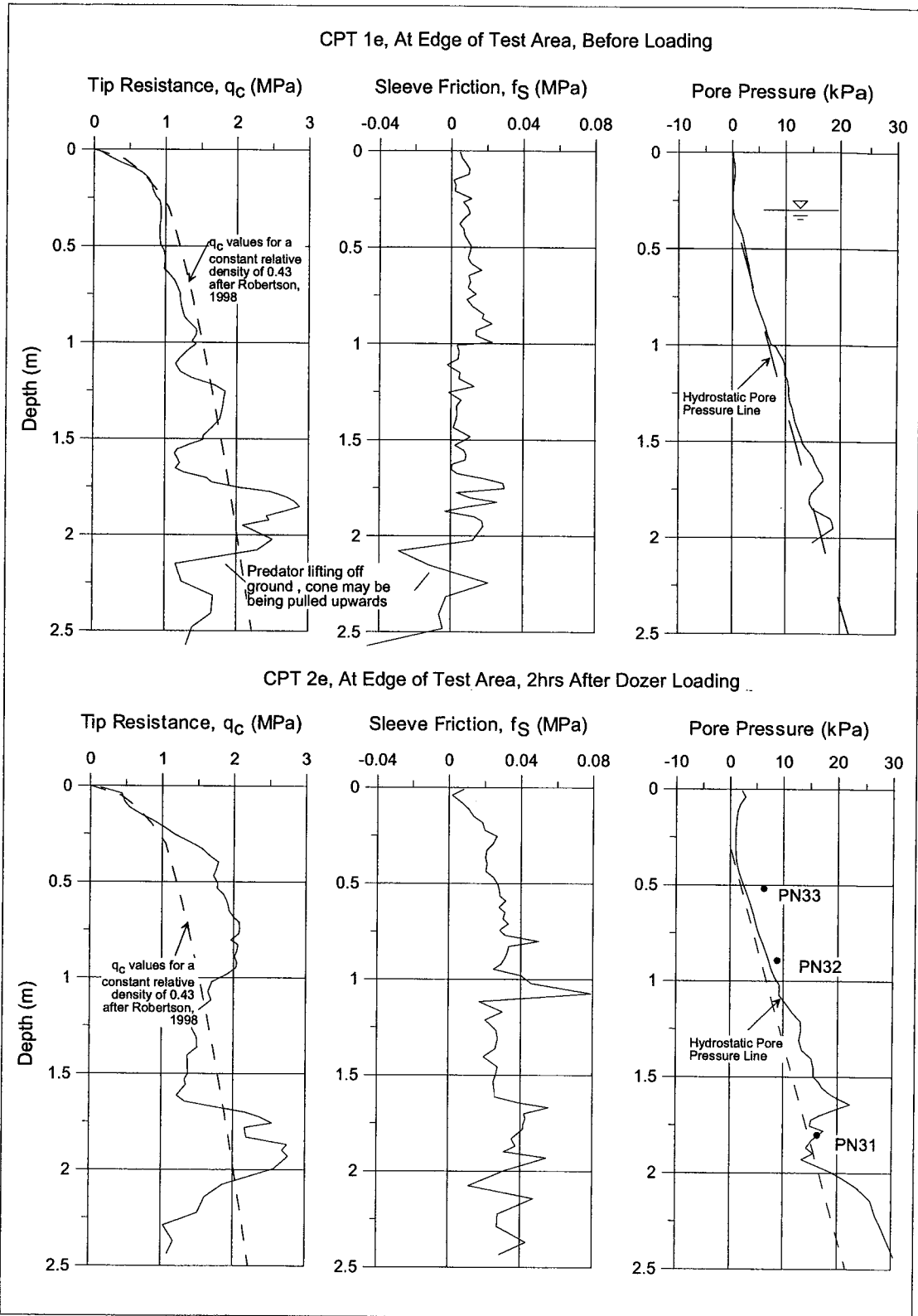


Figure 3.11 CPT Results from the Edge of the Main Test Site

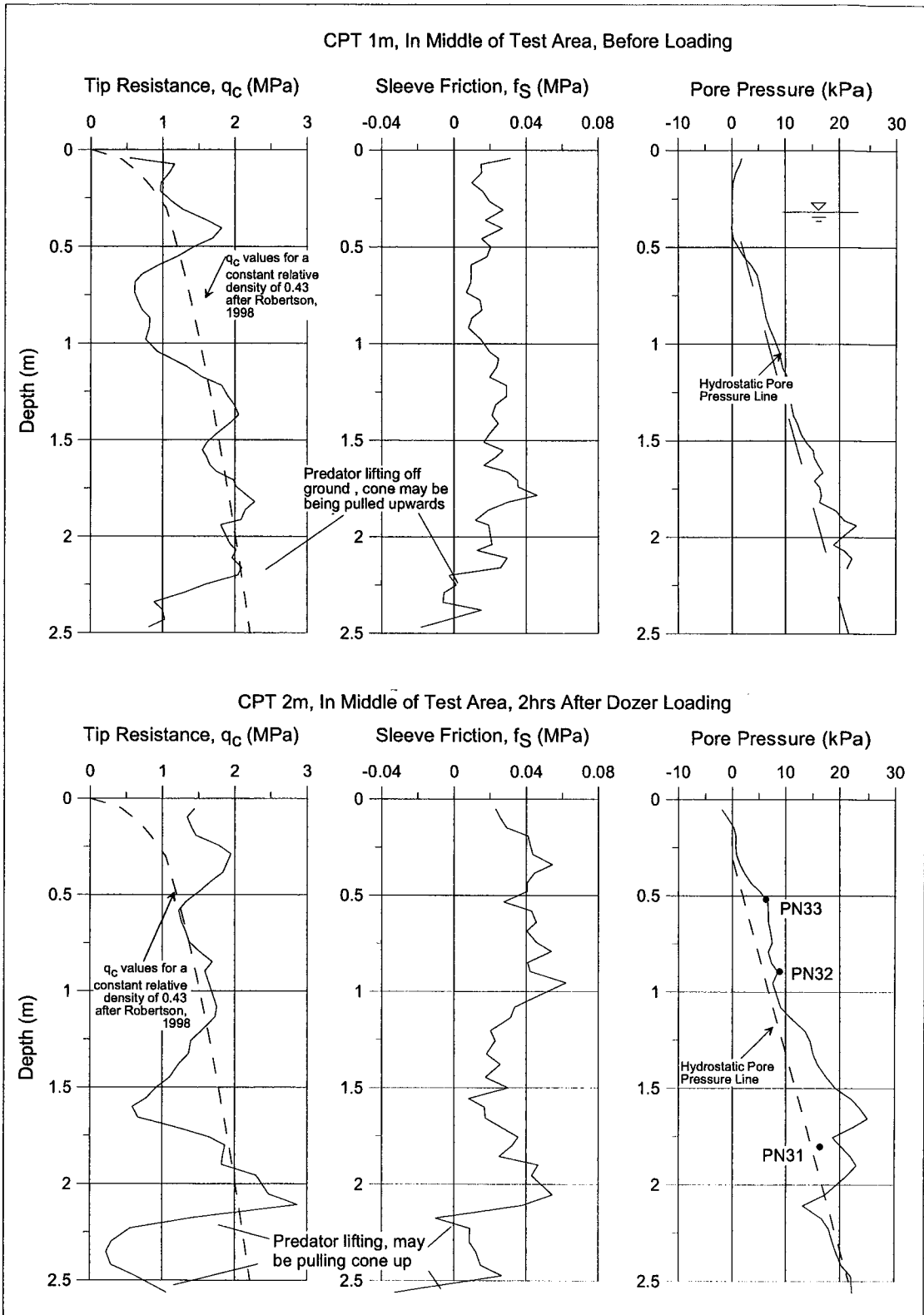


Figure 3.12 CPT Results from Middle of Main Site

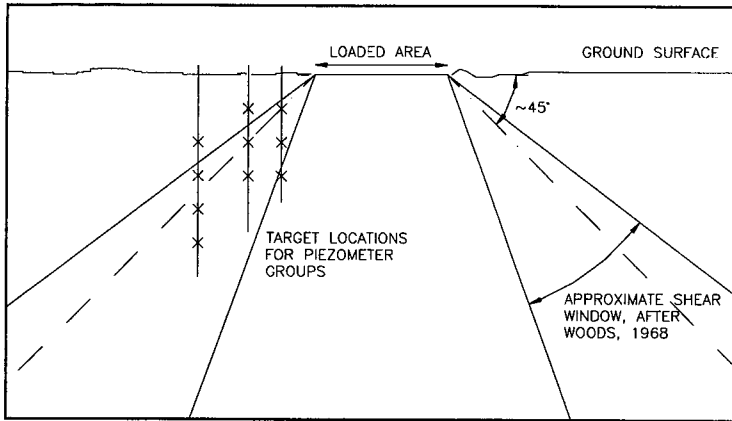


Figure 3.13 Shear Window and Target Piezometer Locations

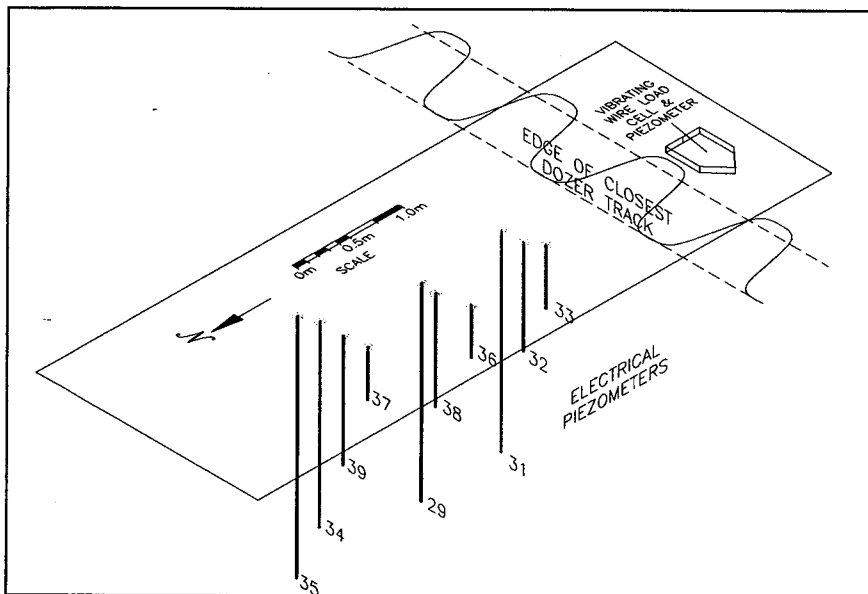


Figure 3.14 Instrument Locations

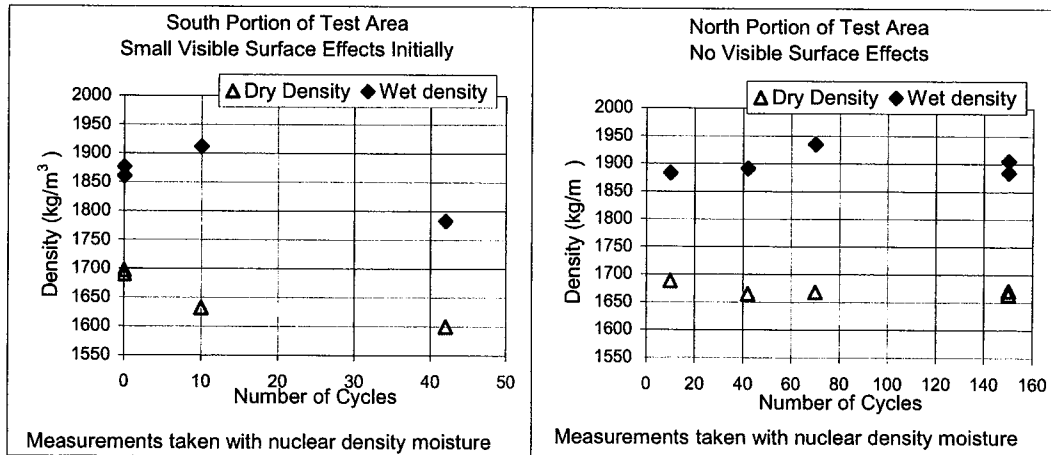


Figure 3.15 Density Variation During Predator Loading at Main Test Site

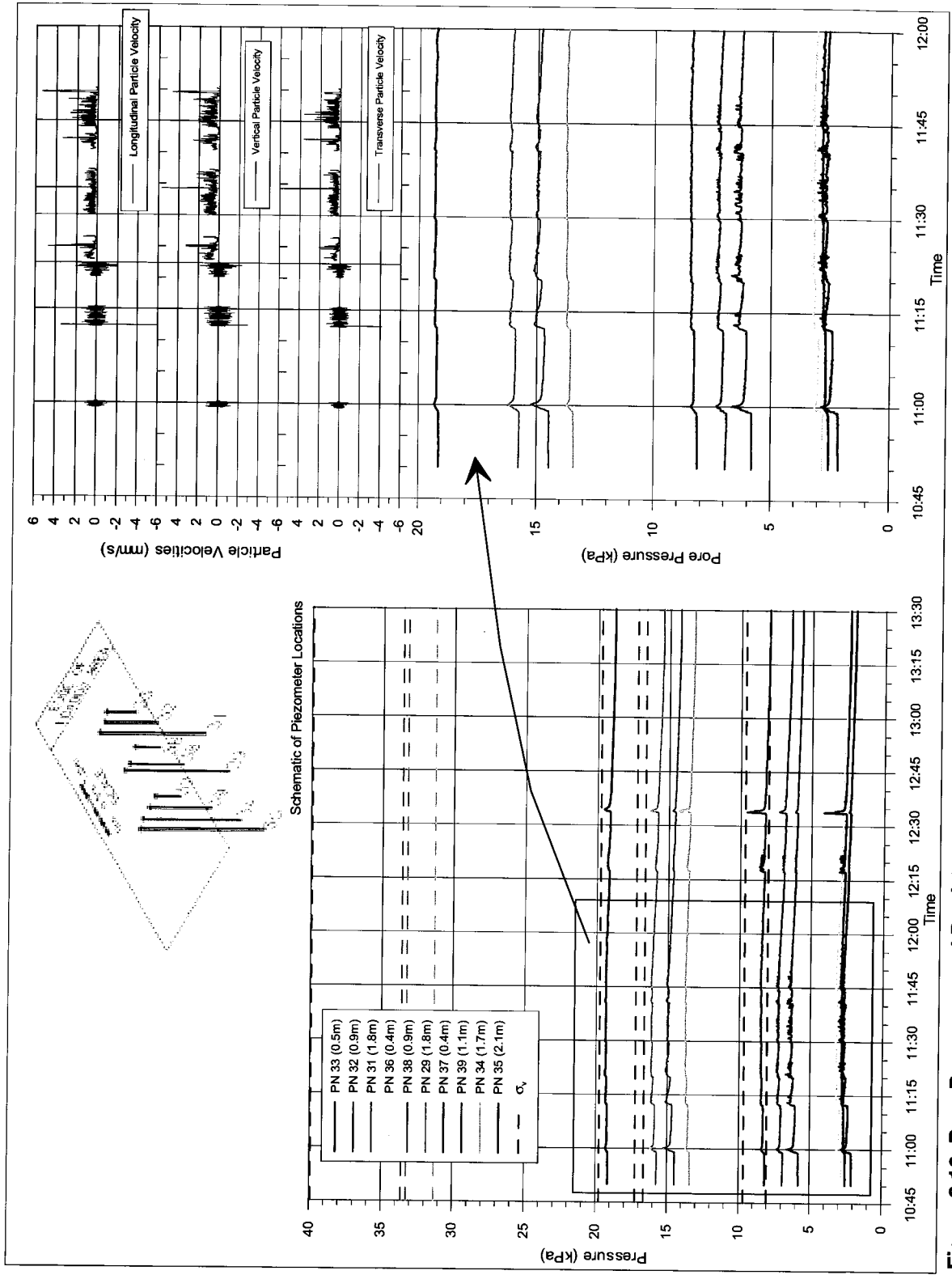


Figure 3.16 Pore Pressures and Particle Velocities Measured During Predator Loading



Figure 3.17 Main Test Site After Predator Loading

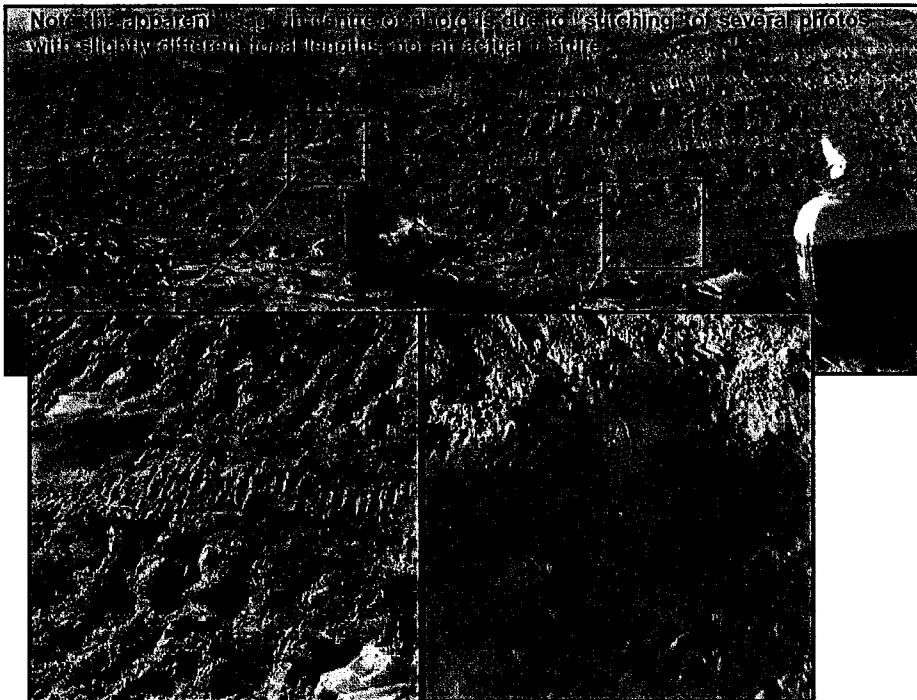


Figure 3.18 Main Test Site After Dozer Loading

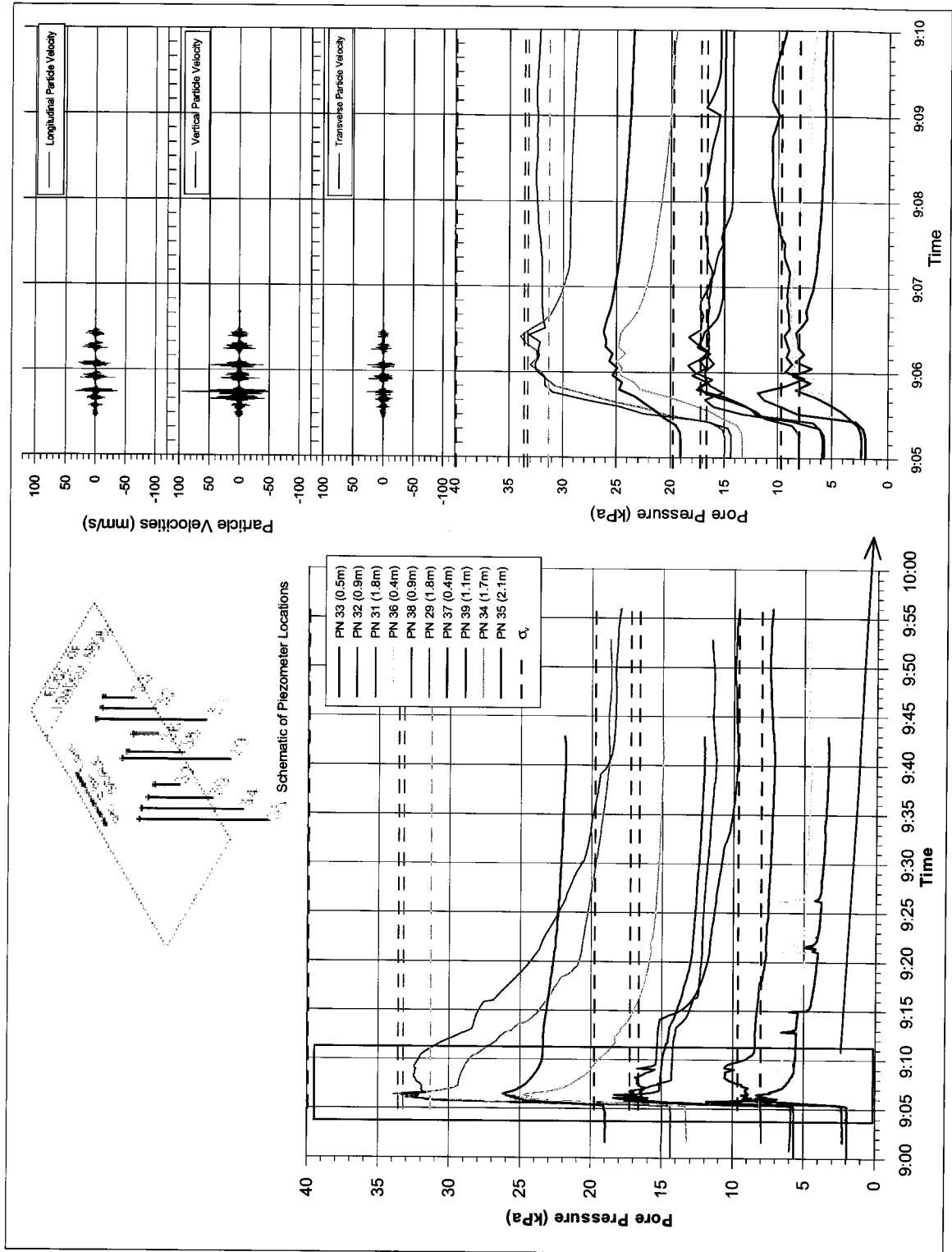


Figure 3.19 Pore Pressure and Particle Velocities Measured During Dozer Loading

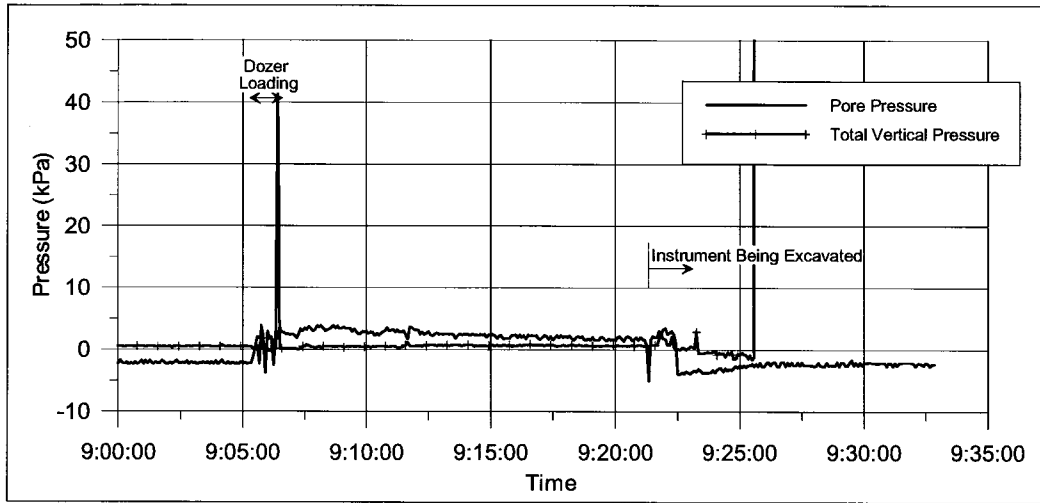


Figure 3.20 Pore Pressure and Load Cell Reading Between Tracks During Dozer Loading

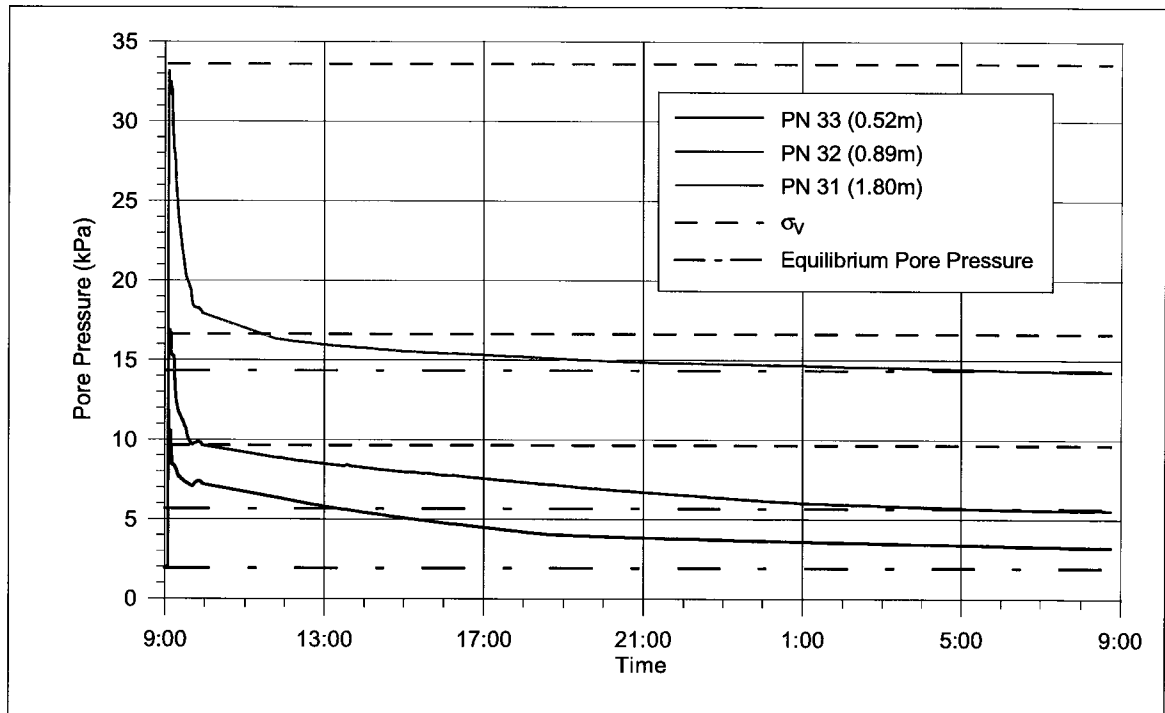


Figure 3.21 Pore Pressure Dissipation at the Main Test Site After Dozer Loading

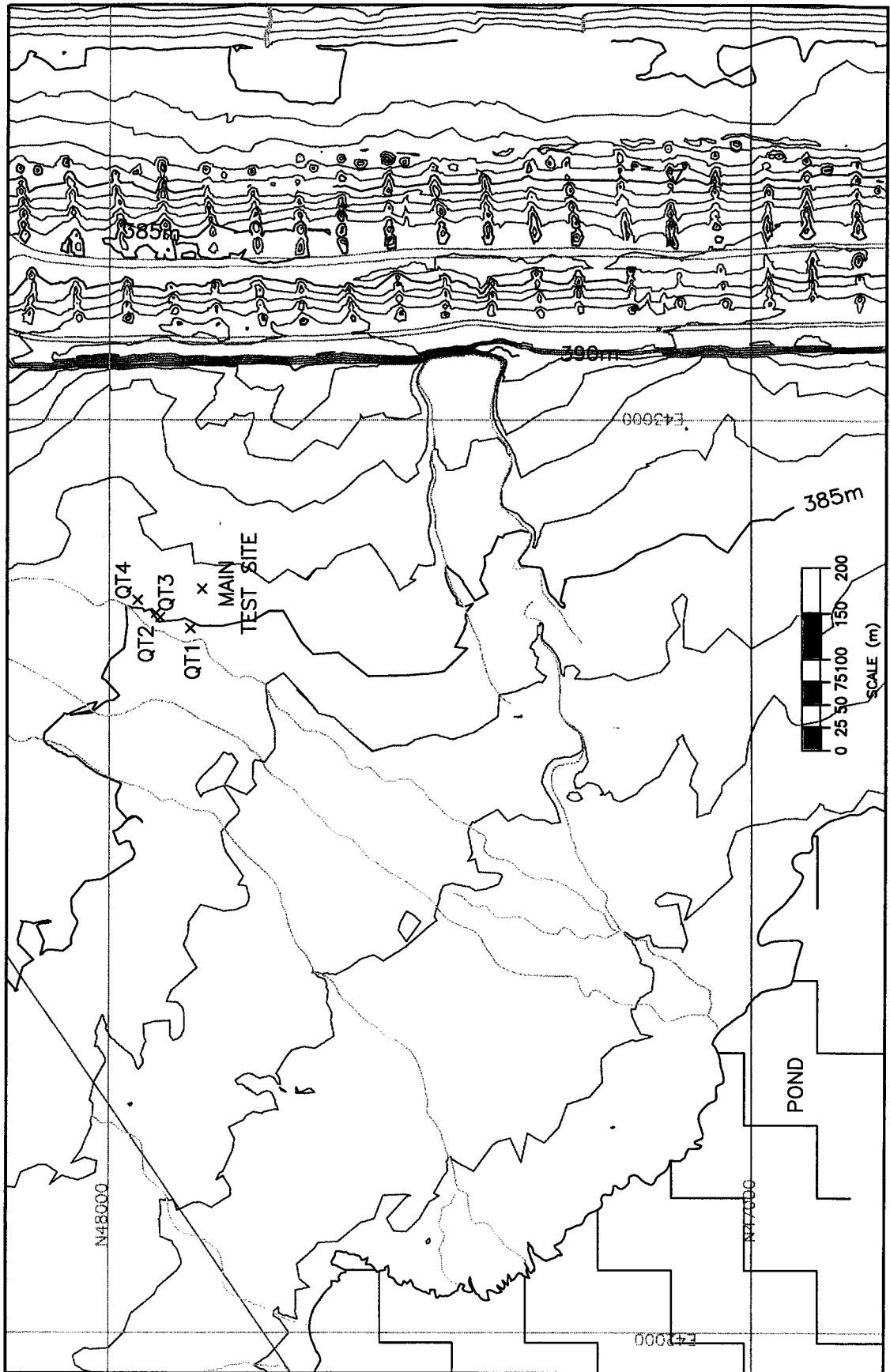


Figure 3.22 Location of Quick Test Sites

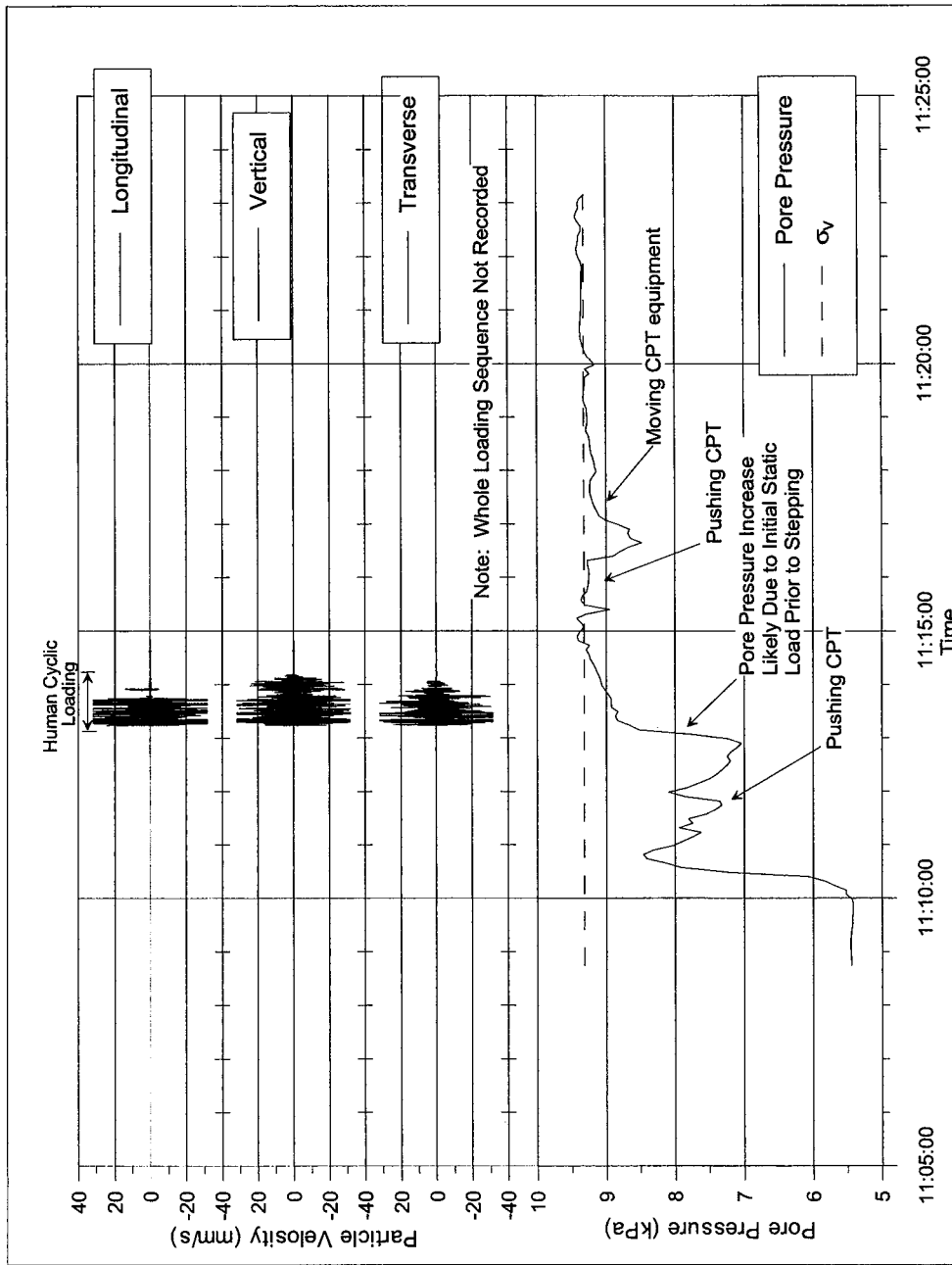


Figure 3.23 Pore Pressure and Particle Velocity to Light Loading at QT1

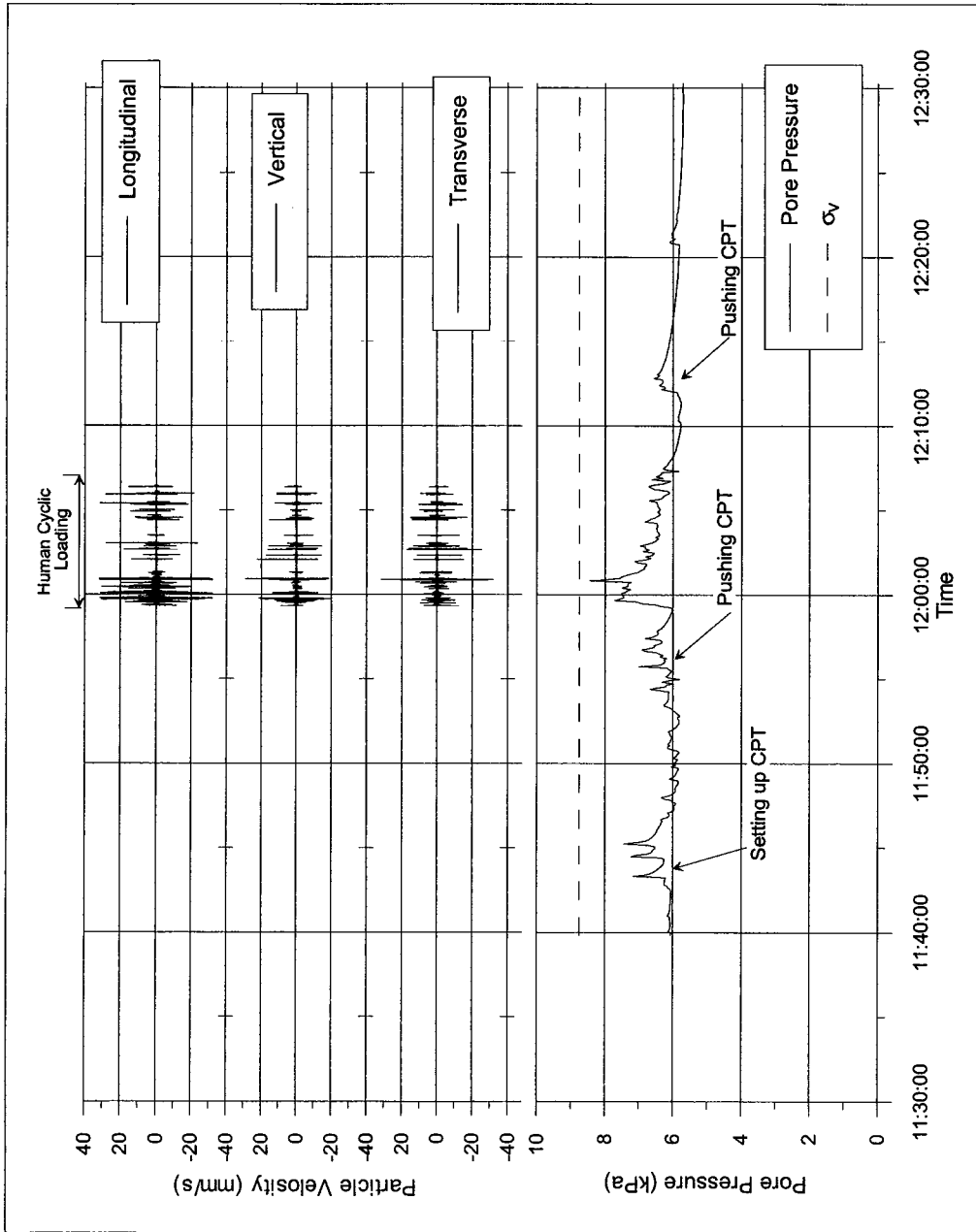


Figure 3.24 Pore Pressure and Particle Velocity to Light Loading at QT2

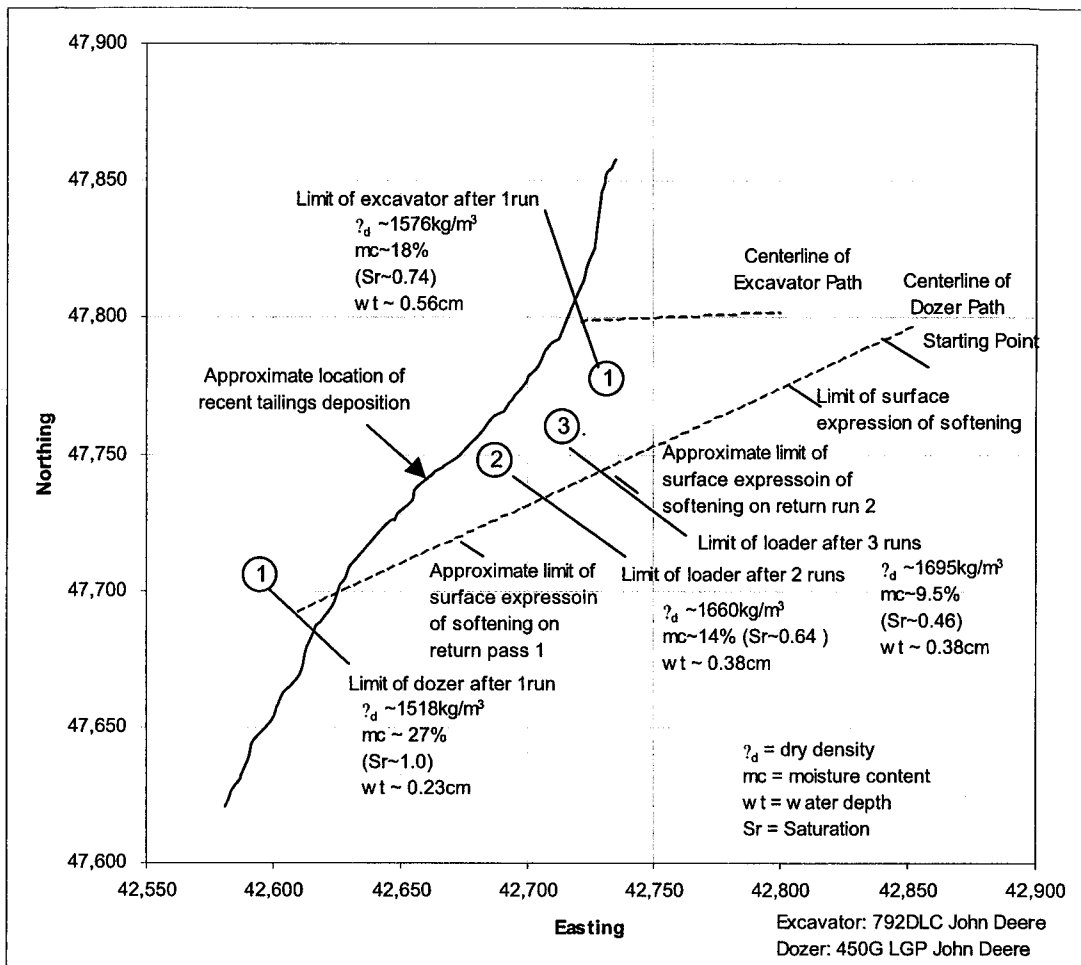


Figure 3.25 Trafficability Results

4.0 LABORATORY PROGRAM

4.1 General

A significant amount of laboratory testing has been carried out on Syncrude tailings over the years and the results are available through published papers (e.g. CANLEX), and Syncrude's internal database and reports. It was therefore decided to carry out a fairly limited laboratory testing program and if the tailings were found to have basic properties consistent with previous studies, the laboratory results of those previous studies would be applied to the main test site.

The mineralogy of Syncrude tailings at Mildred Lake and the Southwest Sand Storage Facility was expected to be fairly consistent and given that the tailings have all been subjected to similar extraction and deposition processes, similarity of grain size distribution between the tailings at the main test site and those used in previous studies was considered sufficient to confirm consistency of basic properties between studies. Grain size distribution tests were therefore carried out on various samples gathered from the test sites.

Density and void ratio measurements were also carried out on samples to identify the in-situ conditions of the deposit. Moisture contents of various samples were determined to allow comparison between laboratory and field measurements and also to provide some insight into the effect of bitumen on water content measurements with the nuclear gauge.

The laboratory test procedures are briefly discussed and the test results are then presented.

4.2 Laboratory Procedures

4.2.1 General

All tests were carried out at the University of Alberta using the laboratory facilities available in the Civil and Electrical Engineering Building. The procedures are only briefly outlined below, as the tests carried out were fairly routine and followed generally accepted procedures.

4.2.2 Moisture Content Determinations

Moisture contents of the bulk samples were determined following generally accepted geotechnical engineering procedures (ASTM, 2000a), whereby the difference in weight between the "wet" and oven-dried sample is used to evaluate the moisture content which is expressed as a percentage relative to the dry weight of soil according to Equation 4-1. Prior to testing, the samples were kept double plastic bagged in a moist room with a relative humidity of 75 percent or greater and temperatures generally between 4 and 6°C. The bulk samples were fairly large (approximately 2 to 5 kg), thus three sub samples were taken from each sample and used for moisture content measurements. In general, unless there was an obvious discrepancy in one measurement that could be explained, the average of the three moisture content measurements was considered representative of the whole sample.

$$m.c. = \frac{M_w}{M_T} \quad \text{Equation 4-1}$$

M_w = Mass of water

M_T = Mass of dry soil

4.2.3 Grain Size Analyses

Grain size analyses were carried out according to generally accepted procedures (ASTM 2000b). The samples were oven dried prior to testing and pulverized to break apart large clumps of tailings sand. Both wet and dry sieving procedures were initially employed and although there was no significant difference in the results from the two procedures, for the majority of the tests, washing was carried out on the finest sieve. The samples were shaken through a series of sieves with opening sizes ranging from 4.75 mm (No. 4 sieve) to 0.045 mm (No. 325 sieve).

The shaker vibrated the column of sieves up and down as it was rotated about a vertical axis. This shaker was chosen over one that only lifted the column up and down as it broke up small clumps of material more effectively. The sieves were shaken for at least 10 minutes. The material retained on a given sieve when washing was not required, was carefully placed into a tin, the sieve was brushed clean and the material was then weighed (as opposed to weighing the sieves before and after shaking). Two methods of washing were employed for comparison. Most commonly, the material retained on the number 325 sieve was washed until the water running through the sieve was clear. The material retained was then washed into a tin and placed in a drying oven for at least 24 hours before being weighed. The material washed through the number 325 sieve was not collected and therefore the amount of material passing the 325 sieve was calculated based on the known dry weight of material placed in the sieves and the cumulative amount of material retained on the various sieves. To confirm that there was not a substantial amount of fines stuck to the larger particle and thus retained on larger sized sieves, another washing procedure was also carried out. Prior to sieving, the sample was dried and weighed and then washed through the 325 sieve and dried and weighed again. The sample was then shaken through the stack of sieves.

4.2.4 Density and Void Ratio Measurements

Densities and void ratios of the tailings were measured at the main field test site and Quick Test Location 4 based on frozen samples and a disturbed sample of known volume. The density of the disturbed sample was calculated from measurement of the volume of the tube used to gather the sample and measurement of the weight and moisture content of the entire sample. The void ratio was then calculated based on a specific gravity of 2.66 as measured for Syncrude tailings during CANLEX (Robertson et al., 2000). The density and void ratio of the frozen samples were similarly based on a measured volume and moisture content but the procedure was somewhat more complicated as explained below.

Bulk density and hence void ratio of the frozen samples were measured following the "Immersion in water" procedures outlined in Head (1992). The method uses Archimedes principle to obtain the volume of the sample based on the submerged weight. Once the volume of the sample is known, the density and void ratio can be calculated based on

the sample weight, moisture content and specific gravity. To avoid migration of water into or out of the sample, the samples were coated in wax prior to submergence.

Prior to testing, the samples were stored double wrapped in plastic, in a cooler surrounded by ice which, in turn, was placed in a deep freezer located inside a large walk in freezer that was maintained at approximately -35 to -40°C . The block and cylindrical tube samples gathered in the field were cut up into smaller samples with a minimum volume of 15 cm^3 using a mitre saw. Trimming was carried out in a freezer with temperatures ranging between -5 and -15°C . Several different types of trimmed samples were used during testing. Initially rectangular samples were cut to allow accurate measurement of the sample volumes using vernier calipers so that the measured immersed volumes could be checked. Irregular sample shapes were used most often however, as they were easier to obtain and resulted in less wastage, particularly from the cylindrical specimens. Protrusions on the irregular samples were trimmed such that re-entrant angles were avoided. The original location of the trimmed samples within the larger sample was recorded. In general, no samples were taken from the upper several centimetres of a sample because there appeared to be significant disturbance in this region. After trimming, if wax coating and immersion could not be immediately carried out, individual samples were placed in a plastic bag, with the air removed and placed in a deep freezer located in a walk-in freezer with temperatures ranging between -35 and -40°C . All samples were tested within 24 hours of being trimmed. Ice crystals were observed on the surfaces of the samples and in general were removed prior to testing.

Trimmed samples were removed from the freezer, in groups of three or four, and kept surrounded by ice in a cooler prior to measurement of its submerged weight. Each frozen sample was weighed and then dipped in melted paraffin wax to create an impermeable seal. Samples were dipped in the wax generally 3 to 5 times until it appeared that a good seal with no cracks had been achieved. The samples were dipped as quickly as possible to minimize any melting of the sample. Generally, if air bubbles were detected in the wax coating, they were removed by creating a small hole in the wax and then re-dipping the sample to seal the hole. It is recognized however that there is typically a thin layer of air trapped between the sample and the wax (Kupper, 1991). The temperature of the wax varied between 70 and 100°C although it was generally maintained at the lower temperatures as recommended. The lower temperatures appeared to cause less cracking of the wax coating although it did appear to create thicker wax layers. In general, it was easier to obtain a good seal on the irregular shaped samples than on the rectangular samples because the wax at the corners of the samples tended to crack. A typical sample, prior to submergence, is shown in Figure 4.1.

The samples were allowed to cool slightly and then the weight of the wax-coated sample was measured. The coated sample was then placed on a hanger attached beneath a scale located in a tub of water at room temperature (approximately 17 to 20°C) as shown in Figure 4.2. Once the surface waves had dissipated and the scale reading stabilized, the submerged weight was recorded. It should be noted, that it took approximately one minute for the scale reading to stabilize and that the samples appeared to steadily gain weight at a rate of 0.01g per 1 to 5 seconds. This may have been due to cooling and the resulting shrinkage of the wax and any air space, which would effectively cause a decrease in volume and an increase in density.

The sample was then retrieved from the tub, and the wax coating was removed, occasionally with some of the outer portions of the sample. It should be noted that for the majority of the samples it did not appear that significant melting or ingress of water had occurred. The samples were then placed in a drying oven for moisture content determination. Initially the weight of the samples was measured after 1, 4 and 5 days in the oven to ensure that sufficient time was allowed for the ice to melt and evaporate. No variation in dry weight was observed at the various times, therefore 24 hours was determined to be a suitable drying time.

4.3 Laboratory Test Results

4.3.1 General

The results of the laboratory tests are summarized and briefly discussed below. A discussion of the results as they pertain to the soil response is presented in Section 5.0. Results of all laboratory tests can be found in Appendix B along with a summary of the relevant information regarding the samples testing.

4.3.2 Moisture Contents

The moisture contents of the samples gathered from the various test sites ranged from 11 to 26 percent. The lower values generally corresponded to samples taken from the unsaturated zone above the phreatic surface prior to any softening while the higher values were generally associated with samples gathered after softening. Generally, bitumen is considered part of the fluid phase when dealing with oil sands (Lord and Cameron, 1985) however, due to the low bitumen concentration in the tailings and because in the field any bitumen in the tailings appeared to be solid, corrections were not made for including bitumen in the fluid phase. To avoid large errors due to this assumption, large chunks of bitumen were removed from any samples prior to moisture content determination although this was generally not necessary as the tailings were fairly clean.

4.3.2.1 Disturbed Bulk Samples

Samples gathered from locations where measurements had also been taken using a nuclear density moisture content gauge were found to have moisture content values within approximately 1 to 2 percent of the value indicated by the gauge as shown in Table 4.1. It should be noted that if there had been significant quantities of bitumen in the tailings, the nuclear gauge readings would have been expected to be higher than the measured laboratory values as the gauges interpret the hydrogen rich bitumen as water (Lord and Cameron, 1985) and since no correction was made in the laboratory, it would have been included in the solid phase in laboratory measurements.

Table 4.1 Moisture Content Comparison Between Laboratory and Field Measurements Taken at the Same Location

Sample	Laboratory Moisture Content (%)	Nuclear Gauge Moisture Content (%)
1 (before loading)	13.1	12.8
21 (after loading)	23.9	25.3
22 (after loading)	23.8	23.9

The average moisture content of the main test site above the phreatic surface, prior to loading based on bulk samples was 15 percent, slightly higher than the 11 percent average measured by the nuclear gauge. These variations were due to different sampling locations and the heterogeneity of sand deposits. Following softening, the average moisture content at the main test site was measured at 24 percent based on both bulk samples and nuclear gauge readings. The moisture content measurements carried out on bulk samples gathered from Quick Test Site 4 also indicated a slight increase in moisture content after softening, from 23 to 25 percent.

Based on moisture content measurements of various disturbed samples gathered during the trafficability study, it appeared that as the tailings were able to sustain more dozer passes without softening, the moisture content in the unsaturated zone above the phreatic surface decreased. At the end of the furthest pass, i.e. softening occurred on the first run, the gathered samples had a moisture content of 25 percent while those gathered at the limits of the second and third runs had moisture contents of 19 to 20 percent and 17 to 18 percent, respectively. The values measured may not be completely indicative of in-situ conditions prior to equipment traffic as the samples were collected after the dozer had completed all the runs and some softening had been induced. The samples were collected at a small distance from the track locations but the moisture content of the samples may have been somewhat affected by induced gradients and the dissipation of excess pore pressures. The moisture contents measured 24 hours later by the nuclear gauge indicated greater differences in the moisture contents of the tailings at the various locations with values of 27, 14 and 10 percent at the ends of the first, second and third runs respectively.

4.3.2.2 Frozen Samples

The tests carried out on the frozen samples indicated a much smaller range in water content values between samples than did the bulk samples and nuclear gauge measurements, particularly at the main test site. This did not appear to be consistent with visual observations, as it appeared that the tailings became significantly wetter upon softening. The equations used to calculate the moisture content of the frozen samples are included in Appendix B because they are slightly different than those used to analyze thawed samples to account for the volume expansion of water during freezing.

Moisture content measurements from frozen samples at the main test site before softening did not agree well with the moisture content measurements from either the bulk samples or the nuclear gauge. The frozen samples indicated a moisture content of between 19 and 23 percent for the tailings deposit at the main site prior to loading and between 22 and 24 percent following softening at the main site. The frozen samples gathered near Quick Test location 4 indicated no change in moisture content, remaining at 22 percent. With the exception of the moisture contents prior to softening at the main test site, the remaining moisture contents agree relatively well with other moisture content measurements. However, based on visual observations and the amount of water brought to surface during softening at Quick Test location 4 it seems unlikely that there was no change in moisture content before and after softening. It was observed upon trimming of some of the after-softening samples that there were tube like voids, possibly piping channels, that were not completely filled with ice. It is unclear whether this unsaturated state was a reflection of the true in-situ conditions or an effect of the apparent friability of the ice and thus caused by trimming of the samples.

The tests carried out on the frozen samples indicated that none of the samples were saturated and that the degree of saturation was fairly consistent between samples. The unsaturated nature of the tailings was not completely unexpected as the samples were gathered near surface and also it has been reported that there can be significant gas content in tailings. However, the similarity of degree of saturation between samples did not appear to be consistent with visual observations as the main test site appeared significantly drier prior to loading than the Quick Test location and there appeared to be a substantial increase in saturation, particularly at the main test site following softening.

A possible cause for the higher moisture content values (and thus saturation) prior to softening at the main test site may be that because the soil was unsaturated, water was drawn towards the freezing front as freezing occurred, similar to the manner in which an ice lens forms. The higher moisture content values, particularly before softening, could also possibly be explained if dilation occurred due to the insertion of the metal tube causing water to flow into the sample. This would have not only increased the amount of water but would have decreased the weight of solids resulting in an increased moisture content. A similar effect may have occurred due to expansion of the soil skeleton as the pore water froze.

4.3.3 Void Ratio and Density

The frozen samples gathered appeared to have retained the macroscopic structure of the tailings reasonably well. Layering in the tailings deposit was visible in the samples gathered prior to softening and there appeared to be evidence of piping channels in some of the samples gathered after softening—as can be seen in Figure 4.3. As discussed however, the moisture contents measured did not always appear consistent with visual observations and this could be expected to affect void ratios.

As with the moisture contents obtained from the frozen samples, the variation in average void ratios measured from the various frozen samples was fairly small. Complete results of the void ratio measurements can be found in Appendix B. The average void ratios measured from the frozen samples indicated a small increase after softening at the main test site and a slight decrease in void ratio after softening at Quick Test location 4. However, the variation in void ratio measured between samples trimmed from the same larger sample was greater than the variation between average values for the larger samples. The small changes measured between before and after softening conditions therefore may not be meaningful. The total range of void ratios measured from the trimmed samples was between 0.67 and 0.93. Within a given sample the total variation was generally not greater than 0.1 and the variation tended to be greatest within samples gathered after softening. There did appear to be a somewhat systematic change to the void ratio measurements within the samples however. There appeared to be a decrease in void ratio with depth. This was reflected by differences between trimmed samples obtained from the same larger sample and also by comparison of the block and tube samples. The block samples were shallower and had higher average void ratios than the deeper cylindrical tube samples. Drying, weathering and low confining stresses could potentially cause higher void ratios near the ground surface. A systematic lateral variation in void ratios was also observed in the tube samples, particularly in those gathered prior to softening. It appeared that there was a decrease in void ratio with distance from the tube varying between 0.87 and 0.82 at the wall of the tube to between 0.81 and 0.66 at the edge of the sample. This lateral variation was not

observed in the block samples suggesting that the insertion of the metal tube may have caused disturbance and been responsible for the variation in void ratio. Sampler disturbance is a well-known phenomenon and is reported by many researchers (e.g. Yoshimi et al., 1977; Marcuson and Franklin, 1980; Tokimatsu and Hosaka, 1986; Konrad, 1995) and if the samples were dilative, it would be expected that void ratios would decrease away from the zone of disturbance around the tube.

Because of the systematic variation in void ratios observed, it appeared likely that trimmed samples located away from the surface and central tube, towards the middle and edges of the tube samples, were more representative of in-situ conditions. A representative range of in-situ void ratios based on the frozen samples therefore appeared to be between 0.81 and 0.72. This agreed reasonably well with the void ratio measured from the disturbed tube sample of 0.75.

Frozen bulk densities were measured directly from the samples. If the saturation of the samples was less than 92 percent, as was the case for the majority of the samples, the frozen bulk density is equivalent to the thawed density as the voids can accommodate the water expansion during freezing. If the sample was saturated, however, and no expansion of the soil occurred during freezing, the frozen bulk density would be less than the in-situ value as the amount of water in the sample would be decreased and corrections to the measured frozen density would be required. The calculations are included in Appendix B. Once the bulk density was known and the moisture content measured, the dry density could be calculated using standard phase relationships. The bulk densities of the frozen samples were found to range between 1720 and 1860 kg/m³. The dry densities, however, had a smaller range, between 1440 and 1500 kg/m³. The saturated tailings density was therefore calculated to range between 1900 and 1950 kg/m³. The remoulded samples indicated similar densities with a measured bulk density of 1783 kg/m³ and corresponding dry and saturated densities of 1517 kg/m³ and 1950 kg/m³, respectively.

4.3.4 Grain Size Distributions

The results of the grain size distribution tests carried out on the bulk samples are shown in Figure 4.4. The samples tested were gathered from depths between 0.1 and 2 m and from both before loading and after softening. Two systems for soil classification are shown in the figure, that presented in the Canadian Foundation Engineering Manual (1992) and that used by Syncrude. The results confirm the visual classification of the tailings as a uniform fine to medium sand. The fines content as defined in the Canadian Foundation Engineering Manual, particles smaller than 0.075 mm, ranged between 1 and 5 percent. Fines content as defined by Syncrude, particles smaller than 0.045 mm, appeared to range between 0.2 and 2.2 percent. The coefficient of uniformity was found to range between 1.9 and 2.2. As can be seen in Figure 4.4, the difference between wet and dry sieving was not significant, possibly because of the small amount of fines. The data also do not appear to indicate any significant change in grain distribution with depth in the upper few meters. Another comparison between samples collected prior to loading and after softening is shown in Figure 4.5. The data in this figure suggests that there was no significant upward washing of fines due to the high gradients and piping that occurred as a result of dozer loading.

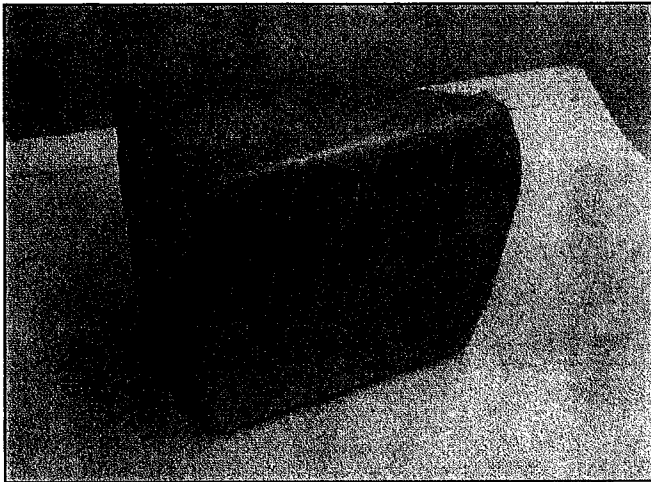


Figure 4.1 Typical Wax Coated Sample Prior To Submergence

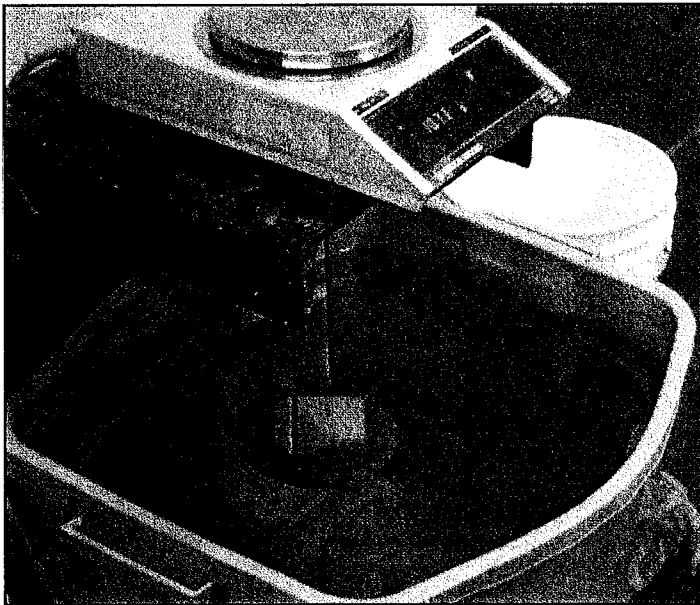


Figure 4.2 Set-up for Measurement of Submerged Weight of Wax Coated Samples

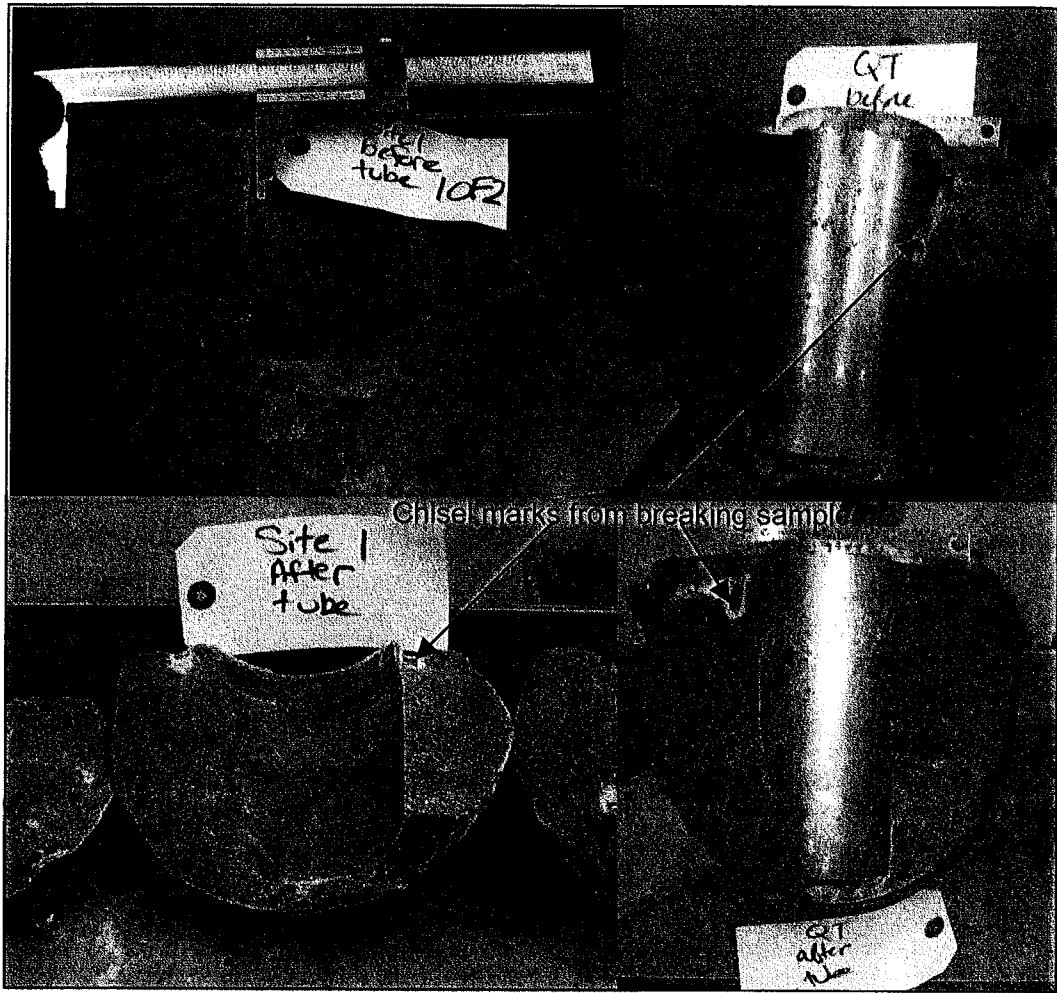


Figure 4.3 Frozen Samples Prior to Trimming

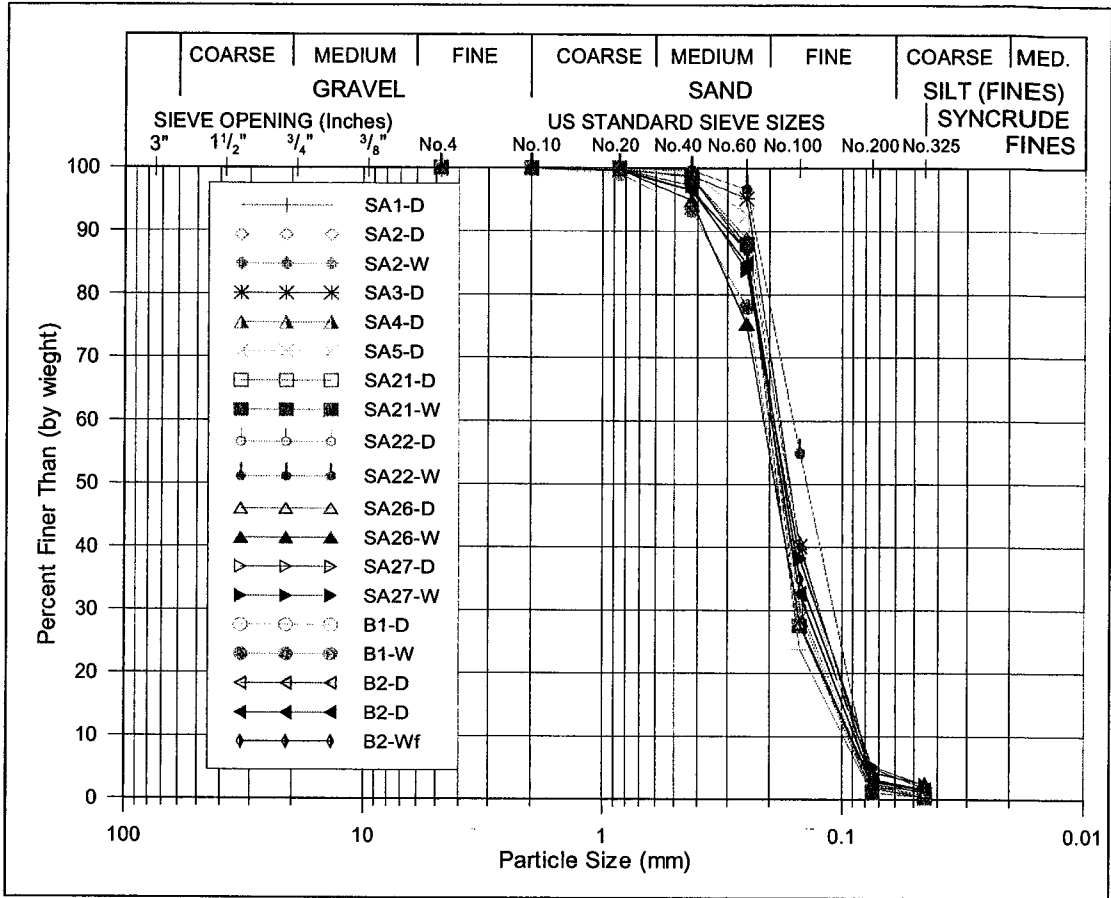


Figure 4.4 Grain Size Distribution of BAW Tailings Sand at Main Test Site

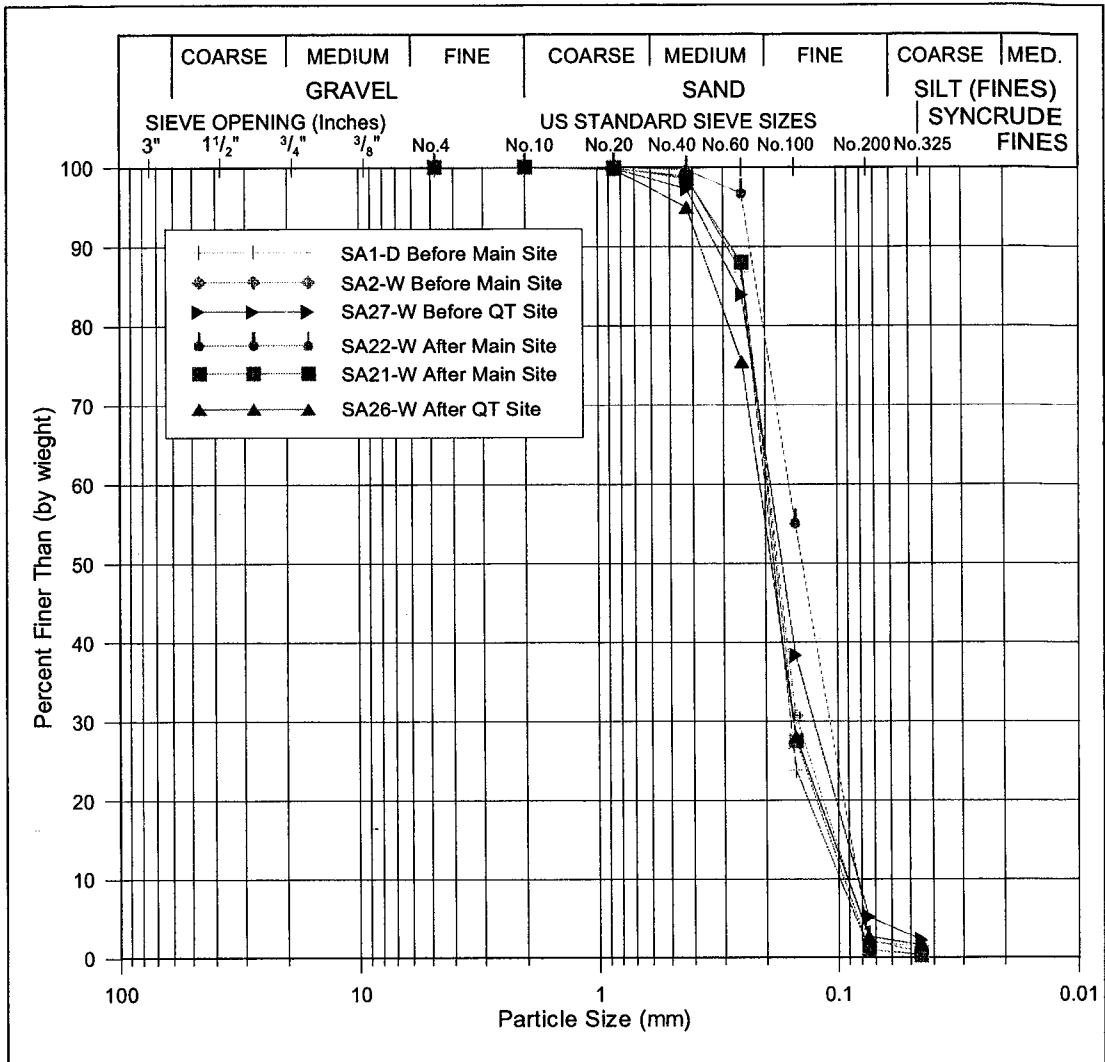


Figure 4.5 Grain Size Distributions Before and After Softening

5.0 DISCUSSION

5.1 General

The data gathered during the field investigation and from laboratory testing were analyzed and compared with published data to explain why the vibratory equipment loading caused softening of the tailings deposit. The following section begins with a discussion of the in-situ conditions of the deposit based on both field and laboratory measurements in an effort to identify what types of load responses would be expected. The analyses and interpretation of the data gathered during the field program are then presented and a mechanism for the occurrence of softening is explained. Factors controlling the softening phenomenon are then discussed. Finally the commonly used charts for the evaluation of liquefaction potential are applied to the main test site and results are extrapolated to other conditions.

5.2 Initial Conditions of Deposit

5.2.1 General

In general, the properties that control the behaviour of a sand can be grouped into two categories, intrinsic properties that cannot be readily altered and environmental or placement conditions. The former includes characteristics such as grain size distribution, particle angularity, and particle mineralogy. It is well known that these characteristics influence the shear strength properties of a sand and many researchers have indicated that they also affect the liquefaction susceptibility and cyclic strength of a deposit (e.g. Sladen et al., 1985; Vaid and Chern, 1985; Poulos et al., 1988; Kramer, 1996). The latter group of characteristics affecting the behaviour of a sand deposits includes factors such as soil fabric, in-situ void ratio, confining stress, and load path. These factors can be modified and varied during laboratory testing. Therefore it would appear reasonable that if the intrinsic properties of the tailings sand at the test sites were similar to other tailings used in previous studies, the results of those previous tests could be applied to the field test site. The tailings at all the Syncrude leases were generally derived from the same geologic unit and were all subjected to the same extraction and hydraulic processing, suggesting that the particle mineralogy and angularity should be consistent for each tailings storage facility. Therefore, if the grain size distribution of the tailings at the test sites were similar to other tailings at Syncrude, particularly other tailings deposited in a similar manner, it would seem reasonable to apply the results from in-situ and laboratory testing carried out at other Syncrude sites to the test sites utilized in this research.

The similarity of the tailings at the main test site to other beach above water (BAW) tailings at Syncrude will first be compared based on CPTs and laboratory grain size distribution tests. Once the similarity is confirmed, test results on Syncrude sand from published data will be used to evaluate the initial state and expected behaviour of the deposit based on the measured in-situ density and void ratio. The expected behaviour of the tailings under load is also evaluated based on the CPT data using several different procedures.

5.2.2 Comparison of the Tailings at the Main Test Site with Other Syncrude Sites

The tailings were characterized visually as a uniformly graded fine to medium sand. The grain size distribution curves obtained from samples gathered at the main test site and at the quick test sites are similar and did not indicate any significant systematic change in fines content with depth in the upper several meters. The grain size distribution curves compare well with the representative grain size curve selected by CANLEX for the Mildred Lake tailings as shown in Figure 5.1. As seen in Figure 5.1, the samples gathered during the current study had a fines content (percent finer than 75 μm) of 1 to 5 percent and a median grain size ranging from 0.15 to 0.19 mm with an average of approximately 0.17 mm. The calculated coefficients of uniformity of the samples ranged from 1.9 to 2.3 with an average value of 2.1. These values are similar to those reported by CANLEX for Syncrude tailings with a median grain size of 0.16, a fines content of approximately 10 percent and a coefficient of uniformity of 2.2 (Robertson et al., 2000).

Syncrude also has a database of tests that have been carried out on their tailings, which was reviewed by HBT AGRA (1992) and can be compared with the tailings encountered in the current study. The fines contents recorded in the database were similar to those measured from the samples gathered during the field program. The database indicated that BAW tailings generally had a fines content (percent finer than 74 μm) between 8 and 14 percent with a total range of 2 to 25 percent and less than 5 percent clay sized (percent finer than 2 μm). The laboratory tests included in the database were carried out on samples with fines contents ranging from 2 to 35 percent, but over half of the samples had fines contents between 5 and 10 percent. Where recorded, the laboratory tailings sand specimens included in the database had less than 2 percent clay sized particles. The higher fines content samples included in the database tended to be tailings sand and sludge mixtures, which had higher clay contents and coefficients of uniformity. The fines contents measured from the samples gathered during the current study, although at the finer end of the range, are similar to the fines contents recorded in the database, particularly when compared with the samples used for lab testing. The coefficient of uniformity for the laboratory tailings sand specimens in the database ranged between 1.5 and 3, which compared well with the 1.9 to 2.3 range measured from the samples gathered at the test sites. Vaid and his co-workers have also carried out significant amounts of testing on Syncrude sand characterized as having a mean grain size of 0.2 mm (Vaid and Sivathayalan, 2000), which is similar to the samples gathered during this study. The good agreement between the grain size distribution of the tailings at the test site and those included in the database and studied as part of CANLEX should allow extrapolation of previous test results from these sources to the test sites used in this study.

The CPTs carried out prior to loading at the main test site were compared to results from various studies carried out on BAW tailings at the Southwest Sand Storage and at the Mildred Lake Settling Basin (HBT AGRA, 1992; Conetec, 2000; Conetec, 2002) and the results were similar. Since the CPT responds to soil behaviour the similarity in CPT results suggests that the tailings at the main test site could be expected to respond to load in a similar manner to other BAW tailings at Syncrude.

5.2.3 In-situ State and Expected Behaviour

The in-situ state of the tailings deposits, prior to loading, was also important to identify since it is a controlling factor in how a sand is expected to behave under monotonic load and in terms of what types of liquefaction are possible.

Density is often considered an indicator of material behaviour. For example there are general rules of thumb related to the friction angle of a “dense” sand versus a “loose” sand. The Troxler data gathered at the main test site indicated that the tailings deposit appeared to be fairly dense in a conventional sense, in that the dry density at the main test site was equal to or greater than 95% of the maximum Standard Proctor density used routinely by Terracon for Syncrude tailings. Generally case histories indicate that liquefaction failures occur in soils with less than 85 percent Standard Proctor density (McRoberts and Sladen, 1992) although McRoberts and Sladen (1992) do refer to laboratory tests carried out by Castro et al. (1982) in which contractive behaviour occurred in sands with densities as high as 92 percent Standard Proctor.

Within liquefaction literature relative density is a more commonly used as a descriptor of density than percent compaction. As discussed in Section 4.3.3, a range of void ratios were measured from the frozen samples gathered during the field investigation. These measured values ranging between 0.72 and 0.81 were significantly larger than the void ratios suggested by the nuclear gauge data averaging 0.57 at the main test site and ranging between 0.65 and 0.82 at the Quick Test locations. Previous studies (HBT AGRA, 1992) indicated that nuclear gauge measurements can produce fairly accurate dry densities (often within $\pm 50 \text{ kg/m}^3$) and, as shown in Table 3.2, the measured moisture contents appeared fairly consistent with laboratory measurements. Therefore it was expected that void ratios of the near surface tailings could be calculated from the nuclear gauge readings with reasonable accuracy. The discrepancy between the void ratios estimated from the nuclear gauge readings and the frozen samples cannot be entirely explained at present. The nuclear gauge measurements penetrated deeper than the frozen samples and there did appear to be a tendency of decreasing void ratio with depth, which could account for slightly lower void ratios based on nuclear gauge measurements. Also, any air trapped in the frozen samples during measurement would tend to increase the void ratios measured from the samples. There is also a very high degree of variability in void ratio even within a sand deposit that appears to be homogeneous (Robertson et al., 2000). To assess the reasonableness of the measured void ratios, a survey of void ratios measured in-situ at Syncrude during previous studies was made.

The CANLEX investigations indicated that the average void ratio for the tailings encountered at Mildred Lake was 0.77, however the void ratios were generally determined for tailings that were at greater depths than in the current study and in general were targeting suspected looser beach below water (BBW) zones. Two studies, Küpper (1991) and HBT AGRA (1992), included measurement of surficial void ratios from frozen block samples. As expected there was a range in the measured void ratios, from 0.65 to 0.80 with most of the values falling between 0.72 and 0.76, which is consistent with the results from the frozen samples gathered at the main test site. A representative average value for the void ratio of the tailings at the test sites was therefore estimated as 0.76. Using the maximum and minimum void ratios determined during CANLEX of 0.958 and 0.522 respectively (Robertson et al., 2000), this corresponds to a relative density of 45 percent. Generally this would correspond to a

medium dense sand (e.g. Seed and Lee, 1966; Seed, 1983). However, as noted by both Ishihara (1993) and Vaid and Chern (1985), relative density is often not sufficient to define the state of a sand, particularly when dealing with stresses outside the stress range typically encountered in geotechnical practice. For example, Vaid and Chern (1985) reported dilative response of tailings sand with initial relative densities of 15 percent at low confining stresses and contractive response of the same tailings sand with an initial relative density of 70 percent under high confining stresses.

An assessment of the in-situ stresses in the deposit was therefore also necessary to define the state of the soil prior to equipment loading. The initial in-situ stresses were not measured during the field investigation, but rather stresses were evaluated using the measured saturated density (1925 kg/m^3) and an estimated horizontal to vertical stress ratio, K_0 of 0.5 based on the CANLEX research data (Wride et al., 2000). This value is also close to what would be expected for a normally consolidated young soil. A plot of void ratio versus mean effective stress is shown in Figure 5.2 with the steady state line adopted by CANLEX for Syncrude tailings. For completeness, all of the trimmed samples, including samples from the upper portions and near the cylindrical tube, which generally had larger void ratios, and the void ratios estimated from the nuclear gauge measurements are shown in the Figure. Note that if a higher K_0 was used in the evaluation, the data points would plot farther to the right on Figure 5.2, but would still fall on the same side of the CANLEX steady state line.

All of the data points from this study plot beneath the CANLEX steady state line, as shown in Figure 5.2, and are therefore considered dense of critical state, which means that the tailings should exhibit dilative behaviour at large strains, particularly in triaxial compression. This conclusion also appears to be supported by data presented in HBT AGRA (1992) and Kupper (1991).

Based on these Figures, theoretically the BAW tailings deposit at the main test site could be susceptible to cyclic liquefaction or cyclic mobility but not to flow liquefaction although limited liquefaction may be possible. It is noted, however, that none of the tests carried out to determine the steady state line were carried out at the very low confining stresses experienced near ground surface and that the steady state line in this area is an extrapolation of test data. Some researchers (e.g. Tatsuoka et al., 1986; Been et al., 1991; and Ishihara, 1993) have suggested that the steady state line may curve and flatten at low stresses possibly levelling off to a single void ratio. The measured values however plot well below both the steady state line and the maximum void ratio measured for Syncrude tailings during CANLEX.

The state of a deposit can also be estimated directly from CPT data. Three methods were used to estimate the state parameter; those proposed by Been et al. (1988), Plewes et al. (1992) and Been and Jeffries (1992). These methods define the state parameter as the difference between the in-situ void ratio and the void ratio at critical state at constant mean effective stress. Been et al. (1988) proposed a relationship between the state parameter and the normalized penetration resistance and dynamic pore pressure. This relationship was based on large calibration chamber tests carried out on sands and on field tests carried out on clays and silty material with the dynamic pore pressure accounting for the difference in drainage conditions between the various soil types. The procedures proposed by Plewes et al. (1992) and Been and Jeffries (1992) are based on the Been et al. (1988) relationship and are dependant on the slope of the steady state line in void ratio: log mean effective stress space (λ_{ss}) but allow for a

varying steady state friction angle in their equation for k^* . The other difference between the three methods is the proposed relationship for determining λ_{ss} . The Been et al. (1988) method required that λ_{ss} be a known value based on laboratory or other testing. Plewes et al. (1992) proposed a relationship between λ_{ss} and the normalized friction ratio measured by the CPT based on field results from clays and silts and laboratory chamber tests on sands. Been and Jefferies (1992) proposed a relationship for λ_{ss} based on the Soil Behaviour Index, I_c , calculated from CPT measurements according to Jefferies and Davies (1991).

Steady state parameters of $\phi_{ss}=33^\circ$ and $\lambda_{ss} = 0.0152$ as suggested by CANLEX (Byrne et al., 2000; Robertson et al., 2000) were used in the equations to calculate the state parameter from the CPTs carried out at the main test site. Complete equations used in the analyses as well as individual plots and a summary of the results can be found in Appendix C. The three methods all indicated that the tailings had a negative state parameter with the Been et al. (1988) relationship producing the most negative values. The remaining two methods produced very similar results with average state parameters of -0.18 and -0.15. The Plewes et al. (1992) method was the only one that indicated a few points with a positive state parameter. CANLEX findings suggested that the Plewes et al. (1992) method was most applicable to Syncrude tailings and the results of this method are therefore plotted in Figure 5.3.

A negative state parameter as defined in the methods discussed above indicates that the in-situ void ratio is less than the void ratio at critical state, i.e. the state lies below the steady state line in void ratio mean effective stress space. Therefore, the analyses of the CPT data agreed with the findings from the analyses of the measured void ratios and indicate a dilative response, at least at large strains. These findings appear to agree in general with findings presented by various researchers with regards to the behaviour of BAW tailings. Vaid and Chern (1985) reported on large number of cyclic undrained tests on tailings sand, which covered a wide range of initial states and did not observe a true flow liquefaction (i.e. completely strain softening) response in any of the samples although they did observe limited liquefaction reaching a quasi steady state in some of the samples. Robertson et al. (2000) reported that of the 53 frozen tailings samples gathered at Syncrude none exhibited strain-softening behaviour when tested in triaxial compression, extension or in simple shear; all exhibited dilation and strain hardening behaviour, at least at large strains and most of the samples exhibited no loss in strength.

5.2.4 Penetration Resistance

There are many relationships between penetration resistance to cyclic liquefaction susceptibility as discussed in Section 2.4.3. A large amount of field experience and case histories have been used to relate the standard penetration resistance, corrected for overburden pressure and normalized to 60 percent energy transfer (SPT $(N_1)_{60}$) to liquefaction susceptibility and there exist many correlations between CPT measurements and $(N_1)_{60}$ values. There are also criteria for the liquefaction susceptibility of a deposit based directly on CPT measurements. In order to get a general idea of the range of behaviours predicted at the main test site, several methods including normalized CPT resistance and equivalent SPT values, were used to analyse the CPT data gathered at the main test site with respect to cyclic liquefaction susceptibility. The complete equations used in the analyses of the CPT data as well as plots of the results can be found in Appendix C.

The NCEER recommended procedure (Youd and Idriss, 2001) for evaluating the liquefaction susceptibility to earthquake loading from CPT data follows the method proposed in Robertson and Wride (1998). This method is an iterative procedure whereby a clean sand equivalent tip resistance (q_{c1N-cs}) is calculated from the measured tip resistance based on a suggested relationship between the soil behaviour index (I_c), and was described in Section 2.4.3.3. Limiting values of q_{c1N-cs} have been suggested for identifying expected sand response to load. For q_{c1N-cs} values greater than 60 MPa dilative behaviour, which is typically associated with cyclic liquefaction or cyclic mobility type behaviour, is expected. For q_{c1N-cs} values less than 40 MPa contractive behaviour, a requirement for flow liquefaction, is expected and between q_{c1N-cs} values of 40 and 60 MPa lies a "grey zone" in which either behaviour should be expected (Robertson and Fear, 1995). Analyses of the data following the procedure suggested in Robertson and Wride (1998) indicated that 76 percent of the data obtained from the CPTs carried out at the main test site had q_{c1N-cs} values greater than 60 MPa, 17 percent of the data fell in the "grey zone" and the remaining 7 percent of the data had q_{c1N-cs} values slightly less than 40 MPa. The average q_{c1N-cs} was 73 MPa, which appeared fairly consistent with depth (refer to Appendix C). The CPT tip resistance data also tended to indicate dilative behaviour when compared to limiting values of q_c with effective overburden pressure suggested by Sladen and Hewitt (1989), Robertson et al. (1992), and Ishihara (1993). These analyses also appear to support the findings that the tailings would be expected to behave predominantly in a dilative manner. Similarly, location of the data on the normalized soil behaviour chart proposed by Jefferies and Davies (2002) indicated dilatant behaviour.

Standard penetration blow counts (N values) are also commonly used to evaluate liquefaction resistance and there exist many empirical correlations between CPT measurements and SPT blowcounts. In general, the methods fall into one of two broad categories. SPT values can be estimated from the measured tip resistance based on empirical correlations dependant on mean grain size determined from index testing (e.g. Robertson and Campanella, 1985; Seed and DeAlba, 1986; Stark and Olson, 1995). Alternatively, there are correlations that use the soil behaviour index in the conversion from CPT tip resistance to SPT blowcount, which incorporates the effect of grain size directly and alleviates the necessity of index testing (e.g. Jefferies and Davies, 1993; Lunne et al., 1997). To calculate the normalized SPT blowcount, a correction for overburden must also be made and can be applied either to the calculated SPT values or to the CPT data prior to conversion. The calculated SPT values are for the type of material tested, e.g. a silty sand, and if clean sand values are desired, further corrections must be applied if applicable.

Many methods for calculating SPT values from the gathered CPT data were used in this study and are included in Appendix C. A very wide range of SPT values were calculated, with $(N)_{60}$ values ranging between 1 and 9, increasing with depth. When compared with boundaries proposed by Ishihara, 1993 the N_{60} values in general did not suggest flow behaviour. Average $(N_1)_{60}$ values ranged from 4.5 to 10 and average clean sand $(N_1)_{60-cs}$ values ranged from 5.5 to 17. The SPT blowcounts which were calculated from CPT data which had been normalized for overburden were fairly consistent with depth, tended to be slightly larger than SPT blowcounts which were normalized for overburden following conversion from non-normalized CPT data and in general agreed more closely with CPT-SPT conversions developed specifically for Syncrude tailings during CANLEX. The SPT blowcounts normalized for overburden after conversion from

CPT data also showed a trend of increasing blowcount with depth suggesting that the overburden correction factor, which was somewhat arbitrarily limited over most of the depth of interest, significantly affected the results.

It was noted that although the conversions indicated a significant correction for fines content, index testing did not indicate large fines contents. The CPT responds to soil behaviour rather than specific grain sizes however, and the Syncrude tailings were very fine, with an average D_{50} less than 0.2 mm. Based on soil behaviour charts the tailings was classified as a sand to silty sand and when compared to various CPT liquefaction susceptibility charts, a D_{50} as measured is typical of a silty sand (refer to section 2.4.3.3), thus a fines correction may be justified.

A general survey of past field data was carried out to identify typical SPT values for Syncrude BAW tailings because of the wide range in the converted SPT values and because of the trend of increasing SPT $(N_1)_{60}$ value with depth. Typical $(N_1)_{60}$ values for Syncrude BAW tailings appeared to range between 8 and 20 (HBT AGRA, 1992; Klohn Crippen, 1998; Wride et al., 2000). This range appeared to agree reasonably well with the values estimated from overburden corrected CPT data and from the site specific relationship developed during CANLEX. More weight was therefore placed on these estimates because of their agreement with previous work and because of their apparent stability with depth. Based on these findings, representative values of 9 and 11 were selected for $(N_1)_{60}$ and $(N_1)_{60-cs}$, respectively.

Generally, clean sand $(N_1)_{60}$ values less than 10 are considered potentially liquefiable while values greater than 15 tend to indicate only limited deformations (Fear and McRoberts, 1995). These limits decrease with increasing fines content. The majority of the converted SPT data appeared to be located within the "grey zone", on the boundary between liquefaction and non-liquefaction, which is reasonably consistent with the "no flow" classification of the N_{60} data.

5.3 Response of Deposit to Cyclic Equipment Loading

5.3.1 General

Significant local softening of BAW tailings was observed in response to cyclic loading by people, and light and heavy equipment. The cyclic equipment loading can be divided into three main components. Firstly, the equipment was driven back and forth across the test site, cyclically loading and unloading the site. Secondly, the equipment was tracked and therefore as the tracks rolled, local cycling of the load occurred as the tracks loaded and unloaded small areas of tailings. Finally, the overall vibration of the equipment itself also induced some cyclic loading.

In general, when lighter loads were applied, such as a person stepping, softening of the tailings only occurred in areas where the water table was very close to the surface and particularly in what appeared to be more recent deposits. In these areas as softening occurred, the area around the applied load appeared to form a raised ring. This rising of the surface was not evident when heavier loads were applied. In general surficial evidence of softening observed during the field tests involving equipment loading included undulation of the surface, the formation of cracks and water pumping to surface often creating sand boils.

5.3.2 Pore Pressure Response

The pore pressures measured in response to light equipment (Predator) loading and heavier equipment (dozer) loading presented in Sections 3.5.5 and 3.5.6 are re-plotted in Figure 5.4 and Figure 5.5 in terms of change in pore pressure. These two figures also show the approximate vertical effective stress prior to loading. The pore pressure response was extremely rapid, lagging only very slightly behind the load application (refer to graphs in Sections 3.5.5 and 3.5.6). The pore pressures also appeared to cycle somewhat in phase with the applied load. This appears to be more obvious in the pore pressures measured during Predator loading where the effects of individual loading events can be observed. Cycling of the pore pressure in response to load appeared to be most pronounced in the piezometers closest to the ground surface while the deeper piezometers tended to indicate a more gradual, consistent increase in pore pressure. However, the record increment was relatively slow (generally every 3 seconds) in comparison to the apparent vibration frequency (35 to 7 Hz) and therefore some cycling of the pore pressures may not have been captured during monitoring. This apparent pore pressure cycling is similar to the cyclic triaxial test results published by Seed and Lee (1966) in which the pore pressure built up in a medium dense sample as it was cycled through a hydrostatic stress state.

As can be seen from Figures 5.5 and 5.6 the dozer caused significantly higher excess pore pressures than the Predator. The Predator loading generated excess pore pressures well below the effective overburden pressures and therefore the effective stresses within the tailings deposit did not drop significantly and softening was not pronounced. The dozer loading, however, caused excess pore pressures equal to the effective overburden pressure and therefore conditions of zero effective stress within a fairly large amount of soil, accounting for the difference in the observed softening response. The variation in changes in pore pressure with depth and location during dozer loading are shown in Figure 5.6.

From Figure 5.6, it can be observed that during dozer loading, the two closest rows of piezometers, located within 150 cm of the closet track and to a maximum depth of 180cm, and the piezometer 250 cm from the track at 0.5 m depth recorded maximum pressures essentially equivalent to or slightly higher than the original overburden pressure (note that because the overburden pressures increased with depth the maximum pore pressure also increased with depth). The deeper piezometers in the further row, located at a horizontal distance of 225 to 230 cm from the closest track, showed maximum excess pore pressures less than the effective overburden pressure. As shown in the Figure, in terms of percentage of overburden pressure, the maximum pore pressures decreased with depth from approximately 100 percent at a depth of 0.5 m to approximately 35 percent at a depth of 2.15 m. The decrease appeared linear with depth over at least the first 1.7 m and then decreased more rapidly. If considered in terms of maximum excess pore pressure however, the readings in the last row of piezometers increased with depth for at least the first 1.7 m before beginning to decrease. It is interesting to note that at a distance of 1.7m from the load, the shear window proposed by Woods (1968), where which one would expect excess pore pressure to be generated, should be located at a depth roughly equal to the location of the peak pore pressure. In general, it appeared that the maximum excess pore pressures occurred at a slightly later time with depth but there was no obvious trend with respect to distance from the source.

Figure 5.7 shows a somewhat different response as a result of Predator loading. The maximum excess pore pressures in terms of percentage of effective overburden pressure decreased with distance from the load and with depth similar to the dozer loading response, although peak pore pressures never approached the original overburden pressure. The magnitude of the maximum excess pore pressures however also decreased with distance from the loaded area and either decreased or was constant with depth, unlike during dozer loading.

Maximum excess pore pressure contours are shown in Figure 5.8 and 5.10 for the Predator and dozer response. The contours of maximum excess pressures were created based on the maximum values recorded in the field, regardless of when the peak pore pressures occurred. The temporal variation with respect to the occurrence of maximum pore pressures recorded at the various transducers was generally not very significant nor was the difference in magnitude between the values recorded within the time over which the peak pore pressures occurred at the different transducers. The contours were constructed by drawing Delauney triangles between the piezometer tip locations and assuming a linear distribution of maximum excess pore pressure between the tip locations to locate points of equal maximum excess pore pressure. Since under perfectly undrained behaviour, any increase in load would be translated to an increase in pore pressure, a typical elastic stress distribution of a static load is shown in Figure 5.10 for comparison with the measured excess pore pressures.

The measured maximum excess pressures caused by the Predator loading are similar to the elastic stress distribution, with slight variations near the surface as shown in Figure 5.9 and Figure 5.10. The dozer however caused maximum excess pore pressure contours very different from those predicted by elastic theory. Under dozer loading, the zone of influence is significantly larger and is more of a horizontally elongated ellipse or a dumbbell shape than the egg shape predicted by elastic theory. The horizontally elongated shape may be due to a higher hydraulic conductivity in the horizontal direction caused by the method of tailings deposition. The large maximum pore pressure magnitudes and the extent of the area can possibly be explained by general plasticity behaviour. As the pore pressures increased locally around the equipment, the material softened and yielded, redistributing load to adjacent areas, thereby causing pore pressures to increase, which in turn caused those areas to yield and shed load outward in an expanding zone of influence. The dumbbell shape of the maximum pore pressure contours explains why much of the water brought to surface was concentrated near the loaded area. Flow paths should be perpendicular to the equipotential lines and as the pore pressure contours approach the loaded area they begin to slope downwards, funnelling a significant amount of flow towards the loaded area.

The excess pore pressures took approximately 20 hours to completely dissipate in the tailings located deeper than approximately 0.8 m and substantially longer in the upper portion of the tailings deposit (refer to Figure 3.21, Section 3.5.6). Initially dissipation occurred fairly quickly, however, as the pore pressures dissipated, the gradient driving the dissipation of the pore pressure decreased and the process slowed. Because of the very low gradients in the upper portions of the deposit, and because the pore pressures likely dissipated at least partly towards the surface, the upper pore pressure transducer located at a depth of 0.5 m still recorded some excess pore pressures 24 hours after loading.

5.3.3 Tailings Properties Following Softening

Following softening, bulk and frozen samples were gathered at the main test site and CPTs were carried out near to the original CPT locations to allow comparison with initial conditions. As described in Section 3.5.8, quick tests applying light loading were also carried out to try to examine any changes in tailings properties occurring as a result of softening. Moisture contents appeared to increase significantly after softening, particularly at the main test site, and clearly the stiffness of the softened area decreased immediately following loading. Otherwise, there did not appear to be significant changes to the tailings properties when conditions several hours after softening were compared with the initial conditions prior to softening.

Unlike the original cyclic load tests carried out prompting this research (refer to Section 1.0) in which significant decreases in dry density were observed as a result softening, in general the current tests tended to indicate a relatively constant dry density. The nuclear gauge measurements carried out at the main test site did indicate an eight percent decrease in dry density after softening, which is of the same order as suggested by the initial tests. Nuclear gauge measurements carried out during the Quick Tests however did not indicate any significant change in dry density after softening, nor did the results of void ratio measurements on the frozen samples, although in general, the tests appeared to indicate slight increases in void ratio, on the order of 0.02 which is within the range of expected scatter in measured values and not significant. The latter observations would appear to be consistent with the small strains measured by the seismograph located 0.55m from the equipment tracks. The discrepancy between the nuclear gauge and frozen sample measurements cannot be completely explained. At the main test site the nuclear gauge measurements were carried out closer to the location of the equipment tracks than the location from which frozen samples were gathered, and therefore would likely have been influenced by higher straining. As discussed in Section 3.5.7.4, the nuclear gauge readings were carried out well after loading and frost had formed in the upper several centimetres of the deposit. Although this layer was removed and measurements were made on material that had not frozen, it may be possible that the soil skeleton could have expanded slightly due to the formation of the frost layer above, although one would generally expect that if it occurred, this effect should have been limited to only the upper portion of the deposit immediately underlying the frost. Significant amounts of bitumen would tend to increase the moisture content measured by the Troxler and hence decrease the dry density compared to what was measured in the laboratory, however, there was no visual evidence of significant amounts of bitumen after softening.

The discrepancy between the quick test results and the initial test results presented in Section 1.0 may be the result of testing procedure. Nuclear gauge measurements in the Quick Tests were carried out approximately 40 to 50 cm from the location of load application, outside the area of major disturbance. It is unknown exactly how the original tests were carried out, but if the measurements were carried out closer to the area of load application, they would record the effects of significantly higher straining. Furthermore if the measurements were taken with significant surface water present, the dry density would certainly have decreased.

The CPT tests carried out prior to and two hours after softening did not indicate any significant, systematic change in either tip resistance or sleeve friction, although the measured pore pressure following softening had increased. This would tend to indicate

that the strength properties remained fairly constant. From CPTs carried out during the quick tests it was qualitatively observed that during and immediately following cyclic loading, when pore pressures were equal to the overburden pressure, tip resistance was reduced. This was likely a result of the upward pore pressure gradients and resulting decreased effective stress, rather than an actual loss in strength of the tailings sand. It therefore appeared that the tailings properties were in general not significantly altered as a result of softening with a possible exception of the tailings located very close to the applied load where a decrease in density may have occurred. Visual observation of the frozen samples did appear to indicate that the original horizontal layering present in the tailings had been changed to a more homogeneous appearance (see Figure 4.3, Section 4.3.3).

5.3.3 Imposed Stresses

The measured particle velocities presented previously in Figures 3.15 and 3.18 were used to estimate the dynamic stresses imposed on the tailings deposit by the equipment. The recorded velocities were cyclic and appeared to be somewhat sinusoidal about zero stress. The cause of the negative velocities is thought to be due to the vibration of the equipment itself. The motor and other rotating components likely caused the machines to vibrate and transmit shear stresses to the soil in all directions.

In order to interpret the measured particle velocities and convert them to dynamic stresses, some consideration was given to wave propagation theory. In general there are two distinct types of waves that transmit vibrations: Rayleigh and body waves (Gutowski and Dym, 1976). Rayleigh waves are surface waves that propagate radially outward from the source on a cylindrical wave front. They can also occur at density interfaces and at the phreatic surface. Body waves, which include both compression and shear waves, propagate mainly through the soil mass along hemispherical wave fronts (Woods, 1968). As installed during the field program, the seismograph generally measured compressional waves in the longitudinal direction and shear waves in the vertical and transverse directions. Due to the seismograph's proximity to the surface, it would also record Rayleigh waves. A simple plot of the measured particle velocities, shown in Figure 5.11, indicated that during a pass, the recorded motion appeared to be dominated by body waves (more diagonal traces) whereas between passes, the particle motion recorded appeared to be dominated by Rayleigh waves (more circular or elliptical traces). Since the particle motions during equipment passes were significantly larger than between passes the stresses were analyzed assuming only body wave transmission. Since the body waves appeared to dominate the measured particle velocities, it was also assumed that the particle velocities measured on surface at a given distance from the track were the same as the particle motions induced at a radius the same distance from the tracks in any direction within the tailings deposit. This last assumption may not be strictly valid as body and Rayleigh waves attenuate at different rates on the ground surface and within the soil mass (Gutowski and Dym, 1976). However, due to the small distance under consideration, the assumption was considered reasonable. The assumption of wave type affects the rate of attenuation of particle velocities and the applicability of the assumed attenuation is discussed in Sections 5.4.3 and 5.4.4.2.

To simplify the problem further, the transverse particle velocities, which were significantly lower than the particle velocities in the remaining two directions, were ignored (i.e. the problem was simplified to plane strain calculations). Therefore in

calculating dynamic stresses from the particle velocities, normal stresses were assumed to be imposed normal to a circle centred about the dozer tracks due to the compression wave particle velocities (longitudinal) and shear stresses were assumed to be imposed by the vertical particle velocities acting in a direction tangential to the circle at the point of interest as shown in Figure 5.12.

The effect of the attenuation of particle velocity with distance from the source was also considered when the point of interest was different than the distance between the recorded particle velocities and the equipment. There are two components to the attenuation of vibrations with distance, geometric damping and material damping (Woods and Jedele, 1985). There exist many theoretical relationships for the attenuation of vibrations and many studies have been carried out to determine attenuation characteristics of construction and traffic induced vibrations, particularly with regards to subways and trains (e.g. Gutowski and Dym, 1976; Woods and Jedele, 1985; Chua et al., 1992; and Kim and Lee, 1998). With respect to induced shear stresses causing liquefaction, the waves of most concern are likely body shear waves and their attenuation with depth.

A common expression to account for both geometric and material damping is (Woods and Jedele, 1985; Kim and Lee, 1998):

$$w_2 = w_1 \left(\frac{r_1}{r_2} \right)^n e^{-\alpha(r_2-r_1)} \quad \text{Equation 5-1}$$

Where: w_i =velocity at location i
 r_i =distance to location i
 α =material damping coefficient
 n =geometric damping coefficient

Kim and Lee (1998) summarized the work of previous researchers and compared the predicted attenuation relationships with data gathered in the field. Some of their findings were used to estimate an attenuation relationship for the main test site. The variable n accounts for geometric damping and appeared to depend mainly on the type of waves being transmitted and also on the type of energy source. When estimating the attenuation of body waves from one point source on the surface to another point on surface, the suggested n value was 2.0; when they estimated the attenuation of a point source at depth (i.e. waves travelling through the soil mass rather than on surface) they found an n value of 1 to be more appropriate (Kim and Lee, 1998). Woods and Jedele (1985) also suggested a value of 1 for the geometric damping of body waves through a soil mass. The material damping coefficient, α , depends on the type of material transmitting the waves and on the frequency of the vibration. For a competent soil, such as sand, the material damping coefficient was suggested to have a range of 0.003 to 0.01 m^{-1} for a frequency of 5Hz and a range of 0.03 to 0.01 for a frequency of 50Hz. Kim and Lee (1998) found that using these values, the predicted values compared well with field data gathered for vibration induced by friction pile driving and short train loading (less than 16 passenger cars). In these cases, the field data was gathered mainly from surface monitoring locations.

As part of this study, the seismograph monitored frequencies in addition to particle velocities and indicated that the Predator had a of 37 Hz, whereas the dozer had a frequency of 7 Hz. The mid-range values for material damping coefficients recommended by Kim and Lee (1998) of 0.007 m^{-1} and 0.02 m^{-1} were used for the dozer and Predator, respectively, based on the recorded vibration frequencies of the equipment and assuming “competent” soil. A geometric damping coefficient of 1 was also used, as it was the attenuation of body waves with depth that was of interest. The applicability of these values to the main test site will be discussed in Section 5.4.4.2.

Based on elasticity theory, dynamic stresses are related to peak particle velocities by the following equations (Dowding, 1985):

$$\sigma_{dynamic} = c_p \rho v_p \quad \text{Equation 5-2}$$

$$\tau_{dynamic} = c_s \rho v_p \quad \text{Equation 5-3}$$

where: c_p =compression wave velocity
 c_s =shear wave velocity
 ρ =material density
 v_p =particle velocity

The shear wave velocity of the tailings deposit was estimated based on the measured CPT tip resistance according to correlations developed by Wride et al. (2000) as part of the CANLEX project. The correlations indicated that near the ground surface the average shear wave velocity was approximately 80 m/s. The compression wave velocity was then estimated as 135 m/s based on elastic theory, using an assumed Poisson’s ratio of 0.33 and a density of 1900 kg/m^3 . These values agree well with the general rule of thumb that the compression wave velocity is between 1.8 and 2.3 times the shear wave velocity (Hunt, 1984).

The dynamic stresses were calculated according to Equations 5-2 and 5-3 at the locations of selected piezometers for both Predator and dozer loading. The vertical and horizontal dynamic stresses were then calculated using the Mohrs circle to allow superposition with the in-situ stresses. The major and minor principal stresses and their orientation were then evaluated. The measured pore pressures were linearly extrapolated between recording times and then used to calculate the mean effective stress and the stress path could then be plotted. A summary of this procedure is included in Appendix D. The combined stresses were very dependent on the assumed initial stress state. The calculated stress paths for both the Predator and dozer loading scenarios are shown in Figure 5.13 and Figure 5.14 for assumed initial stress ratios (K_0 values) of 0.5 and 1 respectively. The stress paths under dozer loading are shown only for the first three passes, as it was clear that softening had occurred during this period.

In both Figures 5.14 and 5.15, the initial portions of the stress path were not captured, this is likely because the vibration level required to trigger the seismograph caused some initial increase in pore pressure. Figure 5.13 indicates that there was no significant softening of the tailings deposit under Predator loading. Dozer loading however produced a very different response as shown in Figure 5.14. The negative effective stresses shown for the dozer loading were expected because the measured pore

pressures were in excess of the vertical overburden pressure and therefore the mean effective stresses had to become negative, particularly if the stress ratio is less than unity.

It was thought that a stress ratio of 0.5 was likely more representative of initial stress conditions however, as pore pressures increased and the deposit softened, it may be that the stress conditions began approaching hydrostatic conditions in response to decreasing effective stresses. A more representative stress path may be obtained by a gradual transition from a condition of $K_0=0.5$ to $K_0=1.0$, which would tend to keep the stress path less negative. An approximation of the effect of varying stress ratio of the stress path is shown in Figure 5.15. Also, as softening was induced, towards the left portion of the stress path in Figure 5.14, the stiffness of the material decreased. This was not accounted for in the calculation of the induced stresses, as there was no way of knowing the magnitude of the change. It would however result in a reduction of the applied stresses. A tension cut-off could have been specified in the analyses to prevent negative effective stresses but it was thought that the behaviour indicated by the data would be instructive. Furthermore, the fact that cracks were observed in the deposit as it softened indicated that there may in fact have been tension induced in the deposit. If the deposit were able to sustain small amounts of tension, the typical stress paths shown in Section 2.3.4, Figure 2.5e may be expected to shift to the left as seen in Figure 5.14.

It is noted that the stress path recorded during dozer loading is quite similar to the typical stress path shown in Figure 2.5e, for cyclic mobility shifted left and slightly downward. The dozer stress path appeared to move to the left as the magnitude of cyclic stresses increased. Significant softening can be observed, as can conditions of zero effective stress. Although not shown in Figure 5.14, which shows only the first few loading passes, Figure 3.18 (see Section 3.5.6) indicates that straining halted once the cyclic load was removed, although the pore pressures remained elevated for a short time. Examining Figure 5.14, it appears that shear stress reversal could only have occurred in the deposit if the stresses in the tailings deposit approached hydrostatic. It is unlikely that the initial stress ratio was 1.0, although with the shallowness of the deposit this condition could possibly have been approached. Based on the measured results and the field observations it would appear that as pore pressures increased and effective stresses decreased, the soil behaved more like a fluid and the in-situ stress ratio likely changed and approached unity. Also as the shear stress ratio approached 1.0 shear stress reversal developed resulting in cyclic liquefaction as defined by CANLEX (refer to section 2.2)

The CPTs carried out approximately 2 hours after loading also support the occurrence of cyclic liquefaction. No significant change in the tailings properties was indicated by the CPT results. This suggested that there was no dramatic loss of strength in the tailings as would be expected of a cyclic liquefaction type behaviour.

5.3.4 Causes of Softening

5.3.4.1 General

The upper, unsaturated portion of the BAW tailings deposit at the main test site likely softened as result of the upward gradients induced because of the excess pore pressures developed in the tailings located below the phreatic surface. As suggested by Seed (1979), the hydraulic gradients induced due to excess pore pressures generated

by liquefaction of material below the phreatic surface caused upward flow of water, as evidenced by the observed formation of sand boils and increased saturation of the surficial materials, resulting in a softened or "quick" condition on surface, which stabilized with the dissipation of the pore pressures. However, the trigger or cause of softening was related to the development of excess pore pressures in the tailings deposit, interpreted as being dense of critical state, located below the phreatic surface.

There are several mechanisms by which a deposit, initially dense of critical state, may generate excess pore pressures. In the past, distinction has been made between vibration, which causes the densification of any cohesionless soil looser than the minimum void ratio, and shear deformation, which typically results in dilation of dense sands (e.g. Cassagrande, 1940). However, it appears that vibration is simply small strain shear and although small and large strain behaviour sometimes require different soil models, they are both part of the same phenomenon.

Vaid and Sivathayalan (2000) suggested another possibility: that pore pressure gradients caused during short-duration loading can cause small expansive volumetric strains, changing the response of the soil. The volume expansion can transform a sand, which was initially dense and would have been strain hardening into a looser state which is strain softening. This latter mechanism however will not be discussed in any more detail as measurements were not gathered in the field that would allow an assessment of the occurrence of this mechanism.

5.3.4.2 Pore Pressure Generation Mechanisms

It is well known that cohesionless soils densify under vibratory loading. If this response were to control the behaviour of cyclically loaded sands then all sands loaded cyclically would have a tendency to contract and generate pore pressure as suggested by Castro (1975), Martin et al. (1975), Poulos et al. (1985), and McRoberts and Sladen (1990). There are several potential causes for the generation of excess pore pressures in the tailings at the test sites when subjected to cyclic loading.

The equipment loading caused both compression (P) and shear (S) waves to be imparted on the soil. The compression waves travel the fastest and likely caused an initial increase in pore pressure. The S-waves that followed would then have caused shear stresses within the soil mass. As pointed out by McRoberts and Sladen (1990) most sands initially contract and therefore generate additional pore pressure when sheared. In particular they indicate that even for dense sands the initial response at low strains is generally contractive. For the Syncrude tailings, the state appeared to be reasonably close to the steady state line and at low confining pressures likely had a significant contractive portion to the shear strain response (e.g. Ishihara, 1993). Thus a cyclic shear load could cause initial contraction at each load application causing pore pressures to build up.

The complex load path followed by the tailings during dozer loading may also have enhanced contractive behaviour of the tailings during shear. Various researchers have indicated that a sand becomes more contractive when it is loaded in simple shear or extension rather than triaxial compression (e.g. Kuberis and Vaid, 1988; Kuberis et al., 1988; Vaid et al., 1990; Yoshimine et al., 1999). The load path illustrated in Figure 5.14 was clearly not triaxial compression and could have caused a more contractive response than would be expected based on simple triaxial compression tests. Furthermore it has

been proposed that rotation of principal stresses alone, without any increase in deviatoric stress can also cause straining (Arthur et al., 1980; Vaid et al., 1990). Sivathayalan and Vaid (2002) showed that movement of the orientation of the principal load direction towards the plane of deposition can cause a dilative material to become contractive. The amount of stress rotation experienced during dozer loading was calculated based on the superposition of dynamic stresses and in-situ stresses as discussed in Section 5.3.3. As can be seen in Figure 5.16, the initial in-situ stress ratio conditions greatly affect the amount of stress rotation that occurs, although in both cases shown, sufficient rotation likely occurred to potentially increase the initial contractiveness of the tailings response.

The strains induced during loading by both the Predator and the dozer were relatively small, indicating that the initial small strain response of the tailings sand to load likely controlled the majority of its response. Based on the measured particle velocities and using the assumptions discussed in Section 5.3.3, strains in the ground at a depth of 0.5m were evaluated for both dozer and Predator loading. During dozer loading, the maximum strain measured at 0.5 m was 0.1 percent. However this was a significantly elevated measurement that occurred only once. In general during dozer loading the maximum strains were between 0.05 and 0.02 percent. By contrast, during Predator loading, the maximum strain at 0.5 m from the equipment was 0.04 percent and in general strains reached a maximum of 0.002 percent. These measured strain levels are shown on the shear strain versus pore pressure development curve presented by Dobry and Ladd (1980) in Figure 5.17. The curve was developed based on results of 10 cycles of loading on a sand with a relative density of 60 percent and indicates a minimum strain of 0.01 percent is required to cause any increase in pore pressure, which is similar to the threshold strain proposed by others based on laboratory results and theoretical considerations (Dobry and Swiger, 1979). For more cycles of loading (i.e. as occurred at the main test site) the pore pressures would be expected to build up to higher levels. However, the figure is useful in showing that the strains induced at the main test site under dozer loading were sufficient to cause pore pressures to build up whereas in general the strains caused by the Predator at a distance of 0.5m were not sufficient to cause an increase in pore pressure.

5.3.4.3 Evaluation of the Softening Mechanisms

The tests carried out during the field program cannot identify what specific mechanism caused the pore pressure generation. What does appear to be confirmed is that the tailings deposit softened under equipment loading due to cyclic liquefaction. Increased pore pressures were generated because of an initial contractive shear deformation. However, large strains induced locally could cause local shear strain behaviour and dilation of the dense deposit. Local high straining is likely the cause of the very large decreases in dry density recorded throughout cyclic loading during the small-scale tests carried out by Syncrude and presented in Section 1.0. The cyclic loading applied by human loading (stepping) caused significant straining in the vicinity of the loaded area with the foot locations sinking somewhat and the surrounding area rising. The local large strains likely caused the onset of local dilative behaviour while the cyclic loading itself caused increases in pore pressure. As discussed previously, these large strains were not measured in other testing possibly because sampling was carried out at greater distances from the point of load application.

5.3.5 Factors Affecting Behaviour

5.3.5.1 General

The tests carried out at the main test site, the Quick Test locations and during the trafficability study indicated that softening was more likely to occur as the loading equipment got larger, as the phreatic surface got nearer the surface or as the saturation and moisture content increased. The applied cyclic load and presence of water therefore appeared to be the main factors that controlled whether softening would be triggered. Other factors such as fines content, topography and ageing appeared to have a smaller effect on the tailings response however these effects were only observed qualitatively.

5.3.5.2 Cyclic Load

The effect of increasing cyclic load is fairly obvious. As the magnitude of the cyclic load increases, the amount of stress induced in the ground increases and softening can be more readily triggered. This is clearly evidenced by the increasing ease with which deposits were softened by the Predator, dozer and excavator. It appeared however, that it was not simply stress that was the driving factor in determining whether softening would occur. For example, the Predator exerted a stress of approximately 4.5 kPa while a person stepping would exert approximately 10 kPa stress yet it appeared that the Predator could induce softening more readily than a person. This can likely be attributed to the relationship between peak particle velocity, and thus induced strain or dynamic stress, to the applied energy. Energy depends not on stress but on mass and velocity (e.g. Woods and Jedele, 1985). Therefore it would appear that the speed with which equipment is driven, its vibration frequency, duration of load, and the equipment mass, rather than the stress it applies, affects the softening behaviour.

5.3.5.3 Phreatic Surface Location and Moisture Content

The presence of water is required for pore pressures to develop and cause softening; thus, it is not surprising that the location of the phreatic surface is an important factor controlling the response of BAW tailings to equipment loading. As the phreatic surface gets deeper, the overburden pressures acting on saturated tailings increase, decreasing the applied cyclic stress ratio and the applied stresses have more distance over which to spread out and attenuate further decreasing the applied cyclic stress ratio. Therefore, the applied stresses in the saturated tailings decrease as the phreatic surface gets deeper. Also, as the phreatic surface becomes deeper, there is a much greater thickness of unsaturated soil above the location of increased pore pressure. This would increase the volume of soil through which pore fluid would have to pass in order to reduce effective stresses and saturate the tailings at the surface. It would also tend to reduce the hydraulic gradient causing upward flow of water.

The effect of moisture in the area above the phreatic surface was evidenced by the changing responses to load observed during the field testing and caused significant problems during the field test. As discussed in Section 3.2, the main test site was selected initially based on the ability of the area to be softened by the light Predator vehicle. However, four days later when testing was carried out, the Predator could not induce softening. The main difference between the two cases was that on the night before the site was selected, it had rained very heavily. The phreatic surface, measured

by the location of free water in test pits, did not appear to have altered much between the two days, varying from approximately 30 cm depth on the morning the site was selected following the precipitation event, to 35 cm depth 4 days later. Significant differences in the degree of saturation of the material above the phreatic surface however was observed between the two days. The CPTs carried out on the site selection day indicated that there was significant moisture in the upper portion of the unsaturated zone, enough to cause positive pore pressure readings above the phreatic surface, possibly indicative of a wetting front moving through the tailings (refer to Figure 3.21, Section 3.5.7.2). Four days later, however, there was a surficial layer of soil that appeared essentially dry and the majority of the tailings above the phreatic surface appeared to be moist rather than wet.

This effect of moisture above the phreatic surface was also evident in an area to the west of the main test area. A boundary was found beyond which, the Predator could not cause softening. The phreatic surface appeared consistent across the boundary at 24 to 25 cm and there were no obvious sudden changes in the tailings; the only observed difference was the moisture content above the phreatic surface. The area that could be softened by the Predator had moisture contents in the upper parts of the deposit of 22 percent compared to 18 percent at the boundary where softening could no longer be caused.

The influence of both the location of phreatic surface and moisture or degree of saturation in the upper tailings was also apparent in the trafficability study. The portion of the trafficability study in which the dozer made several runs up and down the beach over the same tracks indicated that the moisture content above the phreatic surface decreased and the phreatic surface deepened slightly in the region where the tailings were able to sustain more runs as shown in Table 5.1. As the moisture content or saturation of the unsaturated increases, compaction upon loading could cause saturation and the zone is then able to generate excess pore pressures upon successive load cycles. No significant changes in density were indicated by the nuclear gauge measurements at the various locations. As discussed in Section 3.5.9, the bulk samples were gathered immediately following loading and the Troxler measurements were made significantly later after any excess pore pressures had dissipated, likely accounting for the differences in moisture content.

Table 5.1 Variation in Phreatic Surface and Water Content at Trafficability Locations

Limit of Pass Number	Depth to Phreatic Surface (m)	Water Content (%)	
		Bulk Samples	Nuclear Gauge
1	0.23	25	27
2	0.30	19	14
3	0.35	17	10

The location of the phreatic surface and the occurrence of increased moisture contents in the unsaturated zone appeared to be somewhat influenced by local topography. In local low spots the groundwater level tended to be closer to the surface. The locally low topography also introduced the possibility of local upward gradients. Both of these effects would decrease the initial effective stresses allowing cyclic liquefaction to be triggered by lower magnitudes of cyclic stress than would be required elsewhere.

5.3.5.4 Fines Content

General observations made during the reconnaissance portion of the field program suggested that fines content also had an influence on the response of the tailings deposit. In general, areas with increased fines appeared to soften more easily under fewer cycles of load but no quantitative field tests were carried out due to lack of time. Locally low topography appeared to cause an increase in the concentration of fines content, likely due to water ponding during deposition. This would then locally increase the ease with which softening was triggered.

A material with increased fines content would also be expected to retain more moisture above the phreatic surface as the capillary zone of a fine material is typically larger than that of a coarse material. A finer soil may also dry out more slowly following a precipitation event. Both of these factors would increase the moisture content of the unsaturated zone, which would tend to make it easier to trigger softening. The presence of fines may also tend to lower the steady state line (Sladen et al., 1985; Poulos et al., 1988) potentially resulting in more contractive behaviour if the void ratio remained unchanged. If all else remained constant, the presence of fines would also tend to decrease penetration resistance that would generally indicate decreased resistance to liquefaction.

5.3.5.5 Ageing

An increase in resistance to softening also appeared to occur with ageing. Newly deposited tailings appeared to soften much more easily than tailings that were a year or two old. A similar observation has been made by Syncrude (Syncrude, 2002). Comparing the results of the Trafficability Study carried out by Syncrude (2002) with the field tests also appeared to indicate an increased resistance to softening with age. The main test site was located near the section line used for trafficability testing in Cell 31 by Syncrude in 2001. It appears that the main test site was located in an area that was "untrafficable" for the excavator in 2001. However, during the field test the excavator was able to travel beyond the main test site, as far as the location of newly deposited tailings.

It is unclear however, what defined an area as "untrafficable" in the previous trafficability study. The excavator caused some cracking and brought water to the surface although in a single pass at the main test site the effects were relatively minor. The excavator was in fact used to carry out work at the main test site, retrieving the installed piezometers, although significant softening of the area did occur over the approximately 10 to 15 minutes it took to carry out the work. The draft trafficability report also did not include the depth to phreatic surface at the individual locations so it is unclear if the improved trafficability was a result of ageing only or also due to a change in the location of the phreatic surface or degree of saturation of the tailings above the groundwater level. Another difficulty in comparing the two results is that the first study was carried out in November when there was frost and ice on the surface of the beach.

It does appear reasonable to expect an increased resistance to softening with ageing of a deposit based on other studies however. CANLEX indicated that in general, older deposits have an increased resistance to liquefaction (Wride et al., 2000). Howie et al. (2002) indicated that for very loose sands, ageing increased the stiffness of the material and also caused reduced volume reduction during shear. An increased stiffness with

age would tend to reduce the strains imposed in the ground due to equipment traffic and thus decrease the potential for the generation of excess pore pressures.

5.3.5.6 Density

Variation in density would generally be expected to have a significant impact on liquefaction type behaviour. The influence of density, however, could not be investigated in the field program because no obvious, systematic change in density was identified up the beach in the area around the main test site. In general it would be expected that as the deposit became denser, i.e. the initial void ratio reduced, the deposit would withstand more cycles of loading before softening occurred. However, because the behaviour appears to be a cyclic liquefaction type phenomenon, and because the induced strains are small, likely keeping the response dominantly in the initial contraction phase, increasing the density of the deposit slightly may not significantly increase the resistance of the tailings to softening. This appears to be supported by field observations, in which compaction did not seem to have a huge beneficial effect on the trafficability of tailings (McKenna, personal communication, 2002).

5.4 Comparison of Field Observations with Liquefaction Susceptibility Analyses

5.4.1 General

The most common preliminary method of assessing the liquefaction susceptibility of a deposit in geotechnical practice is the use of the CSR/CRR – $(N_1)_{60}$ chart presented by Seed et al. (1985) and modified slightly by the National Centre for Earthquake Engineering Research (NCEER) in 1998 or the similar CSR/CRR- q_{1c} charts, which were discussed in detail in Section 2.4.3.3. The relationships were based on case records of sites that were subjected to earthquake loading or laboratory determined cyclic resistance ratios. In developing the charts, liquefaction included not only cases where significant lateral movements or failure had occurred but also those in which the evidence consisted only of sand boils and ground cracking without any significant lateral movements or failure. Although there has been criticism of this method of identifying liquefaction, as opposed to cyclic mobility, (e.g. Fear and McRoberts, 1995), it would appear that these cases may be similar in nature to what was observed during the field test. It is therefore possible that the CRR – $(N_1)_{60}$ or q_{1c} charts may be able to predict the cyclic liquefaction of the main test site.

There are however several inherent difficulties with applying the CRR – $(N_1)_{60}$ or CRR – q_{c1} charts to the application in question. Firstly, although the equipment loading appeared to be cyclic, it is still very different than an earthquake. The equipment loading was much more localized, and induced smaller strains than would large earthquake loading. Furthermore, the depths of interest in this case are generally fairly shallow typically less than a few meters depth while in the case history data used to generate the CRR charts, the majority of the data points were from depths greater than 4m. Regardless, the CRR – $(N_1)_{60}$ or q_{1c} chart would be a logical preliminary method of assessing the likelihood of cyclic liquefaction or cyclic mobility at the main test site. Hryciw et al. (1990) used the chart to successfully back analyze a similar situation in which flow failure of a loose sand deposit occurred when it was subjected to vibratory loading during a seismic reflection survey.

5.4.2 Calculation of the Cyclic Stress Ratio and Penetration Resistance

In order to apply the CSR/CRR charts, representative SPT or CPT penetration values were required as well as an estimate of the applied average cyclic shear stress ratio. As discussed in Section 5.2.4, based on many analyses of the CPT data and a review of previous field data, an average clean sand $(N_1)_{60}$ value of 11 was considered representative of the tailings below the phreatic surface. Based on the CPT data itself, representative values for q_{c1} and q_{c1cs} of 4 and 7, respectively, were identified.

Calculation of the induced cyclic shear stress ratio required knowledge of the effective overburden pressure and the applied cyclic shear stress. The former was based on the measured bulk densities of the tailings discussed in Section 4.3.3, the measured depth of the phreatic surface and the particular depth of interest. The relationship between cyclic shear stress and particle velocity used by Hryciw et al. (1990) to analyze the liquefaction flow failure of a road embankment as a result of stresses induced by vibratory tampers is presented below and was adopted in the analyses to calculate the cyclic shear stress. The particle velocity attenuation relationship discussed in Section 5.3.3 was used to calculate particle velocities at any depth of interest.

Assuming plane wave propagation, shear strain is related to the peak vector resultant of particle velocity and shear wave velocity according to Equation 5-4 (Hryciw et al., 1990). Combining this equation with the well-known relationships between shear stress, shear strain, shear modulus, shear wave velocity and material density as given in Equations 5-5 and 5-6 generates Equation 5-7. This last equation was used to calculate the cyclic shear stress at the various depths of interest. By carrying out the appropriate substitutions this equation becomes identical to that presented earlier for dynamic shear stresses based on elastic theory.

$$\gamma = \frac{v_p}{c_s} \quad \text{Equation 5-4}$$

$$\tau = G\gamma \quad \text{Equation 5-5}$$

$$c_s^2 = \frac{G}{\rho} \quad \text{Equation 5-6}$$

$$\tau = (G\rho)^{0.5} v_p \quad \text{Equation 5-7}$$

Where: v_p = particle velocity
 c_s = shear wave velocity
 G = shear modulus
 τ = shear stress
 γ = shear strain
 ρ = shear strain

The shear modulus for the tailings at the main test site was evaluated from the shear wave velocity and material density according to Equation 5-6. The shear wave velocity was estimated based on the correlation developed during CANLEX between CPT tip resistance and the normalized shear wave velocity for Syncrude tailings. It should be noted however that the shear wave velocity used to calculate the shear modulus was the actual shear wave velocity (c_s), not the value normalized for overburden (c_{s1}). This was

done to reflect the fact that the shear wave velocity (and thus the shear modulus) near the surface was likely lower than at depth. Since the measured excess pore pressures indicated that under dozer loading, the affected area was approximately 5 m in depth, c_s was calculated for the average depth of 2.5 m. The average shear modulus calculated in this manner was 20 MPa, which is reasonable for this deposit based on values previously used at Syncrude (Klohn-Crippen, 1998; Byrne et al., 2000). The equations used and plots of the results can be found in Appendix D. There could be justification for using a smaller shear modulus for analyzing Predator loading where the depth of influence was clearly shallower however, for simplicity, all analyses were carried out assuming a shear modulus of 20 MPa. It was recognized that measured in this way, the shear modulus values represent the small strain shear stiffness G_{max} . The strains imposed by the equipment were quite small particularly at the onset of pore pressure generation, which triggered softening, therefore no reduction in the measured stiffness values were made.

The cyclic stress ratios used in the liquefaction susceptibility charts were based on the average cyclic stresses for a magnitude 7.5 earthquake, calculated as suggested by Seed and Idriss (1971). As indicated by Seed and Idriss (1982) this corresponds to 15 cycles of the average shear stress induced by the earthquake. Seed and Idriss (1971) indicated that the average stress was typically equivalent to 65 percent of the maximum stress. Simply using the maximum recorded particle velocity to calculate the induced shear therefore did not seem appropriate. Two methods for selecting an appropriate particle velocity with which to calculate the shear stress were evaluated. Since the shear stress was directly proportional to particle velocity, one method used to select the appropriate peak particle velocity was to use a velocity equal to 65 percent of the maximum vector resultant particle velocity. The number of cycles exceeding this velocity was estimated from the monitoring record and a correction factor was applied, as appropriate, following the procedures used by Seed and Idriss (1982) to develop magnitude scaling factors which were briefly discussed in Section 2.4.2. The second method used to select an appropriate particle velocity consisted of selecting the particle velocity from the monitoring record that had 15 cycles equal to or greater than it. This velocity was then used with no correction factor. Figure 5.18 shows the results of the two analyses, values of 67 and 43 mm/s were obtained from calculating 65% of the maximum peak particle velocity and the 15 cycle velocity respectively. However as observed in the figure, the peak velocity recorded appeared to be an outlier and likely did not significantly affect the response, using a more realistic maximum velocity of 75 mm/s and calculating 65% of that velocity yields an average velocity of 49 mm/s, very close to the 15 cycle velocity. The 15 cycle particle velocity was used in the analyses as it was most consistent with the methods used to develop the charts.

The particle velocities in Figure 5.18 were measured at 0.55m from the edge of the track and as discussed in Section 5.3.3 it was assumed that the same particle velocities occurred at any point 0.55m from the load within the soil mass. The particle velocities at various depths of interest were then calculated based on the assumed attenuation relationship discussed in Sections 5.3.3 and 5.4.4.2 using a geometric damping coefficient of 1. The shear stress and cyclic stress ratio were then calculated using a shear modulus of 20 MPa and a bulk density of 1925 kg/m³. The applied cyclic stress ratios were plotted with the corresponding representative penetration resistance and the resulting predicted behaviour was compared to the observed behaviour.

5.4.3 Comparison of Predicted Behaviour With Observations

The results of the liquefaction susceptibility analyses based on the $CRR-(N_1)_{60}$ charts as well as the $CRR-q_{c1}$ charts for clean and silty sands are presented in Figure 5.19. In the silty sand CPT analyses, the representative penetration resistance, uncorrected for fines content of 4 MPa where as the other two analyses used clean sand values of 11 and 7 for the SPT and CPT analyses respectively. Figure 5.19 indicates that with the phreatic surface located at a depth of 35cm, the conditions caused by the Predator loading at the phreatic surface fall below the liquefaction boundary. However, when the phreatic surface is located at a depth of 25 cm, the conditions caused by Predator loading at the phreatic surface fall above the liquefaction boundary. These findings agree well with the occurrence and non-occurrence of softening observed at the main test site. The dozer loading, with the phreatic surface at a depth of 35 cm, is shown in Figure 5.19 to cause conditions that fall well above the liquefaction boundary at a depth of 1 m. The conditions at a depth of 0.5 m plot so far above the boundary that the point does not appear in Figure 5.19. The conditions caused by the dozer loading at a depth of 2 m plot just below the liquefaction boundary. Close to the dozer, pore pressures equal to the overburden were recorded to a depth of 1.8 m. Although elevated excess pore pressures likely also existed deeper, where there were no piezometers installed to record them, the results coincide well with the observed behaviour.

5.4.4 Factors Influencing Predicted Behaviour

5.4.4.1 General

The predicted behaviour appeared to match well with the observed behaviour. However, the analyses involved several assumptions, such as the attenuation of the particle velocities with depth and a constant representative penetration resistance, and involved several material properties including density and shear modulus. A discussion of the sensitivity of the analyses results to the various factors is therefore presented below.

5.4.4.2 Attenuation Relationship

The assumed attenuation relationship had a great influence on the predicted behaviour when compared to the prediction if no attenuation was assumed. The latter assumption is clearly incorrect so a small sensitivity study was carried out to assess the effects of the material and geometric damping coefficients used in the assumed attenuation relationship.

It was found that the calculated cyclic stress ratios were not very sensitive to the values selected for the material damping within the ranges summarized by Kim and Lee (1998). Therefore the use of average values of 0.007 m^{-1} and 0.02 m^{-1} for the dozer and Predator, respectively, based on their recorded vibration frequencies and a "competent" soil appeared reasonable. It was noted that even if the larger material damping coefficient used for Predator loading was used to analyze the dozer loading the results were not significantly altered. The value used for the geometric damping coefficient, n , influenced the calculated stresses to a greater degree and its effect was therefore examined in greater detail.

It was recommended that n should vary between 1 and 2 for the attenuation of body waves (Woods and Jedele, 1985; Kim and Lee, 1998; Kramer 1996). In general, it

seems that body wave attenuation on the surface should have $n=2$ while body wave attenuation within the soil mass should have $n=1$. However, it would seem that there would have to be a gradual transition between the two conditions as clearly a soil particle on the surface must move somewhat similarly to the particle adjacent to it that is not on the surface. No information was readily available regarding this so comparisons of predicted behaviour and observed behaviour for $n=1$ and $n=2$ for three cases were carried out. The cases considered were dozer loading with a phreatic surface at 0.35 m in which softening did occur, Predator loading with the phreatic surface at 0.35 m in which softening did not occur and Predator loading with the phreatic surface at 0.25 m in which softening did occur provided sufficient moisture content existed above the phreatic surface. It was found that the best fit between predicted and observed behaviour occurred when a geometric damping coefficient of 1 was used, consistent with the transmission of body waves through a deposit. These calculations and the resulting plots are included in Appendix D.

5.4.4.3 Effective Overburden Pressure

It is readily apparent from Figure 5.19 that the applied cyclic stress ratio varies dramatically with depth. At shallow depths, although the cyclic stress may be low compared to earthquake conditions, the low overburden pressure causes the cyclic stress ratio to be very large. Because the CSR is calculated as shear stress divided by effective overburden stress and the overburden stresses are quite low, the solution is also very sensitive to the location of the phreatic surface. As is indicated by the plots for Predator loading with different phreatic surfaces, a small increase in the location of the phreatic surface can cause the deposit to be classified as potentially liquefiable. This result correlates well with the observed behaviour.

Similarly, the calculated cyclic stress ratio does depend somewhat on the density of the material however to a much lesser degree. Lower density would cause a reduction in both the effective overburden stress as well as in the calculated induced shear stress (see Equation 5-6). The latter is proportional to the square root of density and therefore would decrease a lesser amount than the effective overburden pressure resulting in a net increase in the cyclic stress ratio. An increased density would also tend to increase the penetration resistance however and this effect would likely be greater than the effect of density on the CSR and would likely result in a decreased liquefaction potential.

5.4.4.4 Shear Stiffness

The effect of shear modulus on the predicted liquefaction behaviour was also examined. In general, stiffer soils produce lower strains for a given stress and should therefore be less susceptible to liquefaction. In the preceding analyses however, the strains were a measured quantity and therefore since the soil shear stiffness is used to calculate stresses from strains, its effect is reversed. Increasing the estimated stiffness of the material resulted in an increase in the calculated induced stresses and an increased predicted liquefaction susceptibility. The predictions of cyclic liquefaction at the main test site however were not extremely sensitive to the selected shear modulus value; although the calculated cyclic stress ratio varied with the shear stiffness, the shear modulus could be varied from 10 to 30 MPa without significantly changing the prediction of occurrence of liquefaction at the main test site. The solution appeared to be much more sensitive to the location of the phreatic surface and the geometric damping coefficient than to the shear modulus.

5.4.4.5 Penetration Resistance

Penetration resistance has a very clear and major effect on the analyses; the liquefaction potential increases and decreases with increasing and decreasing penetration resistance. A non-representative penetration resistance would invalidate the entire analyses. The normalized penetration resistance would tend to increase with a multitude of factors including the density, age, coarseness and in-situ stresses.

5.5 Extrapolation of Liquefaction Prediction to Other Sites

The prediction of softening based on the cyclic stress – penetration charts appeared to correlate well with the observed behaviour at the main test site. Although the methods clearly don't include effects such as increased or varying moisture contents above the phreatic surface they may provide a good starting point for preliminary screening of similar sites. However, because of the assumptions involved in the analyses, any trends would only be applicable to sites with BAW tailings similar to those at the main test site in terms of gradation, stiffness, representative penetration values, in-situ density and also would have to be subjected to similar loading conditions.

The simplest case to consider is BAW tailings with similar properties under similar dozer loading with a varying phreatic surface location. The minimum depth of the phreatic surface to prevent softening was calculated assuming that softening would not be triggered if the induced cyclic stress ratio at the phreatic surface was less than the critical value. For an $(N_1)_{60}$ value of 11 or a q_{C1N} value of 75, the critical CSR to trigger liquefaction is approximately 0.12 (see Figure 5.19). Assuming that the 15 cycle velocity does not differ from that recorded at the main test site, the phreatic surface would have to be at a depth of approximately 1.5 m to minimize the potential for softening under dozer loading. It should be noted that in calculating this depth, a bulk density of 1675 kg/m^3 , lower than that used in the previous analyses, was used to reflect the fact that above the phreatic surface, the tailings are unsaturated. If the loading changed however so that there were significantly more or less loading cycles, the 15 cycle particle velocity would likely change and therefore the required depth of the phreatic surface would also change.

To attempt to capture the effect of longer loading duration, the minimum depth of the phreatic surface was also calculated based on 65 percent (the average after Seed and Idriss, 1971) of the maximum velocity corrected for a large number of cycles. As the number of cycles increases the shear stress ratio required to cause zero effective stress conditions approaches a constant value and the corresponding limiting correction factor of 1.5 was used to correct for many cycles. This does assume, however, that the magnitude of the applied particle velocities do not differ substantially from those recorded at the main test site. In this case, the required depth of the phreatic surface to minimize the potential for softening was estimated as 2.0 m. This case can be somewhat generalized by plotting the calculated applied cyclic stress ratio generated by the dozer with depth assuming that the phreatic surface is coincident with the depth of interest as shown in Figure 5.20. The penetration resistance required to have a cyclic resistance ratio equal to the applied cyclic stress for clean sands is shown on the bottom axis based on the relationship proposed by Seed et al. (1985). Figure 5.20 would however be applicable only to sites with similar soil and equipment loading conditions. Field measurement of particle velocities resulting from different types of equipment

would allow development of similar charts for each piece of equipment and allow estimation of cyclic liquefaction potential under a variety of conditions.

A somewhat more useful extrapolation of the field data may be an estimate of the maximum permissible peak particle velocity to prevent softening with depth of the phreatic surface. To carry out these calculations, it was again assumed that there was a constant critical cyclic stress ratio at which cyclic liquefaction would be triggered resulting in softening of the deposit. The properties of the BAW tailings at the main test site were used as representative tailings properties. In particular it was assumed that the shear modulus was 20 MPa, the in-situ material bulk density above the phreatic surface averaged 1675 kg/m^3 , representative penetration resistance values were 11 and 75 for $(N_1)_{60}$ and q_{C1N} , respectively, corresponding to a critical CSR of 0.12 and that the particle velocity attenuation relationship described previously was appropriate. At each depth of interest, the particle velocity required on the surface to produce a CSR equal to the critical CSR of 0.12 was calculated. The maximum velocity was then calculated following the same logic as for calculating the required depth of the phreatic surface for dozer loading; the critical velocity was assumed to be 65 percent of the maximum recorded velocity, and to account for many loading cycles, the limit correction from DeAlba's (1976) work of 1.5 was applied. These calculations are for a factor of safety of 1.0, i.e. liquefaction is just triggered and excess pore pressures are close to overburden pressure. Idriss (1998) indicated that residual pore pressures of greater than 25 to 40 percent are often of concern. Idriss (1998) presented results from Marcuson and Hynes (1989) which indicated that for sands, maintaining pore pressure below the 25 to 40 percent threshold corresponded to a factor of safety of approximately 1.3 against liquefaction since. Since large excess pore pressures are a concern with respect to the softening phenomenon, calculations were also carried out for a factor of safety of 1.3. The results are plotted in Figure 5.21. These calculations have also been included in Appendix D.

Application of Figure 5.21 would require that particle velocities be recorded in a manner similar to the one employed at the main test site and would require validation of the assumptions inherent in the calculations. Also, as the phreatic surface becomes deeper, it would be expected that increased pore pressures could potentially have less and less effect on the surface and that there may be a limiting depth below which excess pore pressure generation would have no effect on surface. Ishihara (1985) proposed a relationship for the thickness of a non-liquefiable surface layer required to prevent ground damage. The relationship indicated that there was a depth below which liquefaction caused by earthquake loading would not cause surface damage, ranging from 3 to 10 m depending on surface acceleration. Andrus and Stokoe (2000) presented data which appeared to indicate similar findings. Maximum surface accelerations measured at the main test site during dozer loading were in the range of 0.3 to 0.4g, which would suggest a required non-liquefiable layer thicknesses of 6 to 10 m. These values do not seem consistent with visual observations. Clearly the attenuation of equipment induced vibrations is very different from the propagation of earthquake stresses possibly invalidating these relationships. Further investigations in this area may be helpful.

In order to produce a relationship that could be used directly for preliminary screening of sites, a relationship between the equipment mass and particle velocity was examined. If such a relationship could be established then the required depths of the phreatic surface calculated in Figure 5.21 could be related directly to vehicle mass. As discussed in

Section 5.3.5.2, peak particle velocity can be related to input energy and distance from the source (Woods and Jedele, 1985). Therefore, provided that the equipment is driven at relatively similar speeds and that the frequency of the equipment does not vary enough to significantly affect the energy it would appear reasonable that peak particle velocity should depend on the mass of the equipment. Since the equipment used to examine this relationship did have different frequencies, the effect of frequency may be somewhat embedded in any relationship developed.

The maximum vector resultant velocity recorded during Predator and dozer loading was plotted versus the equipment mass as shown in Figure 5.22. It is recognized that there are not sufficient data points to confidently extrapolate the field data however, also shown in Figure 5.22 are the relationships developed by Woods and Jedele (1985) for maximum particle velocities associated with construction activities. Although the data provided by Woods and Jedele is in terms of energy (J) while the field data is plotted in terms of mass, the slopes of the lines appear very similar. The magnitudes of the recorded particle velocities also appear reasonable as the field data was gathered at a location closer to the source than that presented by Woods and Jedele. This comparison appears to suggest that a tentative relationship between recorded particle velocities and equipment mass is justified. However, the absolute maximum particle velocities recorded during both Predator and dozer loading appeared to be isolated events that were not repeated enough to dominate the response of the tailings. As shown in Figure 5.22, the relationship between equipment mass and more representative maximum velocities is slightly steeper than that based on the absolute maximum velocities and seemed a more realistic relationship based on the analyses carried out at the main test site.

The tentative relationship between the maximum recorded vector resultant particle velocities and equipment mass was applied to the estimated maximum allowable particle velocities for increasing depth of the phreatic surface as calculated for Figure 5.21. This produced a preliminary relationship between equipment mass and required depth to the phreatic surface as shown in Figure 5.23 for factors of safety against triggering of liquefaction of 1.0 and 1.3. It should be noted that this relationship is based on several significant assumptions. It was assumed that the particle velocity attenuation with depth followed the relationship presented in Equation 5-1 with a material damping coefficient of 0.007 and a geometric damping coefficient of 1 for depths greater than 0.55m. It was assumed that softening would not be triggered provided the induced cyclic stress ratio at the phreatic surface was less than 0.12; i.e. that a $(N_1)_{60}$ value of 11 or a q_{C1N} value of 75 is appropriate for the tailings, and that the charts adopted by the NCEER (Youd and Idriss, 2001) after Seed et al. (1985) and Robertson and Write (1998) correctly define the "liquefaction" susceptibility at the location of interest. It was assumed that the deposit subjected to loading was similar to the BAW tailings at the main test site with a shear modulus of 20 MPa and an average density above the phreatic surface of 1675 kg/m³. It is also likely that the relationship is only applicable to tracked equipment; equipment or vehicles with tires may have different loading characteristics and thus a different relationship. Finally a very significant and tentative assumption was made concerning the relationship between particle velocity and equipment mass as shown in Figure 5.22. Furthermore, the relationship does not account for the effect of a wetting front due to a recent heavy precipitation event. This effect however would likely be most significant when dealing with shallow water levels and light equipment. The relationship also does not account for a significant saturated capillary zone above the phreatic surface.

The curves derived for Figure 5.23 using factors of safety of 1.0 and 1.3 are likely conservative because they consider essentially infinite load cycles and do not take into account limiting depths. It is therefore likely that the curves could be moved vertically upward. For example, if 65 percent of the maximum recorded particle velocity is assumed to be representative of the average stresses induced without requiring an additional correction for essentially infinite loading cycles, the curve can be moved upwards as indicated in Figure 5.23 by the heavier dashed line. Furthermore, if the concept of a limiting depth below which liquefaction of the tailings has no effect on surface is valid, a cutoff would exist similar to that shown by the heavy horizontal dashed line in Figure 5.23. Clearly site specific information and further testing could improve the relationship considerably and would likely result in a less conservative relationship. The graph in Figure 5.23 indicates that it is possible to develop a relationship between equipment mass and required depth to phreatic surface and provides a starting point for future testing. Information regarding particle velocities for specific equipment and their attenuation would also be particularly useful in improving the relationship.

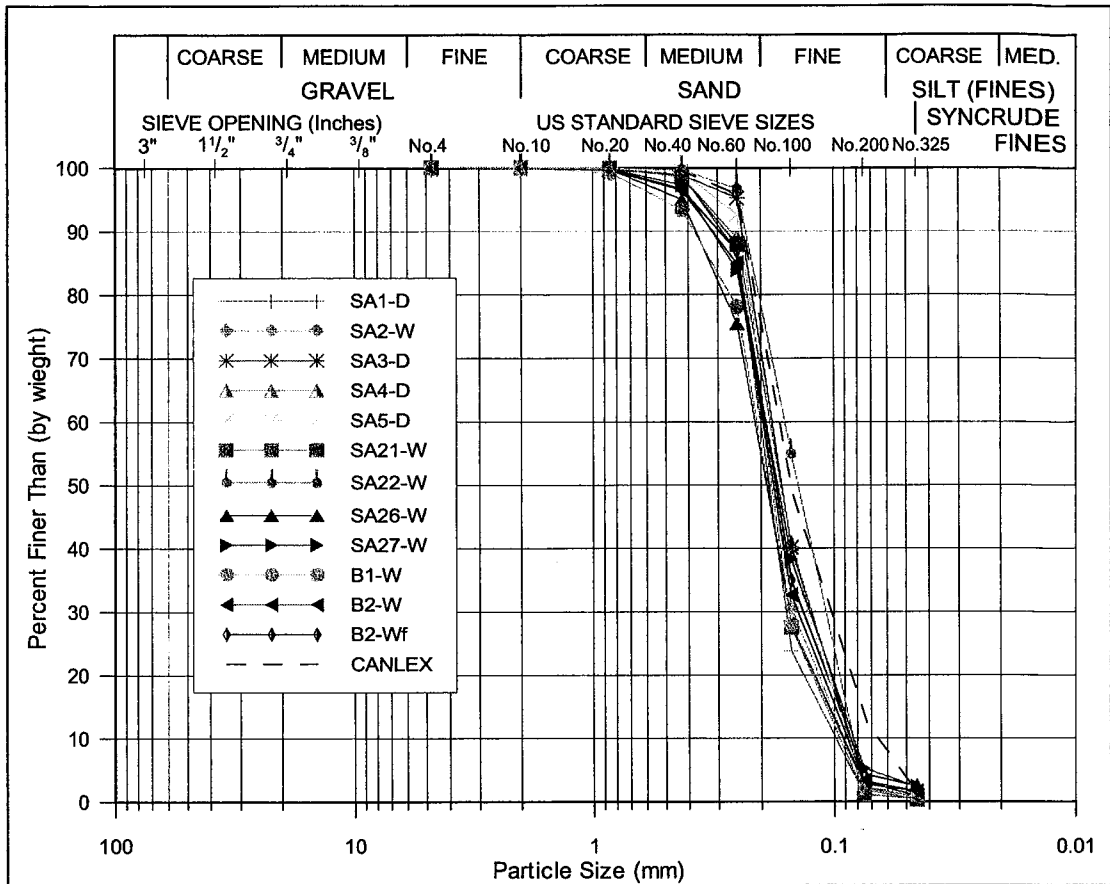


Figure 5.1 Comparison of Grain Size Distribution at Test Sites With Results from CANLEX

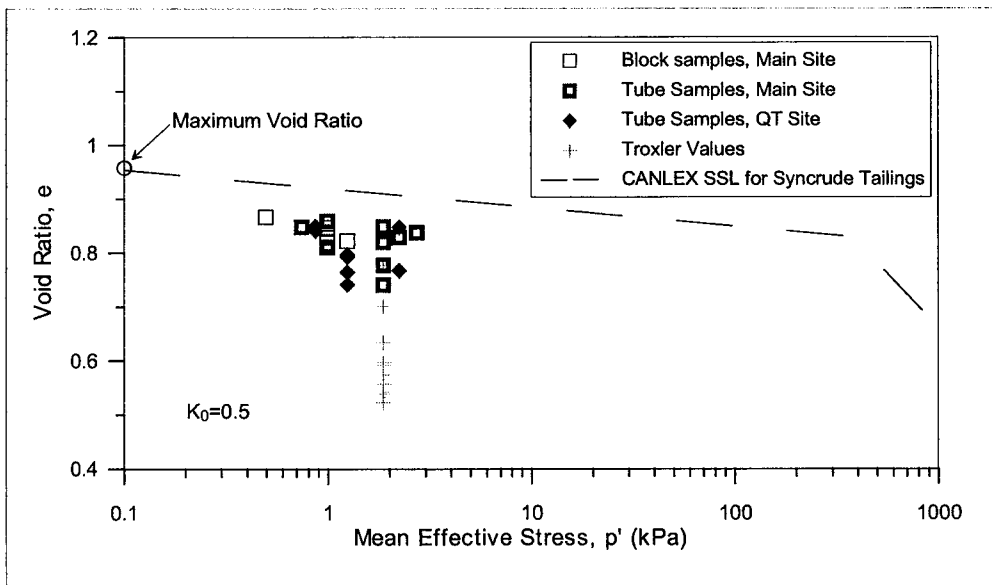


Figure 5.2 Initial State Conditions at the Main Test Site

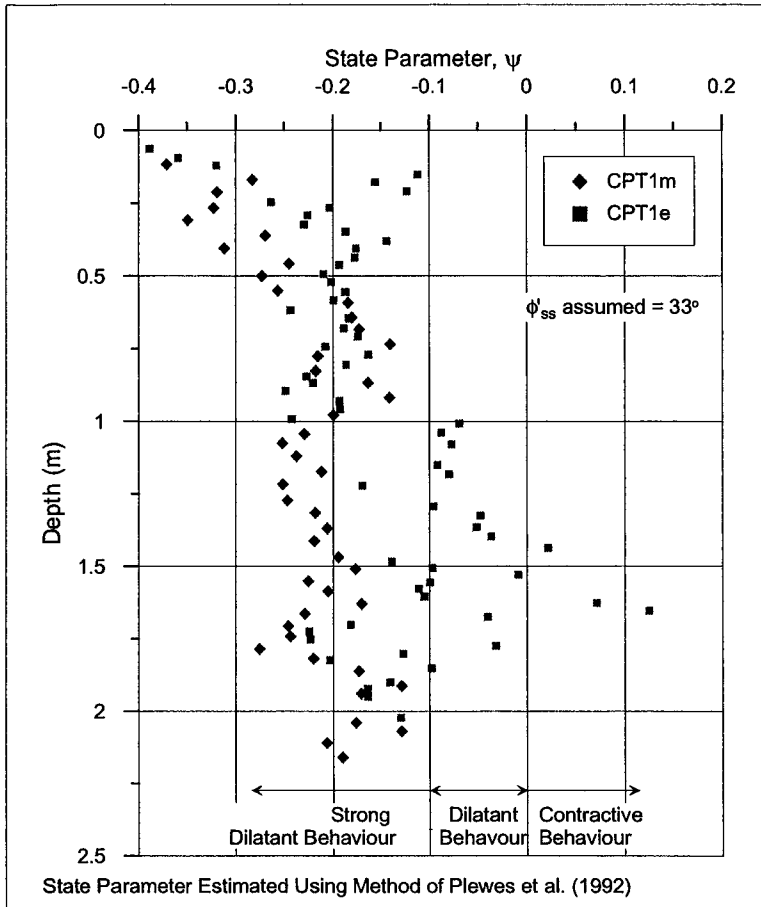


Figure 5.3 State Parameter Estimate from CPT Data at Main Test Site

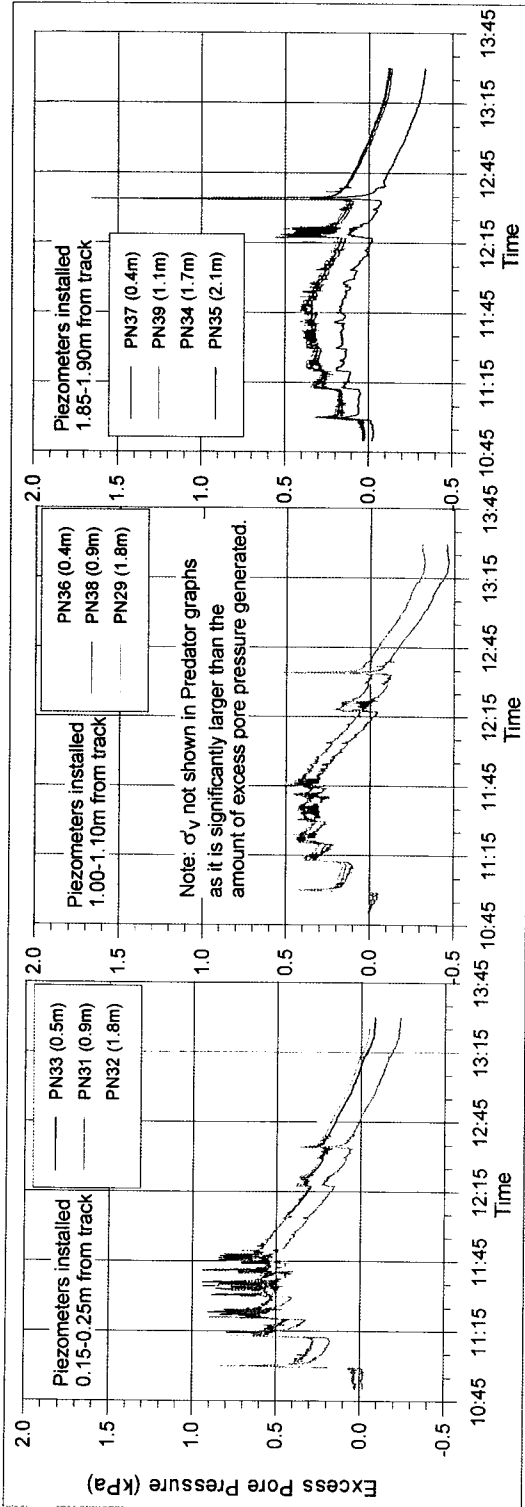


Figure 5.4 Excess Pore Pressures Measured During Predator Loading

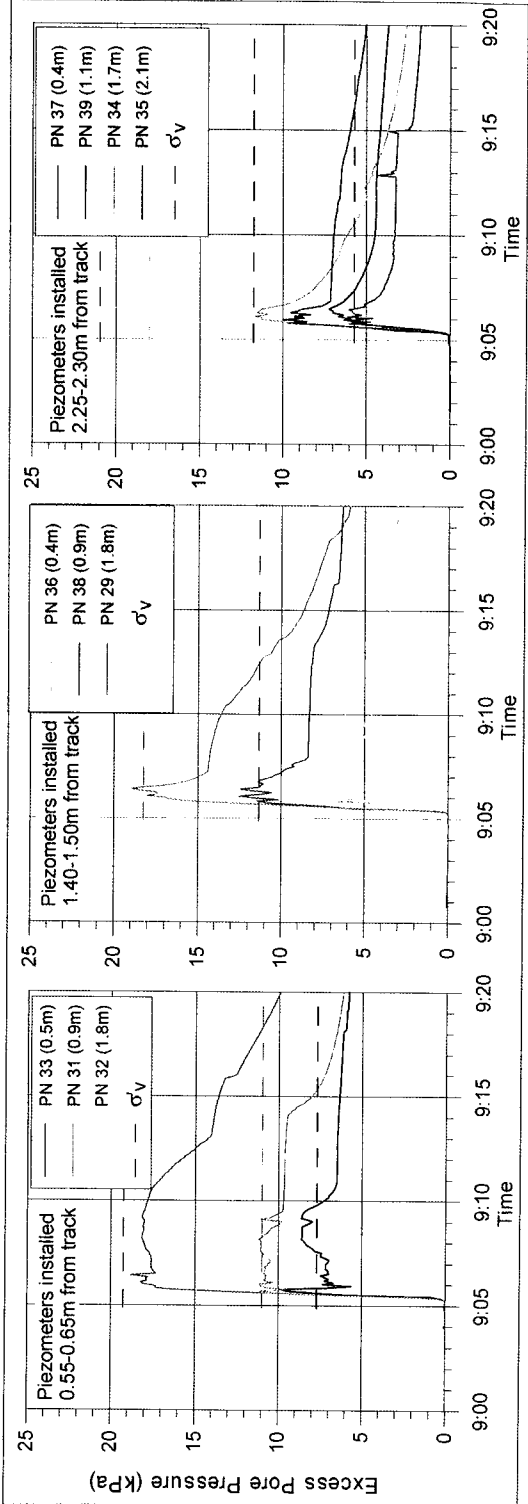


Figure 5.5 Excess Pore Pressures Measured During Dozer Loading

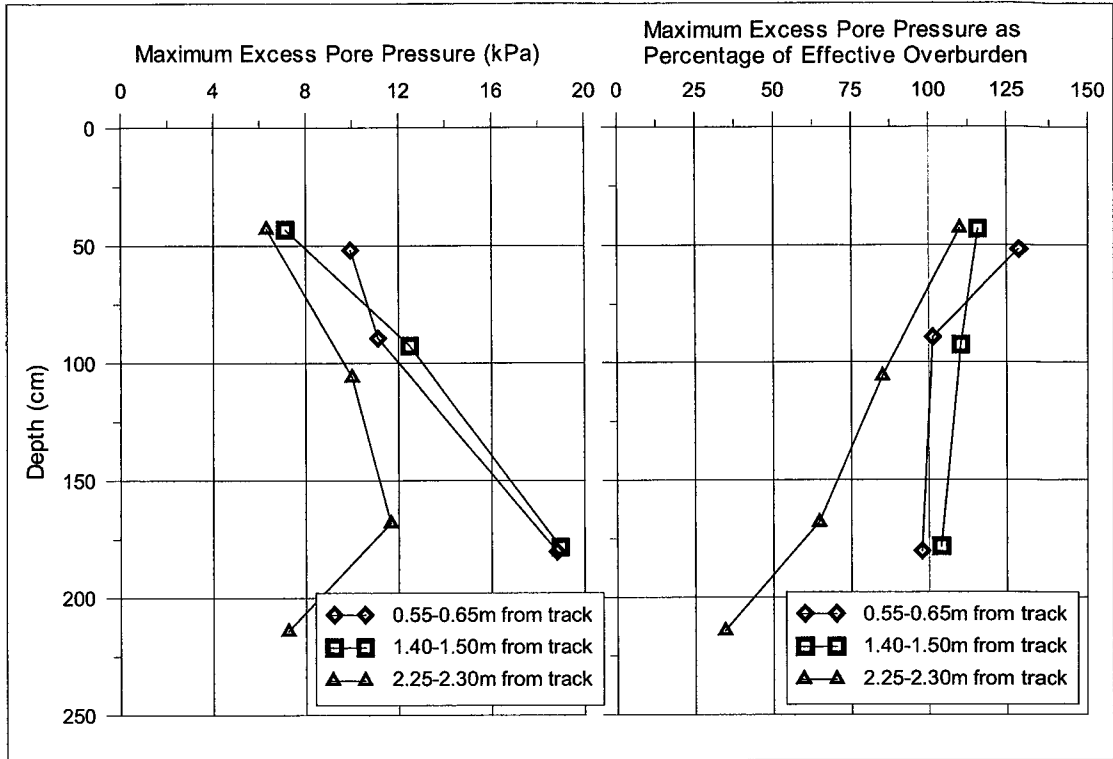


Figure 5.6 Variation in Maximum Excess Pore Pressure Within Tailings Deposit During Dozer Loading

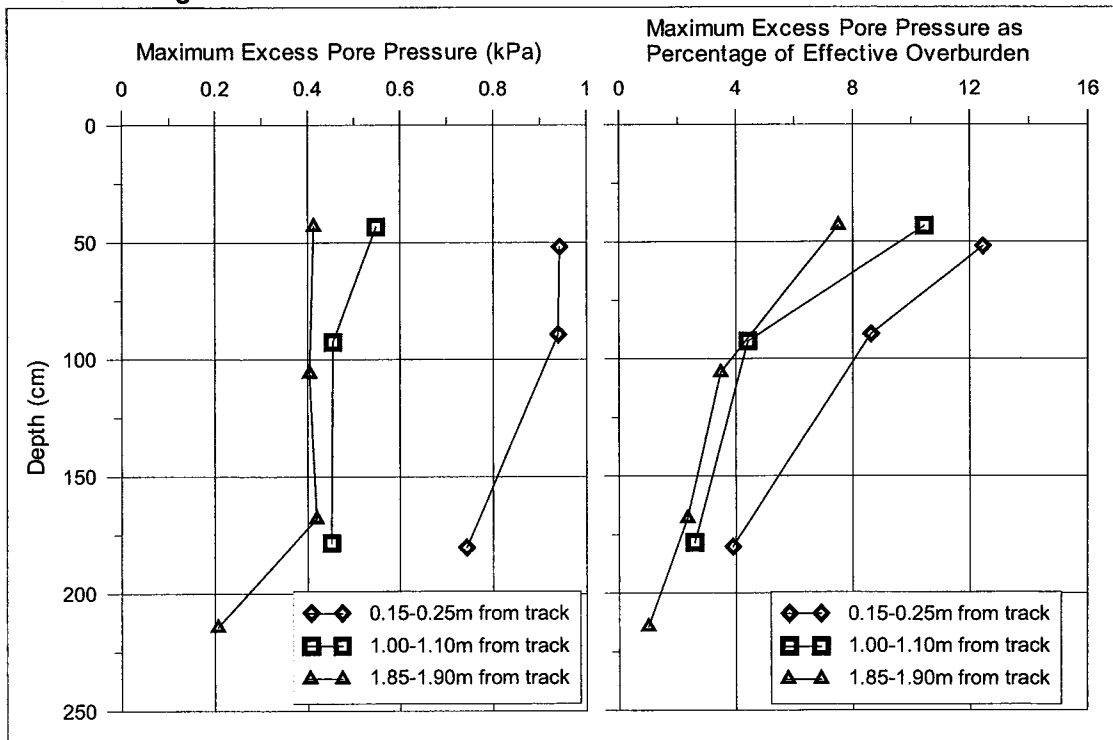


Figure 5.7 Variation in Maximum Excess Pore Pressure Within Tailings Deposit During Predator Loading

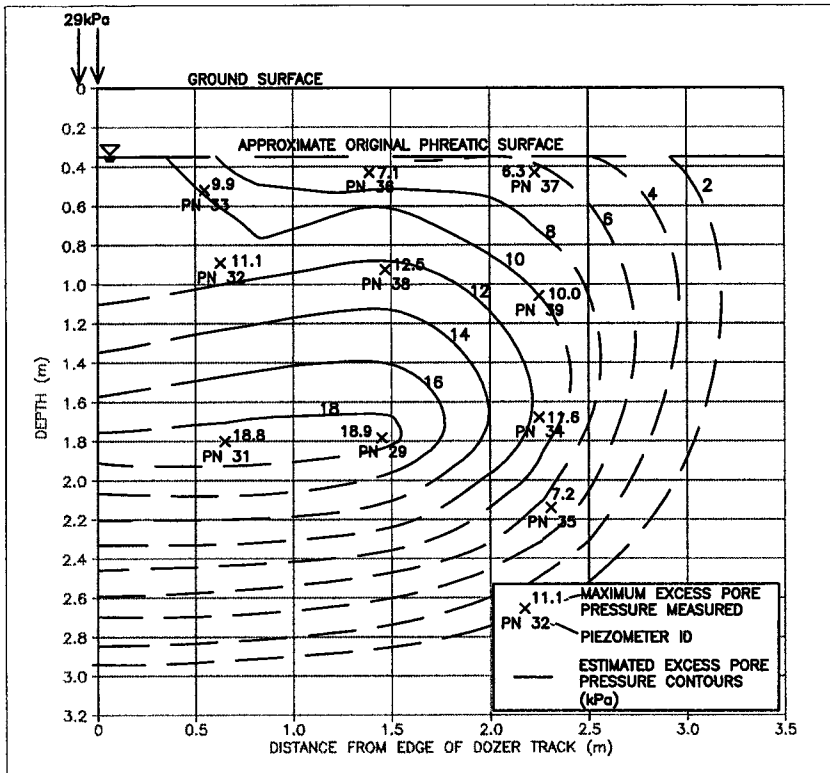


Figure 5.8 Contours of Maximum Excess Pore Pressure Generated by Dozer Loading

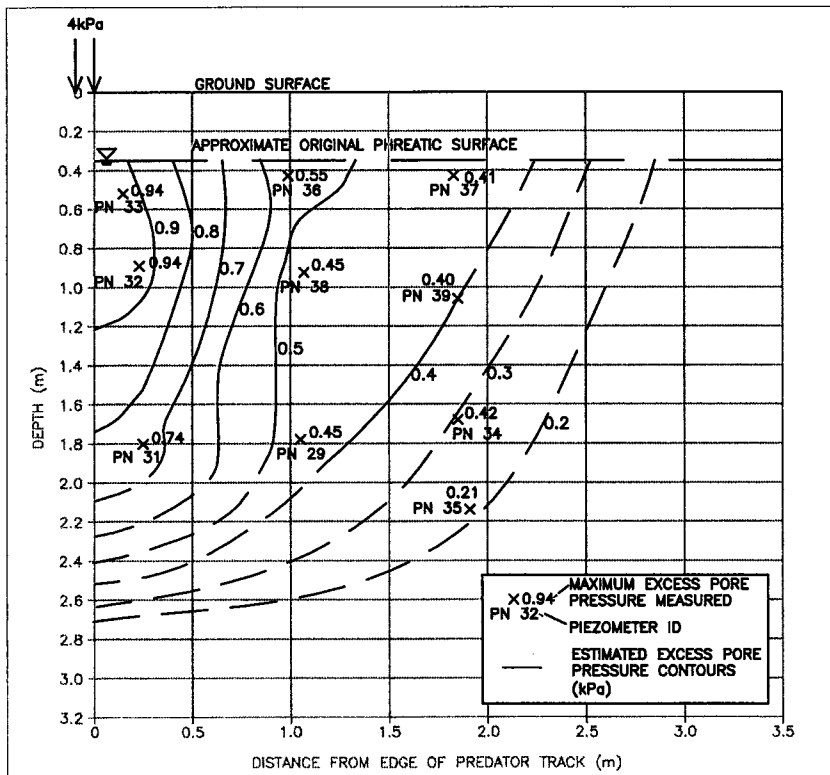


Figure 5.9 Contours of Maximum Excess Pore Pressure Generated by Predator Loading

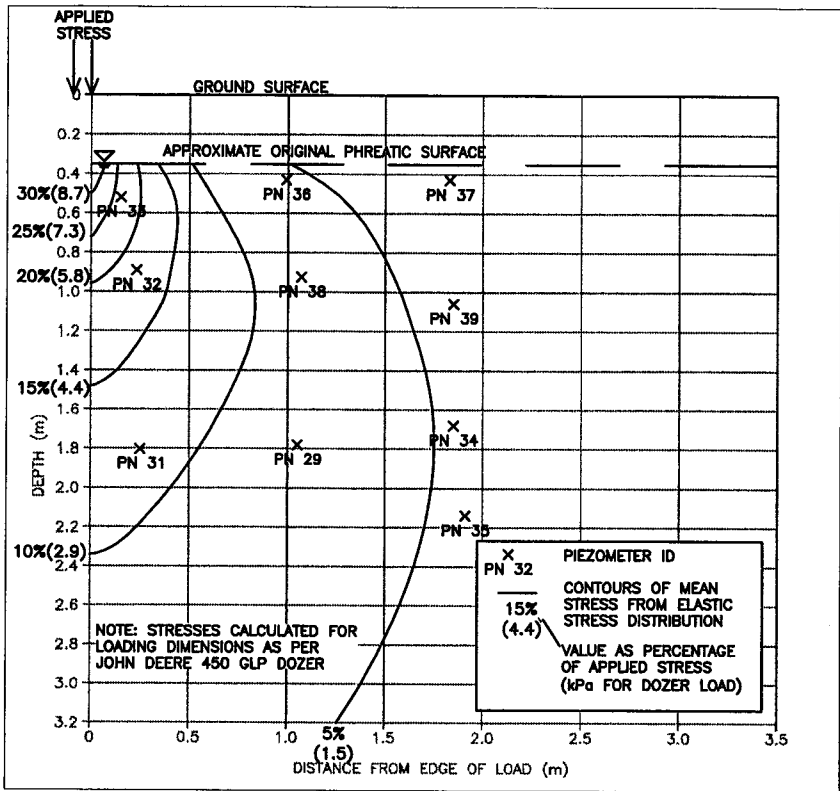


Figure 5.10 Typical Elastic Distribution of Load

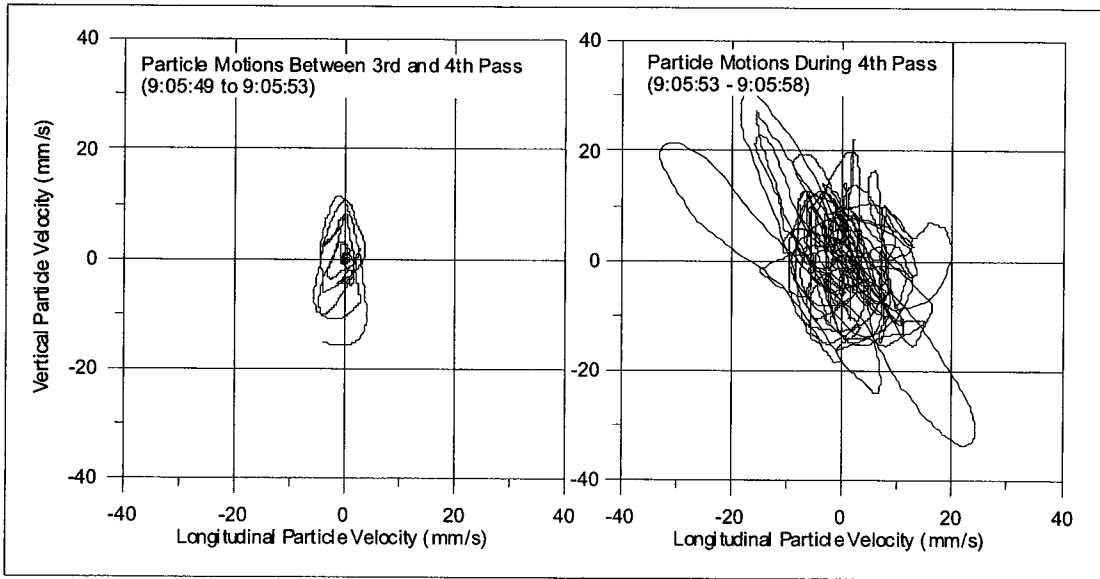


Figure 5.11 Particle Motions Recorded During Dozer Loading

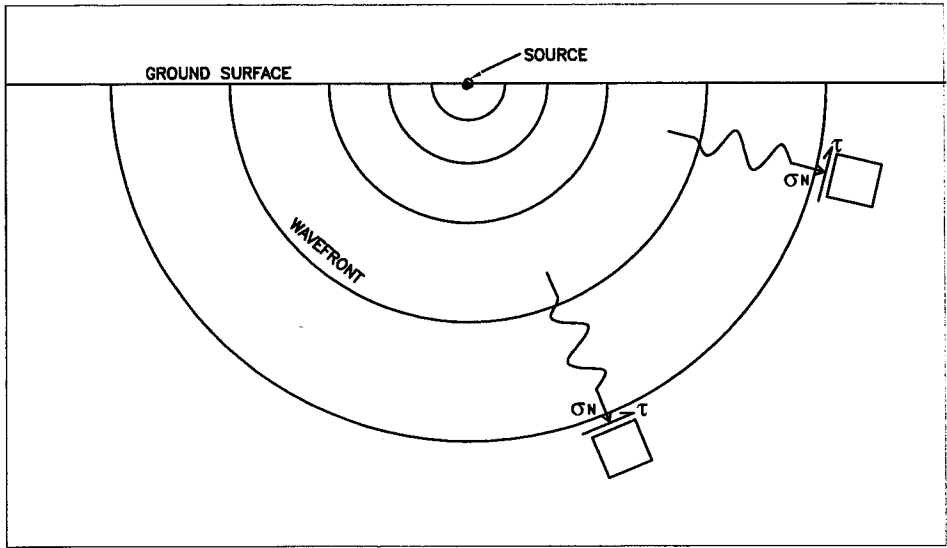


Figure 5.12 Schematic of Assumed Wave Propagation

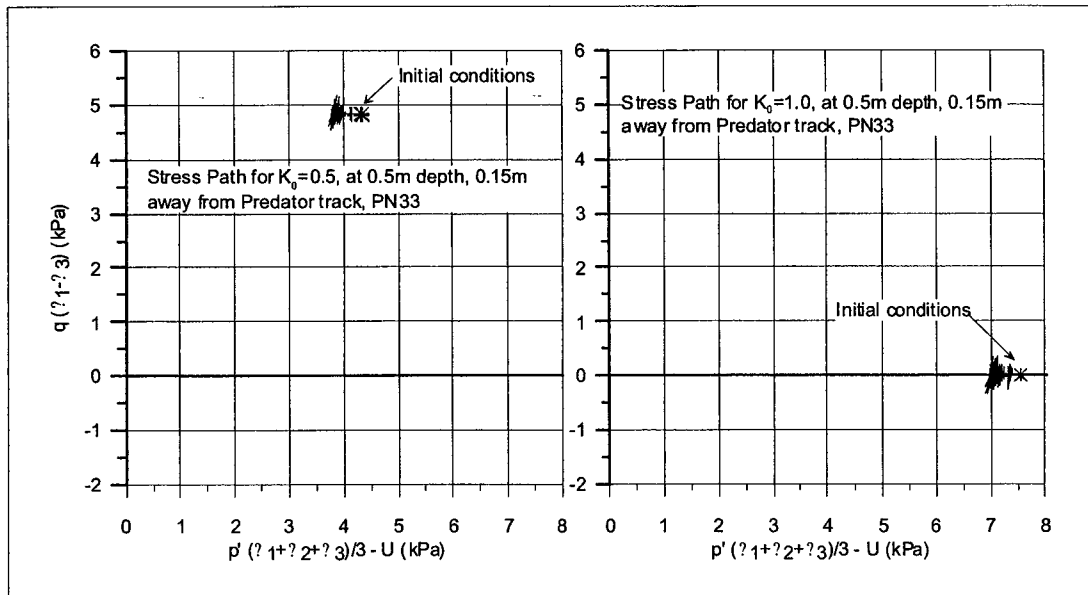


Figure 5.13 Stress Path at PN 33 (Depth of 0.5m) During Predator Loading

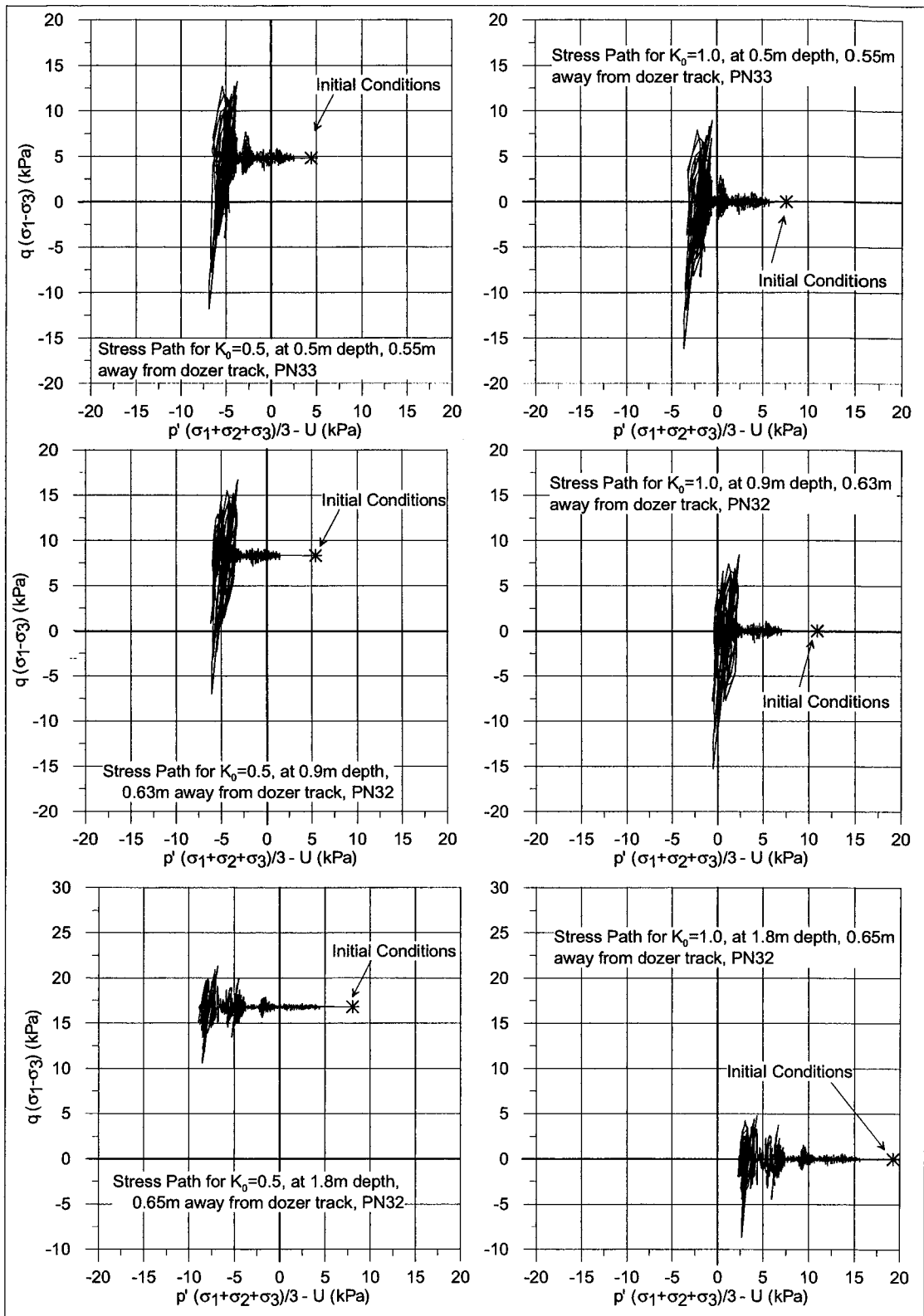


Figure 5.14 Stress Path at PN 33, 32 and 31 (depths of 0.5, 0.9 and 1.8m) During Dozer Loading

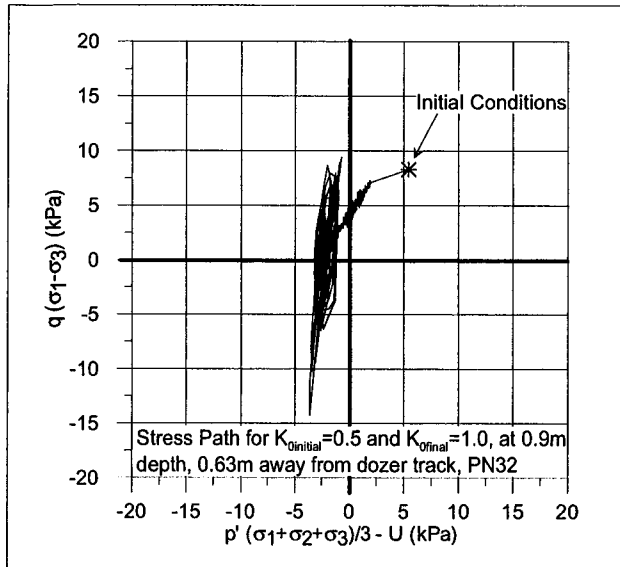


Figure 5.15 Approximate Stress Path at PN32 During Dozer Loading with a Varying K_0

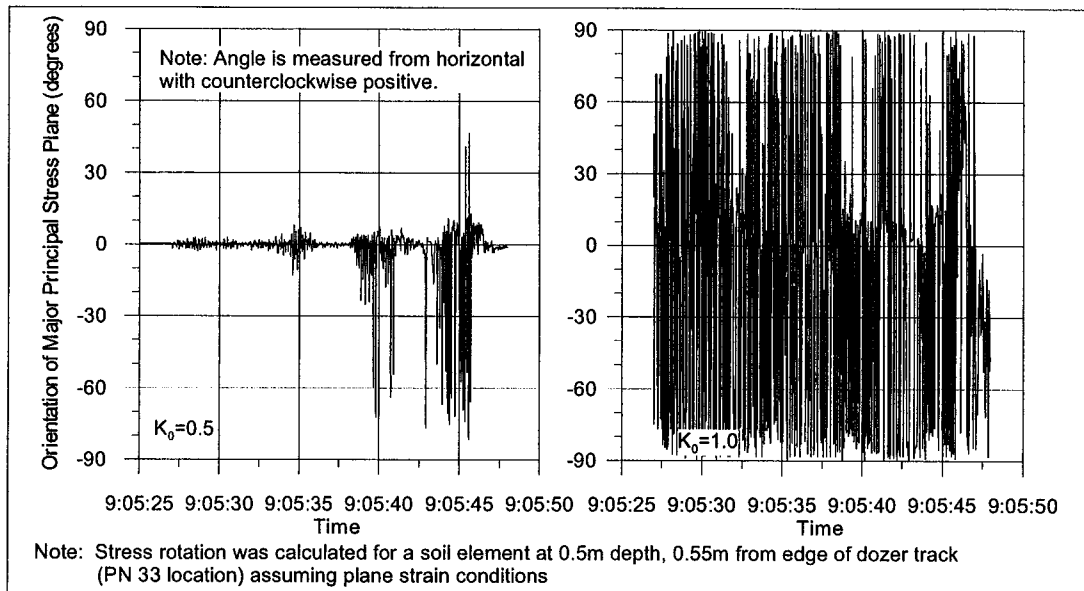


Figure 5.16 Stress Rotation During Dozer Loading

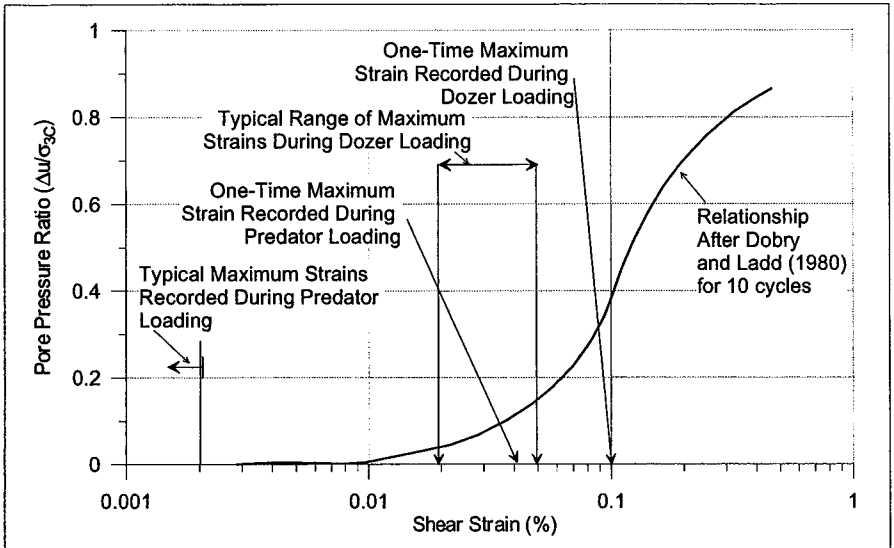


Figure 5.17 Cyclic Strain - Pore Pressure Generation Relationship Compared to Strains Measured During Field Test

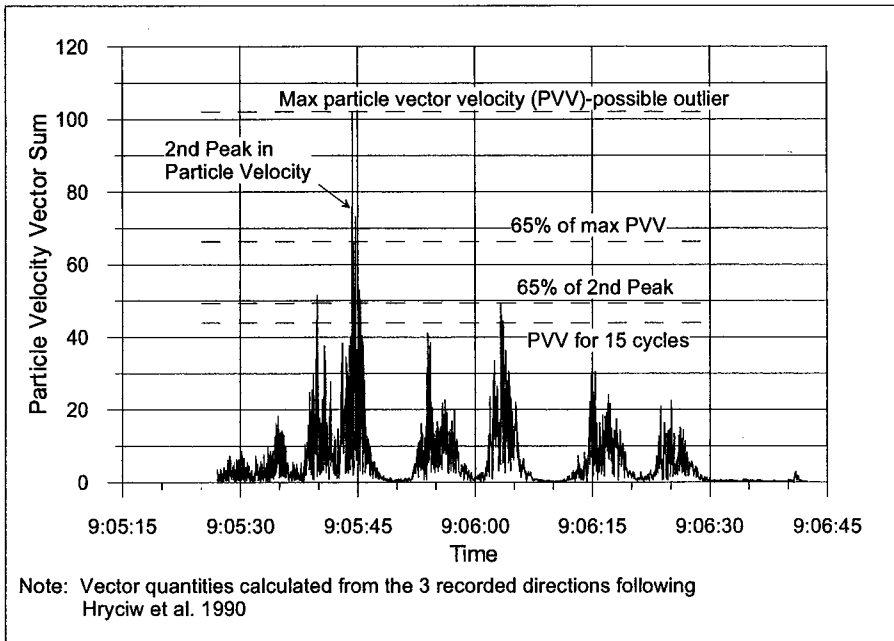


Figure 5.18 Resultant Vector Particle Velocities Used in Calculation of Cyclic Stress Induced During Dozer Loading

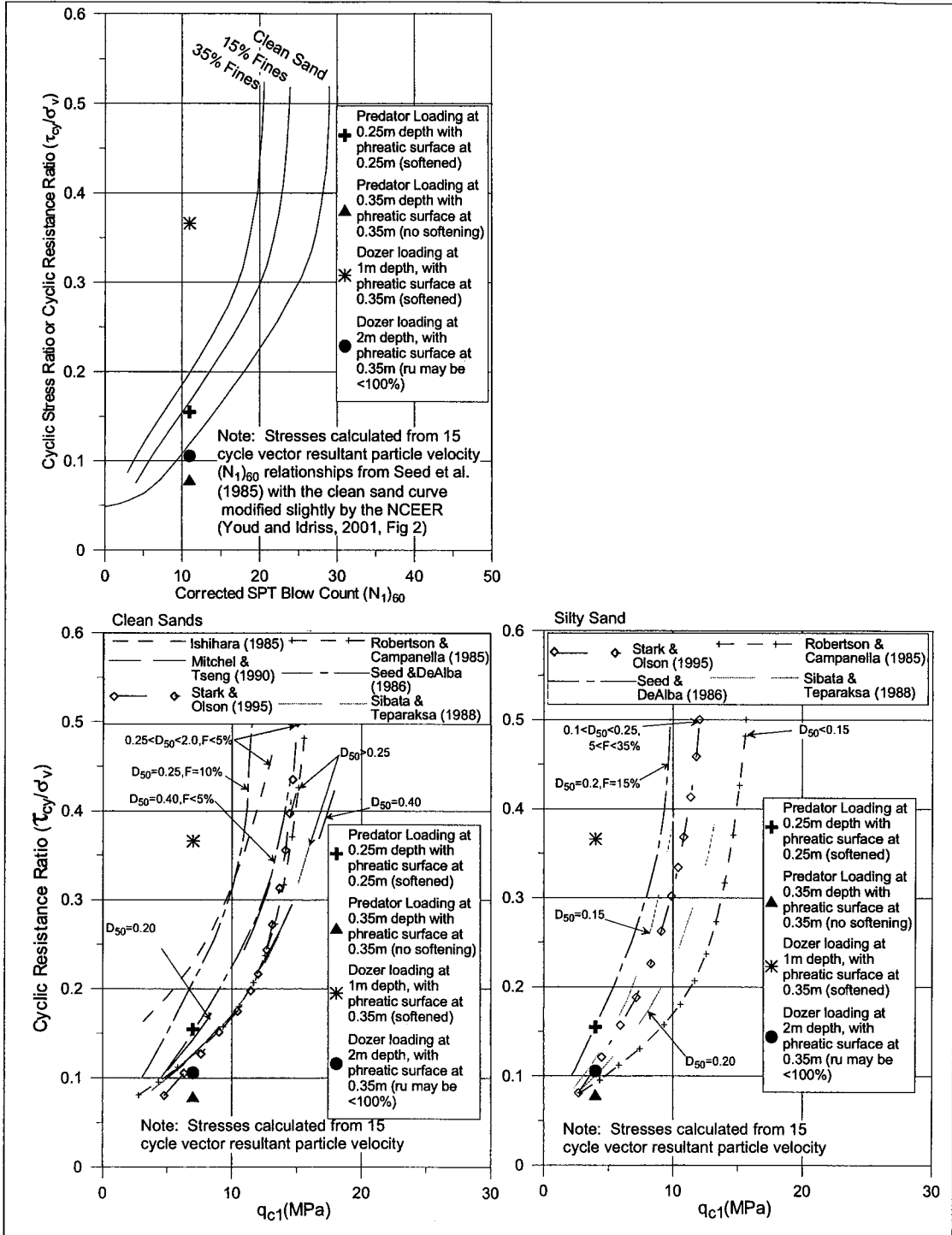


Figure 5.19 Predicted Liquefaction Response of the BAW Tailings at the Main Test Site

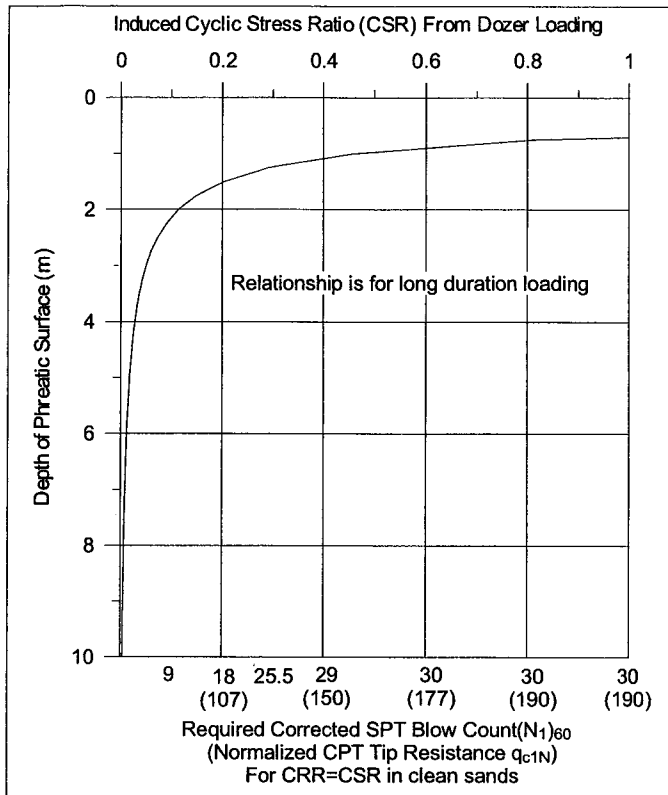


Figure 5.20 Cyclic Stress Ratio Vs Depth for Dozer Loading

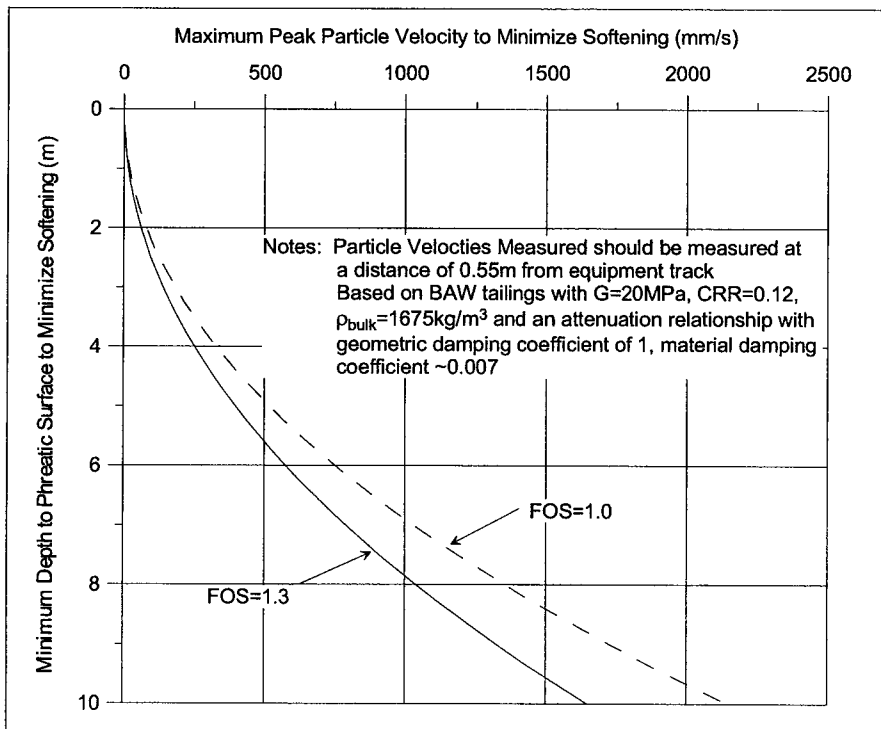


Figure 5.21 Maximum Peak Particle Velocity vs. Depth to Phreatic Surface to Minimize Softening

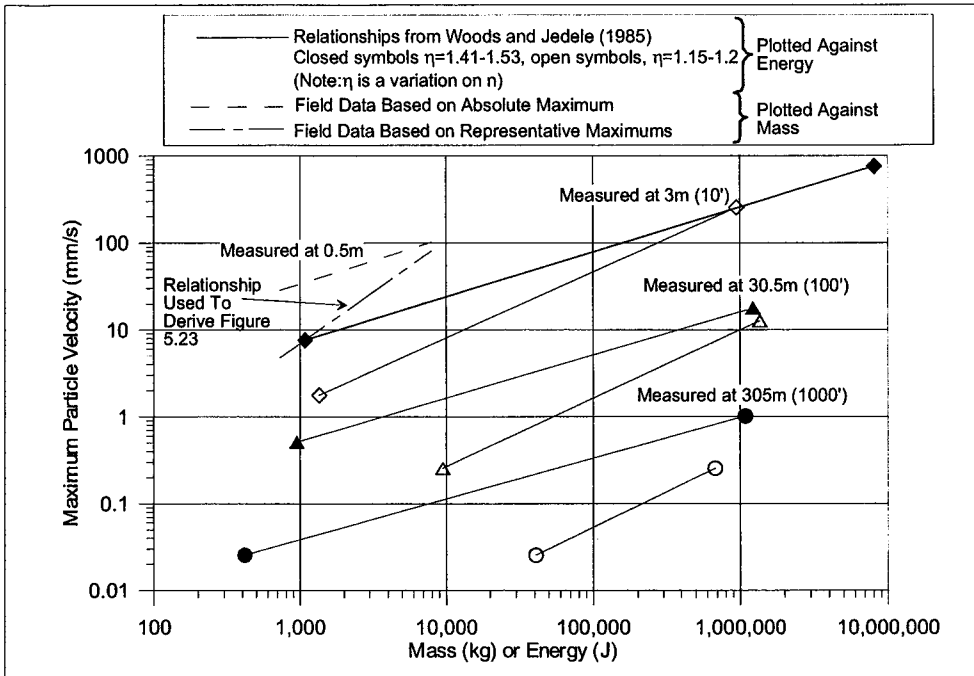


Figure 5.22 Tentative Particle Velocity, Equipment Mass and Energy Relationships

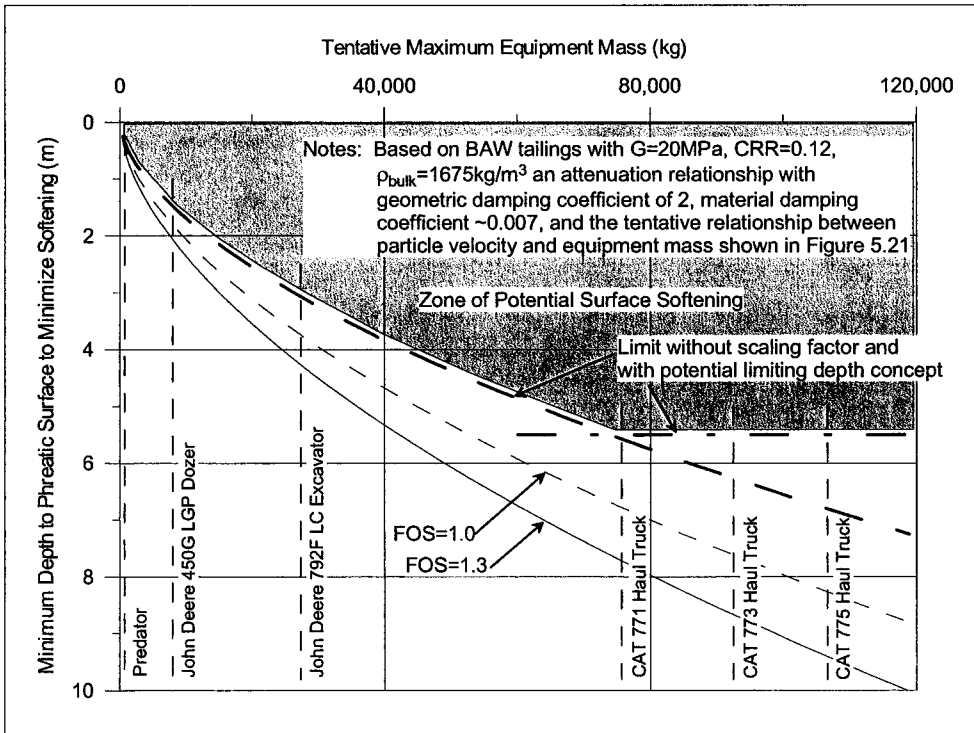


Figure 5.23 Tentative Relationship Between Equipment Mass and Required Depth to Phreatic Surface

6.0 CONCLUSIONS

The softening of dense BAW tailings when subjected to equipment loading at Syncrude was replicated in instrumented field tests. Tests were carried out to check the assertion that the in-situ tailings were in fact dense. Pore pressures and particle velocities were monitored during equipment loading to allow an understanding of the mechanisms involved. Further testing was carried out after softening to investigate if any significant changes to the tailings properties had occurred as a result of softening. A short trafficability study was also carried out, mainly for comparison with previous work.

Shallow frozen samples gathered at the site by radial freezing appeared to successfully capture the in-situ density of the tailings. The method employed was described in detail and could be improved by greasing the tube, by installing strain gauges to monitor straining as a result of freezing, and by longer freezing times. It could also likely be adapted to depths of up to a meter or two by using a longer sampling tube and a small auger for cleaning out the tube. Frozen block samples gathered as described in HBT AGRA (1992) also appeared to be a reliable method of obtaining representative samples, but do require longer freezing times than were utilized in the present study. Based on a comparison of the measured densities and void ratios from the frozen samples with steady state lines developed previously for Syncrude tailings sand, it was confirmed that the in-situ state of the BAW tailings at shallow depths was generally dense of the steady state line. Analyses of CPT data gathered during the field program independently confirmed these findings.

The BAW tailings were first subjected to light equipment loading which did not induce softening. Larger equipment was then used to load the area and softening did occur, evidenced on surface by undulation of the ground, cracking and sand boils. The pore pressures measured during loading indicated that under a sufficiently large cyclic load pore pressures in dense BAW tailings did build up significantly and caused conditions of essentially zero effective stress in a significant volume of the deposit. Examination of the pore pressures indicated that the affected area was significantly larger than would be expected based on typical rules of thumb; the dozer with tracks 61 cm wide appeared to cause excess pore pressure reaching greater than 50 percent of the overburden pressure at distances of up to 3 m from the edge of the track.

Analyses of the measured particle velocities allowed calculation of the induced dynamic stresses. Coupled with the measured pore pressures and an estimate of the original in-situ stress state, this allowed the stress path during loading to be evaluated. The stress paths indicated that under a sufficiently large cyclic load significant softening occurred and the effective stress was decreased to essentially zero. The stress paths also indicated that only if the stress state was nearly isotropic did shear stress reversal occur. Previous testing indicated that the initial stress condition was more likely anisotropic with a stress ratio less than unity. However as pore pressures increased and effective stress decreased, the soil likely behaved more like a fluid, as suggested by the undulations observed on the surface, and in-situ stress conditions likely approached isotropic causing shear stress reversal to occur. Under smaller cyclic loads, no significant softening was observed. These findings led to the conclusion that cyclic liquefaction was the cause of the observed softening response.

Tests carried out following softening did not indicate large variations in the properties of the tailings. The moisture content and saturation of the tailings increased significantly

after softening but no other significant changes were observed. Nuclear density gauge readings indicated large decreases in the dry densities of the tailings very near the loading location. This was generally not supported by the results of the frozen samples or Troxler measurements carried out at the Quick Test locations. The discrepancy may have been due to the differences in the proximity of the measurement locations to the location of load application and large local staining. Difficulties encountered with gathering frozen samples of sufficiently large size to produce representative samples of the tailings after softening at the main test site in the short amount of time available may also have accounted for some of the differences. CPT measurements gathered following softening did not indicate any significant decrease in tailings strength as a result of softening. This agreed with the interpretation of the tailings as being initially dense of steady state and subjected to cyclic liquefaction.

It was suggested that the increase in pore pressure could be attributed an initial contractive response of sands subjected to relatively small shear strains, particularly in the pre softening stage. It was proposed that if large shear strains developed then the dilative response of the tailings would begin to control the behaviour. Dilation at large strains could possibly be the cause of the large increases in dry density observed in the initial tests carried out by Syncrude and presented in Section 1.0 where significant local straining likely occurred.

Various factors were identified which appeared to affect the response of the tailings deposit. The main factors appeared to be the magnitude and duration of the vibrations, the elevation of the phreatic surface and the saturation or moisture content of the unsaturated zone. Increases in these factors increased the relative ease with which softening occurred, although the latter factor is likely more influential when the phreatic surface is shallow than when it is deep. It also appeared that if the moisture content in the unsaturated zone above the phreatic surface increased, the BAW tailings were more likely to soften, possibly because it allowed for quicker saturation and the development of increased pore pressures in the near surface soils. Although not evaluated quantitatively, it appeared that fines content increased the likelihood of softening whereas ageing appeared to decrease the likelihood of softening. Areas of low topography were generally most prone to softening because these areas typically had an increased fines content, a shallower phreatic surface and higher moisture content in the unsaturated zone, possibly due to the concentration of surface run-off.

Charts typically used in geotechnical practice to evaluate liquefaction susceptibility under earthquake loading were applied to the observed cyclic liquefaction response since this behaviour was considered liquefaction in the development of the charts. If an appropriate attenuation relationship was used to correlate the measured particle velocities to particle velocities at different locations, the predicted response from the charts correlated well with observed behaviour. The method of analysis was then extended to extrapolate the results of the field program to other conditions. A relationship between maximum vector resultant particle velocity recorded at the ground surface 0.55 m from the edge of an equipment track and the required depth to the phreatic surface to minimize softening was developed, since this is the distance from the tracks where all measurements were taken in this research. A tentative relationship between maximum vector resultant particle velocity and equipment mass was also developed. These two relationships were combined to produce another tentative relationship between equipment mass and required depth of the phreatic surface to minimize softening potential. As with most empirical relations, these relationships were

based on many assumptions. The relationship between equipment mass and particle velocity is very approximate and should be confirmed on a site and equipment specific basis prior to being used on an operational basis. The attenuation relationship for particle velocity with distance from the source should also be confirmed. Finally the relationships were based on BAW tailings with a representative $(N_1)_{60}$ value of 11, a shear modulus of 20 MPa, an average density of 1675 kg/m³ above the phreatic surface and the assumption that the Seed et al. (1985) relationship between penetration resistance and cyclic resistance ratio as modified by the NCEER (Youd and Idriss, 2001) correctly identifies the occurrence of large excess pore pressures. The calculated curves are likely very conservative and can be altered if the assumption of essentially infinite loading cycles is removed and if the concept of a limiting depth below which liquefaction of the tailings does not impact the surface is valid. Further work and testing could likely result in a significantly less conservative relationship. Also, the effect of a wetting front due to heavy rain or a significant zone of nearly saturated tailings above the phreatic surface was not included in the relationships.

Based on the findings presented in this report, it would appear that the options available to avoid causing softening of similar BAW tailings when subjected to equipment loading are fairly limited. The dynamic shear strains that lead to cyclic liquefaction could be reduced or the depth to the phreatic surface could be increased, such that the imposed cyclic stresses are reduced below critical levels within the zone of saturated tailings. Further densification of the deposits would likely be difficult to achieve as the deposit appeared to be at a reasonably dense state relative to any densification that could be obtained by equipment sufficiently light enough to travel the area. Furthermore, because the behaviour appeared to be caused by cyclic liquefaction, significant improvement of the behaviour in response to densification may be limited.

The amount of dewatering or the thickness of a working platform necessary for reclamation using conventional methods could be minimized by gathering site-specific data to optimize the relationships presented herein. Field tests in BAW tailings using different types of reclamation equipment to confirm or determine an appropriate particle attenuation relationship both along the surface and with depth from running equipment would be useful. The effect of equipment speed and natural frequency on maximum particle velocity and attenuation should also be investigated. Efforts to improve the tentative relationship between equipment mass, or simply equipment type, and maximum particle velocity would also be similarly useful. It would also be of interest to identify if there is a depth below which increased pore pressures do not affect the surface. Finally, measurements of the capillary zone, its saturation and potential for liquefaction would be useful for incorporating this aspect into a relationship between equipment mass and required depth to phreatic surface to prevent surficial softening.

If the mechanism causing the initial generation of pore pressures is to be better understood controlled laboratory testing would likely be required. Monotonic and cyclic testing at low confining stresses to explore the strain ranges of contractive and dilative behaviour may aid in identifying the mechanisms causing excess pore pressures. Comparison of drained and undrained cyclic testing of dense BAW tailings may also be useful in identifying the cause of the increased pore pressures. Model laboratory tests that simulate equipment loading may also be useful in understanding the mechanism causing softening. Void ratios could be measured at various points throughout loading and comparisons of drained versus undrained behaviour could possibly be valuable.

7.0 REFERENCES

- Alarcon-Guzaran, A., Leonards, G.A., and Charneau, J.L. 1988. Undrained Monotonic and Cyclic Strength of Sands. *Journal of Geotechnical Engineering, ASCE*, Vol.114, pp. 1089-1109.
- Ambraseys, N. N. 1988. Engineering Seismology. *Earthquake Engineering and Structural Dynamics*, 17, pp. 1-105.
- Andrus, R. D., and Stokoe, K.H. 2000. Liquefaction Resistance of Soils from Shear Wave Velocity. *Journal of Geotechnical and Geoenvironmental Engineering, ASCE*, Vol.126(No.11), pp. 1015-1025.
- Andrus, R. D., and Stokoe, K.H., II. 1997. Liquefaction Resistance Based on Shear Wave Velocity. NCEER Workshop on Evaluation of Liquefaction Resistance of Soils, National Center for Earthquake Engineering Research, Buffalo, Technical Report NCEER-97-0022, Youd, pp. 89-128.
- Andrus, R. D., Stokoe, K.H., and Roesset, J.M. 1991. Liquefaction of Gravelly Soil at Pence Ranch during the 1983 Borah Peak Earthquake. *Soil Dynamics and Earthquake Engineering*, Southampton, England, pp. 251-262.
- Arango, I. 1996. Magnitude Scaling Factors for Soil Liquefaction Evaluations. *Journal of Geotechnical Engineering, ASCE*, Vol.122(11), pp. 929-936.
- Arthur, J. R. F., Chua, K.S., Dunstan, T., and Rodriguez del C., J.I. 1980. Principal Stress Rotation: A Missing Parameter. *Journal of Geotechnical and Geoenvironmental Engineering, ASCE*, Vol. 106(GT4), pp. 419-433.
- ASTM. 1996 D5311-92(1996) Standard Test Method for Load Controlled Cyclic Triaxial Strength. *Book of Standards Volume 04.08*, p.
- ASTM. 2000. D422-63 Standard Test Method for Particle-Size Analysis of Soils. *Annual Book of ASTM Standards*, Vol. 04.08, pp.
- ASTM. 2000. D2216-98 Standard Test Method for Laboratory Determination of Water (Moisture) Content of Soil and Rock by Mass. *Annual Book of ASTM Standards Volume 04.08*, pp.
- Ayoubian, A., and Robertson, P.K. 1998. Void ratio redistribution in undrained triaxial extension tests on Ottawa sands. *Canadian Geotechnical Journal*, Vol.35, pp. 351-359.
- Been, K. 1999. The Critical State Line and Its Application to Soil Liquefaction. *International Symposium on the Physics and Mechanics of Soil Liquefaction*, Baltimore, Maryland, USA, Lade, pp. 195-203.
- Been, K., and Jeffries, G. 1985. A State Parameter for Sands. *Geotechnique*, Vol.35(No.2), pp. 99-112.

- Been, K., and Jeffries, M.G. 1992. Towards Systematic CPT Interpretation. Wroth Symposium, Oxford, U.K., pp. 44-55.
- Been, K., Crooks, J.H.A., and Jefferies, M.G. 1988. Interpretation of Material State from the CPT in Sands and Clays. ICE Conference on Penetration Testing in the UK, Birmingham, U.K., pp. 215-218.
- Been, K., Jefferies, M.G., and Hachey, J. 1991. The Critical State of Sands. *Geotechnique*, Vol.41(No. 3), pp. 365-381.
- Blunden, B. G., McLachlan, C.B., and Kirby, J.M. 1992. A Recording System for Measuring In-situ Soil Stresses Due to Traffic. *Soil and Tillage Research*, Vol. 25, pp. 35-42.
- Burland, J. B. 1990. On the compressibility and Shear Strength of Natural Clays. *Geotechnique*, Vol.40(No.3), pp. 329-378.
- Byrne, P. M., Puebla, H., Chan, D.H., Soroush, A., Morganstern, N.R., Cathro, D.C., Gu, W.H., Phillips, R., Robertson, P.K., Hofmann, B.A., Wride (Fear), C.E., Segoo, D.C., Plewes, H.D., List, B.R., and Tan, S. 2000. CANLEX full scale experiment and modelling. *Canadian Geotechnical Journal*, Vol.37, pp. 543-562.
- Canadian Geotechnical Society, Technical Comiteee on Foundations. 1992. *Canadian Foundation Engineering Manual*.
- Casagrande, A. 1940. Characteristics of Cohesionless Soils Affecting the Stability of Earth Fills. *Contributions to Soil Mechanics, 1925-1940*, Boston Society of Engineers, pp. 257-276.
- Casagrande, A. 1979. Liquefaction and Cyclic Deformation of Sands A Critical Review. *Harvard Soil Mechanic Series*, No. 88, pp. 1-50.
- Castro, G. 1975. Liquefaction and Cyclic Mobility of Sands During Cyclic Loading. *Journal of the Geotechnical Engineering Division, ASCE*, Vol.101(GT6), pp. 551-569.
- Castro, G., and Poulos, S.J. 1977. Factors affecting liquefaction and cyclic mobility. *Journal of the Geotechnical Engineering Division, ASCE*, Vol.103(No.GT6), pp. 501-516.
- Castro, G., Enos, J.L., France, J.W., and Poulos, S.J. 1982. Liquefaction Induced by cyclic loading. *NSF/CEE-82018*. 325
- Chua, K. H., Balendra, T., and Lo, K.W. 1992. Groundborne Vibrations Due to Trains in Tunnels. *Earthquake Engineering and Strutural Dynamics*, Vol. 21, pp. 445-469.
- National Research Council. 1985 *Liquefaction of soils during earthquakes*. p.
- Conetec Investigations Ltd. 2002 *Historical Data Reduction Review and Analysis of Mildred Lake Settling Basin and the SWSS Facility*. June 11, 2002, p.

- Conetec Investigations Ltd. 2000 Presentation of Cone Penetration Test Data, East Toe Berm, Mildred Lake. June 12, 2000, p.
- Coop, M. R., and Atkinson, J.H. 1993. The mechanics of cemented carbonate sands. *Geotechnique*, Vol.43(No.2), pp. 53-67.
- Davies, M. P., and Campanella, R.G. 1994. Selecting Design Values of Undrained Strength for Cohesionless Soils. 47th Canadian Geotechnical Conference, Halifax, Nova Scotia, 1, pp. 176-186.
- Davies, M. P., McRoberts, E.C., Martin, T. 2001. Static Liquefaction of Tailings - Fundamentals and Case Histories. Tailings Dams 2002, Association of State Dam Safety Officials, U.S. Society on Dams, April 29-May 1, Las Vegas, pp. 233-255.
- DeAlba, P., Seed, H.B., and Chan, C.K. 1976. Sand Liquefaction in Large-Scale Simple Shear Tests. *Journal of the Geotechnical Engineering Division, ASCE*, Vol. 102(GT9), pp. 909-927.
- Desrues, J., Chambon R., Mokni, M., and Mazerolle, F. 1996. Void ratio evolution inside shear bands in triaxial specimens studied by computed tomography. *Geotechnique*, Vol.46(No. 3), pp. 529-546.
- Dobry, R., and Ladd, R.S. 1980. Discussion - Soil Liquefaction and Cyclic Mobility Evaluation for Level Ground During Earthquakes and Liquefaction Potential: Science Versus Practice. *Journal of Geotechnical Engineering, ASCE*, Vol. 106(No. GT6), pp. 720-724.
- Dobry, R. a. S., W.F. 1979. Threshold Strain and Cyclic Behaviour of Cohesionless Soils. Austin Texas, pp. 521-525.
- Dowding, C. H. 1985. Blast Vibration Monitoring and Control, Englewood Cliffs, NJ : Prentice-Hall. 297 p.
- Fear, C. E., and McRoberts, E.C. 1995. Reconsideration of Initiation of Liquefaction in Sandy Soils. *Journal of Geotechnical Engineering, ASCE*, Vol.121(3), pp. 249-261.
- Fear, C. E., and Robertson, P.K. 1995. Estimating the Undrained Strength of Sands: a theoretical framework. *Canadian Geotechnical Journal*, Vol.32(No.4), pp.
- Finn, W. D. L., Ledbetter, R.H., and Wu, G. 1994. Liquefaction in Silty Soils: Design and Analysis. *Ground Failures Under Seismic Conditions: Proceedings of Sessions Sponsored by the Geotechnical Division of the American Society of Civil Engineers in Conjunction with the ASCE National Convention in Atlanta, Georgia, October 9-13, 1994, New York, ASCE*, pp. 51-76.
- Finn, W. D. L., Pickering, D.J., and Bransby, P.L. 1971. Sand Liquefaction in Triaxial and Simple Shear Tests. *Journal of the Soil Mechanics and Foundation Division, ASCE*, Vol. 97(No. SM4), pp. 639-659.

- Froese, C. R., Barlow, J.P. 2001. Geological Controls on Directionally Drilled Pipeline Installations in Northeastern Alberta. 2001 an Earth Odyssey, pp. 27-32.
- GEO-SLOPE International Ltd. 2002 SeepW Manual For Finite Element Seepage Analysis - Version 5.11. 455 p.
- Grozic, J. H. L., Robertson, P.K., and Morganstern, N.R. 2000. Cyclic Liquefaction of Loose Gassy Sand. Canadian Geotechnical Journal, Vol.37, pp. 843-856.
- Gutowski, T. G., and Dym, C.L. 1976. Propagation of Ground Vibration: A Review. Journal of Sound and Vibration, Vol. 49(2), pp. 179-193.
- Harder, L. R., Jr., and Seed, H.B. 1986. Determination of Penetration Resistance for Coarse-Grained Soils Using the Becker Hammer Drill. Report UCB/EERC-86/06.
- HBT AGRA Ltd. 1992 Syncrude Canada Ltd. In-Pit Perimeter Dyke System Laboratory Testson Tailings Sand, Report No. 10, Volume I. February, 1992, p.
- HBT AGRA Ltd. 1992 Syncrude Canada Limited In-Pit Perimeter Dyke System Update on Consideration of Sand State. Report No.11, December, 1992, 54 p.
- Head, K. H. 1992. Moisture Content and Index Tests. Manual of Soil Testing, Pentech Press, London, pp. 59-114.
- Howie, J. A., Shozen, T., and Vaid, Y.P. 2002. Effect of Ageing on Stiffness of Very Loose Sand. Canadian Geotechnical Journal, Vol.39, pp. 149-156.
- Hryciw, R. D., Vitton, S., and Thomann, T.G. 1990. Liquefaction and Flow Failure During Seismic Exploration. Journal of Geotechnical Engineering, ASCE, Vol.116(No. 12), pp. 1881-1899.
- Hunt, R. E. 1984. Geotechnical Engineering Investigation Manual, McGraw-Hill Book Company, New York. 983 p.
- Hynes, M. E., and Olson, R.S. 1999. Influence of Confining Stress on Liquefaction Resistance. International Workshop on Physics and Mechanics of Soil Liquefaction, Balkema, Rotterdam, The Netherlands, pp. 145-152.
- Idris, M. 1998. Evaluation of Liquefaction Potential, Consequences and Mitigation, An Update. Presentation to Vancouver Geotechnical Society, Vancouver, BC, pp.
- Ishihara, K. 1985. Stability of Natural Deposit During Earthquakes. Eleventh International Conferenceon Soil Mechanics and Foundation Engineering, San Fransisco, Volume 1, pp. 321-376.
- Ishihara, K. 1993. Liquefaction and Flow Failure During Earthquakes. Geotechnique, 43(No. 3), pp. 351-415.
- Ishihara, K., Sodekawa, M. and Tanaka, Y. 1978. Effects of Overconsolidatio on Liquefaction Characteristics of Sands Containing Fines. Dynamic Geotechnical

- Testing STP 654, Philadelphia: American Society for Testing and Material, pp. 246-264.
- Ishihara, K., Tatsuoka, F., Yasuda, S. 1975. Undrained Deformation and Liquefaction of Sand Under Cyclic Stresses. *Soils and Foundations*, Vol.15(No. 1), pp. 29-44.
- Jefferies, M. G. 1999. A Critical State View of Liquefaction. International Symposium on the Physics and Mechanics of Soil Liquefaction, Baltimore, Maryland, USA, Lade., pp. 221-235.
- Jefferies, M. G., and Davies, M.P. 1991. Soil Classification by the Cone Penetration Test: Discussion. *Canadian Geotechnical Journal*, Vol. 28, pp. 173-176.
- Jefferies, M. G., and Davies, M.P. 1993. Use of CPTu to Estimate Equivalent SPT N160. *Geotechnical Testing Journal*, December 1993, pp. 459-468.
- Jefferies, M. G., Been, K., and Hachey, J.E. 1990. Influence of Scale on the Constitutive Behaviour of Sands. 43rd Canadian Geotechnical Engineering Conference, Laval University, Quebec, Vol.1, pp. 263-273.
- Kayen, R. E., Mitchell, J.K., Seed, R.B., Lodge, A., Nishio, S., and Coutinho, R. 1992. Evaluation of SPT-, CPT-, and Shear Wave-Based Methods for Liquefaction Potential Assessments Using Loma Prieta Data. 4th Japan-US Workshop on Earthquake Resistant Design of Lifeline Facilities and Countermeasures for Soil Liquefaction, National Center for Earthquake Engineering Research, Buffalo, Vol.1, Hamada, pp. 177-204.
- Klohn-Crippen. 1998 Mildred Lake East Toe Berm, Final Design Report. January, 26, 1998, 13 p.
- Kim, D.-S., and Lee, J-S. 1998. Source and Attenuation Characteristics of Various Ground Vibrations. *Geotechnical Earthquake Engineering and Soil Dynamics III*, Proceedings of a Specialty Conference, Aug 3-6, 1998, University of Washington, Seattle, WA, 2, Dakoulas, pp. 1507-1517.
- Konrad, J.-M. 1993. Undrained Response of Loosely Compacted Sands During Monotonic and Cyclic Compression Tests. *Geotechnique*, Vol.43(No. 1), pp. 69-89.
- Konrad, J.-M., Pouliot, N., and Hofmann, B.A. 1995. Evaluation of the Performance of Laval's Large Diameter Sampler in Loose to Medium Dense Sands. pp.
- Kramer, S. L. 1996. *Geotechnical Earthquake Engineering*, Prentice Hall, New Jersey. 653 p.
- Kuberis, R. H., and Vaid, Y.P. 1988. Sand sample preparation - the slurry deposition method. *Soils and Foundations*, Vol.24(4), pp. 107-118.
- Kuberis, R. H., Negussy, D., and Vaid, Y.P. 1988. Effect of gradation and fines content on the undrained response of sands. Conference on Hydraulic Fill Structures, ASCF Geotechnical Special Publication 21, pp. 330-345.

- Kupper, A. 1991. Design of Hydraulic Fill, Ph.D, University of Alberta, Edmonton. 497
- List, B. R., and Lord, E.R.F. 1996. An Overview of Syncrude's Tailings Management Practices From Research to Implementation. CIM, pp.
- Lodge, A. L. 1994. Shear Wave Velocity Measurements for Subsurface Characterization, Ph.D. Dissertaion, University of California, Berkeley, California.
- Lord, E. R., and Cameron, R. 1985. Compaction Characteristics of Athabasca Tar Sand. 38th Canadian Geotechnical Conference, pp. 359-368.
- Lunne, T., Robertson, P.K., and Powell, J.J.M. 1997. Cone Penetration Testing In Geotechnical Engineering, E&FN Spon An Imprint of Routledge. 312 p.
- Lupini, J. F., Skinner, A.E., and Vaughan, P.R. 1981. The drained residual strength of cohesive soils. Geotechnique, Vol.31(No. 2), pp. 181-213.
- Marcuson, I., W.F., and Franklin, A.G. 1980. State of the Art of Undisturbed Sampling of Cohesionless Soils. Geotechnical Engineering, 11, pp. 31-53.
- Marcuson, W. F., III. 1978. Definition of Terms Related to Liquefaction. Journal of the Geotechnical Engineering Division, ASCE, Vol., 104(9), pp. 1197-1200.
- Martin, G. R., Finn, W.D.L., and Seed, H.B. 1975. Fundamentals of Liquefaction Under Cyclic Loading. Journal of the Geotechnical Engineering Division, ASCE, Vol. 101(GT5), pp. 423-438.
- McKenna, G. 2002. personal communication to Wood. Edmonton.
- McRoberts, E. C., and Sladen, J.A. 1990. Observations on Static and Cyclic Sand Liquefaction Methodologies. 43rd Canadian Geotechnical Conference, Prediction and Performance in Geotechnique, Quebec, Vol.1, pp. 215-226.
- McRoberts, E. C., and Sladen, J.A. 1992. Observation on static and cyclic sand liquefaction methodologies. Canadian Geotechnical Journal, Vol.29, pp. 650-665.
- Mitchell, J. K., and Tseng, D.-J. 1990. Assessment of Liquefaction Potential by Cone Penetration Testing. H. Bolton Seed Memorial Symposium, Berkeley, California, Vol.2, Duncan, pp. 335-350.
- Nova, R. a. H., T. 1981. A Unified Approach to the Modelling of Liquefaction and Cyclic Mobility of Sands. Soils and Foudations, Vol. 21(No. 4), pp. 13-28.
- Olson, S. M., and Stark, T.D. 2002. Liquefied Strength Ratio From Liquefaction Flow Failure Case Histories. Canadian Geotechnical Journal, 39, pp. 629-647.
- Optimum Instruments Ltd. 2002. Data Dolphin Users Manual.
- Pestana, J. M., and Whittle, A.J. 1995. Compression model for cohesionless soils. Geotechnique, Vol.45(4), pp. 611-631.

- Plewes, H. D., Davies, M.P., and Jeffries, M.G. 1992. CPT Based Screening Procedure for Evaluating Liquefaction Susceptibility. 45th Canadian Geotechnical Conference, Toronto, pp. 4-1 - 4-9.
- Poulos, S. J. 1981. The steady state of deformation. Journal of the Geotechnical Engineering Division, ASCE, Vol.107(No. GT5), pp. 553-562.
- Poulos, S. J., Castro, G., and France, J.W. 1985. Liquefaction Evaluation Procedure. Journal of Geotechnical Engineering, ASCE, Vol.111(No. 6), pp. 772-792.
- Poulos, S. J., Castro, G., France, J.W. 1988. Liquefaction evaluation procedure, Reply. Journal of the Geotechnical Engineering Division, ASCE, Vol.116, pp. 165-185.
- Raper, R. L., and Erbach, D.C. 1990. Prediction of Soil Stresses Using the Finite Element Method. Transactions of the ASAE, Vol.33(No. 3), pp. 725-730.
- Robertson, P. K. 1994. Suggested Terminology for Liquefaction. 47th Canadian Geotechnical Conference, pp. 277-286.
- Robertson, P. K. 2001. personal communication to Wood. Edmonton.
- Robertson, P. K., and Campanella, R.G. 1985. Liquefaction Potential of Sands Using the Cone Penetration Test. Journal of the Geotechnical Engineering Division of the ASCE, Vol.22(No. 3), pp. 298-307.
- Robertson, P. K., and Fear, C.E. 1995. Liquefaction of Sands and Its Evaluation. The First International Conference on Earthquake Geotechnical Engineering, Tokyo, Ishihara, pp.
- Robertson, P. K., and Wride (Fear), C.E. 1998. Evaluating cyclic liquefaction potential using the cone penetration test. Canadian Geotechnical Journal, Vol.35, pp. 444-459.
- Robertson, P. K., and Wride (Fear), C.E. 1998. Evaluating Cyclic Liquefaction Potential Using the CPT, University of Alberta Final Submission to the NCEER Workshop. Edmonton. 56
- Robertson, P. K., Woeller, D.J., and Finn, W.D.L. 1992. Seismic Cone Penetration Test for Evaluating Liquefaction Potential Under Cyclic Loading. Canadian Geotechnical Journal, 29, pp. 686-695.
- Robertson, P. K., Wride (Fear), C.E., List, B.R., Atukorala, U., Biggar, K.W., Byrne, P.M., Campanella, R.G., Cathro, D.C., Chan, D.H., Czajewski, K., Finn, W.D.L., Gu, W.H., Hammamji, Y., Hofmann, B.A., Howie, J.A., Hughes, J., Imrie, A.S., Konrad, J.-M., Kupper, A., Law, T., Lord, E.R.F., Monahan, P.A., Morganstern, N.R., Phillips, R., Piche, R., Plewes, H.D., Scott, D., Sego, D.C., Sobkowicz, J., Stewart, R.A., Watts, B.D., Woeller, D.J., Youd, T.L., Zavodni, Z. 2000. The CANLEX project summary and conclusions. Canadian Geotechnical Journal, 37, pp. 563-591.

- Roscoe K.H., S., A.N., and Wroth, C.P. 1958. On the yielding of soils. *Geotechnique*, 8(1), pp. 22-52.
- Roscoe, K. H., Schofield A.N., and Thurairajah R. 1963. An evaluation of test data for selecting a yield criterion for soils. *Laboratory Shear Testing of Soils*, American Society for Testing and Materials Special Publication 361, pp. 111-128.
- Schmid, I. C. 1995. Vehicle Interaction and Terrain Results from 10 Years of Research at IKK. *Journal of Terramechanics*, Vol.32(No. 1), pp. 3-26.
- Seed, H. B. 1979. Soil Liquefaction and Cyclic Mobility Evaluation for Level Ground During Earthquakes. *Journal of the Geotechnical Engineering Division, ASCE*, Vol.105(No. GT2), pp. 201-255.
- Seed, H. B. 1983. Earthquake Resistant Design of Earth Dams. *Seismic Design of Earth Dams and Caverns*, ASCE, New York, pp. 41-64.
- Seed, H. B. 1987. Design Problems in Soil Liquefaction. *Journal of the Geotechnical Engineering Division, ASCE*, Vol.113(No. 8), pp. 827-845.
- Seed, H. B., and De Alba, P. 1986. Use of SPT and CPT for Evaluating the Liquefaction Resistance of Sands. *Use of In-situ Tests in Geotechnical Engineering*, ASCE, Geotechnical Special Publication, Vol.6, pp. 281-302.
- Seed, H. B., and Idriss, I.M. 1971. Simplified Procedure for Evaluating Soil Liquefaction Potential. *Journal of the Soil Mechanics and Foundations Division, ASCE*, Vol.97(No. SM9), pp. 1249-1273.
- Seed, H. B., and Idriss, I.M. 1982. *Ground Motions and Soil Liquefaction During Earthquakes*, Earthquake Engineering Research Institute, Berkeley, California. 134 p.
- Seed, H. B., and Lee, K.L. 1966. Liquefaction of Saturated Sands During Cyclic Loading. *Journal Soil Mechanics and Foundation Division, ASCE*, Vol.92(No. SM6), pp. 105-134.
- Seed, H. B., and Lee, K.L. 1967. Undrained Strength Characteristics of Cohesionless Soils. *Journal of the Soil Mechanics and Foundations Division, ASCE*, Vol.93(No. SM6), pp. 333-359.
- Seed, H. B., and Peacock, W.H. 1971. Test Procedures for Measuring Soil Liquefaction Characteristics. *Journal of the Soil Mechanics and Foundations Division, ASCE*, Vol.97(No. SM8), pp. 1099-1119.
- Seed, H. B., Idriss, I.M., and Arango, I. 1983. Evaluation of Liquefaction Potential Using Field Performance Data. *Journal of the Geotechnical Engineering Division, ASCE*, Vol.109(3), pp. 458-482.
- Seed, H. B., Mori, K., Chan, C.K. 1975. Influence of Seismic History on the Liquefaction Characteristics of Sand. Report No. EERC 75.

- Seed, H. B., Pyke, R.M. and Martin, G.R. 1978. Effect of Multidirectional Shaking on Pore Pressure Development in Sands. Journal of the Geotechnical Engineering Division, ASCE, Vol.104(No. GT1), pp. 27-44.
- Seed, H. B., Singh, S., Chan, C.K., and Vilela, T.F. 1982. Considerations in Undisturbed Sampling of Sands. Journal of Geotechnical Engineering, ASCE, Vol.108(No. GT2), pp. 265-283.
- Seed, H. B., Tokimatsu, K., Harder, L.F., and Chung, R.M. 1984. The Influence of SPT Procedures in Soil Liquefaction Resistance Evaluations. UCB/EERC-84/15. 50
- Seed, H. B., Tokimatsu, K., Harder, L.F., and Chung, R.M. 1985. Influence of SPT Procedures in Soil Liquefaction Resistance Evaluations. Journal of Geotechnical Engineering, ASCE, Vol.111(No. 12), pp. 1425-1445.
- Seed, R. B., and Duncan, J.M. 1986. FE Analyses: Compaction-induced Stresses and Deformations. Journal of Geotechnical Engineering, ASCE, Vol.112(No. 1), pp. 23-43.
- Seed, R. B., and Harder, L.F. Jr. 1990. SPT based analysis of cyclic pore pressure generation and undrained residual strength. H. Bolton Seed Memorial Symposium, pp. 351-376.
- Shibata, T., and Teparaska, W. 1988. Evaluation of Liquefaction Potentials of Soils Using Cone Penetration Tests. Soils and Foundations, Vol.28(2), pp. 49-60.
- Sivathayalan, S., and Vaid, Y.P. 2002. Influence of Generalized Initial State and Principal Stress Rotation on the Undrained Response of Sands. Canadian Geotechnical Journal, Vol. 39, pp. 63-76.
- Sladen, J. A., and Hewitt, K.J. 1989. Influence of Placement Method on the In-situ Density of Hydraulic Sand Fills. Canadian Geotechnical Journal, Vol. 26, pp. 453-466.
- Sladen, J. A., D'Hollander, R.D., and Khran, J. 1985. The liquefaction of sands, a collapse surface approach. Canadian Geotechnical Journal, Vol.22, pp. 564-578.
- Sobkowicz, J. C., and Handford, G.T. np. The Application of State of the Art Liquefaction Concepts at Syncrude Canada Ltd., pp. 15.
- Society, J. G. 1998. Remedial Measures Against Soil Liquefaction, from Investigation and Design to Implementation, AA. Balkeman, Rotterdam. p.
- Stark, T. D., and Mesri, G. 1992. Undrained Shear Strength of Liquefied Sands for stability analysis. Journal of Geotechnical Engineering, ASCE, Vol.118(No. 11), pp. 1727-2747.
- Stark, T. D., and Olson, S.M. 1995. Liquefaction resistance using CPT and case histories. Journal of Geotechnical Engineering, Vol.121(12), pp. 856-869.

- Stewart, R. A., Kilpatrick, B.L., and Cattanach, J.D. 1990. The Use of Becker Penetration Testing for Liquefaction Assessment of Coarse Granular Overburden. 43rd Canadian Geotechnical Conference, Prediction and Performance in Geotechnique, Quebec, Quebec, Vol.1, pp. 275-283.
- Suzuki, Y., Tokimatsu, K., Koyamada, K., Taya, Y., and Kubota, Y. 1995. Field Correlation of Soil Liquefaction Based on CPT. International Symposium on Cone Penetration Testing, CPT'95, Linkoping, Sweden, 2, pp. 583-588.
- Sy, A. 1997. Twentieth Canadian Geotechnical Colloquium: Recent Developments in the Becker Penetration Test 1986-1996. Canadian Geotechnical Journal, Vol.34, pp. 952-973.
- Sy, A., and Campanella, R.G. 1993. Dynamic Performance of the Becker Hammer Drill and Penetration Test. Canadian Geotechnical Journal, Vol. 30, pp. 607-610.
- Sy, A., and Campanella, R.G. 1994. Becker and Standard Penetration Tests (BPT-SPT) Correlations with Consideration of Casing Friction. Canadian Geotechnical Journal, Vol.31(3), pp. 343-356.
- Syncrude Canada Ltd. 2002 Southwest Sand Storage Facility 2001 Trafficability Site Characterization Program. April 2002, 11 p.
- Syncrude Canada Ltd. 2003 Syncrude Canada Ltd. Southwest Storage Facility 2002 Performance Report. February 29, 2003, 43 p.
- Tatsuoka, F., Ochi, K., Fujii, S. and Okkamoto, M. 1986. Cyclic Undrained Triaxial and Torsional Shear Strength of Sands for Different Sample Preparation Methods. Soils and Foundations, Vol.26(3), pp. 23-41.
- Terzaghi, K., Peck, R.B. and Mesri, G. 1996. Soil Mechanics in Engineering Practice, 3rd edition, 3rd, John Wiley and Sons Inc. 549 p.
- Thurairajah, R. 1961. Some Shear Properties of Kaolin and of Sand, Ph.D., Univerisity of Cambridge, Cambridge, U.K.
- Tokimatsu, K., and Hosaka, Y. 1986. Effects of Sample Disturbance on Dynamic Properties of Sand. Soils and Foudations, Vol.26(No. 1), pp. 53-64.
- Tokimatsu, K., and Uchida, A. 1990. Correlation Between Liquefaction Resistance and Shear Wave Velocity. Soils and Foudations, Vol. 30(2), pp. 33-42.
- Tokimatsu, K., and Yoshimi, Y. 1984. Criteria of Soil Liquefaction with SPT and Fines Content. 8th World Conference on Earthquake Engineering, San Fransisco, California, Vol.3, pp. 255-262.
- Troxler Electronic Laboratories. 2002. Manual of Operation and Instruction Model 3430 (and Model 3430-M) Surface Moisture-Density Gauge.
- Vaid, Y. P. 1994. Liquefaction of Silty Soils. Ground Failures Under Seismic Conditions: Proceedings of Sessions Sponsored by the Geotechnical Division of the

American Society of Civil Engineers in Conjunction with the ASCE National Convention in Atlanta, Georgia, October 9-13, 1994, pp. 1-16.

- Vaid, Y. P., and Chern, J.C. 1985. Cyclic and Monotonic Undrained Response of Saturated Sands. *Advances in the Art of Testing Soils Under Cyclic Conditions*, Khosla, pp. 120-147.
- Vaid, Y. P., and Finn, W.D.L. 1979. Static Shear and Liquefaction Potential. *Journal of the Geotechnical Engineering Division, ASCE*, Vol.105(GT10), pp. 1233-1246.
- Vaid, Y. P., and Sivathayalan, S. 2000. Fundamental Factors Affecting Liquefaction Susceptibility of Sands. *Canadian Geotechnical Journal*, Vol.37, pp. 592-606.
- Vaid, Y. P., Sayao, A., Hou, E., and Negussey, D. 1990. Generalized Stress-Path-Dependent Soil Behaviour With a New Hollow Cylinder Apparatus. *Canadian Geotechnical Journal*, Vol.27, pp. 601-616.
- Vaid, Y. P., Stedman, J.D., and Sivathayalan, S. 2001. Confining Stress and Static Shear Effects in Cyclic Liquefaction. *Canadian Geotechnical Journal*, Vol.38, pp. 580-591.
- Valera, J. E., Michael, M., Traubenik, L., Egan, J.A., and Kaneshiro, J.Y. 1994. A Practical Perspective on Liquefaction of Gravels. *Ground Failures Under Seismic Conditions: Proceedings of Sessions Sponsored by the Geotechnical Division of the American Society of Civil Engineers in Conjunction with the ASCE National Convention in Atlanta, Georgia, October 9-13, 1994*, pp. 241-256.
- Vreugdenhil, R., Davis, R., and Berrill, J. 1994. Interpretation of Cone Penetration Results in Multilayered Soils. *International Journal for Numerical Methods in Geomechanics*, Vol.18, pp. 585-599.
- Whitman, R. V. 1971. Resistance of Soil to Liquefaction and Settlement. *Soils and Foundations*, Vol. 11(No. 4), pp. 59-68.
- Woods, R. D. 1968. Screening of Surface Waves in Soil. *Journal of the Soil Mechanics and Foundations Division, ASCE*, Vol.94(No. SM4), pp. 951-979.
- Woods, R. D., and Jedele, L.P. 1985. Energy-Attenuation Relationships from Construction Vibrations. *Vibration Problems in Geotechnical Engineering*, Detroit, Michigan, October 22, *Gazetas*, pp. 229-247.
- Wride (Fear), C. E., Robertson, P.K., Biggar, K.W., Campanella, R.G., Hofmann, B.A., Hughes, J.M.O., Kupper, A., and Woeller, D.J. 2000. Interpretation of in situ test results from the CANLEX sites. *Canadian Geotechnical Journal*, 37, pp. 505-529.
- Yoshimi, Y., Hatanaka, M., Oh-Oka, H. 1977. A Simple Method for Undisturbed Sand Sampling. *IXth International Conference on Soil Mechanics and Foundation Engineering, Soil Sampling Specialty Session 2, Tokyo*, 1, pp. 23-28.
- Yoshimi, Y., Tokimatsu, K and Ohara, J. 1994. In situ liquefaction resistance of clean sands over a wide density range. *Geotechnique*, Vol.44(No. 3), pp. 479-494.

- Yoshimine, M., Robertson, P.K., and Wride (Fear) C.E. 1999. Undrained shear strength of clean sands to trigger flow liquefaction. *Canadian Geotechnical Journal*, Vol.36, pp. 891-906.
- Youd, T. L., and Garris, C.T. 1995. Liquefaction-Induced Ground-Surface Disruption. *Journal of Geotechnical Engineering, ASCE*, Vol. 121(No. 11), pp. 805-809.
- Youd, T. L., and Idriss, I.M. 1997. Proceedings of the NCEER Workshop on Evaluation of Liquefaction Resistance of Soils. Technical Report NCEER-97-0022. 40
- Youd, T. L., and Idriss, I.M. 2001. Liquefaction Resistance of Soils: Summary Report from the 1996 NCEER and 1998 NCEER/NSF Workshops on Evaluation of Liquefaction Resistance of Soils. *Journal of Geotechnical and Geoenvironmental Engineering, ASCE*, Vol.127(4), pp. 297-313.
- Youd, T. L., and Noble, S.K. 1997. Liquefaction Criteria Based on Statistical and Probabilistic Analyses. NCEER Workshop on Evaluation of Liquefaction Resistance of Soils, National Centre for Earthquake Engineering Research, State University of New York at Buffalo, pp. 201-215.
- Zhou, S. G. 1980. Evaluation of the Liquefaction of Sands by Static Cone Penetration Test. Proceedings of the 7th World Conference on Earthquake Engineering, Istanbul, Turkey, Vol. 3, pp. 156-162.

APPENDIX A

**Summary of Field Program Data – Nuclear Gauge Measurements, Piezometer
Readings and Calibration**

PIEZOMETER INSTALLATION DETAILS

Piezometer Serial Number	Row	Distance from Edge of Load (cm)	Burial Depth (cm)
33	1	15	51.8
32	1	23	89.3
31	1	25	180.2
36	2	99	43.2
38	2	107	92.5
29	2	105	178.3
37	3	183	43
39	3	185	105.9
34	3	185	168
35	3	191	214.2
30	1-atm		0
28	2-atm		0

SUMMARY OF PIEZOMETER READINGS FROM PREDATOR LOADING IN TEST AREA

Piezometer Serial Number	Equilibrium Pore Pressure (kPa)	Depth to Phreatic Surface (if Hydrostatic) (m)	Hydraulic Gradient	Total Overburden Pressure (kPa) ¹	Effective Overburden Pressure (kPa) ¹	Peak Pore Pressure During Pred Loading (kPa)	Time at Peak	Peak Pore Pressure Change	
								(kPa)	(% of effective overburden)
33	2.1	0.30		9.66	7.56	3.04	11:35:54 AM	0.94	12.5
32	5.8	0.31	0.00	16.64	10.89	6.70	11:20:59 AM	0.94	8.6
31	14.5	0.33	-0.02	33.59	19.11	15.22	11:00:09 AM	0.74	3.9
36	2.81	0.15		8.05	5.24	3.36	11:45:38 AM	0.55	10.5
38	6.9	0.22	-0.15	17.24	10.32	7.38	11:41:23 AM	0.45	4.4
29	15.7	0.18	0.05	33.23	17.49	16.20	11:41:23 AM	0.45	2.6
37	2.51	0.17		8.01	5.51	2.92	11:37:15 AM	0.41	7.5
39	8.1	0.23	-0.09	19.74	11.64	8.50	11:46:30 AM	0.40	3.5

Piezometer Serial Number	Equilibrium Pore Pressure (kPa)	Depth to Phreatic Surface (if Hydrostatic) (m)	Hydraulic Gradient	Total Overburden Pressure (kPa) ¹	Effective Overburden Pressure (kPa) ¹	Peak Pore Pressure During Loading (kPa)	Time at Peak	Peak Pore Pressure Change	
								(kPa)	(% of effective overburden)
34	13.4	0.32	-0.13	31.31	17.94	13.79	11:47:35 AM	0.42	2.3
35	19.2	0.19	0.28	39.92	20.76	19.37	11:40:55 AM	0.21	1.0
30	-8.17	atm							
28	-1.54	atm							

¹ Based on wet density of 1900kg/m³, avg from Troxler measurements

SUMMARY OF PIEZOMETER READINGS FROM DOZER LOADING IN TEST AREA

Piezometer Serial Number	Equilibrium Pore Pressure (kPa)	Depth to Phreatic Surface (if Hydrostatic) (m)	Hydraulic Gradient	Total Overburden Pressure (kPa) ¹	Effective Overburden Pressure (kPa) ¹	Peak Pore Pressure During Loading (kPa)	Time at Peak	Peak Pore Pressure Change	
								(kPa)	(% of effective overburden)
33	1.9	0.32		9.66	7.71	11.87	9:05:46 AM	9.93	128.7
32	5.7	0.31	0.01	16.64	10.97	16.79	9:06:01 AM	11.12	101.3
31	14.3	0.34	-0.03	33.59	19.24	33.15	9:06:26 AM	18.80	97.7
36	1.90	0.24		8.05	6.15	9.02	9:06:00 AM	7.12	115.8
38	5.9	0.32	-0.17	17.24	11.33	18.39	9:06:05 AM	12.48	110.2
29	15.0	0.26	0.08	33.23	18.25	33.93	9:06:25 AM	18.95	103.8
37	2.28	0.20		8.01	5.73	8.58	9:05:58 AM	6.30	109.9
39	8.0	0.25	-0.08	19.74	11.77	17.97	9:05:58 AM	10.00	85.0
34	13.3	0.33	-0.13	31.31	18.03	24.94	9:06:08 AM	11.66	64.7
35	19.0	0.21	0.25	39.92	20.96	26.18	9:06:28 AM	7.22	34.5
30	-8.83	atm							
28	-1.41	atm							

¹ Based on wet density of 1900kg/m³, avg from Troxler measurements

SUMMARIES OF TEST PIT AND NUCLEAR GAUGE MEASUREMENTS AT ALL TEST SITES AND DURING TRAFFICABILITY STUDY

Summary of beach profiles test pit results, nuclear gauge readings and calculations

Location	Mine Metric		Date	Troxler ^{1,2}			Depth to Phreatic surface (m) ³	Depth of "Wet Zone" Above Phreatic Surface (m)	Calc From Troxler ⁴		Distance from Crest (m)
	Northing	Easting		Dry Density (kg/m ³)	% Standard Proctor	Wet Density (kg/m ³)			Moisture Content (%)	Void Ratio	
QT1 before	47911.5	42772.0	26-Sep-02	1464	82	1841	25.8		0.82	83.93	283
QT3 before	47945.4	42784.4	26-Sep-02	1614	91	1954	21		0.65	86.31	272
QT2 before	47949.3	42788.7	26-Sep-02	1529	86	1919	25.5		0.74	91.71	268
Site 1 - before	47909.0	42794.2	24-Sep-02	1708	96	1926	12.8		0.56	61.03	261
Site 1 - before	47894.6	42813.9	24-Sep-02	1697	95	1877	10.6		0.57	49.70	242
Site 1 - before	47894.2	42811.7	24-Sep-02	1690	95	1861	10.1		0.57	46.83	244
Just N. of site 1	47894.2	42811.7	25-Sep-02					0.35			244
Just N. of site 1	47896.9	42840.7	25-Sep-02					0.34		0.16	215
Beach profile	47901.6	42839.0	24-Sep-02	1721	97	1856	7.8		0.54	38.07	216
Beach profile	47899.1	42864.4	25-Sep-02					0.42			191
Beach profile	47900.7	42862.8	24-Sep-02	1686	95	1791	6.2		0.58	28.57	193
Beach profile	47901.1	42889.0	24-Sep-02	1634	92	1676	2.6		0.63	11.01	166
Beach profile	47896.1	42891.7	25-Sep-02					0.61			164
Beach profile	47898.5	42921.7	25-Sep-02					0.59			134
break in slope	47902.6	42921.9	24-Sep-02	1591	89	1644	3.3		0.67	13.07	134
Beach profile	47899.7	42931.5	25-Sep-02					0.90			124
Beach profile	47905.7	42942.7	24-Sep-02	1652	93	1718	4		0.61	17.44	113
Beach profile	47899.1	42943.8	25-Sep-02					>1m			112
Top of hill	47903.2	42968.1	25-Sep-02					>1m			88
Beach profile	47907.3	42968.3	24-Sep-02	1670	94	1739	4.1		0.59	18.41	87
Beach profile	47910.9	42997.6	24-Sep-02	1629	92	1718	5.5		0.63	23.10	57
Beach profile	47916.6	43054.8	24-Sep-02	1657	93	1765	6.5		0.61	28.58	0

NOTES:

1. All measurements taken with Troxler Model No. 30512, S/N 30512, supplied and operated by Terracon on Sept 26, 2002.
Standard Counts: MS: 705, MS: 2837
2. Maximum dry densi 1780 kg/m³, from Terracon testing
3. Phreatic surface measured in hand dug test pits
4. Calculated from:
$$P_{bulk} = \frac{Gs(1+w)}{1+e} \rho_w \quad Sr = \frac{wG_s}{e} \quad \text{Assuming } Gs = 2.66 \quad \rho_w = 1000 \text{ kg/m}^3$$

Summary of Nuclear Gauge Tests Carried out During Cyclic Loading

Location	Mine Metric		Date	Loading	# of cycles	Troloxer ^{1,2}				Calc From Troloxer ⁴		quadrant
	Northing	Easting				Dry Density (kg/m ³)	% standard proctor	Wet Density (kg/m ³)	Moisture (%)	Void Ratio	Saturation (%)	
Site 1	47894.6	42813.9	24-Sep-02	none	0	1697	95.3	1877	10.6	0.57	50	SE
Site 1	47909.0	42794.2	24-Sep-02	none	0	1708	96.0	1926	12.8	0.56	61	SE
Site 1	47894.2	42811.7	24-Sep-02	none	0	1690	94.9	1861	10.1	0.57	47	SW
Site 1	47894.2	42811.7	24-Sep-02	predator	10	1632	91.7	1912	17.2	0.63	73	SW
Site 1	47894.2	42811.7	24-Sep-02	predator	42	1600	89.9	1783	11.5	0.66	46	SE
Site 1	47894.2	42811.7	24-Sep-02	predator	10	1688	94.8	1883	11.5	0.58	53	N
Site 1	47894.2	42811.7	24-Sep-02	predator	42	1665	93.5	1891	13.5	0.60	60	N
Site 1	47894.2	42811.7	24-Sep-02	predator	70	1668	93.7	1935	16	0.59	72	centre
Site 1	47903.8	42814.6	24-Sep-02	predator	150	1671	93.9	1884	12.7	0.59	57	N-NW
Site 1	47903.4	42809.2	24-Sep-02	predator	150	1664	93.5	1905	14.5	0.60	64	N-NW
Site 1 after	47896.3	42808.7	26-Sep-02	loader	158	1548	87.0	1939	25.3	0.72	94	centre
Site 1 after	47895.7	42806.9	26-Sep-02	loader	158	1568	88.1	1943	23.9	0.70	91	S-centre
QT1 before	47911.5	42772.0	26-Sep-02			1464	82.2	1841	25.8	0.82	84	
QT1 after	47911.5	42772.0	26-Sep-02			1484	83.4	1885	27	0.79	91	
QT2 before	47949.3	42788.7	26-Sep-02			1529	85.9	1919	25.5	0.74	92	
QT2 after	47949.3	42788.7	26-Sep-02			1515	85.1	1926	27.2	0.76	96	
QT3 before	47945.4	42784.4	26-Sep-02			1614	90.7	1954	21	0.65	86	
QT3 during	47945.4	42784.4	26-Sep-02			1564	87.9	1914	22.4	0.70	85	
QT3 during	47945.4	42784.4	26-Sep-02			1586	89.1	1918	20.9	0.68	82	

Summary of trafficability test pit results, nuclear gauge readings and calculations

Location	Mine Metric		Date	Troxler ^{1,2}			Depth to Phreatic surface (m) ³	Depth of "Wet Zone" Above Phreatic Surface (m)	Calc From Troxler ⁴	
	Northing	Easting		Density (kg/m ³)	standard proctor	Density (kg/m ³)			Moisture (%)	Void Ratio
Mark 15, limit of loader	47696.5	42612.5	26-Sep-02	1518	85.2809	1938	0.230	0.000	0.74	97
Mark 20ish, 2nd pass loader	47657.6	42730.4	26-Sep-02	1660	93.2584	1891	0.380	0.180	0.60	61
Mark 24, 3rd pass loader	47748.7	42740.3	26-Sep-02	1695	95.2247	1856	0.385	0.130	0.57	44
location, ~ limit of hoe	47882.7	42794.6	26-Sep-02	1576	88.5393	1867	0.560	0.180	0.69	71

NOTES:

1. All measurements taken with Troxler Model No. 30512, S/N 30512, supplied and operated by Terracon on Sept 26, 2002.
Standard Counts: MS: 705, MS: 2837
2. Maximum dry densi 1780 kg/m³, from Terracon testing
3. Phreatic surface measured in hand dug test pits
4. Calculated from: $G_s(1+w) \rho_w \quad Sr = \frac{wG_s}{e}$

$$\rho_{bulk} = \frac{1+e}{1+w} \rho_w \quad Sr = \frac{wG_s}{e}$$

Assuming Gs= 2.66
 $\rho_w = 1000 \text{ kg/m}^3$

SAMPLE SUMMARY, COLLECTED FROM SYNCRUDE'S SOUTH WEST SAND STORAGE FACILITY IN CELL 31

Sample Number	Location			Depth	Date	Comments
	Description	Northing	Easting			
SA1	Main Test Site (Site 1) SE corner of loaded area	47894.62	42813.89	0 - 30cm	24-Sep-02	Before softening, at troxler 1 location
SA2	Main Test Site (Site 1) South edge of loaded area			0 - 20cm	24-Sep-02	Before softening, density measurement, tube A, full
SA3	South of main (Site 1) test area			0 - ~25cm	24-Sep-02	After softening in this area
SA4	South of main (Site 1) test area			40cm	24-Sep-02	After liquefaction in this area
SA5	~9.5m West of Main Test area			0 - 25cm	24-Sep-02	Area that wouldn't liquefy, sample from above water table
SA6	~11m West of Main Test Area			0 - 25cm	24-Sep-02	Area that would just liquefy, sample from above water table
SA7	~12.5m West of Main Test Area			0 - 24cm	24-Sep-02	Area that would liquefy, sample from above water table
SA8	~2-3m North of Main Test Area			16cm	25-Sep-02	Above water table, before loading
SA9	~2-3m North of Main Test Area			0 - 8cm	25-Sep-02	Above water table, before loading
SA10	SW of Site 1 test pit w/ backhoe	47882.71	42794.59	~1 - 1.5m	25-Sep-02	Large test pit with backhoe, unloaded area
SA10B	SW of Site 1 test pit w/ backhoe	47882.71	42794.59	~1.5-2.5m	25-Sep-02	Large test pit with backhoe, unloaded area
FR1B-tube	~7m Southeast of test area Main Test Area			0 - 27cm	25-Sep-02	Unloaded area, note sample split into two on site, samples frozen for 5.5hrs
FR1B-block	~7m Southeast of test area Main Test Area			0 - 13cm	25-Sep-02	Unloaded area, freezing for 5.5 hrs
FR1A-tube	Site 1 edge of loaded area, near instrumentation			0 - 20cm	25-Sep-02	Loaded area after softening, freezing for 5.5 hrs
FR1A-block	Site 1 center of loaded area between tracks			0 - 10cm	25-Sep-02	Loaded area after softening, freezing for 5.5 hrs
SA11 M26	Trafficability, furthest excavator location	47797.2	42721.56	0 - 56cm	25-Sep-02	Furthest excavator point

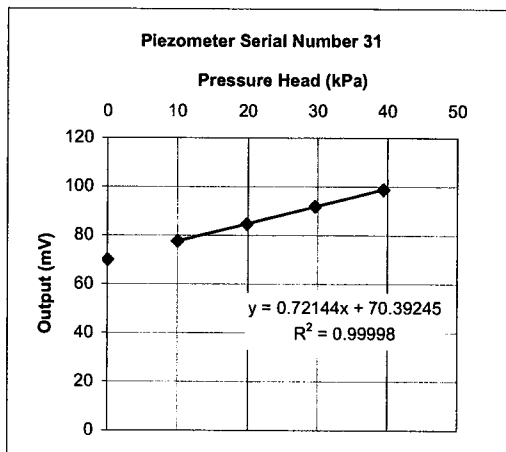
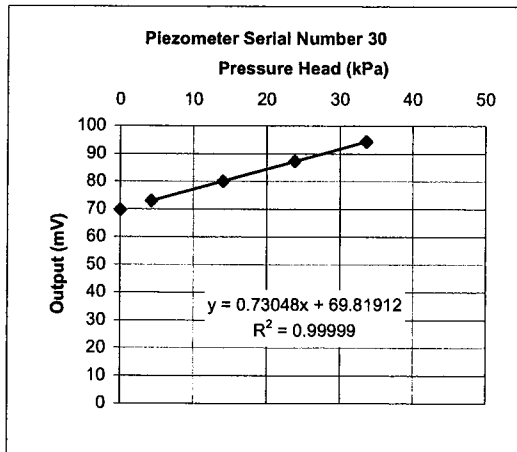
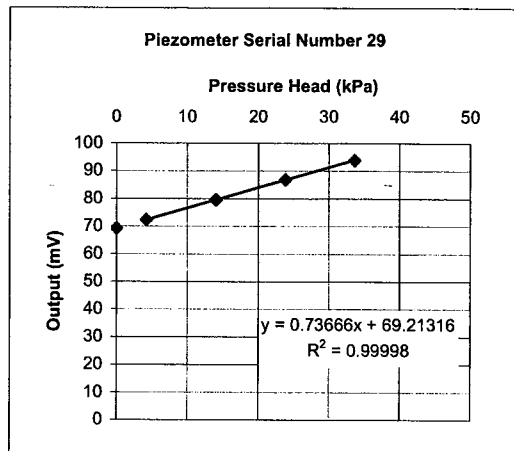
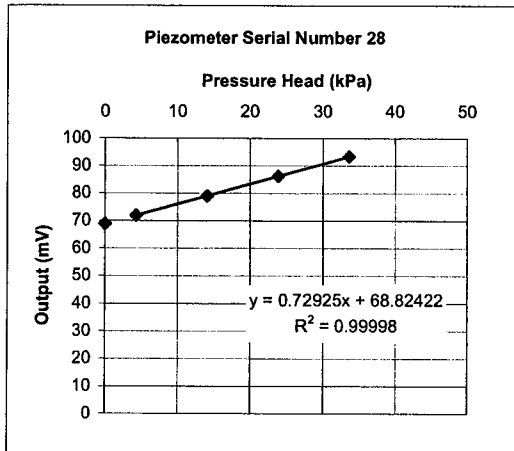
Sample Number	Location				Date	Comments
	Description	Mine Metric		Depth		
		Northing	Easting			
SA12 M15	Trafficability, furthest dozer location	47692.58	42608.22	0 - 23 cm	25-Sep-02	Furthest dozer point (1 pass)
SA13 M20	Trafficability, end of dozer 2nd pass	47735.07	42705.82	20-38cm	25-Sep-02	Second dozer pass
SA14 M20	Trafficability, end of dozer 2nd pass	47735.07	42705.82	5-10cm	25-Sep-02	Second dozer pass
SA15 M24	Trafficability, end of dozer 3rd pass	47743.61	42729.33	5-10cm	25-Sep-02	Third dozer pass
SA16 M24	Trafficability, end of dozer 3rd pass	47743.61	42729.33	20cm	25-Sep-02	Third dozer pass
SA17 M24	Trafficability, end of dozer 3rd pass	47743.61	42729.33	33cm	25-Sep-02	Third dozer pass
SA 20	Near QT2 before loading	47949.33	42788.69	0 - 20 cm	26-Sep-02	From inside freezing tube, before loading
SA 21	After softening site 1 at Troxler location 1	47911.54	42771.98	5 - 25 cm	26-Sep-02	From site 1 loaded area, between tracks, in line with instruments
SA 22	After softening site 1 at Troxler location 2	47895.7	42806.9	5 - 25cm	26-Sep-02	From site 1 loaded area, between tracks, 2m West of instruments
SA 23	QT2 after softening	47949.33	42788.69	0 - 15cm	26-Sep-02	After loading, couldn't get very deep because of sluffing
SA 26	QT3 after softening	47969.02	42803.03	0 - 20cm	26-Sep-02	From inside freezing tube, after loading (by foot), tube pushed to 3cm above surface
SA 27	Near QT3 to represent initial conditions	47964.81	42799.66	0 - 20cm	26-Sep-02	From inside freezing tube, undisturbed area, similar to loaded area (by foot), tube pushed
FRQT-B	Near QT3 to represent initial conditions	47964.81	42799.66	0 - 20cm	26-Sep-02	Radial freezing undisturbed area, freezing for about 2 hrs
FRQT-A	QT3 after softening	47969.02	42803.03	0 - 20cm	26-Sep-02	Radial freezing loaded area, freezing for about 2 hrs
Bucket 1, B1	Site 1, instrument area			1m	26-Sep-02	From instrumentation area, back row
Bucket 2, B2	Site 1, instrument area			2m	26-Sep-02	From instrumentation area, test pit by backhoe
Bucket 3, B3	Site 1, loaded area			15-65cm	26-Sep-02	From loaded area, samples gathered from many small, hand dug test pits

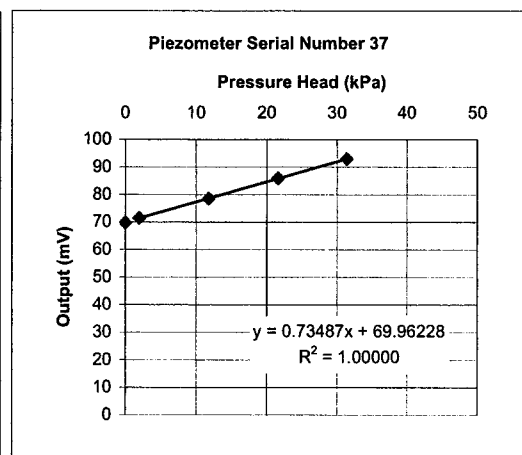
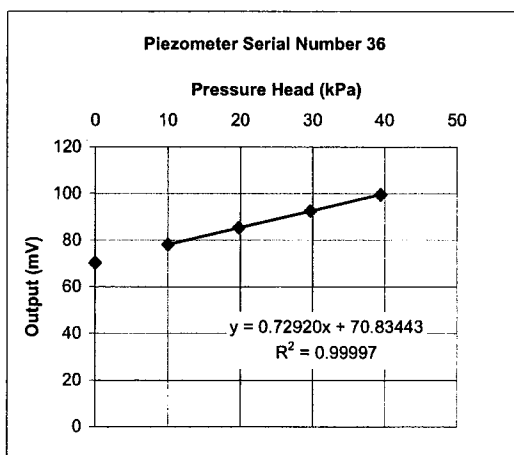
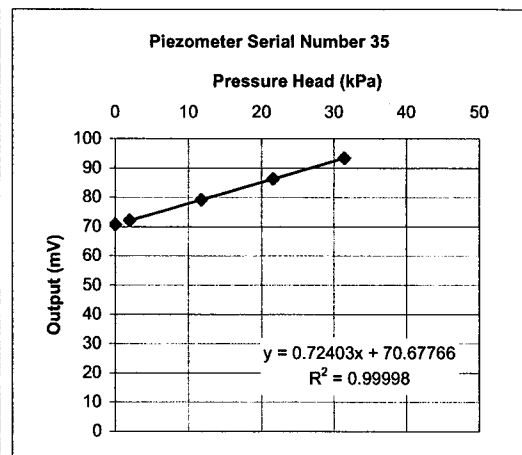
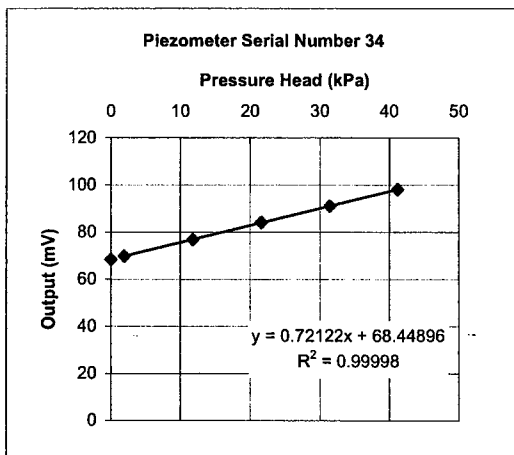
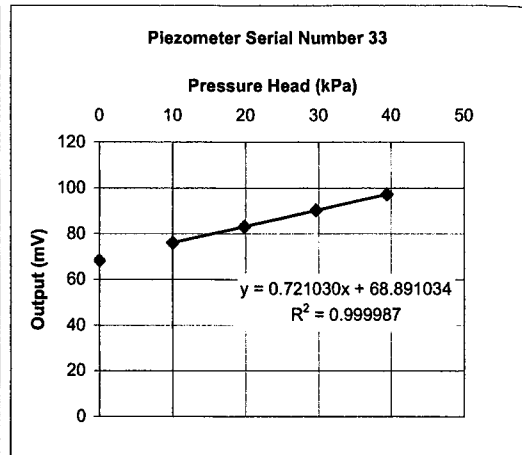
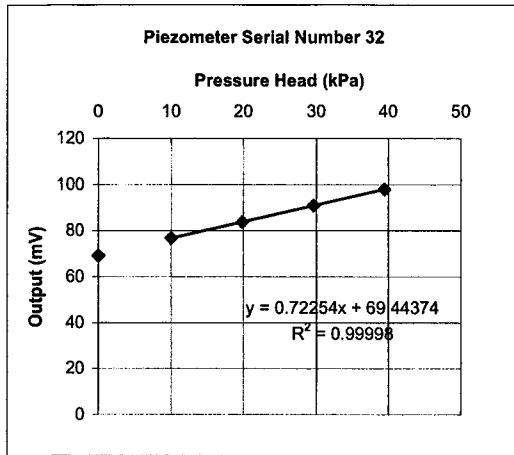
PIEZOMETER CALIBRATION

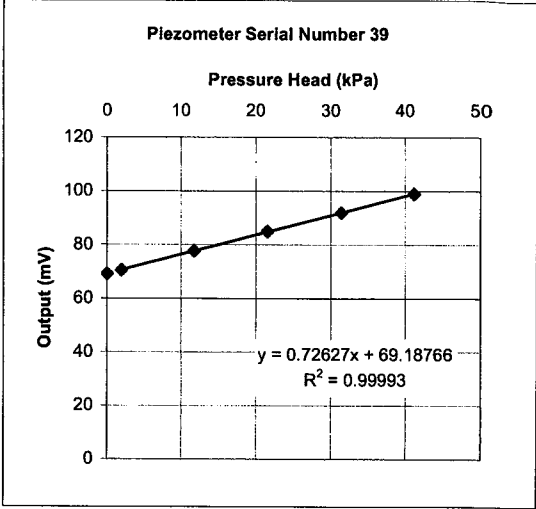
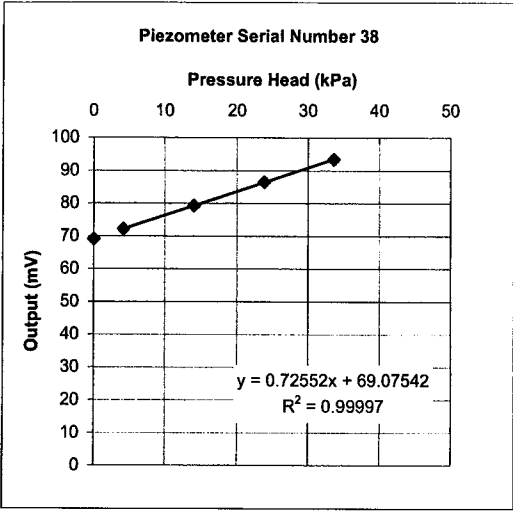
Carried out September 20, 2001 in well installed in Detcon's Shop at Syncrude Site
 Weather was overcast and cold (~8 degrees)

Piezo SN	0 Reading	Calibration	
		(mV/kPa)	(mV/cm head)
33	68.392	0.721	0.071
32	69.048	0.723	0.071
31	69.985	0.721	0.071
36	70.292	0.729	0.072
30	69.766	0.730	0.072
38	69.113	0.726	0.071
29	69.276	0.737	0.072
28	68.921	0.729	0.072
39	69.093	0.726	0.071
34	68.413	0.721	0.071
37	69.820	0.735	0.072
35	70.733	0.724	0.071

PIEZOMETER CALIBRATION CURVES







APPENDIX B

Laboratory Samples, Calculations and Results

SUMMARY OF SAMPLES TESTED

Sample ID	Description	Depth	Tests Carried Out		
			Moisture Content	Void Ratio & Density	Grain Size
SA1	Main Test Site SE corner of loaded area, before loading	0 - 30cm	Y		Y
SA2	Disturbed density sample, Main TestSite South edge of loaded area, near instruments, before softening	0 - 20cm	Y	Y	Y
SA3	South of Main Test Area, After softening in this area	0 - ~25cm	Y		Y
SA4	South of Main Test Area, After softening in this area	40cm	Y		Y
SA5	~9.5m West of Main Test area that wouldn't soften, above phreatic surface	0 - 25cm	Y		Y
SA6	~11m West of Main Test Area that would just soften, above phreatic surface	0 - 25cm	Y		
SA7	~12.5m West of Main Test Area that would soften, above phreatic surface	0 - 24cm	Y		
SA8	~2-3m North of Main Test Area, above phreatic surface before loading	16cm	Y		
SA9	~2-3m North of Main Test Area above phreatic surface before loading	0 - 8cm	Y		
SA11	Trafficability, furthest excavator location	0 - 56cm	Y		
SA12	Trafficability, furthest dozer location	0 - 23 cm	Y		
SA13	Trafficability, end of dozer 2nd pass	20-38cm	Y		
SA14	Trafficability, end of dozer 2nd pass	5-10cm	Y		
SA15	Trafficability, end of dozer 3rd pass	5-10cm	Y		
SA16	Trafficability, end of dozer 3rd pass	20cm	Y		
SA17	Trafficability, end of dozer 3rd pass	33cm	Y		
SA21	After softening site 1 at Troxler location 1, in between tracks, in line with instruments	5 - 25 cm	Y		Y
SA22	After softening site 1 at Troxler location 2, in between tracks, west of instruments	5 - 25cm	Y		Y
SA26	From inside freezing tube, after loading (by foot), tube pushed to 3cm above surface	0 - 20cm	Y		Y
SA27	From inside freezing tube, undisturbed area, similar to loaded area (by foot), tube pushed from surface	0 - 20cm	Y		Y
FR1B-B	~7m Southeast of test area Main Test Area, representing initial conditions, block sample, 5.5 hours freezing	0 - 13cm	Y	Y	
FR1B-T	~7m Southeast of test area Main Test Area, representing initial conditions, radial freezing tube sample, 5.5 hours freezing	0 - 27cm	Y	Y	
FR1A-B	Center of loading area between tracks, after softening, block sample, 5.5 hours freezing	0 - 10cm	Y	Y	
FR1A-T	Center of loading area between tracks, after softening, radial freezing tube sample, 5.5 hours freezing	0 - 20cm	Y	Y	
FRQT-B	"Undisturbed" area near QT3, radial freezing tube sample, 2 hours freezing	0 - 20cm	Y	Y	
FRQT-A	QT3 radial freezing tube sample, 2 hours freezing	0 - 20cm	Y	Y	
B1	Main test site from instrumentation area, back row	1m			Y
B2	Main test site from instrumentation area	2m			Y

SUMMARY OF VOID RATIO, DENSITY AND MOISTURE CONTENT DETERMINATIONS ON FROZEN SAMPLES

Initial Condition Samples

Large Sample ID	Trimmed Sample ID	Moisture Content (%)	Bulk Density (Thawed) (kg/m ³)	Dry Density (kg/m ³)	Void Ratio	Saturation (%)	Saturated Density (kg/m ³)	Comments
FR1B-B	MT *	19.2	1692	1420	0.87	58.6	1884	
FR1B-B	MB *	19.6	1739	1454	0.82	63.2	1905	
FR1B-B	MO *	18.7	1703	1435	0.85	58.5	1893	
FR1B-B	EI *	18.5	1727	1457	0.82	60.0	1907	
FR1B-B	EO *	19.1	1726	1449	0.83	61.2	1902	
average		19.4	1716	1437	0.84	60.9	1895	
FR1B-T	B	24.8	1800	1442	0.84	78.5	1898	seal may have cracked
FR1B-T	M TUBE	22.9	1789	1456	0.82	73.9	1907	possible air bubble
FR1B-T	MET	22.2	1752	1434	0.85	69.3	1893	
FR1B-T	MEB *	24.3	1854	1491	0.78	83.0	1928	seal may have cracked
FR1B-T	MEB redip	25.3	1908	1522	0.74	90.7	1948	
FR1B-T	EM-T	21.8	1736	1426	0.86	67.3	1888	
FR1B-T	EB *	24.2	1799	1449	0.83	77.3	1902	
FR1B-T	REM *	21.1	1773	1464	0.81	69.0	1911	
FR1B-T	REB *	23.5	1770	1434	0.85	73.3	1893	
average		23.3	1799	1459	0.82	75.7	1908	
FRQT-B	TI	21.2	1718	1418	0.87	64.6	1863	
FRQT-B	MI	22.3	1790	1464	0.81	72.8	1911	
FRQT-B	BI	25.5	1868	1488	0.78	86.7	1927	
FRQT-B	UI2	20.1	1728	1439	0.84	63.2	1896	
FRQT-B	M12	22.2	1836	1503	0.76	77.0	1936	
FRQT-B	M13	22.4	1803	1473	0.80	74.3	1917	
FRQT-B	B12	26.8	1818	1434	0.85	83.7	1893	
FRQT-B	ME *	22.5	1810	1478	0.79	75.1	1920	
FRQT-B	ME2 *	21.8	1801	1478	0.79	73.0	1920	
FRQT-B	ME3 *	21.0	1785	1475	0.80	69.8	1918	
FRQT-B	TO	21.1	1712	1413	0.88	64.0	1880	
FRQT-B	MO *	21.9	1820	1493	0.78	74.9	1930	
FRQT-B	BO *	24.3	1847	1485	0.78	82.2	1925	
FRQT-B	UO2	19.6	1714	1433	0.85	61.2	1892	
FRQT-B	MO2 *	22.3	1861	1522	0.74	79.6	1948	
FRQT-B	BO2 *	24.1	1861	1500	0.77	83.3	1934	
average		22.6	1826	1490	0.78	76.9	1928	
Minimum		26.8	1908	1522	0.88	90.7	1948	
Maximum		18.5	1692	1413	0.74	58.5	1880	

Note: * indicates values used to calculate representative averages, i.e. located away from surface and tube
 Trimmed sample ID: T=top, M=middle, B=bottom, E=edge, I=inner, O=outer

After Softening Samples

Large Sample ID	Trimmed Sample ID	Moisture Content (%)	Bulk Density (Thawed) (kg/m ³)	Dry Density (kg/m ³)	Void Ratio	Saturation (%)	Saturated Density (kg/m ³)	Comments
SA1A-B	MMT *	22.9	1795	1461	0.81	71.1	1925	
SA1A-B	MMB *	21.8	1744	1431	0.85	68.3	1890	
SA1A-B	ME1 *	21.9	1747	1433	0.85	68.0	1894	
SA1A-B	ME2 *	23.0	1756	1428	0.86	74.4	1874	
SA1A-B	E	21.4	1664	1370	0.93	68.6	1815	
SA1A-B	chunk *	22.1	1746	1430	0.85	60.8	1927	
average		22.3	1757	1437	0.85	68.5	1902	
SA1A-T	TI	23.2	1754	1424	0.86	71.4	1887	
SA1A-T	BI	26.9	1793	1413	0.88	81.5	1880	very wet after wax removed
SA1A-T	ME2 *	26.7	1698	1340	0.98	72.4	1834	
SA1A-T	ME *	22.2	1762	1442	0.84	70.2	1898	filled void (crack) with wax - unrealistically low??
SA1A-T	ME3 *	24.0	1731	1397	0.90	70.7	1870	
SA1A-T	BRE *	21.2	1803	1488	0.78	71.9	1927	
SA1A-T	TO *	21.1	1823	1505	0.76	73.6	1937	
SA1A-T	BO *	25.5	1865	1487	0.78	86.2	1926	
average		23.4	1780	1443	0.84	74.2	1898	
QT-A	TI	22.6	1767	1441	0.84	71.4	1897	
QT-A	MI	22.5	1897	1548	0.71	83.9	1964	
QT-A	M12	21.5	1869	1538	0.72	78.9	1957	
QT-A	TI2	24.2	1775	1430	0.85	75.1	1890	
QT-A	ME *	21.8	1869	1534	0.73	79.4	1955	
QT-A	ME2 *	23.1	1875	1522	0.74	82.8	1948	
QT-A	TO *	22.4	1791	1463	0.81	73.2	1911	
QT-A	MO *	22.6	1888	1540	0.72	83.0	1959	
QT-A	TO2 *	24.3	1798	1446	0.83	77.4	1901	
QT-A	MO2 *	21.2	1923	1588	0.67	83.8	1988	
QT-A	BO2	20.9	1928	1595	0.66	83.6	1993	very wet after wax removed
average		22.6	1857	1516	0.75	79.9	1943	
Maximum		26.9	1928	1595	0.98	86.2	1993	
Minimum		20.9	1664	1340	0.66	60.8	1815	

Note: * indicates values used to calculate representative averages, i.e. located away from surface and tube
Trimmed sample ID: T=top, M=middle, B=bottom, E=edge, I=inner, O=outer

EQUATIONS USED TO CALCULATE MOISTURE CONTENT, VOID RATIO AND DENSITY OF FROZEN SAMPLES

If the sample was saturated in-situ, the 9% volume expansion of water must be accounted for as, providing that the soil skeleton didn't expand and water was free to drain during freezing, the amount of water trapped as ice would be less than the amount of water there initially. If however the sample was less than 91% saturated then since $S_r = V_w/V_v$ the volume of voids filled with air would provide enough room for the water to expand and therefore the amount of water trapped as ice is representative of the amount of water in the soil in-situ.

Constants:

Wax density (g/cm^3)	0.93
Density of Water (g/cm^3)	1.00
Density of Ice (g/cm^3)	0.917
Gs tailings:	2.65

Equations Used:

$$\text{average} = \frac{1}{n} \sum_{i=1}^n d_i$$

$$\text{Frozen Volume (V}_F) = h_{\text{avg}} * l_{\text{avg}} * b_{\text{avg}}$$

$$\text{Frozen weight (M}_F)$$

$$\text{Sample+wax weight (M}_{F+W})$$

$$\text{Submerged weight (M}_{\text{sub}})$$

Frozen Bulk Density Calcs:

$$\text{Total Volume of Sample and wax (V}_{TF}) = M_{F+W} - M_{\text{sub}}$$

$$\text{Mass of Wax (M}_W) = M_{F+W} - M_F$$

$$\text{Volume of wax (V}_W) = M_W / \rho_w$$

$$\text{Volume of frozen soil (V}_{FS}) = V_{TF} - V_W$$

$$\text{Frozen Bulk Density (}\rho_{BF}) = M_F / V_{FS}$$

If sample is < 91% saturated then:

$$\text{Frozen Bulk Density (}\rho_{BF}) = \text{Thawed bulk density (}\rho_b) = M_F / V_{FS}$$

Moisture Content Calcs:

$$\text{Tare weight (M}_{wcT})$$

$$\text{Tare + frozen weight (M}_{wcT+FS})$$

$$\text{Tare + dry weight (M}_{wcT+D})$$

$$\text{Weight of frozen soil (M}_{wcFS}) = M_{wcT+FS} - M_{wcT}$$

$$\text{Weight of ice (M}_{wc_{ice}}) = M_{wcT+FS} - M_{wcT+D}$$

$$\text{Weight of dry soil (M}_{wc_{DS}}) = M_{wcT+D} - M_{wcT}$$

If sample is < 91% saturated then:

$$\text{Ice content (w}_{ice}) = \text{Moisture content (w)} = M_{wc_{ice}} / M_{wc_{DS}} * 100$$

If sample > 91% saturated then:

$$\text{Ice content (w}_{ice}) = M_{wc_{ice}} / M_{wc_{DS}} * 100$$

$$\text{Moisture content (w)} = w_{ice} / (\rho_{ice} / \rho_{H_2O})$$

Thawed Property Calcs:

Mass of soil in sample (M_s): $M_{TF}/(1+(w_{ice}/100))$

$$\text{Dry density } (\rho_D) = \frac{M_s}{V_{FS}} = \frac{100}{100 + (w * 100)} \rho_B$$

$$\text{Void ratio } (e) = \frac{G_s \rho_w}{\rho_d} - 1$$

If sample is >91% saturated then:

$$\text{Thawed bulk density } (\rho_B) = (M_s + M_s * (w/100)) / V_{FS}$$

SUMMARY OF MOISTURE CONTENT AND DENSITY DETERMINATIONS ON DISTURBED BULK SAMPLES

Moisture Content Summary

Sample	Average Moisture Content (%)	Comments	Sample	Average Moisture Content (%)	Comments
SA1	13.11		SA12	24.83	bitumen inclusions
SA2	17.32		SA13	24.94	
SA3	24.02		SA14	13.89	
SA4	26.57		SA15	14.43	
SA5	21.20	large bitumen inclusion	SA16	26.14	
SA6	17.79		SA17	21.28	
SA7	21.71		SA21	23.93	water in sample bag
SA8	23.10		SA22	23.77	water in sample bag
SA9	15.24		SA26	25.25	very very wet
SA11	10.52		SA27	22.53	

Note: $mc = \frac{m_w}{m_s} \times 100\%$

Disturbed Density Sample

Volume of Sample Gathered

	Tube Dimensions (mm)			
	Wall Thickness	Inside Diameter	Height	Height of cutting taper
	2.06	97.58	200.53	5.83
	2.02	97.33	199.52	5.57
	2.02	97.47	199.22	5.48
	2.06	97.43	199.55	5.48
	2.03	97.43	200.23	5.62
	1.94	97.58		5.75
	2.17	97.4		
	2.04	97.39		
		97.53		
average:	2.04	97.46	199.81	5.62

Sample Volume: 0.001491 m³

Wet Sample Weight: 2.6587 kg

Dry Sample Weight: 2.2616 kg

Moisture Content: 17.56 %

Assumed Gs (CANLEX): 2.66

Bulk Density:	1784 kg/m ³
Dry Density:	1517 kg/m ³
Void Ratio:	0.75
Saturated density:	1947 kg/m ³

SUMMARY OF GRAIN SIZE DISTRIBUTIONS

Sample	Depth	Softened	Washed	D10	D50	D60	Cu	% finer than 75µm	% finer than 45µm
SA1-D	0-0.3	N	N	0.100	0.185	0.200	2.0	1.04	0.47
SA2-D	0-0.2	N	N	0.093	0.180	0.200	2.2	1.12	0.27
SA2-W	0-0.2	N	W	0.093	0.180	0.200	2.2	2.05	1.42
SA3-D	0-0.25	Y	N	0.089	0.170	0.177	2.0	3.16	0.83
SA4-D	0.4	Y	N	0.089	0.170	0.180	2.0	2.30	0.81
SA5-D	0-0.25	N	N	0.090	0.170	0.180	2.0	1.71	0.69
SA21-D	0.05-0.25	Y	Y	0.094	0.180	0.200	2.1	1.08	0.31
SA21-W	0.05-0.25	Y	Y	0.094	0.180	0.200	2.1	1.08	0.35
SA22-D	0.05-0.25	Y	N	0.083	0.150	0.155	1.9	1.91	0.33
SA22-W	0.05-0.25	Y	Y	0.083	0.150	0.155	1.9	2.25	0.70
SA26-D	0-0.3	Y	N	0.093	0.190	0.207	2.2	2.44	1.16
SA26-W	0-0.3	Y	Y	0.093	0.190	0.207	2.2	2.72	1.61
SA27-D	0-0.3	N	N	0.083	0.175	0.190	2.3	4.98	1.75
SA27-W	0-0.3	N	Y	0.083	0.175	0.190	2.3	5.25	2.28
B1	0-1	Y	Y	0.096	0.190	0.204	2.1	2.02	0.79
B2	1-2	Y	Y	0.089	0.180	0.190	2.1	3.22	1.58
B2 Wf	1-2	Y	Y	0.085	0.175	0.185	2.2	4.35	2.40
Average ¹ :				0.090	0.176	0.189	2.1	2.60	1.16

Note: 1. If a sample was tested twice (e.g. washed and dry) only the washed result was used in calculating the average

APPENDIX C
CPT Data Analyses,
Estimation of State Parameter and Liquefaction Susceptibility

EQUATIONS FOR CPT DATA REDUCTION AND LIQUEFACTION EVALUATION:

General Equations:

$$q_c = \frac{Q_c}{A_c} \quad q_T = q_c + u_2(1 - a)$$

$$f_s = \frac{F_s - Q_c}{A_s} \quad \text{subtraction cone}$$

$$q_{c1} = C_q q_c$$

$$C_q = \left(\frac{P_a}{\sigma'_{v0}} \right)^n \leq 1.7$$

n depends on material type, 0.5 for sands, 1.0 for clays
 P_a and P_{a2} are reference pressures of 100kPa in the same units as σ'_{v0} and $(q_c - \sigma_{v0})$ respectively

$$q_{c1N} = \frac{q_{c1}}{P_{a2}}$$

$$Q = \left(\frac{q_c - \sigma_{v0}}{P_{a2}} \right) \left(\frac{P_a}{\sigma'_{v0}} \right)^n$$

$$F = \frac{f_s}{q_c - \sigma_{v0}} \times 100\%$$

$$CN = \frac{2.2}{1.2 + 10\sigma'_{v0}}$$

CPT-SPT, Robertson et al. 1983

$$\frac{q_c}{N} = 5.5 \quad q_c \text{ in } kg/cm^2$$

CPT-SPT, Seed and DeAlbda, 1986

$$\frac{q_c}{N_{60}} = 0.37 \quad q_c \text{ in } MPa$$

CPT-SPT Andrus and Youd 1989

$$\frac{q_c}{N_{60}} = 0.31 \quad q_c \text{ in } MPa$$

Robertson and Wride 1998 method of CPT Liquefaction Evaluation

$$Q = \frac{q_c - \sigma_{v0}}{\sigma'_{v0}}$$

$$F = \frac{f_s}{q_c - \sigma_{v0}} \times 100\%$$

Iteration Procedure to Evaluate q_{c1N} and I_c

$$I_c = \left((3.47 - \log Q)^2 + (\log F + 1.22)^2 \right)^{0.5}$$

IF $I_c > 2.6$ then $q_{c1N} = Q$

IF $I_c < 2.6$ then re-evaluate

$$q_2 = \frac{q_c}{P_{a2}} \left(\frac{P_a}{\sigma'_{v0}} \right)^{0.5}$$

$$I_c = \left((3.47 - \log q_2)^2 + (\log F + 1.22)^2 \right)^{0.5}$$

IF I_c remains < 2.6 then $q_{c1N} = q_2$

IF I_c is now > 2.6 then re-evaluate

$$q_{c1N} = \frac{q_c}{P_{a2}} \left(\frac{P_a}{\sigma'_{v0}} \right)^{0.75}$$

Fines Content:

$$FC(\%) = \begin{cases} 0 & \text{If } I_c < 1.26 \\ 1.75 I_c^{3.25} - 3.7 & \text{If } 1.26 \leq I_c \leq 35 \\ 100 & \text{If } I_c > 35 \end{cases}$$

Tip Resistance Correction, for Fines Content:

$$K_c = \begin{cases} 1.0 & \text{if } I_c \leq 1.64 \\ 1.0 & \text{if } 1.64 < I_c < 2.36 \\ -0.403I_c^4 + 5.581I_c^3 - 21.63I_c^2 + 33.75I_c - 17.88 & \text{if } I_c > 1.64 \\ \text{likely non-liquefiable} & \text{if } I_c \geq 2.6 \text{ and } F > 1\% \\ \text{should be evaluated with other criteria} & \text{if } I_c \geq 2.6 \end{cases}$$

Clean Sand Equivalent Tip Resistance:

$$q_{(c1N)CS} = K_c * q_{c1N}$$

SPT Equivalents, From Lunne et al. 1992

$$N_{60} = \frac{q_c}{0.85 \left(1 - \frac{I_c}{4.6} \right)}$$

$$(N_1)_{60} = N_{60} \times CN$$

$$(N_1)_{60_CS} = \begin{cases} 0+1*(N_1)_{60} & \text{if } FC < 5\% \\ e^{1.76 - \frac{190}{FC^2}} + \left(0.99 + \frac{FC^{1.5}}{1000}\right) (N_1)_{60} & \text{if } FC < 35\% \\ 5+1.2*(N_1)_{60} & \text{if } FC > 35\% \end{cases}$$

SPT Equivalent From Corrected CPT Data, After Lunne et al. 1992

$$(N_1)_{60} = \frac{q_{C1N}}{8.5 \left(1 - \frac{Ic}{4.6}\right)} \quad (N_1)_{60-CS} = \frac{q_{C1N-CS}}{8.5 \left(1 - \frac{Ic}{4.6}\right)}$$

Jeffries and Davies 1993 SPT from CPT Method

$$Q_T = \frac{q_T - \sigma_{v0}}{\sigma'_{v0}}$$

$$B_q = \frac{u - u_0}{q_T - \sigma_{v0}}$$

$$Fr(\%) = \frac{f_s}{q_T - \sigma_{v0}} \times 100$$

$$Ic = \left[\left(3 - \log(Q_T(1 - B_q)) \right)^2 + (1.5 + 1.3 \log Fr)^2 \right]^{\frac{1}{2}}$$

Fines Content:

$$FC(\%) = \begin{cases} 0 & \text{If } Ic < 1.3 \\ 42.4 Ic - 54.9 & \text{If } 1.3 \leq Ic \leq 3.65 \\ 100 & \text{If } Ic > 3.65 \end{cases}$$

SPT Equivalents:

$$N_{60} = \frac{q_c}{0.85 \left(1 - \frac{Ic}{4.75}\right)}$$

$$(N_1)_{60} = N_{60} \times CN$$

$$(N_1)_{60_CS} = \begin{cases} 0+1*(N_1)_{60} & \text{if } FC < 5\% \\ e^{1.76 - \frac{190}{FC^2}} + \left(0.99 + \frac{FC^{1.5}}{1000}\right) (N_1)_{60} & \text{if } FC < 35\% \\ 5+1.2*(N_1)_{60} & \text{if } FC > 35\% \end{cases}$$

State Parameter, ψ , Been et. al., 1988

$$q^* = k^* \exp(-m^* \psi)$$

$$q^* = \frac{q_c - p_0}{p'_0} (1 - B_q) \quad k^* = 6 + \frac{0.55}{\lambda - 0.12} \quad m^* = 11.9 - 13.3\lambda$$

Combining these equations gives:

$$\psi = \frac{-\ln \left(\frac{\frac{q_c - p_0}{p'_0} (1 - B_q)}{6 + \frac{0.55}{\lambda - 0.12}} \right)}{11.9 - 13.3\lambda}$$

Value of λ used in analyses: 0.0152

State Parameter, ψ , Plewes et. al., 1992

$$Q_r(1 - B_q) = k \exp(-m \psi)$$

where k and m are:

$$\frac{k}{M} = 3 + \frac{0.85}{\lambda} \quad m = 11.9 - 13.3\lambda$$

M and λ are the slopes of the critical state line in q - p and e - p space respectively and can be evaluated from:

$$M = \frac{6 \sin(\phi_{ss})}{3 - \sin(\phi_{ss})} \quad \lambda = \frac{Fr}{10}$$

Combining these equations gives:

$$\psi = \text{Min} \left\{ \begin{array}{l} 0.2 \\ -\ln \left(\frac{Q_r(1 - B_q)}{\frac{6 \sin(\phi_{ss})}{3 - \sin(\phi_{ss})} \left(3 + 0.85 \times \frac{10}{Fr} \right)} \right) \\ \frac{11.9 - \frac{13.3Fr}{10}}{11.9 - \frac{13.3Fr}{10}} \end{array} \right.$$

Value of ϕ_{ss} used in analyses: 33 degrees

State Parameter Been and Jeffries, 1992

$$Q_p = \frac{q_c - p_0}{p'_0}$$

$$\frac{Q_p}{1 - B_q} = k \exp(-m \psi)$$

where k and m are:

$$\frac{k}{M} = 3 + \frac{0.85}{\lambda} \quad m = 11.9 - 13.3\lambda$$

M and λ are the slopes of the critical state line in q - p and e - v space respectively and can be evaluated from:

$$M = \frac{6 \sin(\phi_{SS})}{3 - \sin(\phi_{SS})} \quad \frac{1}{\lambda} = 34 - 10I_c$$

$$\text{where } I_c = \left\{ \left[3 - \log [Q(1 - B_q) + 1] \right]^2 + (1.5 + 3 \log(Fr))^2 \right\}^{0.5}$$

Combining these equations gives:

$$\psi = \frac{-\ln \left(\frac{Q_p}{(1 - B_q) \left(\frac{6 \sin(\phi_{SS})}{3 - \sin(\phi_{SS})} \right) (3 + 0.83 \times (34 - 10I_c))} \right)}{11.9 - \frac{13.3}{34 - 10I_c}}$$

Lunne et al 1997 Method

I_c is calculated as in the iterative Robertson and Wride 1998 method

Fines Content:

$$FC = 1.75 \times I_c^3 - 3.7$$

Equivalent SPT:

$$\frac{q_c}{P_a N_{60}} = 8.5 \left(1 - \frac{I_c}{4.6} \right)$$

$$(N_1)_{60} = N_{60} \times C_N \quad \text{if } FC < 5\%$$

$$(N_1)_{60-CS} = \begin{cases} e^{1.76 - \frac{190}{FC^2}} + \left(0.99 + \frac{FC^{1.5}}{1000} \right) (N_1)_{60} & \text{if } FC < 35\% \\ 5 + 1.2 * (N_1)_{60} & \text{if } FC > 35\% \end{cases}$$

Wride et al 2000 (CANLEX)

Equivalent SPT:

Note: value in parenthesis is the standard deviation

q_{c1} is in MPa

$$\frac{q_{c1}}{(N_1)_{60}} = 0.44(\pm 0.15)$$

Equations for Calculating Shear Wave Velocities and Shear Modulus:

$$q_{c1} = q_c \left(\frac{P_a}{\sigma'_v} \right)^{0.5} \quad q_{c1} \text{ in MPa and } V_{s1} \text{ in m/s}$$

$$q_{c1} = \left(\frac{V_{s1}}{Y} \right)^4$$

Y avg: 95.6 from CANLEX at Mildred Lake

std dev: 12.1 from CANLEX at Mildred Lake

Y avg: 101.1 from CANLEX at J pit

std dev: 6.3 from CANLEX at J pit

$$V_{s1} = V_s \left(\frac{P_a}{\sigma'_v} \right)^{0.25}$$

where P_a is a reference pressure of 100kPa in the same units as σ'_v .

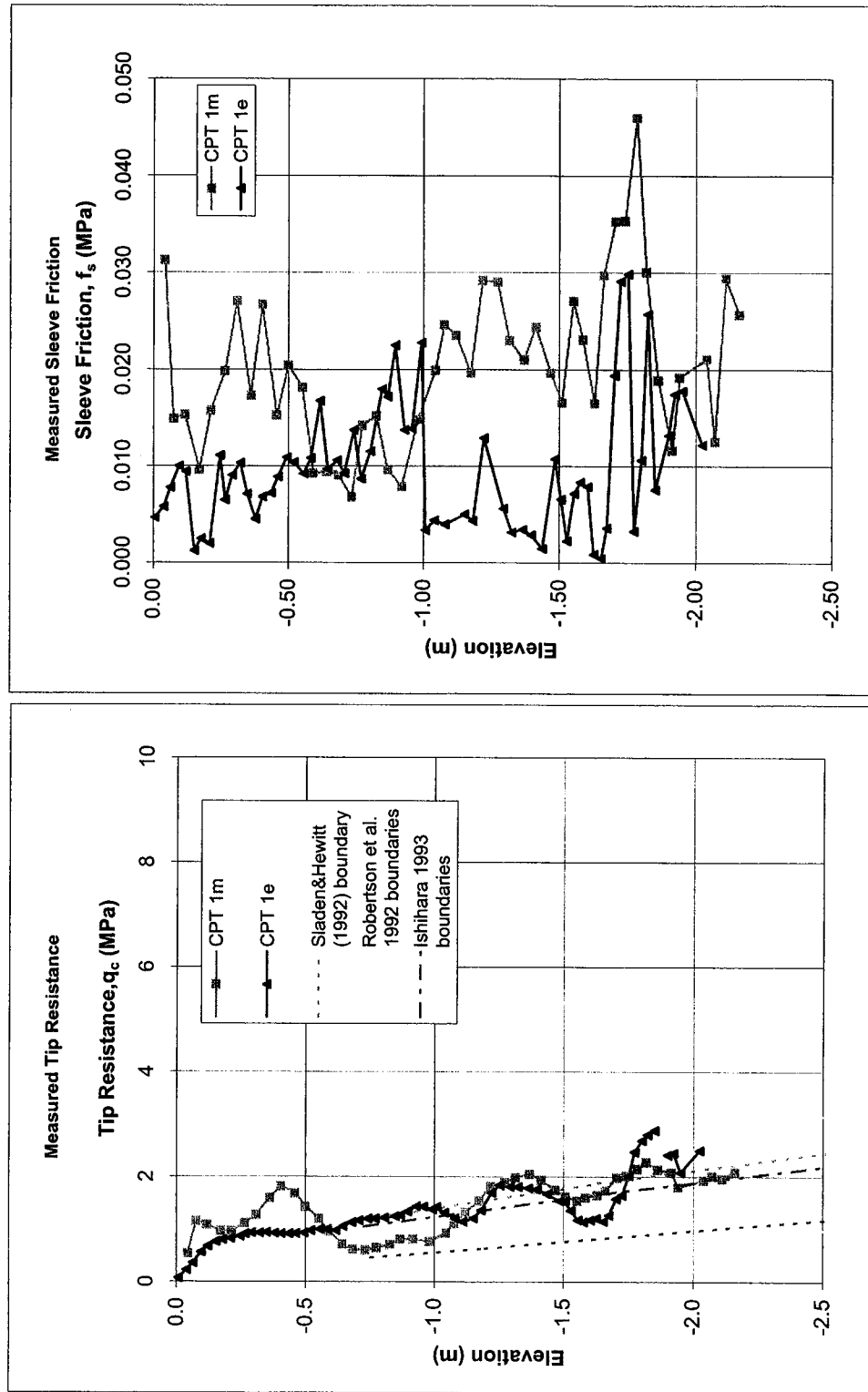
$$G = \rho * V_s^2$$

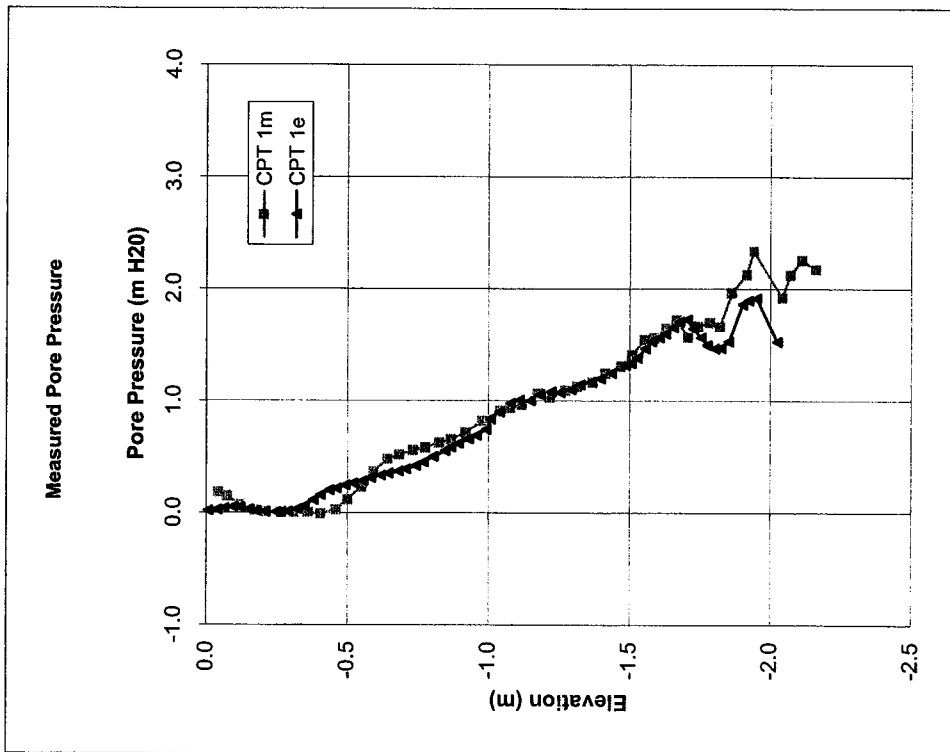
Summary of CPT Liquefaction Interpretation

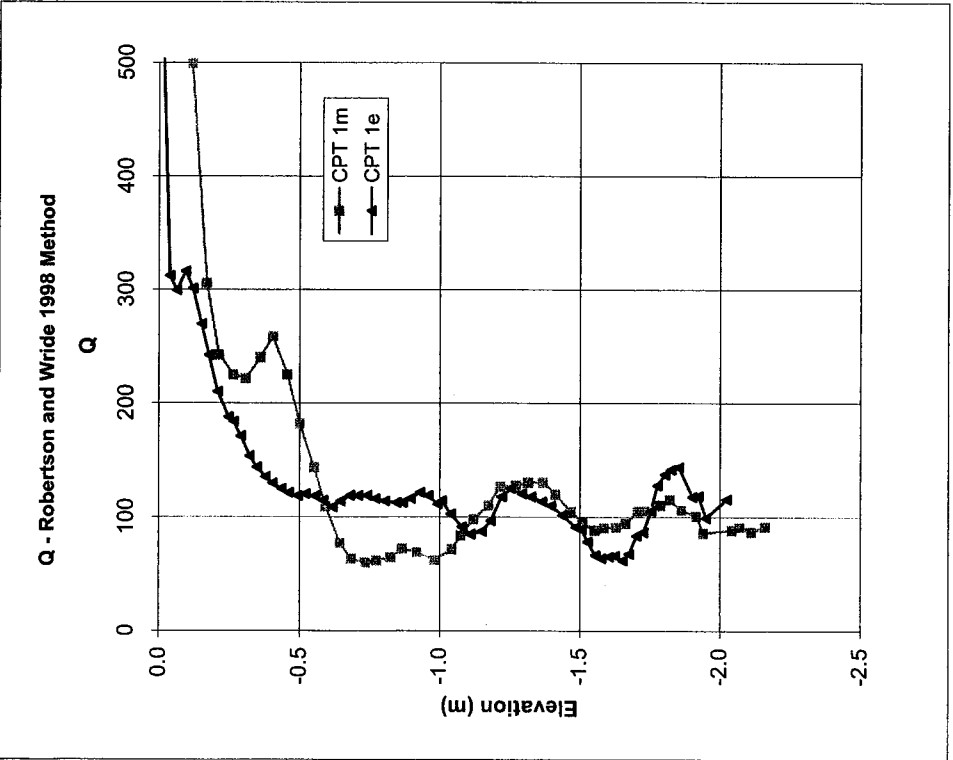
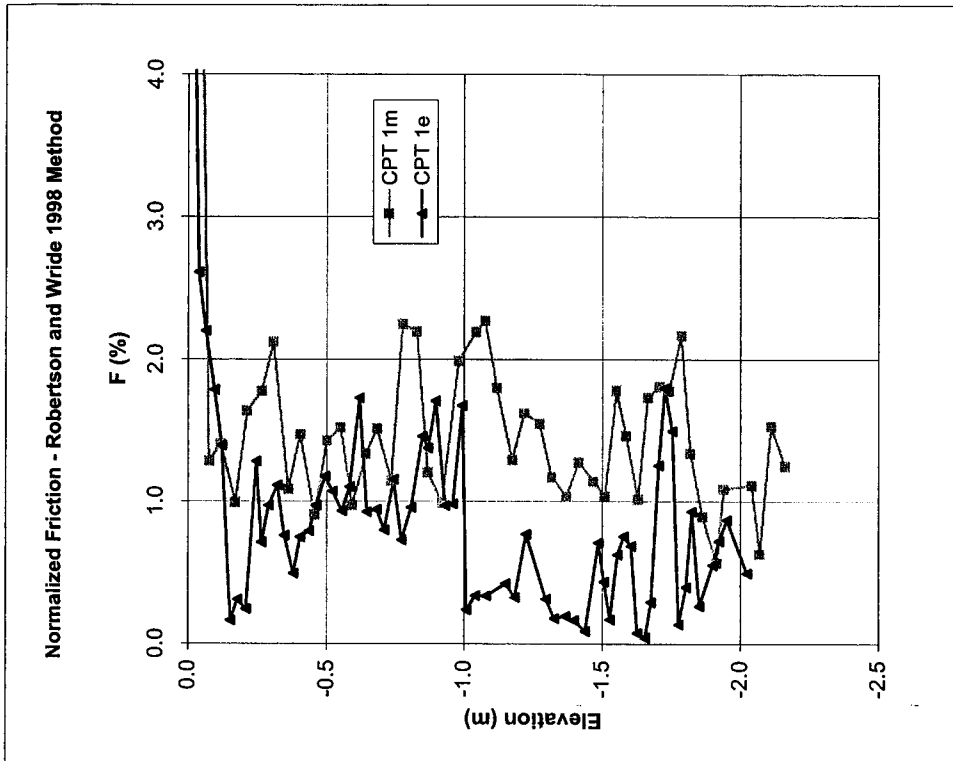
Method	Parameter	Average Values from Below Phreatic Surface		
		CPT 1m	CPT 1e	Both
General	qc (MPa)	1.53	1.48	1.50
	fs (MPa)	0.0208	0.0104	0.0156
Robertson etal SPT	Max SPT	6.7	8.4	7.5
	Min SPT	1.9	2.9	2.4
	Avg SPT	4.6	4.5	4.6
Seed & DeAlba 1986	Max SPT	9.7	12.3	11.0
	Min SPT	2.8	3.8	3.3
	Avg SPT	6.7	6.3	6.5
Andrus & Youd 1989	Max SPT	11.6	14.6	13.1
	Min SPT	3.3	4.5	3.9
	Avg SPT	8.0	7.6	7.8
Robertson & Wride 1998	Q	111.29	108.86	110.07
	F	1.43	0.75	1.09
	lc	2.31	2.15	2.23
	qc1N	41.85	39.73	40.79
	qc1	4.18	3.97	4.08
	FC	23.19	17.74	20.46
	Kc	2.06	1.63	1.84
	qc1Ncs	81.73	63.31	72.52
	N60	3.57	3.22	3.39
	(N1)60	5.78	5.25	5.52
	(N1)60cs	10.25	8.50	9.38
	(N1)60 from qc1N	9.79	8.73	9.26
	(N1)60cs from qc1N	19.36	14.13	16.75
Jeffries and Davies	Qt	111.39	109.09	110.24
	Qt(1-Bq)	111.26	108.99	110.12
	Fr (%)	1.43	0.75	1.09
	lc	1.95	1.58	1.77
	N60	3.03	2.60	2.81
	(N1)60	4.91	4.23	4.57
	F.C.(%)	27.77	13.65	20.71
	(N1)60-cs	9.80	6.63	8.22
Plewes etal.	State Par.	-0.21	-0.14	-0.18
Been and Jeffries	State Par.	-0.13	-0.16	-0.15
Been et al.	State Par.	-0.40	-0.45	-0.43
Lunne et al. 1997	lc	1.99	1.78	1.88
	N60	3.15	2.81	2.98
	(N1)60	5.10	4.59	4.84
	F.C.(%)	10.41	6.38	8.40
	(N1)60-cs	6.32	4.90	5.61

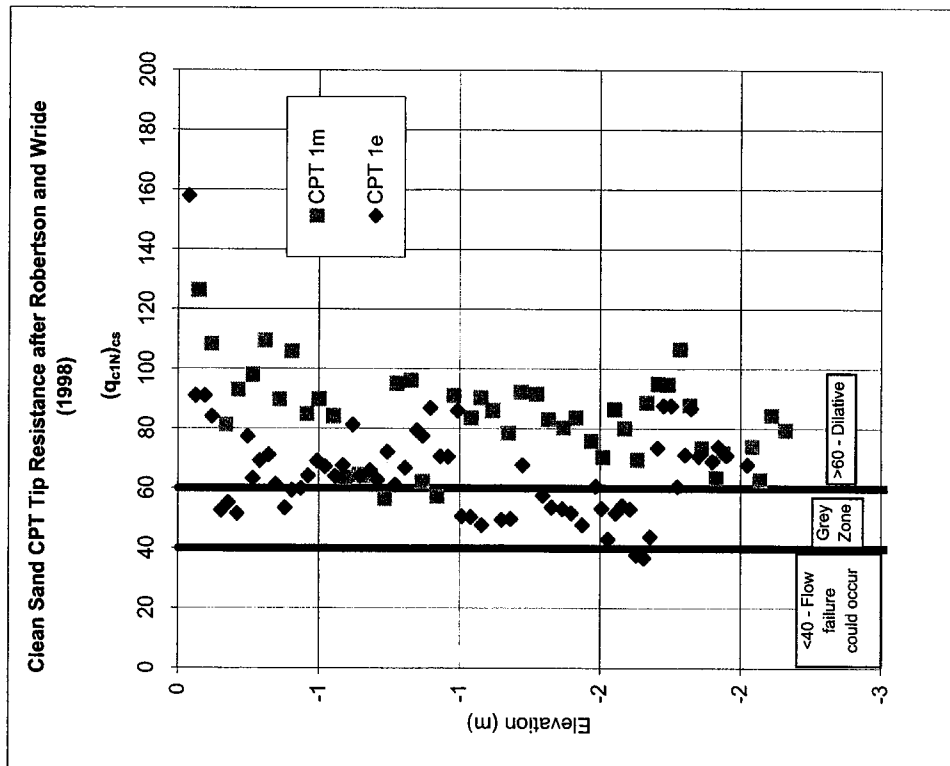
Wride et al. 2000 (CANLEX)	qc1	4.07	3.97	4.02
	(N1)60	9.25	9.03	9.14
	(N1)60 -1 std dev	6.90	6.73	6.82
	(N1)60 +1 std dev	14.04	13.70	13.87
	Vs1 (m/s) avg	134.52	134.41	134.46
	Vs1 (m/s) -1 std dev	117.49	117.40	117.44
	Vs1 (m/s) +1 std dev	151.54	151.42	151.48
	Vs (m/s) avg	82.03	81.07	81.55
	Vs (m/s) -1 std dev	71.65	70.81	71.23
	Vs (m/s) +1 std dev	92.41	91.34	91.88
	G (MPa) avg	13.00	12.67	12.83
	G (MPa) -1 std dev	9.91	9.66	9.79
	G (MPa) +1 std dev	16.49	16.07	16.28

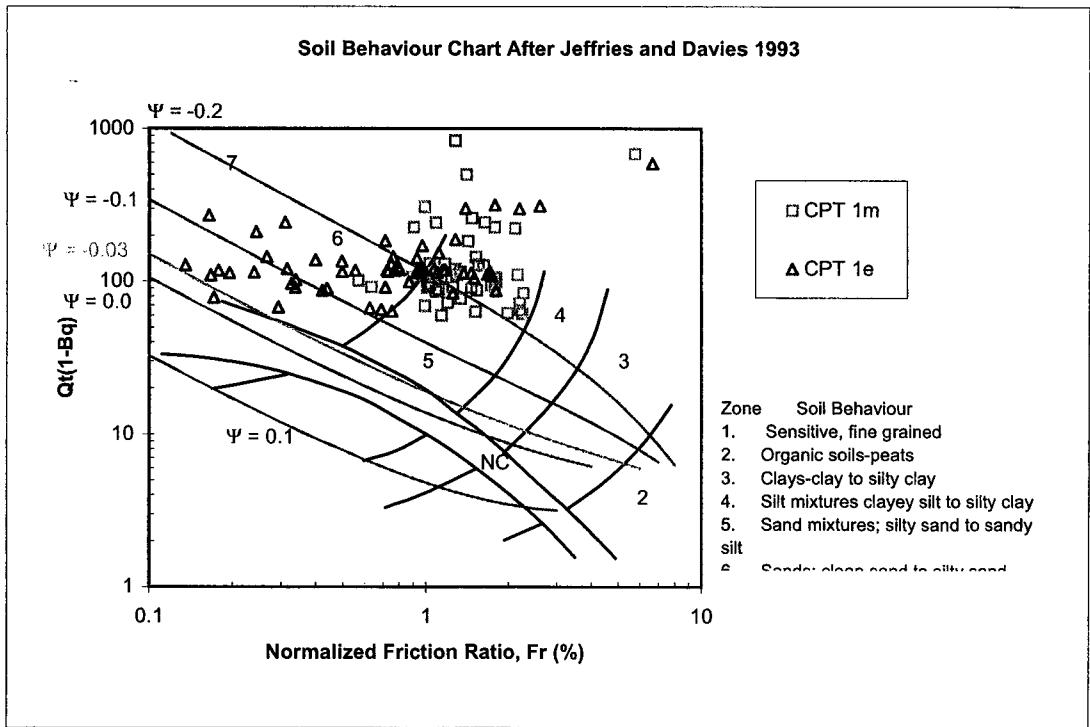
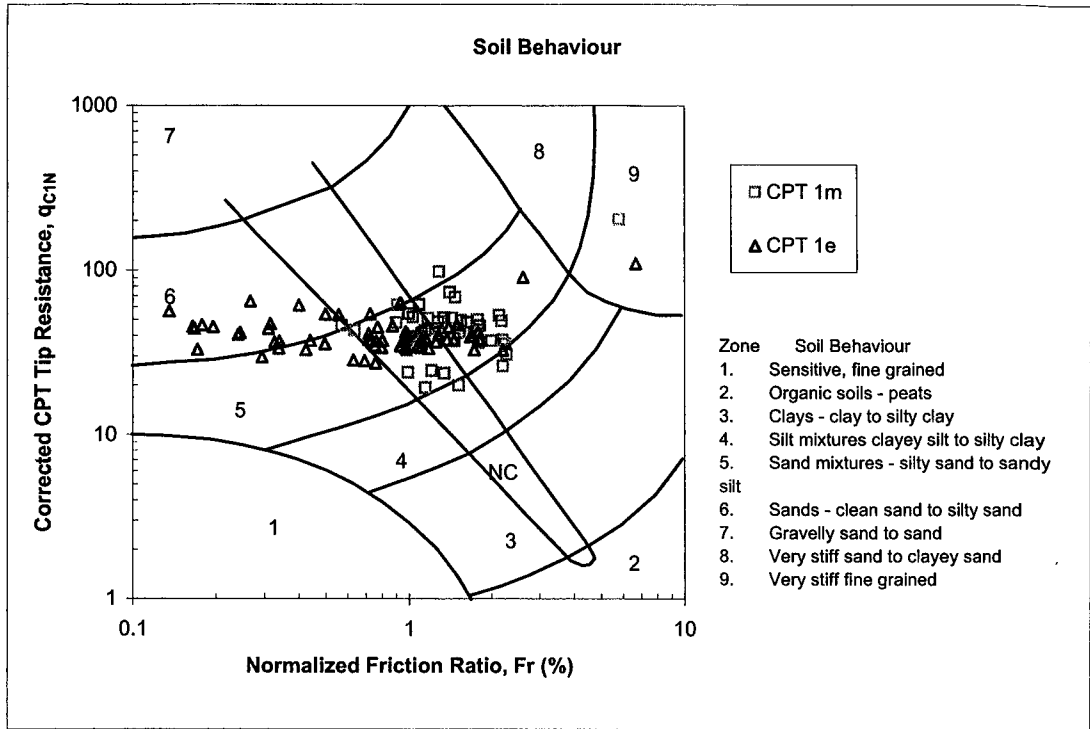
CPT MEASUREMENTS



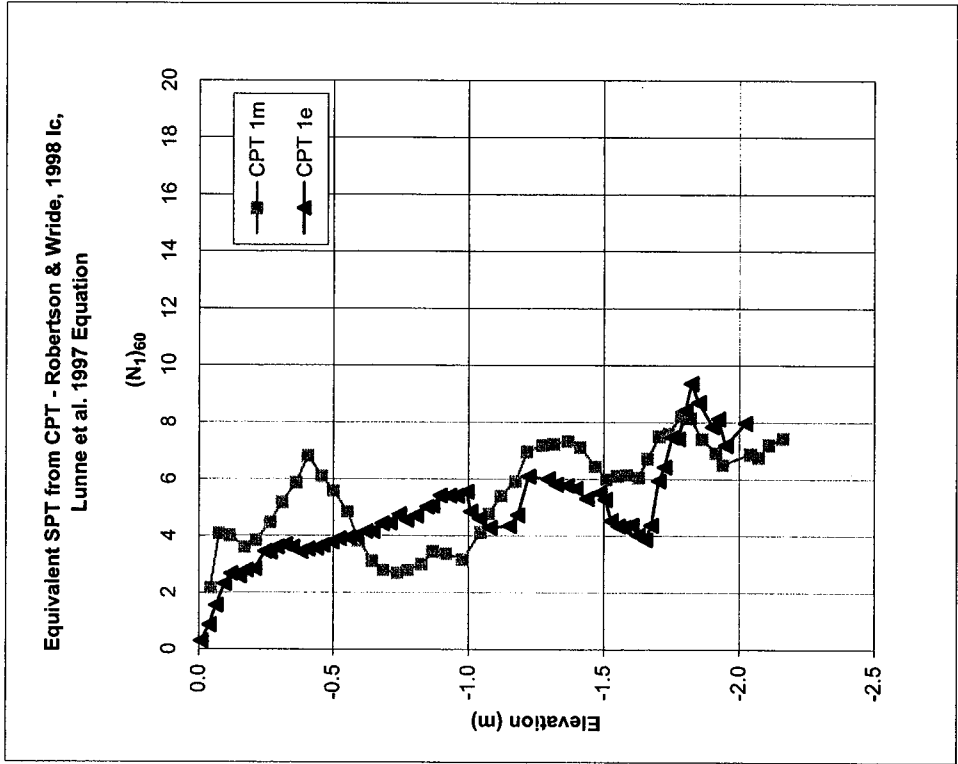
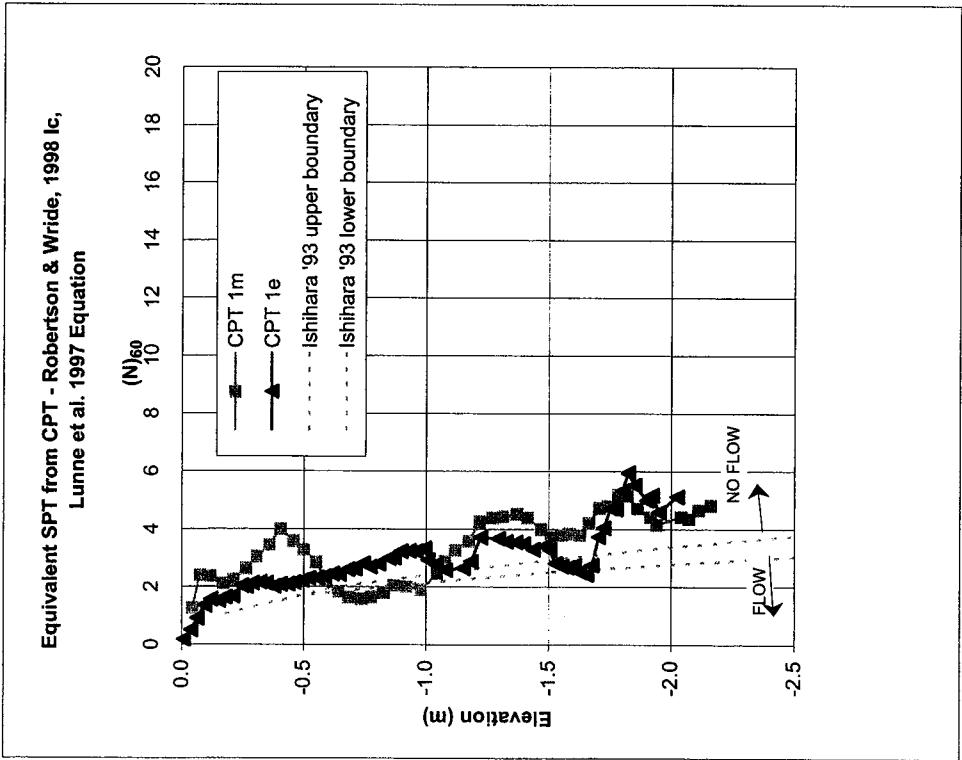


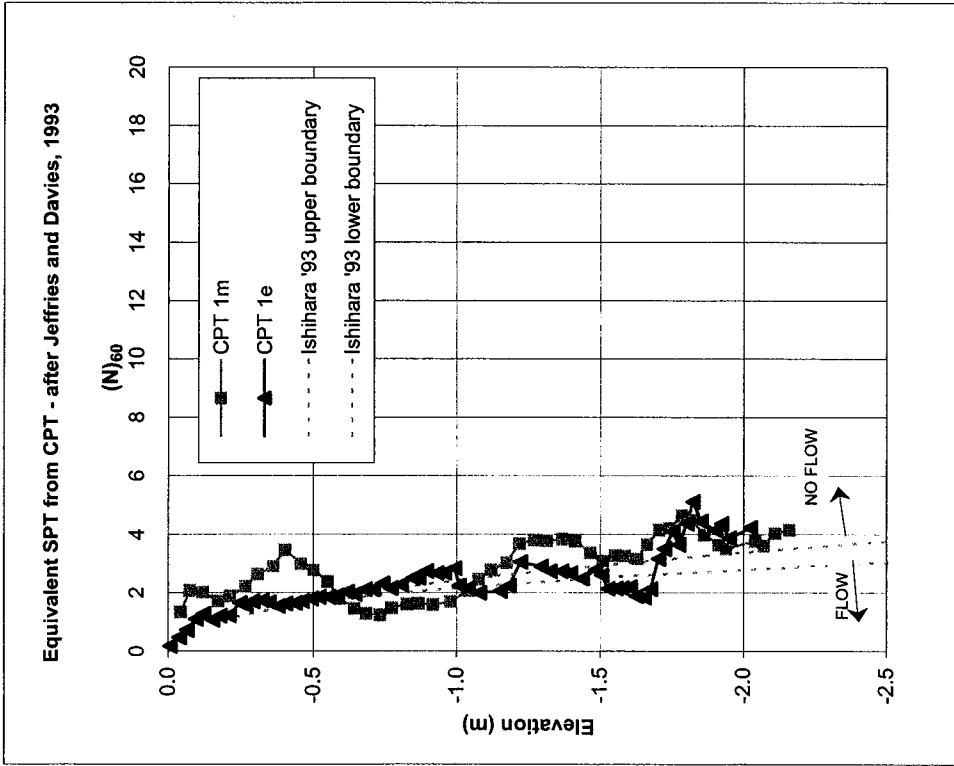
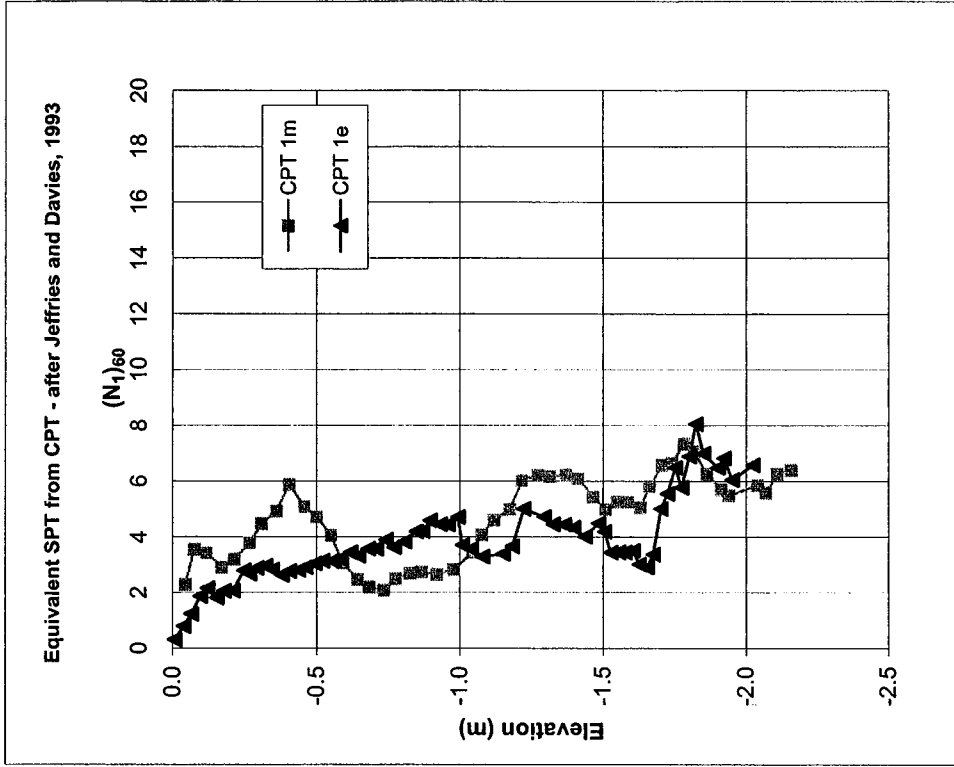


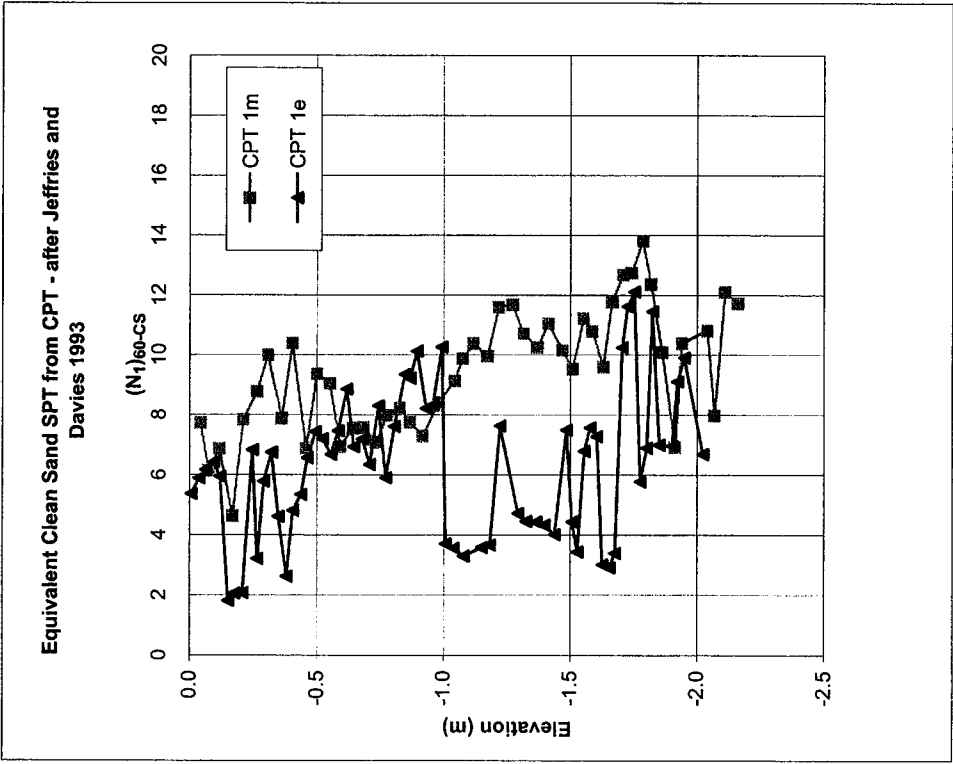
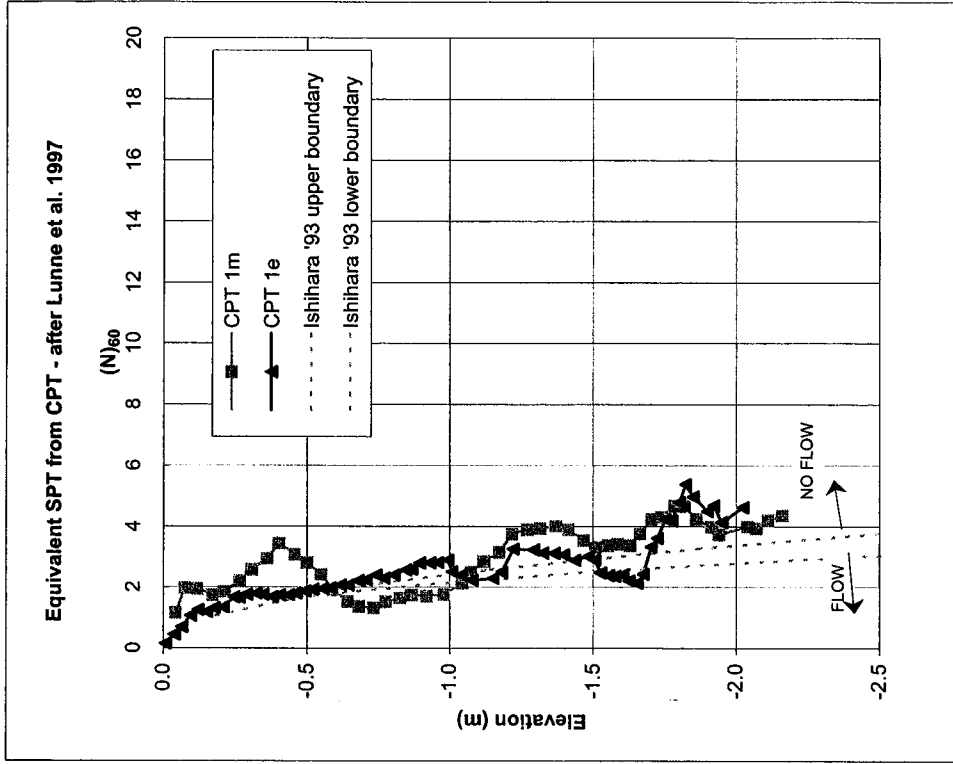


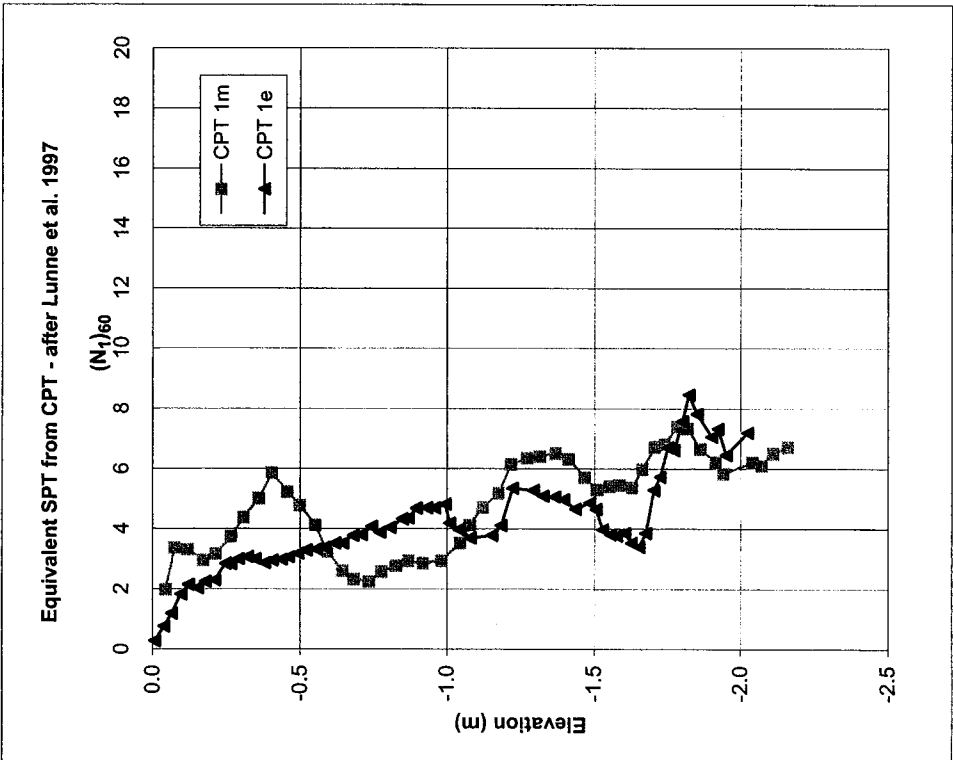
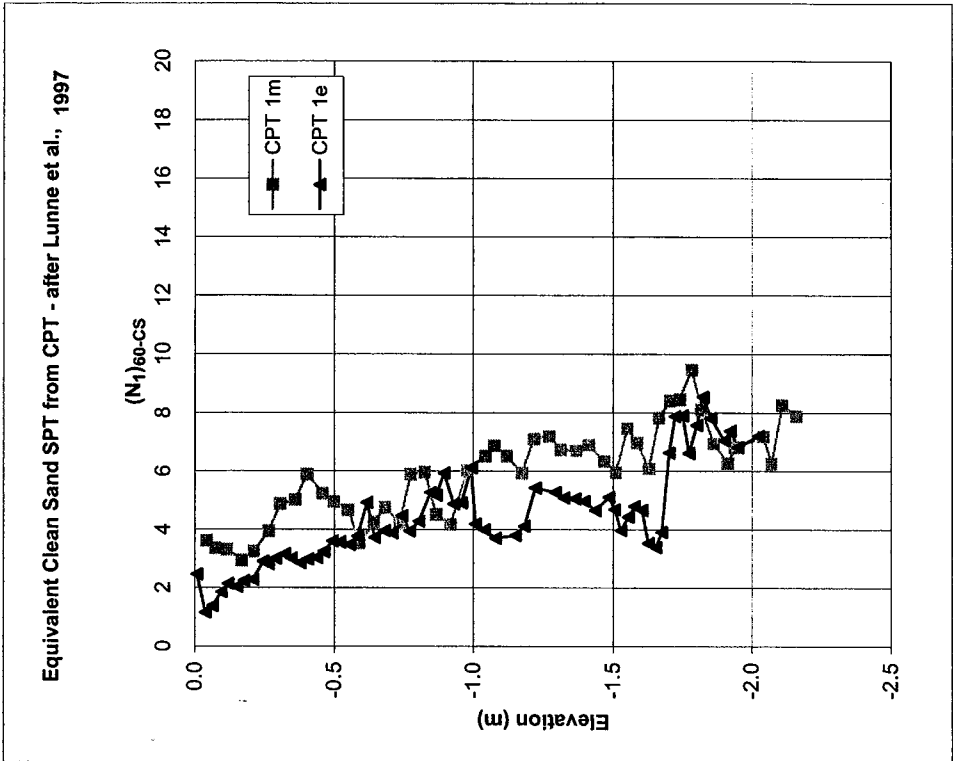


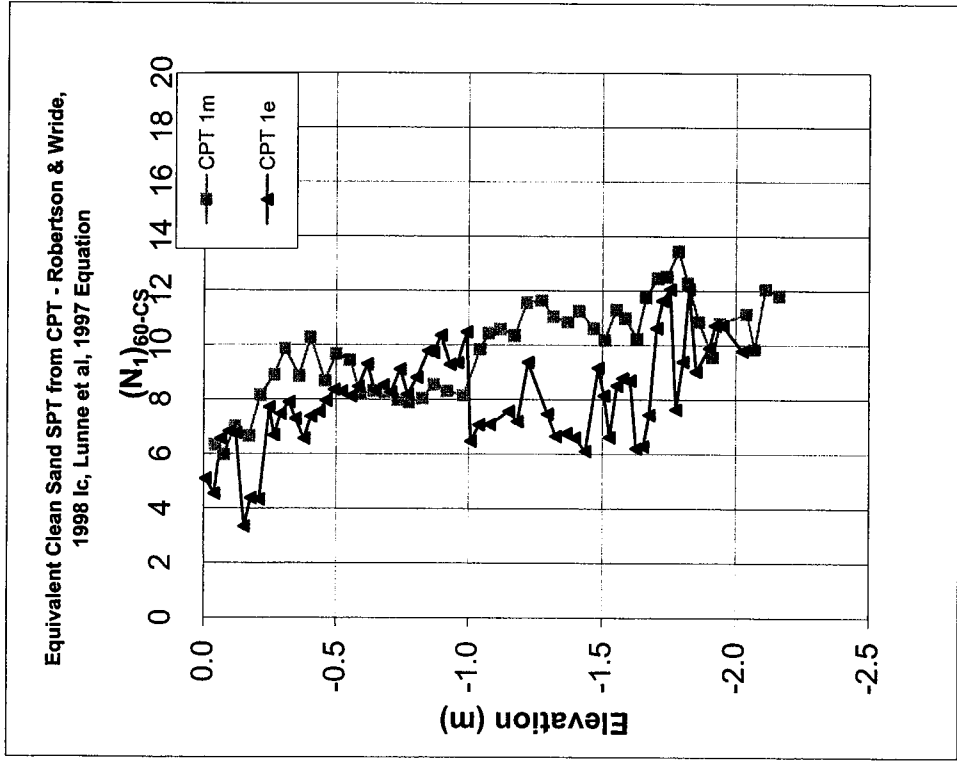
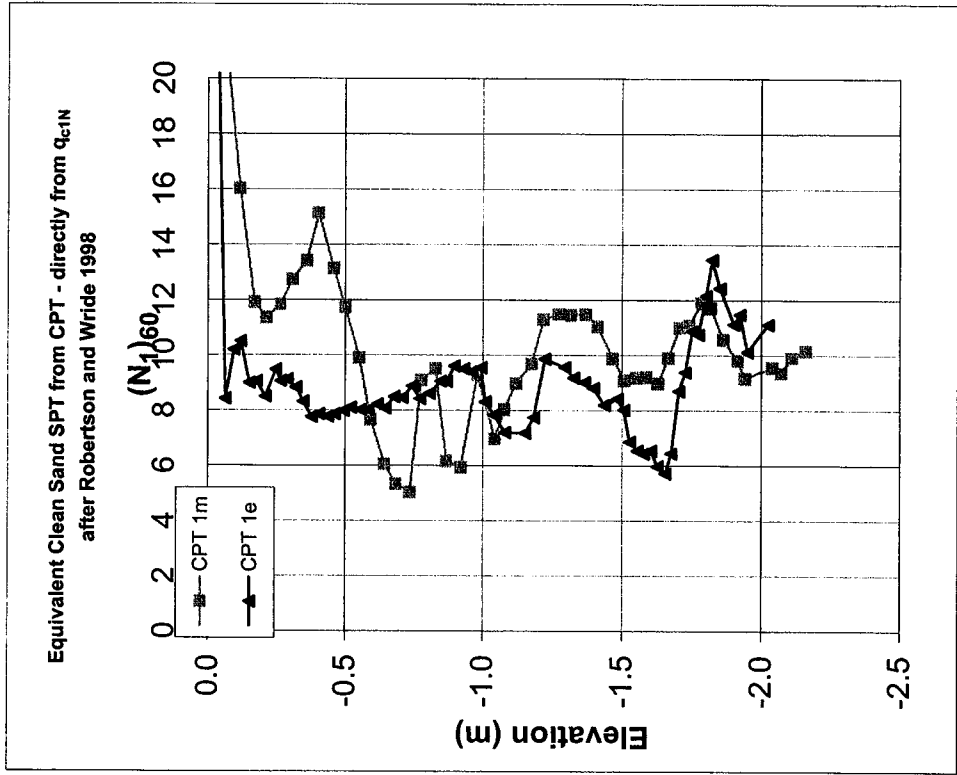
SPT EQUIVALENTS FROM CPT DATA

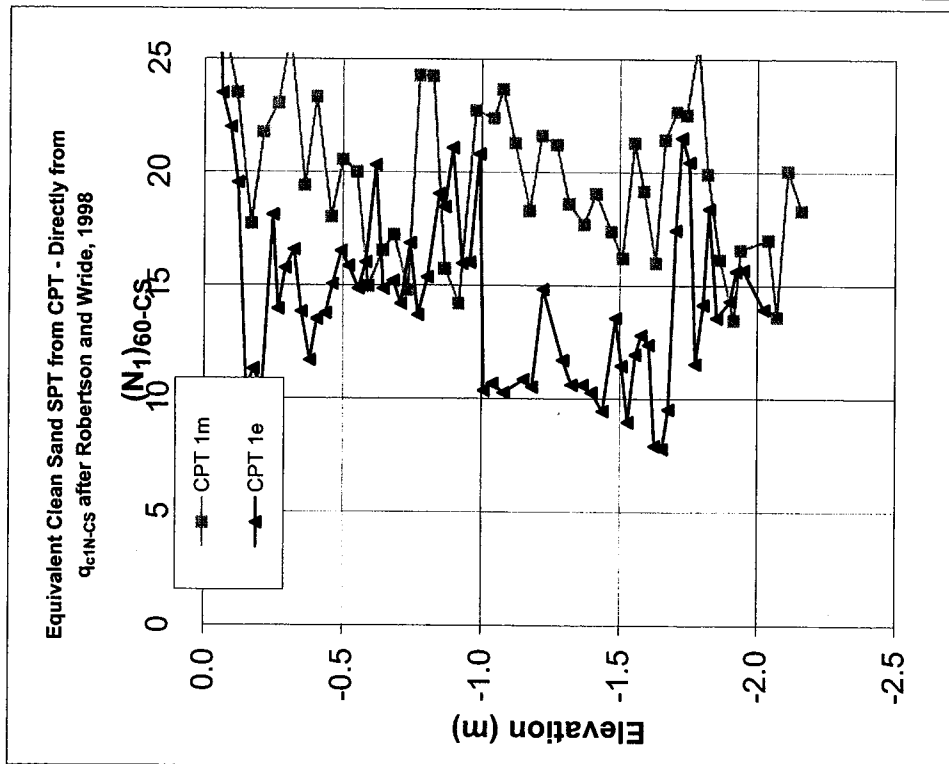
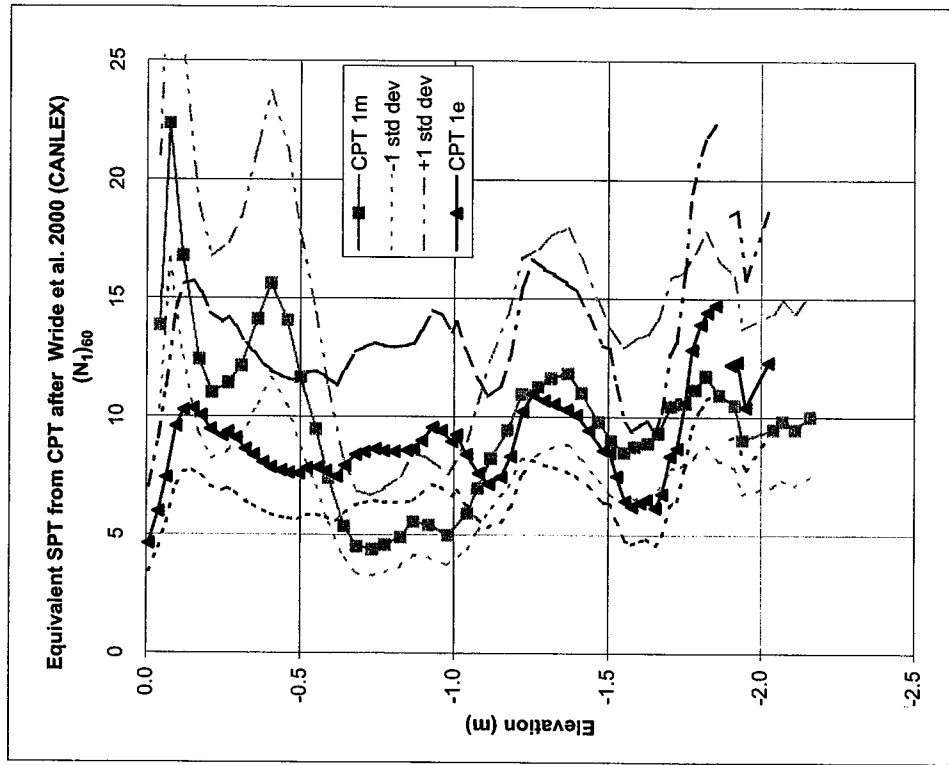


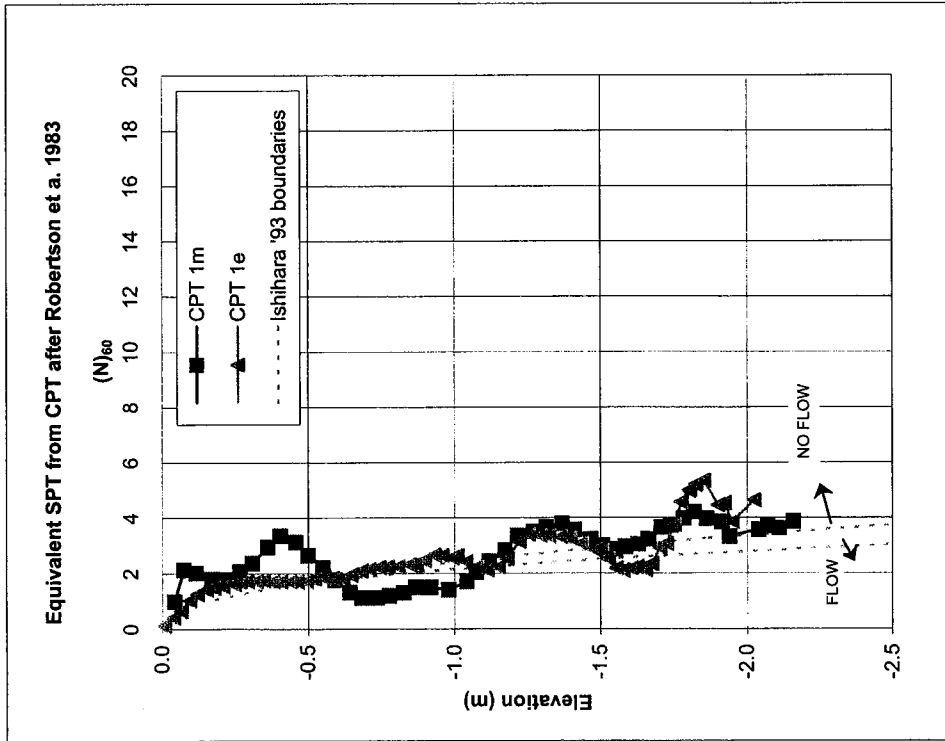
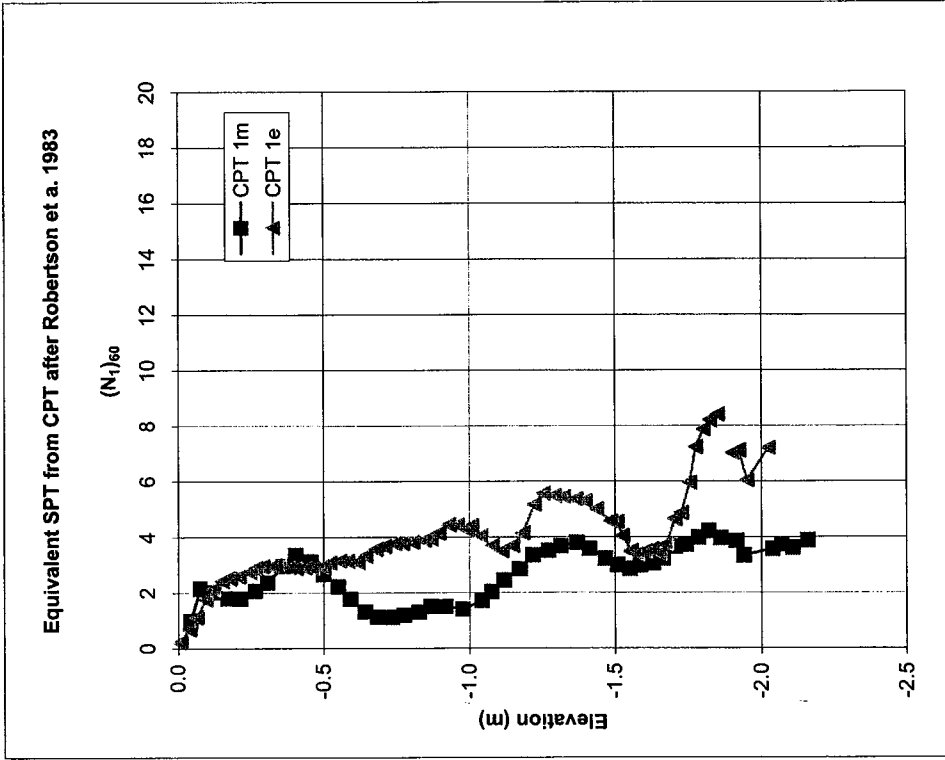


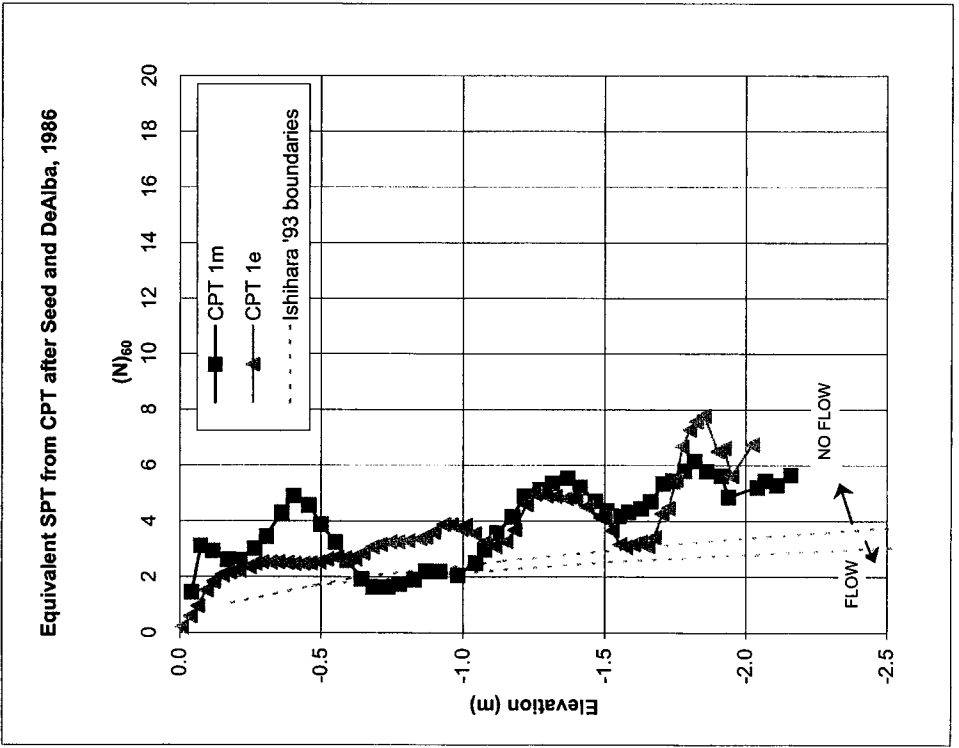
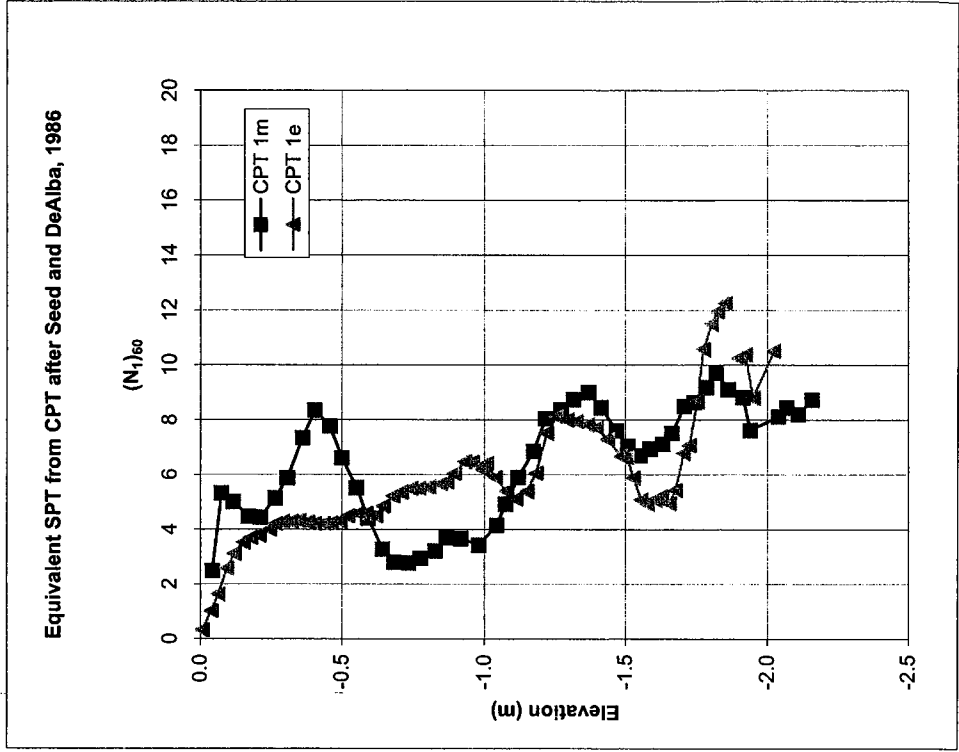


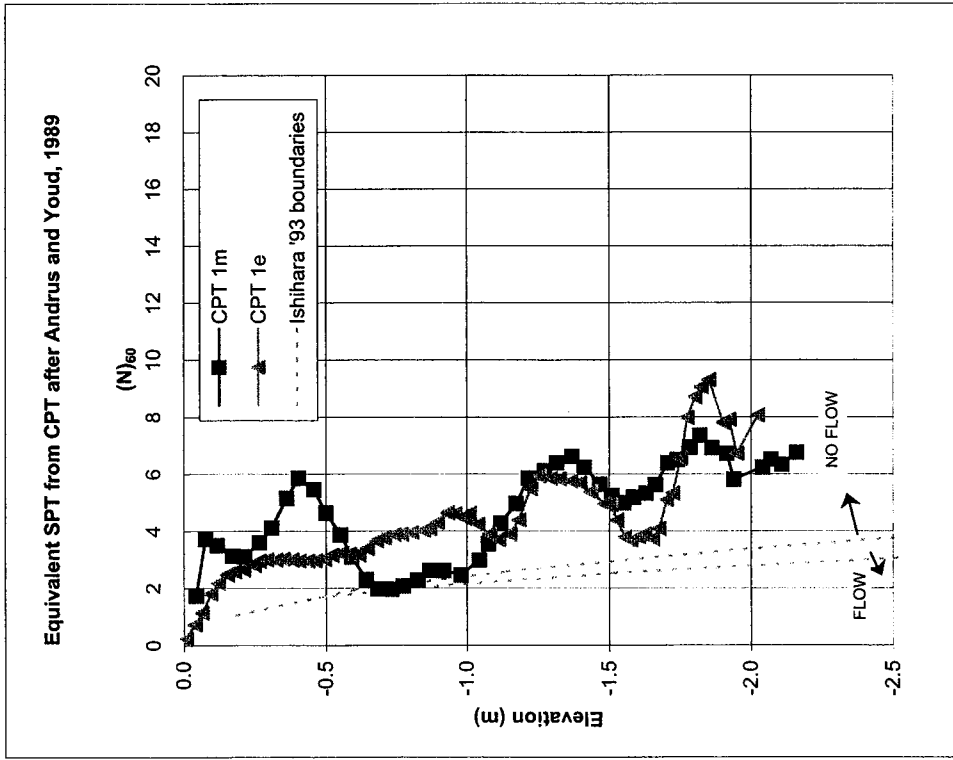
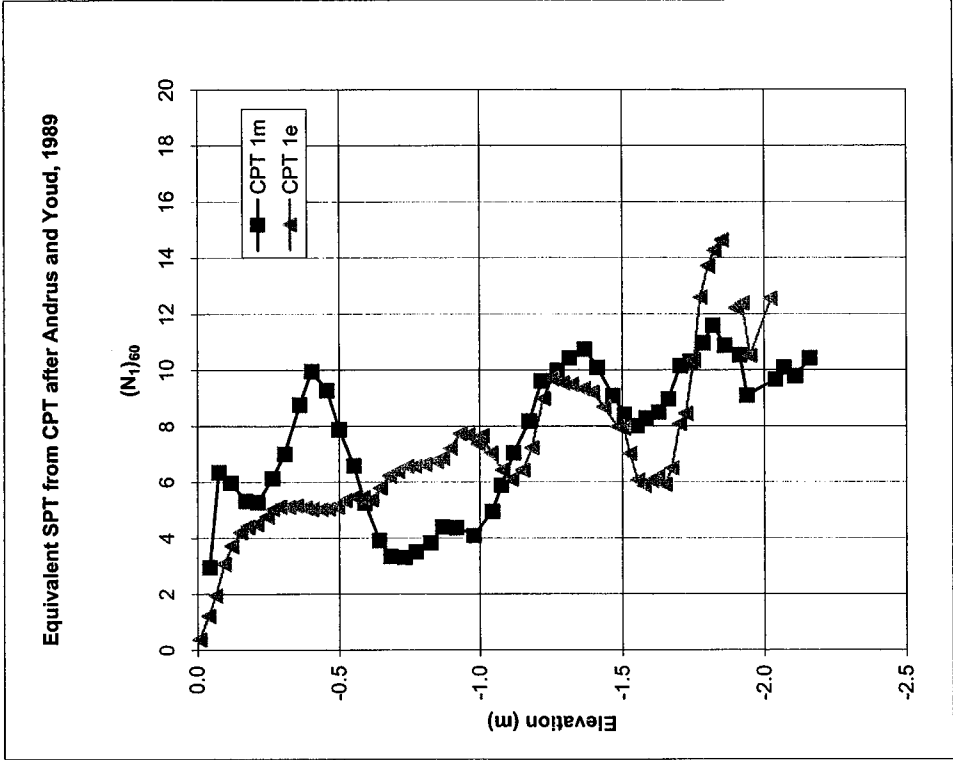




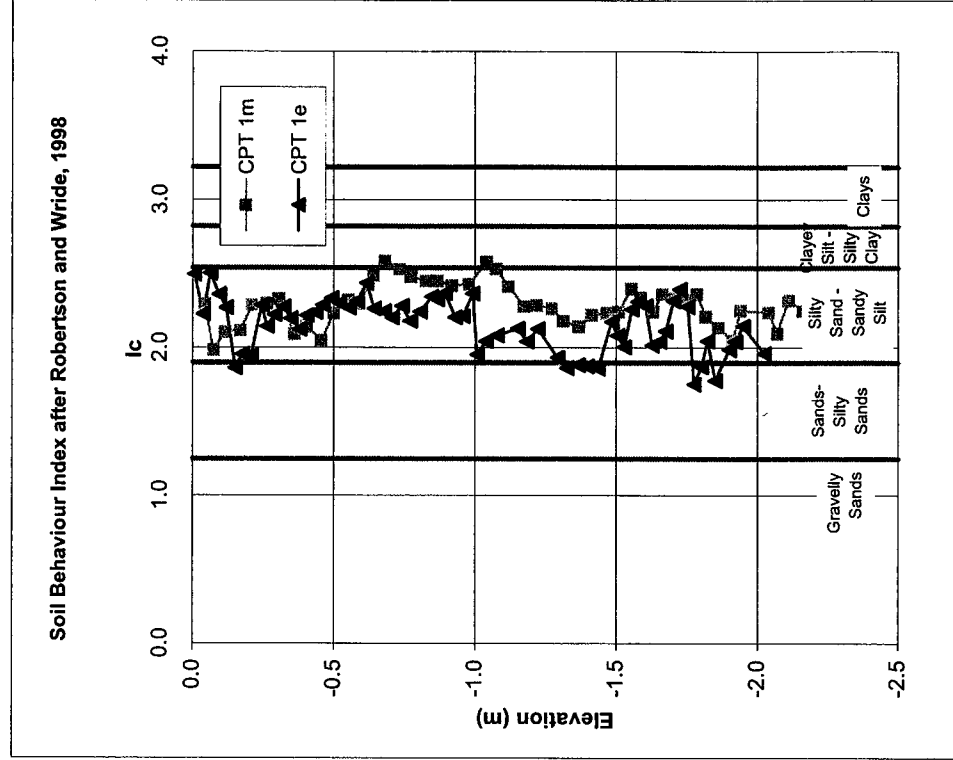
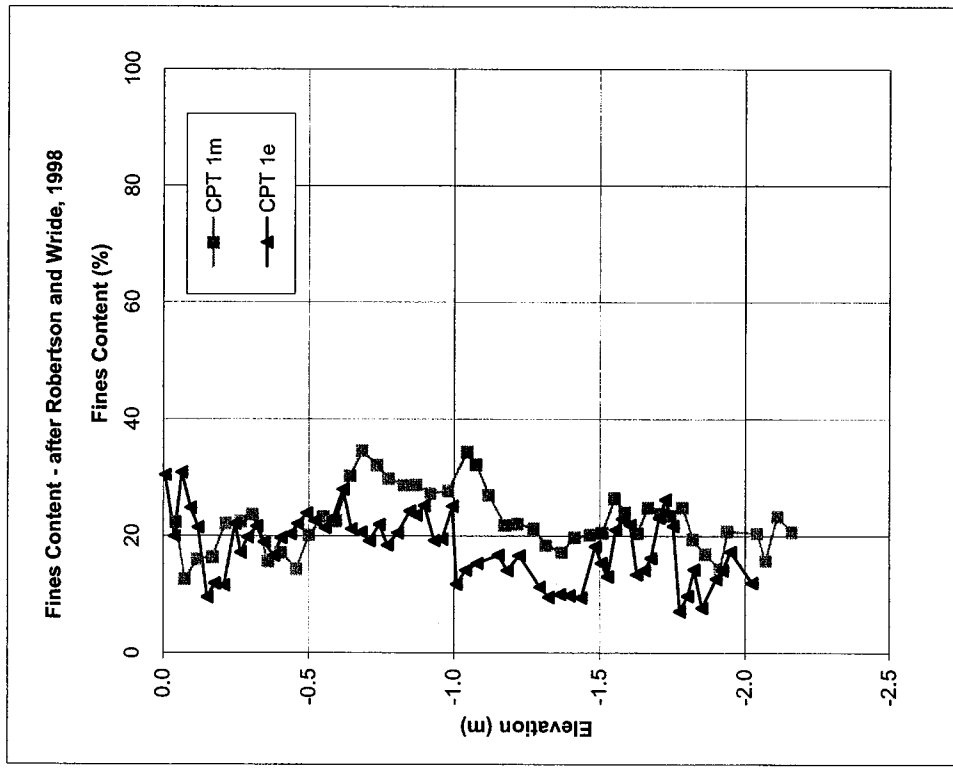


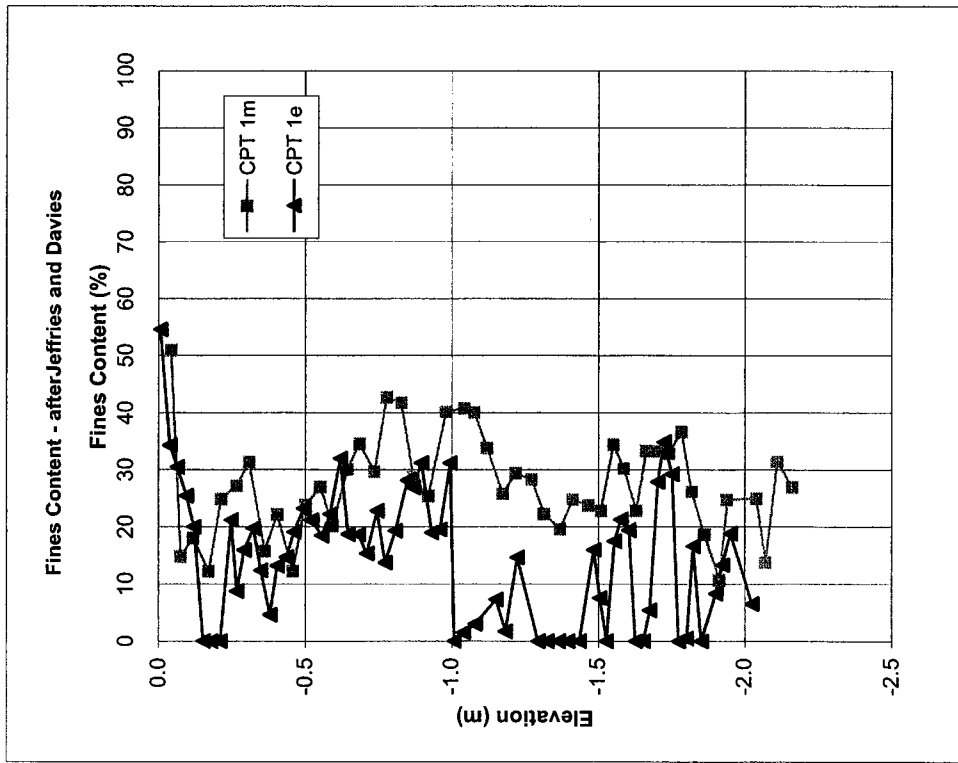
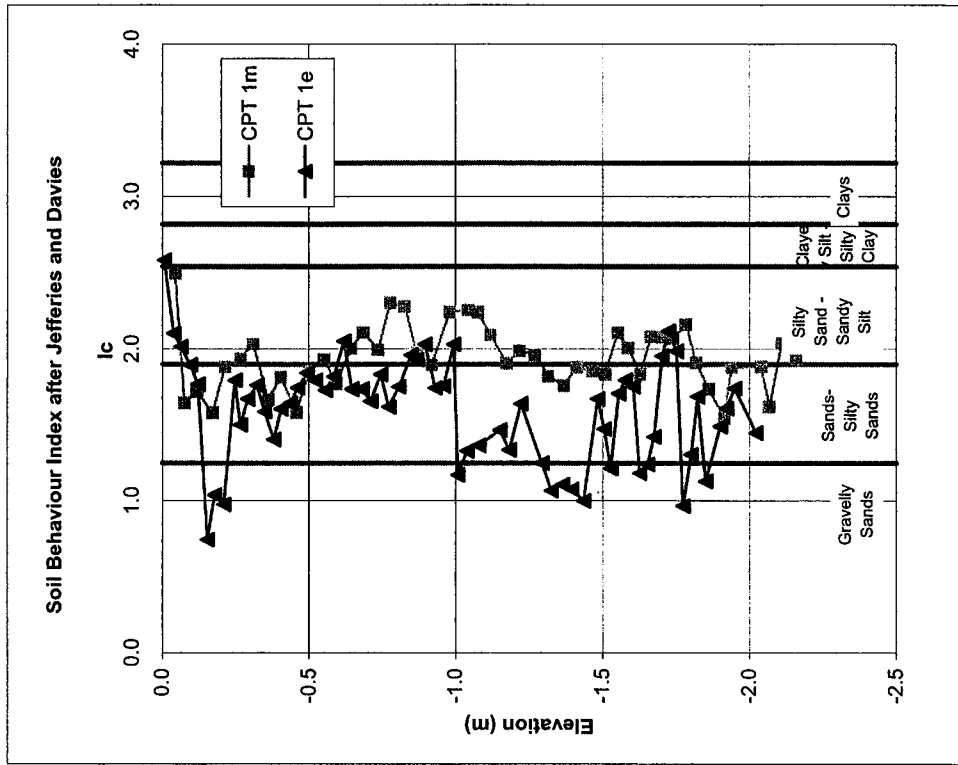


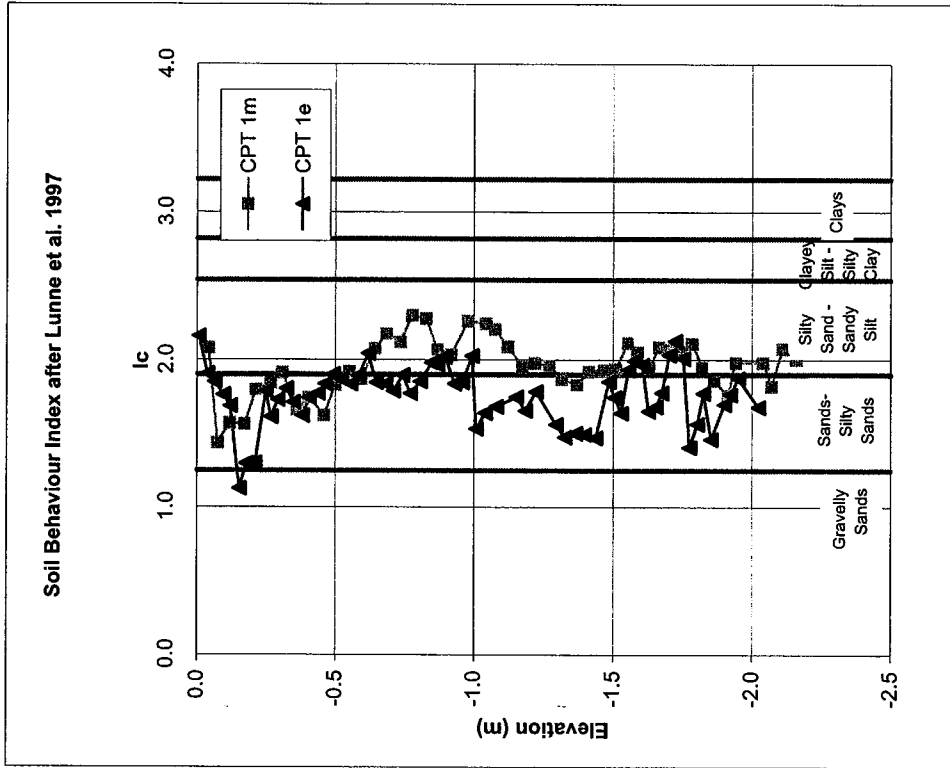
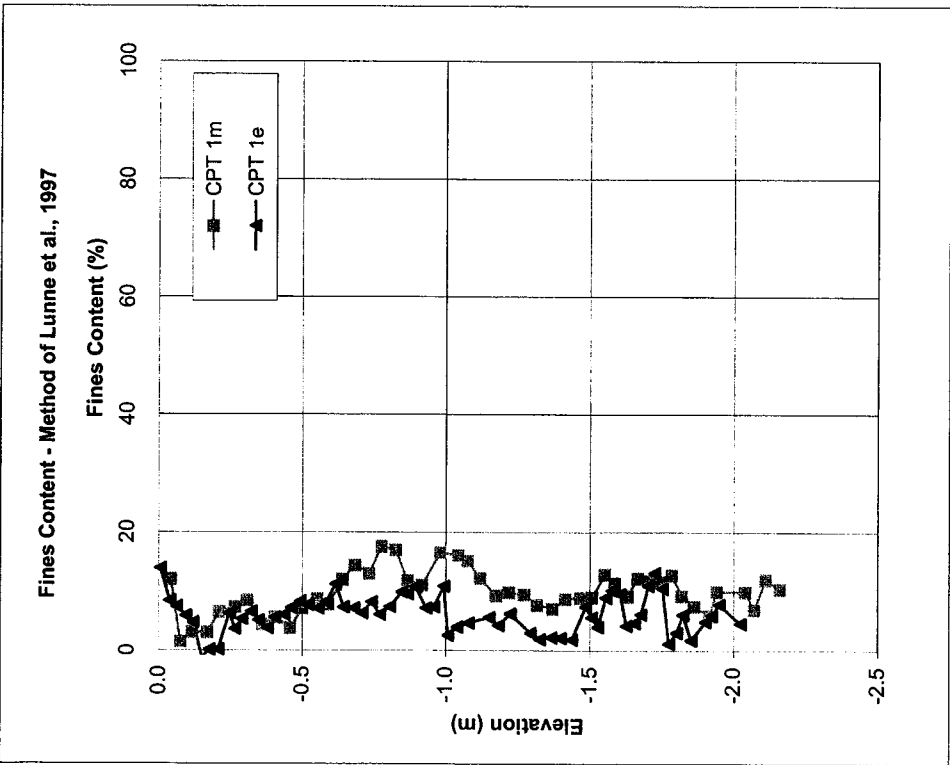




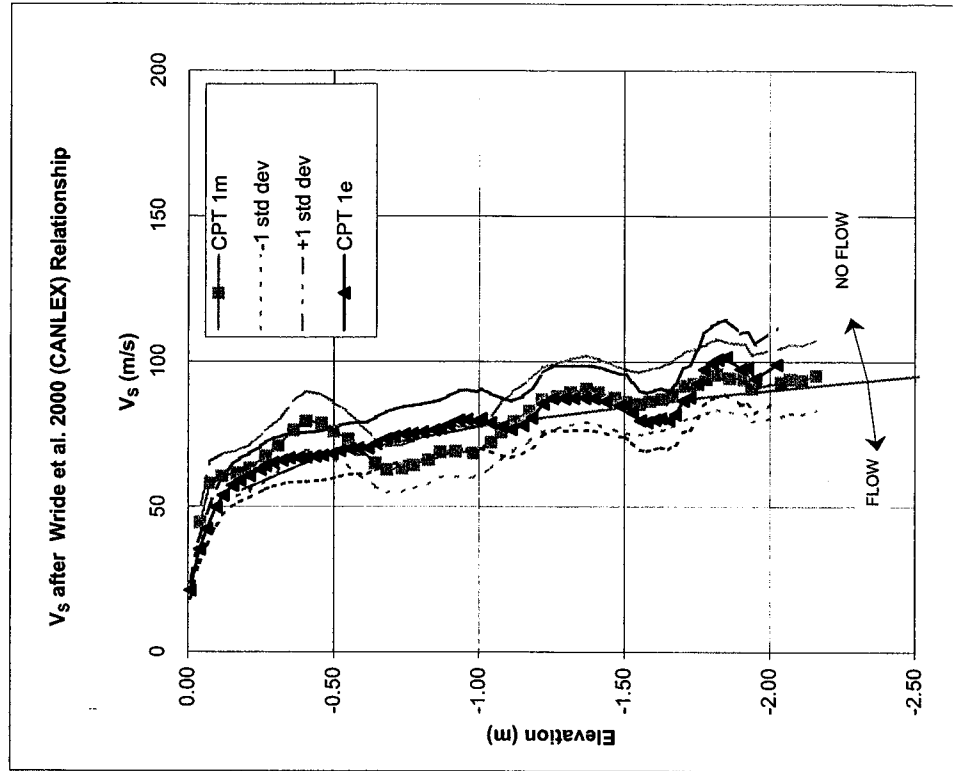
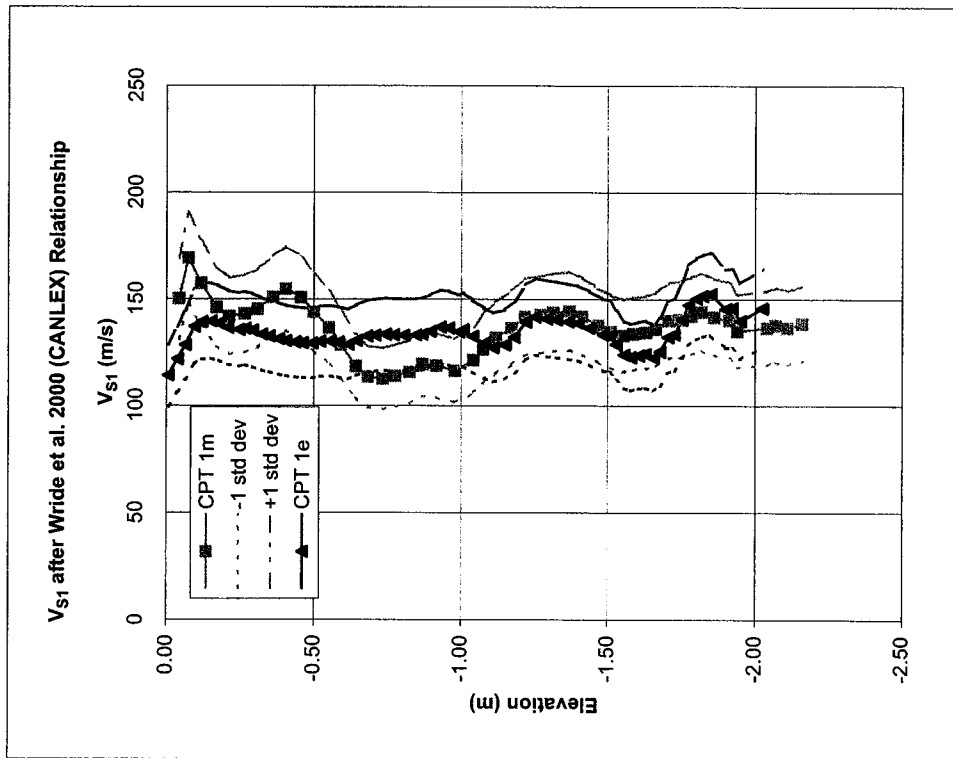
FINES CONTENT AND BEHAVIOUR INDEX

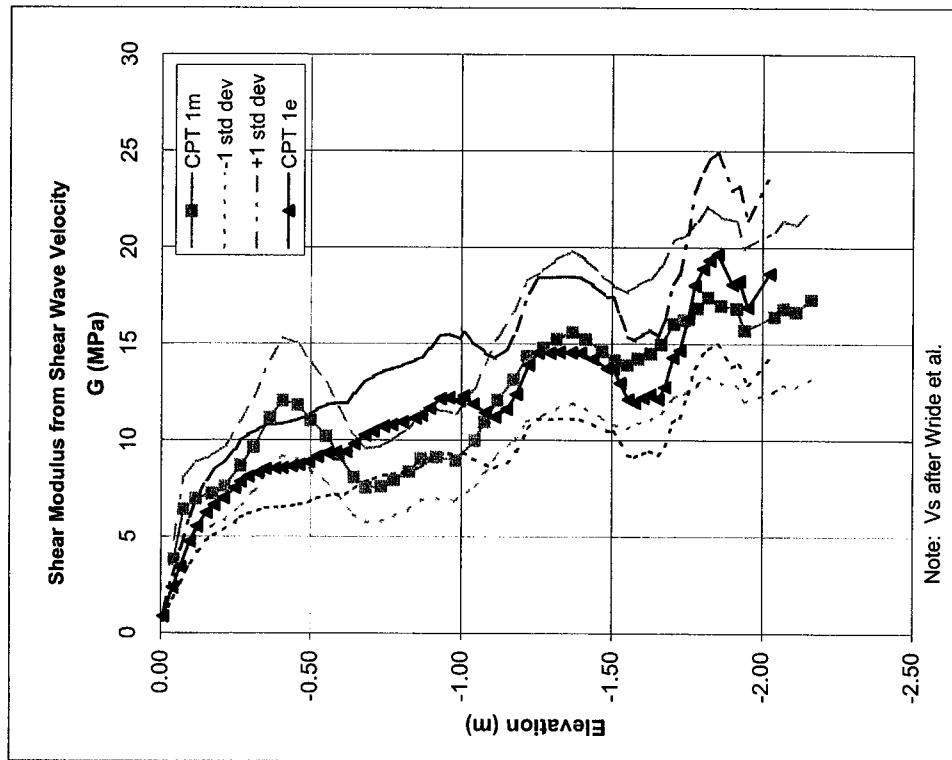






SHEAR WAVE VELOCITY FROM CPT AND SHEAR MODULUS





Note: Vs after Wride et al.

APPENDIX D

**Liquefaction Susceptibility Analyses and
Extrapolation of Field Data**

EQUATIONS USED FOR LLIQUEFACTION ANALYSES

Following Hryciw et al. 1990:

$$G\gamma^2 = v_p^2 \rho$$

$$\tau = G\gamma$$

Particle Velocity Attenuation Relationship:

From Dong-Soo et al. after Bornitz, 1931

$$v_{Pi} = v_{PM} \left(\frac{r_M}{r_i} \right)^n e^{-\alpha(r_i - r_M)}$$

v_{Pi} = particle velocity at depth i
 v_{PM} = measured particle velocity
 r_M = distance from source to measurement location
 r_i = distance from source to location of interest
 n = geometric damping coefficient
 α = material damping coefficient

Calculation of Cyclic Shear Stress Ratio:

$$\gamma_i = \sqrt{\frac{v_{Pi}^2 \times \rho}{G}}$$

$$\tau_i = \gamma_i G$$

$$CSS_i = \frac{\tau_i}{\sigma'_{v0i}}$$

$$CSS_{i7.5} = CSS_i \times SF \quad \text{where } SF = \text{scaling factor dependant on number of cycles}$$

Extrapolation to Other Sites:

$$CSS_i = \frac{\tau_{i-CORR}}{\sigma'_{v0}}$$

CSS_i = induced cyclic stress ratio at depth of interest
 τ_{i-CORR} = induced cyclic shear stress corrected for a large number of cycles at depth of interest

$$\tau_{i-CORR} = (v_{Pi} \sqrt{G \times \rho}) SF \quad SF = 1.5, \text{ limit scaling factor for large number of cycles}$$

$$v_{Pi} = (0.65 v_{PM-max}) \left(\frac{r_M}{r_i} \right)^n e^{-\alpha(r_i - r_M)}$$

v_{PM-max} is found by iteration until CSS_i equals the critical cyclic stress ratio.

For a factor of safety of 1, the critical cyclic stress ratio is 0.12, the cyclic stress resistance for the deposit's penetration resistance, for a factor of safety of 1.3, the critical cyclic stress ratio is 0.092.

Tentative Equipment Mass-Particle Velocity Relationship

$$\log M_i = \frac{\log \left(\frac{v_{pi}}{v_{p0}} \right)}{\beta} + \log M_0$$

M_i = Mass of Interest

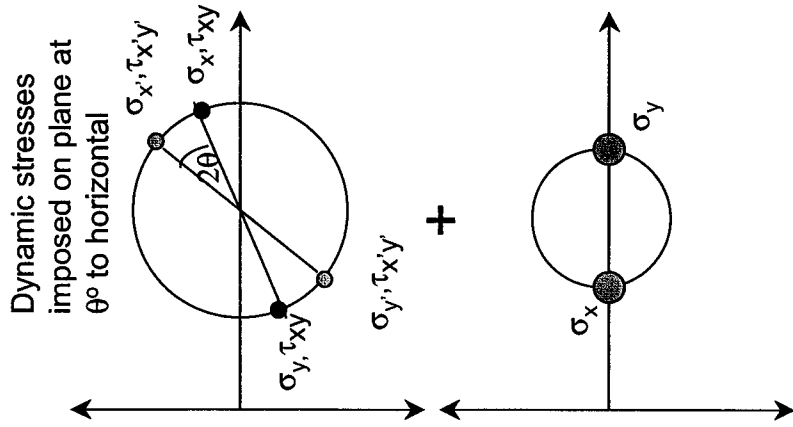
v_{pi} = Velocity of Interest

v_{p0} = Reference Velocity, 65mm/s

B = Slope in log-log space, 1.19

M_0 = Reference Mass, 7800 kg

Mohr's Circle Rotation of Stresses:



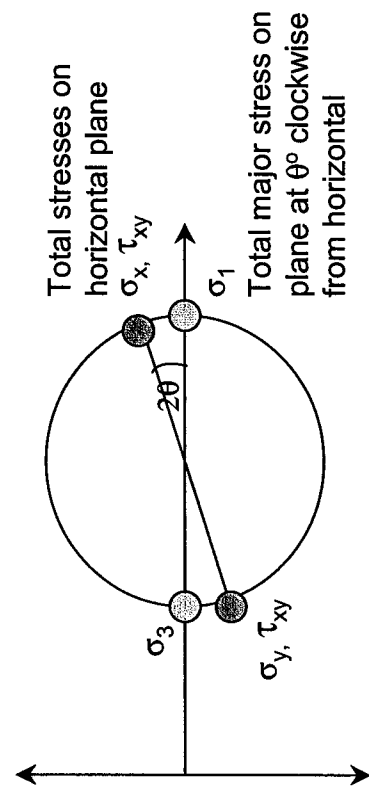
Calculation of Horizontal and Vertical Dynamic Stresses:

$$\sigma_x = \frac{\sigma_{x'} + \sigma_{y'}}{2} + \frac{\sigma_{x'} - \sigma_{y'}}{2} \cos 2\theta - \tau_{x'y'} \sin 2\theta$$

$$\sigma_y = \frac{\sigma_{x'} + \sigma_{y'}}{2} - \frac{\sigma_{x'} - \sigma_{y'}}{2} \cos 2\theta + \tau_{x'y'} \sin 2\theta$$

$$\tau_{xy} = \frac{\sin 2\theta}{2} (\sigma_{x'} - \sigma_{y'}) + \tau_{x'y'} \cos 2\theta$$

Dynamic stresses imposed on horizontal plane



Total major stress on plane at θ° clockwise from horizontal

LIQUEFACTION ANALYSES AT MAIN TEST SITE

Dozer Loading

Particle Velocity Case	Surface Particle Velocity (mm/s)	Density (kg/m ³)	Shear Modulus (MPa)	Geometric Damping, n	Material Damping, α	Depth to Phreatic Surface	Depth of Interest (m)	Particle Velocity at Depth (mm/s)	Number of Cycles	CSS	Scaling Factor for Number of Cycles	CSS ^{7.5}
15 cycles	42	1900	20	2	0.007	0.35	0.5	42.0	15	1.04	1.00	1.04
							1	12.7	15	0.20	1.00	0.20
							2	3.1	15	0.03	1.00	0.03
Maximum	102	1900	20	2	0.007	0.35	0.5	102.0	1	2.53	0.43	1.09
							1	30.8	1	0.49	0.43	0.21
							2	7.6	1	0.07	0.43	0.03
65% of Maximum	66.3	1900	20	2	0.007	0.35	0.5	66.3	3	1.65	0.68	1.12
							1	20.0	3	0.32	0.68	0.22
							2	5.0	3	0.05	0.68	0.03
2nd Maximum Peak (More Representative Max)	77	1900	20	2	0.007	0.35	0.5	77.0	2	1.91	0.60	1.15
							1	23.2	2	0.37	0.60	0.22
							2	5.8	2	0.05	0.60	0.03
65% of 2nd Peak	50.05	1900	20	2	0.007	0.35	0.5	50.1	7	1.24	0.86	1.07
							1	15.1	7	0.24	0.86	0.21
							2	3.7	7	0.03	0.86	0.03
15 cycles	42	1900	20	1	0.007	0.35	0.5	42.0	15	1.04	1.00	1.04
							1	23.0	15	0.37	1.00	0.37
							2	11.4	15	0.11	1.00	0.11
Maximum	102	1900	20	1	0.007	0.35	0.5	102.0	1	2.53	0.43	1.09
							1	55.9	1	0.89	0.43	0.38
							2	27.8	1	0.26	0.43	0.11
65% of Maximum	66.3	1900	20	1	0.007	0.35	0.5	66.3	3	1.65	0.68	1.12
							1	36.4	3	0.58	0.68	0.39
							2	18.0	3	0.17	0.68	0.11
2nd Maximum Peak (More Representative Max)	77	1900	20	1	0.007	0.35	0.5	77.0	2	1.91	0.60	1.15
							1	42.2	2	0.67	0.60	0.40
							2	21.0	2	0.19	0.60	0.12
65% of 2nd Peak	50.05	1900	20	1	0.007	0.35	0.5	50.1	7	1.24	0.86	1.07
							1	27.4	7	0.44	0.86	0.38
							2	13.6	7	0.13	0.86	0.11

Particle Velocity Case	Surface Particle Velocity (mm/s)	Density (kg/m ³)	Shear Modulus (MPa)	Geometric Damping, n	Material Damping, α	Depth to Phreatic Surface	Depth of Interest (m)	Particle Velocity at Depth (mm/s)	Number of Cycles	CSS	Scaling Factor for Number of Cycles	CSS ^{7.5}
15 cycles	42	1900	20	1	0.02	0.35	0.5	42.0	15	1.04	1.00	1.04
							1	22.9	15	0.36	1.00	0.36
15 cycles	42	1900	10	1	0.007	0.35	0.5	42.0	15	0.74	1.00	0.74
							1	23.0	15	0.26	1.00	0.26
							2	11.4	15	0.07	1.00	0.07
							0.5	42.0	15	1.28	1.00	1.28
15 cycles	42	1900	30	1	0.007	0.35	1	23.0	15	0.45	1.00	0.45
							2	11.4	15	0.13	1.00	0.13

Predator Loading

Particle Velocity Case	Surface Particle Velocity (mm/s)	Density (kg/m ³)	Shear Modulus (MPa)	Geometric Damping, n	Material Damping, α	Depth to Phreatic Surface	Depth of Interest (m)	Particle Velocity at Depth (mm/s)	Number of Cycles	CSS	Scaling Factor for Number of Cycles	CSS ^{7.5}
15 Cycle	1.67	1900	20	2	0.02	0.25	0.25	8.1	15	0.34	1.00	0.34
							0.5	2.0	15	0.06	1.00	0.06
Representative Maximum	28.4	1900	20	2	0.02	0.25	1	0.5	15	0.01	1.00	0.01
							0.25	138.3	1	5.78	0.43	2.49
							0.5	34.4	1	0.98	0.43	0.42
65% of Maximum	3.1	1900	20	2	0.02	0.25	1	8.5	1	0.15	0.43	0.06
							0.25	15.1	2-4	0.63	0.67	0.63
15 Cycle	1.67	1900	20	1	0.02	0.25	0.5	3.8	2-4	0.11	0.67	0.11
							1	0.9	2-4	0.02	0.67	0.02
							0.25	3.7	15	0.15	1.00	0.15
Representative Maximum	28.4	1900	20	1	0.02	0.25	0.5	1.8	15	0.05	1.00	0.05
							1	0.9	15	0.02	1.00	0.02
15 Cycle	1.67	1900	20	1	0.02	0.25	0.25	62.9	1	2.63	0.43	1.13
							0.5	31.3	1	0.89	0.43	0.38
Representative Maximum	28.4	1900	20	1	0.02	0.25	1	15.5	1	0.27	0.43	0.12

Particle Velocity Case	Surface Particle Velocity (mm/s)	Density (kg/m ³)	Shear Modulus (MPa)	Geometric Damping, n	Material Damping, α	Depth to Phreatic Surface	Depth of Interest (m)	Particle Velocity at Depth (mm/s)	Number of Cycles	CSS	Scaling Factor for Number of Cycles	CSS ^{7.5}
65% of Maximum	3.1	1900	20	1	0.02	0.25	0.25	6.9	2-4	0.29	0.67	0.19
							0.5	3.4	2-4	0.10	0.67	0.06
							1	1.7	2-4	0.03	0.67	0.02
15 Cycle	1.67	1900	10	1	0.02	0.25	0.25	3.4	15	0.10	1.00	0.10
							0.5	1.7	15	0.03	1.00	0.03
							1	0.8	15	0.01	1.00	0.01
15 Cycle	1.67	1900	30	1	0.02	0.25	0.25	3.4	15	0.17	1.00	0.17
							0.5	1.7	15	0.06	1.00	0.06
							1	0.8	15	0.02	1.00	0.02
15 Cycle	1.67	1900	20	2	0.02	0.35	0.35	4.1	15	0.12	1.00	0.12
							0.5	2.0	15	0.05	1.00	0.05
							1	0.5	15	0.01	1.00	0.01
Representative Maximum	28.4	1900	20	2	0.02	0.35	0.35	70.4	1	2.10	0.43	0.90
							0.5	34.4	1	0.85	0.43	0.37
							1	8.5	1	0.14	0.43	0.06
65% of Maximum	3.1	1900	20	2	0.02	0.35	0.35	7.7	2-4	0.23	0.67	0.15
							0.5	3.8	2-4	0.09	0.67	0.06
							1	0.9	2-4	0.01	0.67	0.01
15 Cycle	1.67	1900	20	1	0.02	0.35	0.35	2.6	15	0.08	1.00	0.08
							0.5	1.8	15	0.05	1.00	0.05
							1	0.9	15	0.01	1.00	0.01
Representative Maximum	28.4	1900	20	1	0.02	0.35	0.35	44.8	1	1.34	0.43	0.58
							0.5	31.3	1	0.78	0.43	0.33
							1	15.5	1	0.25	0.43	0.11
65% of Maximum	3.1	1998	20	1	0.02	0.35	0.35	4.9	2-4	0.14	0.67	0.10
							0.5	3.4	2-4	0.08	0.67	0.05
							1	1.7	2-4	0.03	0.67	0.02
15 Cycle	1.67	1900	10	1	0.02	0.35	0.35	2.4	15	0.05	1.00	0.05
							0.5	1.7	15	0.03	1.00	0.03
							1	0.8	15	0.01	1.00	0.01
15 Cycle	1.67	1900	30	1	0.02	0.35	0.35	2.4	15	0.09	1.00	0.09
							0.5	1.7	15	0.05	1.00	0.05
							1	0.8	15	0.02	1.00	0.02

LIQUEFACTION SUSCEPTIBILITY ANALYSES AT MAIN TEST SITE

Base Case Properties:

Shear Modulus = 20MPa
 Density = 1900 kg/m³
 Geometric Damping Coefficient = 1
 Material Damping Coefficient = 0.007 Dozer
 0.02 Predator
 Surface Particle Velocity = 15 cycle

